Science

24 March 2006 | $10

Climate Change
Breaking the Ice

AAAS

spot goes quantitative

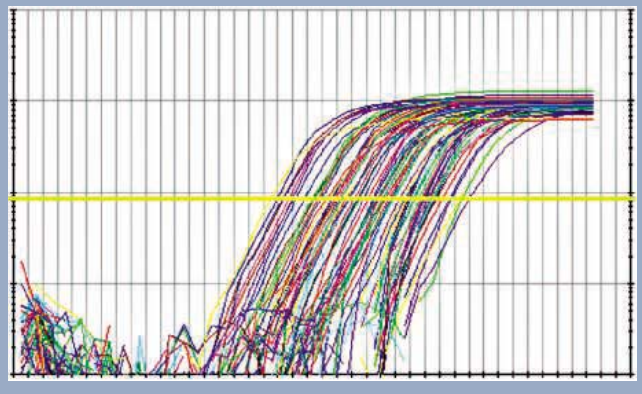

RT² *Profiler*™ PCR Arrays
Monitor expression profiles in your pathway using real-time PCR.

Graduate to a quantitative array...

- **pathway focused:**
  profiles the expression of a panel of genes relevant to a pathway or disease state
- **simple and accurate:**
  simple PCR-based procedure; high sensitivity and wide dynamic range
- **designed for routine use:**
  brings expression profiling to almost any lab with a real-time PCR instrument

PCR Arrays combine microarray profiling capability with real-time PCR performance.

RT² *Profiler*™ PCR Arrays are the ideal tool for monitoring gene expression focused on biological pathways and disease states. With PCR Arrays, you can profile the expression of a thoroughly researched panel of genes plus housekeeping genes and controls in a single 96-well plate.

RT² *Profiler*™ PCR Arrays are available for immunology, cancer, signal transduction and more.

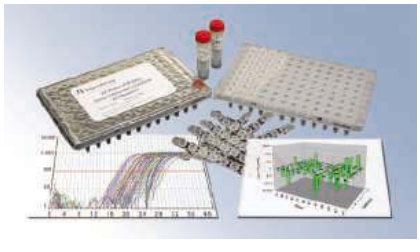

SuperArray Bioscience Corporation

Find the PCR Array for your pathway at www.SuperArray.com.

888-503-3187 (USA) **301-682-9200**

Pathway-Centric Tools and Technology™

Reproducibility.

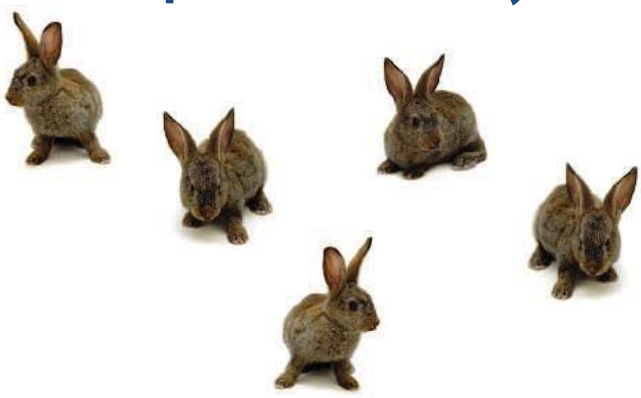

R&D Systems Quantikine® ELISA Kits

re·pro·duc·i·bil·i·ty (rē´prə-doos´ĭ-bĭl´ĭ-tē) 1. An assessment of variability among replicate measurements of the same sample that are expected to produce identical results.

Every Quantikine® ELISA Kit undergoes stringent testing to ensure reproducibility within and between assays.

- **Reproducibility/Precision** is tested with replicate measurements on the same plate and between plates to ensure a low coefficient of variation
- **High Affinity Antibodies** are selected to minimize non-specific binding
- **Diluents** are designed to reduce matrix interference in different sample types
- **Optimized Recovery** of known analyte quantities from different sample types
- **Highly Specific** antibodies are selected to prevent cross-reactivity with related molecules
- **Linearity** is assured across the assay dynamic range
- **Sensitivity** - can detect cytokine levels down to low pg/mL range

For research use only. Not for use in diagnostic procedures except where noted.

Cancer Development Endocrinology Immunology Neuroscience Proteases Stem Cells

www.RnDSystems.com

U.S. & Canada | **R&D Systems, Inc.** | Tel: (800) 343-7475 | info@RnDSystems.com
Europe | **R&D Systems Europe Ltd.** | Tel: +44 (0)1235 529449 | info@RnDSystems.co.uk
Germany | **R&D Systems GmbH** | Tel: 0800 909 4455 | infogmbh@RnDSystems.co.uk
France | **R&D Systems Europe** | Tel: 0800 90 72 49 | info@RnDSystems.co.uk

R&D Systems is a trademark of TECHNE Corporation

R&D SYSTEMS

Quality | Selection | Performance | Results

GE Healthcare

Greater flexibility in histidine-tagged protein purification

Ni Sepharose™ products from GE Healthcare give you greater flexibility and the highest binding capacity available for histidine-tagged protein purification. They also assure maximum target protein activity, thanks to their tolerance of a wide range of additives and negligible nickel ion leakage.

His MultiTrap™ prepacked multiwell plates let you directly apply unclarified lysate for greater convenience and minimized degradation of sensitive target proteins. Ni Sepharose is also available prepacked in His SpinTrap™, His GraviTrap™, HisTrap™ and bulk packs to ensure maximum flexibility in histidine-tagged protein purification.

www.gehealthcare.com/his

imagination at work

YYePG Proudly Presents, Thx for Support

GE01-06

Volume 311, Issue 5768

COVER

Icebergs and ice sheets in Nansen Fjord, Greenland. New measurements indicate that the flow rates of glaciers in Greenland and West Antarctica have increased recently and that the masses of the Greenland and West Antarctic ice sheets have been declining. See News story page 1698, Editorial page 1673, and other related content (also available at www.sciencemag.org/sciext/ice/).

Image: Nevada Wier/CORBIS

DEPARTMENTS

EDITORIAL

NEWS OF THE WEEK

NEWS FOCUS


1704

LETTERS

BOOKS *ET AL.*


1714

POLICY FORUM

PERSPECTIVES

CONTENTS continued >>

Systems Biology — RNA Purification

Standardized RNA solutions guarantee comparable results

Convenient RNA purification

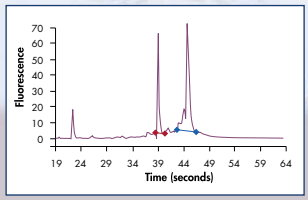

Purification of high-quality RNA

Advance your gene expression research with standardized solutions for RNA purification!

QIAGEN RNA solutions standardize the purification of RNA from biological samples.

Benefits include:

- **Reliability** — highly pure, intact RNA for standardized results in all downstream applications
- **Convenience** — easy-to-use kits with minimal protocol steps
- **Speed** — ready-to-use RNA purified in as little as 25 minutes
- **Versatility** — manual and automated kits for a wide range of sample types, sizes, and throughputs

Visit www.qiagen.com/goto/RNAsolutions to find out more!

QIAGEN

SCIENCE EXPRESS

www.sciencexpress.org

BIOCHEMISTRY

A Voltage Sensor–Domain Protein Is a Voltage-Gated Proton Channel
M. Sasaki, M. Takagi, Y. Okamura
Most of a voltage-gated proton channel consists of a four-transmembrane domain similar to the voltage sensor of other channels.
10.1126/science.1122352

MOLECULAR BIOLOGY

RNA Interference Directs Innate Immunity Against Viruses in Adult *Drosophila*
X.-H. Wang et al.
Insects use small RNA silencing mechanisms to neutralize invading viral pathogens.
10.1126/science.1125694

VIROLOGY

BREVIA: H5N1 Virus Attachment to Lower Respiratory Tract
D. van Riel et al.
The avian influenza H5N1 attaches most efficiently to cell types located deep in the lungs of some mammals, including humans, affecting its pathology and transmissibility.
>> News story p. 1692
10.1126/science.1125548

EVOLUTION

Conservation of RET Regulatory Function from Human to Zebrafish Without Sequence Similarity
S. Fisher, E. A. Grice, R. M. Vinton, S. L. Bessling, A. S. McCallion
A human regulatory gene can substitute for the corresponding gene in zebrafish, conferring tissue-specific expression despite its different sequence.
10.1126/science.1124070

PLANETARY SCIENCE

A Population of Comets in the Main Asteroid Belt
H. H. Hsieh and D. Jewitt
A currently small population of comets exists in the main asteroid belt, differing in origin and temperature from those in the outer solar system.
10.1126/science.1125150

TECHNICAL COMMENT ABSTRACTS

REVIEWS

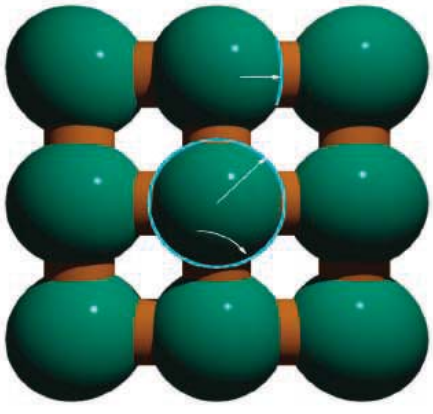

BREVIA

RESEARCH ARTICLE

REPORTS

Create!

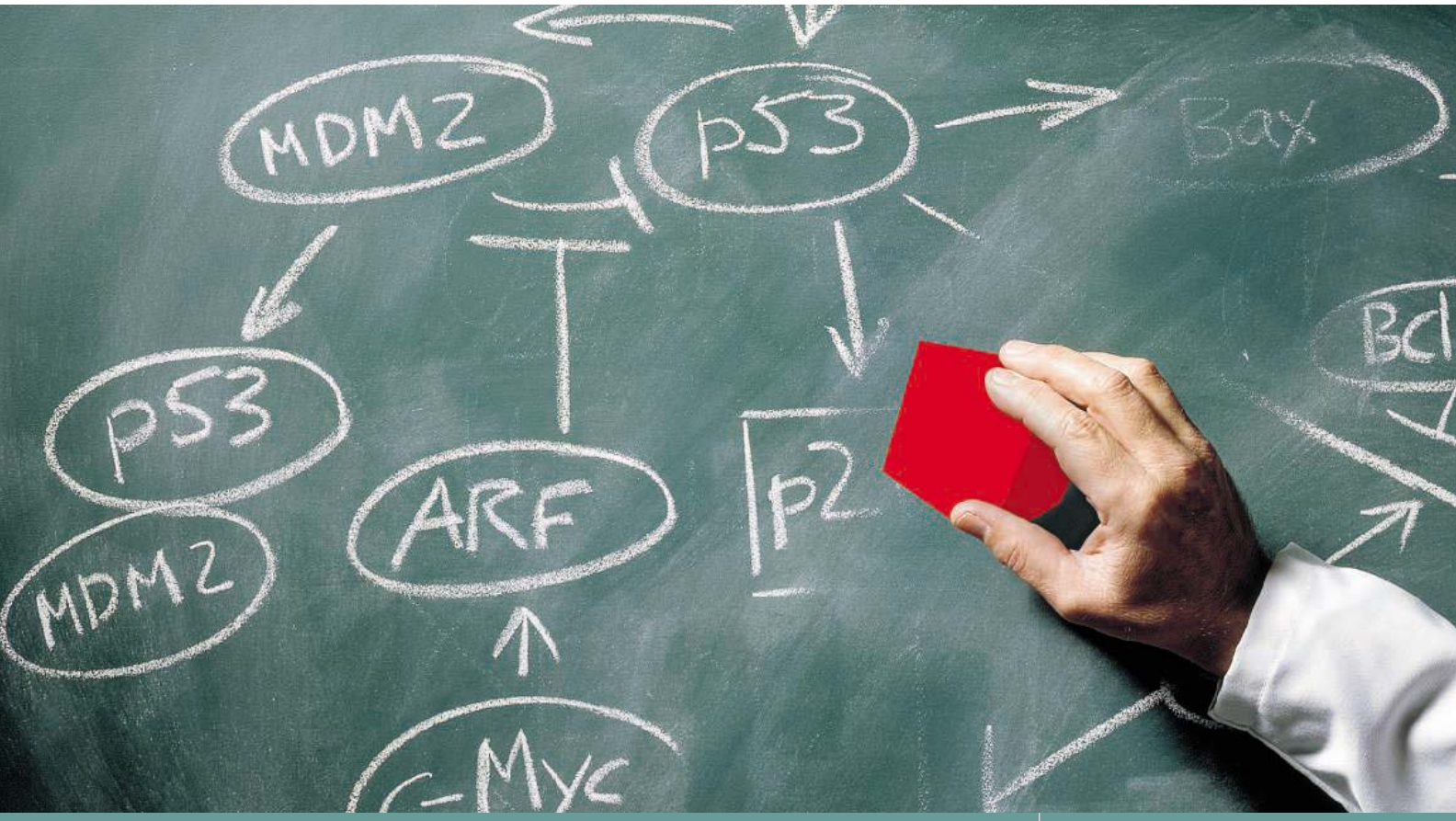

INNOVATION @ WORK

with Sigma, the new leader in RNAi
create your advantage

Faster siRNA manufacturing? 100% transduction efficiency of shRNA constructs? Long and short term silencing?

Sigma has developed the most comprehensive array of cutting edge products for every step of your RNAi experimental design – creating for you a real advantage.

- Taking siRNA manufacturing to a new level by providing a rapid turnaround, high throughput and cost effective service that caters to your siRNA needs
- MISSION™ TRC shRNA libraries, comprising 150,000 pre-cloned shRNA constructs targeting 15,000 human genes and 15,000 mouse genes
- Lentiviral shRNA delivery that boasts flexibility of long and short term silencing, 100% transduction efficiency and enables experimentation with difficult to study cell types such as non-dividing or primary cells

So whether you are determining gene function, analyzing signal transduction or screening for potential drug targets, why not discover how you can create your RNAi advantage.

sigma.com/rnai

Member of the RNAi Consortium

MISSION is a trademark belonging to Sigma-Aldrich Co. and its affiliate Sigma-Aldrich Biotechnology LP.
The RNAi Consortium shRNA library is produced and distributed under license from the Massachusetts Institute of Technology.

Accelerating Customers' Success through **Leadership** in **Life Science, High Technology** and **Service**
SIGMA-ALDRICH CORPORATION • BOX 14508 • ST. LOUIS • MISSOURI 63178 • USA

SIGMA®

REPORTS *CONTINUED...*

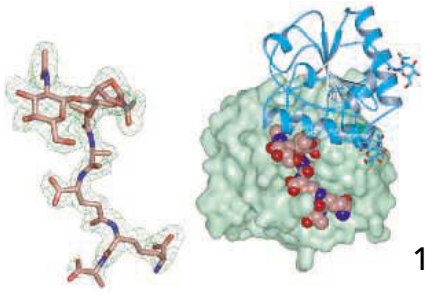

AAAS
ADVANCING SCIENCE, SERVING SOCIETY

SCIENCE (ISSN 0036-8075) is published weekly on Friday, except the last week in December, by the American Association for the Advancement of Science, 1200 New York Avenue, NW, Washington, DC 20005. Periodicals Mail postage (publication No. 484460) paid at Washington, DC, and additional mailing offices. Domestic individual membership and subscription (51 issues): $139 ($74 allocated to subscription). Domestic institutional subscription (51 issues): $650; Foreign postage extra: Mexico, Caribbean (surface mail) $55; other countries (air assist delivery) $85. First class, airmail, student, and emeritus rates on request. Canadian rates with GST available upon request, GST #1254 88122. Publications Mail Agreement Number 1069624. **Printed in the U.S.A.**

Change of address: Allow 4 weeks, giving old and new addresses and 8-digit account number. **Postmaster:** Send change of address to *Science*, P.O. Box 1811, Danbury, CT 06813–1811. **Single-copy sales:** $10.00 per issue prepaid includes surface postage; bulk rates on request. **Authorization to photocopy** material for internal or personal use under circumstances not falling within the fair use provisions of the Copyright Act is granted by AAAS to libraries and other users registered with the Copyright Clearance Center (CCC) Transactional Reporting Service, provided that $18.00 per article is paid directly to CCC, 222 Rosewood Drive, Danvers, MA 01923. The identification code for *Science* is 0036-8075/83 $18.00. *Science* is indexed in the *Reader's Guide to Periodical Literature* and in several specialized indexes.

CONTENTS continued **>>**

One just right for you.

Find your perfect match among the full line of Bio-Rad amplification products.

Bio-Rad is committed to providing you with the best tools for your PCR needs. This dedication is proven by our history of innovation, quality, and regard for researchers' needs.

- The most complete line of thermal cyclers available anywhere
- The only modular real-time cycler upgrade with a thermal gradient; choose from 1 to 5 colors
- Innovative enzymes that work where others fail
- PCR tubes, plates, and sealers for any application
- Dedicated technical support by experienced scientists

PCR License Update

All Bio-Rad's thermal cyclers and real-time systems, including MJ products, are covered by PCR agreements.

Find out more at **www.bio-rad.com/PCRnews**

For more information, visit us on the Web at: **www.bio-rad.com/amplification/**

Photo: Pete with his MiniOpticon™ real-time system and Patty with her DNA Engine Dyad® cycler with a Dual Alpha™ unit and a single Alpha™ unit.

Practice of the patented polymerase chain reaction (PCR) process requires a license. Bio-Rad Thermal Cyclers, whether purchased as complete instruments or as multiple modules, are Authorized Thermal Cyclers and may be used with PCR licenses available from Applied Biosystems. Their use with Authorized Reagents also provides a limited PCR license in accordance with the label rights accompanying such reagents.

Bio-Rad real-time thermal cyclers are licensed real-time thermal cycler(s) under Applera's United States Patent No. 6,814,934 B1 for use in research and for all other fields except the fields of human diagnostics and veterinary diagnostics.

Visit us on the Web at **discover.bio-rad.com**
Call toll free at 1-800-4BIORAD (1-800-424-6723),
outside the US, contact your local sales office.

XX-PCT Proudly Presents, Thx for Support

BIO-RAD

Active MAPK in mouse embryos.

SCIENCE'S **STKE**

www.stke.org SIGNAL TRANSDUCTION KNOWLEDGE ENVIRONMENT

PERSPECTIVE: *BRAF* and *MEK* Mutations Make a Late Entrance
N. Duesbery and G. Vande Woude
Germline mutations in the *KRAS*, *BRAF*, and *MEK1* and *MEK2* genes cause specific developmental syndromes.

PERSPECTIVE: Multiple Thermometers in Mammalian Cells—Why Do Cells from Homeothermic Organisms Need to Measure Temperature?
M. Y. Sherman and V. L. Gabai
Do cells have specific molecular thermometers or simply detect the accumulation of abnormal proteins?

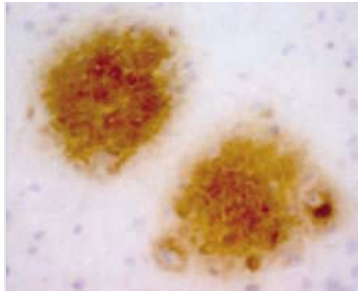

A plethora of plaque types in the human brain.

SCIENCE'S **SAGE KE**

www.sageke.org SCIENCE OF AGING KNOWLEDGE ENVIRONMENT

REVIEW: The Development of Amyloid β Protein Deposits in the Aged Brain
D. R. Thal, E. Capetillo-Zarate, K. Del Tredici, H. Braak
Different types of amyloid β protein deposits offer clues into the development of neurodegeneration.

AGING IN THE ARTS
View a painting of moon goddess Chang E, who purportedly stole the elixir of immortality from her husband.

SCIENCE**NOW**

www.sciencenow.org DAILY NEWS COVERAGE

A (Genetic) History of Violence
Aggressive behavior may be linked to gene variant.

A Lop-Sided Look at Cancer
Breast symmetry seems to be important for predicting cancer risk.

Holey Fiber
Optics technology gets wired.

The fulfillment of teaching science.

SCIENCE **CAREERS**

www.sciencecareers.org CAREER RESOURCES FOR SCIENTISTS

GLOBAL: Scientists as Schoolteachers—Feature Index
R. Arnette
Scientists are finding professional fulfillment from teaching inside and outside of the classroom.

MISCINET: Educated Woman, Chapter 49—The Grad School Success-O-Meter
M. P. DeWhyse
Micella explores the continuum from grad school success to failure.

US: Learning Without Schooling
A. Kotok
Scientists can teach kids in places other than the classroom, but business skills and a touch of showbiz are needed.

EUROPE: A Surfeit of Schoolteachers
C. Berrie
Italy has too many teachers now, but a teacher shortage is predicted for the coming years.

US: An Alternative Approach to an Alternative Career
J. Austin
In parts of the United States, scientists can be teaching just weeks after making the decision to leave the bench.

Competent Cells from New England Biolabs

SUPERIOR COMPETENT *E.COLI* STRAINS FOR CLONING AND PROTEIN EXPRESSION

For many years staff scientists at New England Biolabs have been using their own line of optimized chemically competent *E.coli* cells for cloning and protein expression. These strains have made all the difference to a highly demanding research and production program. Now when you are looking for a versatile cloning strain, rapid colony growth, or tight control of protein expression, you can benefit from the superior performance and high quality of these strains.

- **NEB Turbo Competent *E.coli*** **C2984H**
  Ligate, transform, plate and pick colonies in one day
- **NEB 5-alpha Competent *E.coli*** **C2991H**
  Versatile cloning strain
- **T7 Express Competent *E.coli*** **C2566H**
  High efficiency transformation and protein expression
- **T7 Express I^q Competent *E.coli*** **C2833H**
  Tight control of protein expression
- **dam⁻/dcm⁻ Competent *E.coli*** **C2925H**
  Grow plasmids free of dam and dcm methylation

Advantages:

- Ready to transform – packaged in single-use transformation tubes (20 x 0.05 ml)
- Free of animal products
- 5 minute transformation protocols
- Supplied with outgrowth media and control DNA

	NEB Turbo	NEB 5-alpha	T7 Express	T7 Express I^q	dam⁻/ dcm⁻
Transformation Efficiency (cfu/µg)	$>10^9$	$1\text{-}3 \times 10^9$	$2\text{-}6 \times 10^8$	$2\text{-}6 \times 10^8$	$>2 \times 10^6$
Strain	K12	K12	B	B	K12
T1 Phage Resistant	✓	✓	✓	✓	✓
Blue/White Screening	✓	✓	–	–	–
lac I^q	✓	✓	–	✓	–
Colonies Visible after 8 hours	✓	–	–	–	–
Endonuclease I Deficient	✓	✓	✓	✓	✓
Protease Deficient	–	–	✓	✓	–
Restriction Deficient	✓	✓	✓	✓	✓
M13 Phage Capable (F^+)	✓	✓	–	✓	–
RecA Deficient	–	✓	–	–	–

Chemically Competent *E.coli* Strain Characteristics

For more information and international distribution network, please visit www.neb.com

- **New England Biolabs Inc.** 240 County Road, Ipswich, MA 01938 USA 1-800-NEB-LABS Tel. (978) 927-5054 Fax (978) 921-1350 info@neb.com
- **Canada** Tel. (800) 387-1095 info@ca.neb.com
- **Germany** Tel. (0800) 246 5227 info@de.neb.com
- **UK** Tel. (0800) 318486 info@uk.neb.com
- **China** Tel. 010-82378266 beijing@neb-china.com

NEW ENGLAND BioLabs® Inc.
the leader in enzyme technology

EDITED BY STELLA HURTLEY AND PHIL SZUROMI

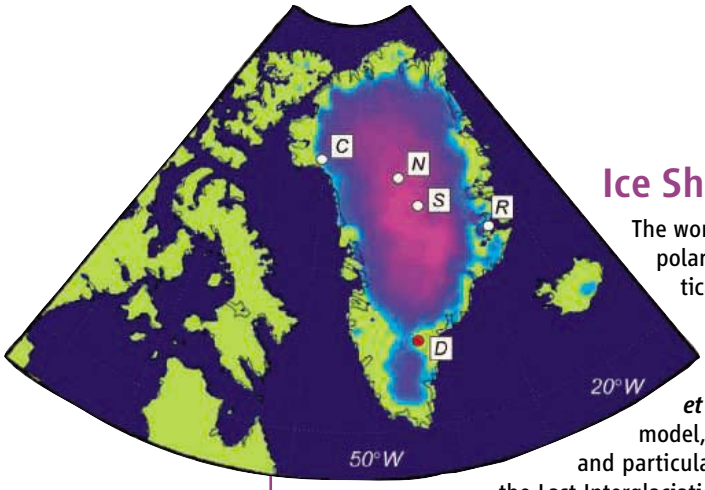

Ice Sheet Stability

The world is warming, and higher temperatures can cause melting of polar ice sheets. How fast will the ice sheets of Greenland and Antarctica disappear, and how fast and far will sea level rise in the coming century? These issues are addressed in a news story by **Kerr** (see the cover), the Editorial by **Hanson and Kennedy**, Perspectives by **Bindschadler** and **Joughin**, and four Reports. **Otto-Bliesner *et al.*** (p. 1751) integrate climate model simulations, an ice sheet model, and paleoclimate data to show that the northern latitudes, and particularly the Arctic, were significantly warmer during the Last Interglaciation, when sea level was several meters higher than at present. They also estimate that the Greenland Ice Sheet contributed between 2.2 and 3.4 meters of sea level rise in the penultimate deglaciation. **Overpeck *et al.*** (p. 1747) compare the model's predictions of warming during the next 130 years to this reconstruction, and conclude that surface temperatures will be as high by the end of this century as they were 130,000 years ago. These conditions would melt enough of the Greenland Ice Sheet to raise sea level by several meters. Determining how quickly Antarctic ice may be disappearing has been difficult to assess. The Gravity Recovery and Climate Experiment (GRACE) satellites were designed to make the needed measurements, and **Velicogna and Wahr** (p. 1754, published online 23 February) show that the mass of the ice sheet has been decreasing by 152 ± 80 cubic kilometers per year from 2002 to 2005, mostly from losses of the West Antarctic Ice Sheet. Contrary to some projections, ice loss around the margins is proceeding faster than the center of the ice sheet is growing. Glacial earthquakes are triggered by the large and sudden sliding of glaciers and can be observed by global seismic networks. **Ekström *et al.*** (p. 1756; see the Perspective by **Joughin**) recorded glacial earthquakes on Greenland and found that these events were more common in summer and that their annual number has doubled since 2002. Both of these findings are consistent with the observed accelerating motion of outlet glaciers from the Greenland Ice Sheet and correlate with its more widespread melting in recent years.

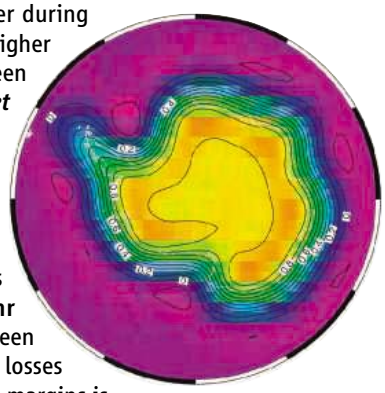

Beating Entropy

It is typically difficult to mix two polymers together or to mix particles into polymers unless there is a strong attraction between the dissimilar materials because entropic effects favor phase separation. **Mackay *et al.*** (p. 1740) show that when the size of the particles is smaller than the radius of gyration of the polymer, the mixed state may be thermodynamically favored because of an increase in surface contacts between the particles and the polymer. However, they also show that processing strategies must be taken into consideration for this favored state to be reached for certain mixtures.

Making Oxygen Glow in the Dark

Aqueous mixtures of organic matter in the environment contain many molecules that, when irradiated by sunlight, can excite dissolved oxygen to its singlet state ($^1O_2$). Highly reactive $^1O_2$ can play a significant role in both the direct degradation of pollutants and the internal chemistry of local bacteria. However, the short lifetime of $^1O_2$ hinders accurate measurements of its concentration. **Latch and McNeill** (p. 1743, published online 23 February; see the Perspective by **Hassett**) use a hydrophobic probe molecule to trap $^1O_2$ from deep within the suspended pockets of organic matter and then quantify concentrations with induced chemiluminescence. They measure values more than 100 times greater than those found with traditional probes that fail to penetrate the organic phase. A kinetic model based on competing quenching and diffusion rates accounts well for the partitioning.

Bloated and Not-So-Bloated Genomes

Eukaryotic genomes are bloated with so-called "junk" DNA including introns, mobile elements, and large intergenic regions. Curiously, animal mitochondrial genomes are tiny, essentially junk-free, and conserved in gene structure, whereas plant mitochondrial genomes are relatively large, dull repeats, and loose on structure rigid conservation of gene structure. What underlies these very different patterns of genome size and complexity? **Lynch *et al.*** (p. 1727) review how mutation rates correlate with organelle genome complexity, being for the most part much higher in animal mitochondria than in plant mitochondria, which suggests that nonadaptive evolutionary forces play a critical role in shaping the structure of organelle genomes and possibly nuclear genomes. A stumbling block in annotating bacterial genomes is the presence of pseudogenes. **Ochman and Davalos** (p. 1730) review systematic methods for identifying pseudogenes in particular genomes, using the well-studied *Escherichia coli* as an example.

Plankton Biogeography

Prochlorococcus is the most common oxyphototroph in the open ocean and plays a key role in ocean-based fixation of CO_2, oceanic primary production, and the composition of the marine ecosystem. **Johnson *et al.*** (p. 1737) show that closely related strains (>97% similarity in 16*S*

Continued on page 1671

CREDITS (TOP TO BOTTOM): OTTO-BLIESNER *ET AL.*; VELICOGNA AND WAHR

introducing the

Time MACHINE

the MINI PREP 96

Fully Automatic plasmid and genomic DNA purification at the push of a button.

START
ENTER

Your time is valuable.

MACCONNELL RESEARCH

800.466.7949 www.macconnell.com

Continued from page 1669

ribosomal RNA) have dramatically different distribution patterns in the water column, and indeed over the entire Atlantic Ocean. These closely related microbes appear to have ecologically distinct roles related to temperature, light, and competitors. **Coleman *et al.*** (p. 1768) analyzed two closely related *Prochlorococcus* strains and found that diversity was concentrated in genomic islands, putatively acquired via lateral gene transfer mediated by phage. Genomic islands may be a fundamental mechanism for niche differentiation across microbial systems (see the news story by **Pennisi**).

A Foe Motif

Pattern recognition receptors recognize conserved components found in pathogens, but not in the host, are central to the innate immune response. **Chang *et al.*** (p. 1761) describe the crystal structure at 2.1 angstrom resolution of tracheal cytotoxin (TCT), a fragment of a peptidoglycan specific to Gram-negative bacteria, bound to the ectodomains of the peptidoglycan recognition proteins LCa and LCx. The structure shows how a specificity determinant of Gram-negative bacteria is recognized in the complex and how TCT induces heterodimerization of LCa and LCx to activate downstream signaling.

Adding Oxygen to the Evolutionary Mix

What was the effect of developing the ability to use oxygen safely in metabolic reactions? **Raymond and Segrè** (p. 1764; see the Perspective by **Falkowski**) modeled how metabolic networks would have evolved from the Late Archean to Late Proterozoic periods of Earth's history. The complexity of networks that could use oxygen increased to levels far beyond those seen before the presence of oxygen. Comparisons between enzyme distributions and phylogenies suggest that adaptation to oxygen occurred after the major phylum-level divergences.

Rethinking β-Islet Cell Replacement

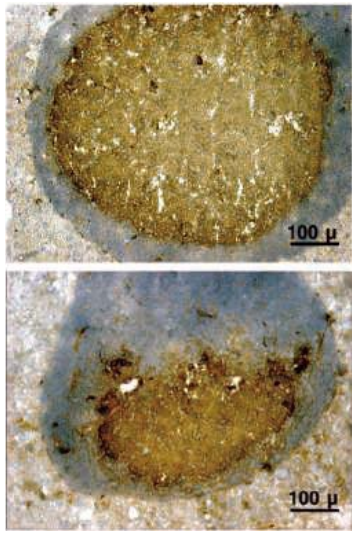

Type 1 diabetes mellitus (T1DM) occurs when the insulin producing β-islet cells of the pancreas become depleted through autoimmune attack. As well as finding means of limiting this destructive immune response, a great deal of research effort is being placed in finding ways of regenerating β-islet cells. It had been reported that spleen cells could reverse T1DM by replacing lost β-islet cells through transdifferentiation when injected together with an immune adjuvant into diabetic mice [*Science* **302**, 1223 (2003)]. Three groups (**Chong *et al.***, p. 1774; **Nishio *et al.***, p. 1775; and **Suri *et al.***, p. 1778) now report that the same protocol does result in some reversal of established T1DM in the same mouse model, but not via spleen cell transdifferentiation (see the news story by **Couzin**). Simple injection of the immune adjuvant alone promoted recovery. Presumably, the immune-modifying activity of the adjuvant provides a window of opportunity for the few remaining β-islet cells to proliferate to the extent that they become a sufficient source of insulin. Although these studies do not support the contribution of spleen cell transdifferentiation to the reversal of T1DM, they do provide hope for future development of immune-based therapies for the condition.

A Trojan Horse to Battle Cancer

One of the major hurdles in cancer therapy is delivering drugs efficiently to the tumor cell target. **Thorne *et al.*** (p. 1780) addressed this problem by designing a "Trojan horse" therapy in which immune effector cells that naturally migrate to tumors (cytokine-induced killer, or CIK cells) were used to deliver a potent oncolytic virus (vaccinia) to tumors growing in mice. The CIK cells transported the virus deep within the tumors to provide a uniform distribution of infection. The viral infection in turn enhanced tumor cell killing by the CIK cells and significantly inhibited tumor growth. Although each component of the therapy had been shown previously to have antitumor activity, the combination proved to be much more effective.

CREDIT: CHONG *ET AL.*

www.roche-applied-science.com

Keep it easy!

cOmplete Protease Inhibitor Tablets

cOmplete protection.
cOmplete convenience.

cOmplete *EASYpacks* foil strips make using cOmplete Tablets even more convenient than ever before.
cOmplete Lysis kits combine cOmplete, Mini Tablets in convenient *EASYpacks* with a ready-to-use lysis reagent.

For more information, please visit
www.keep-it-easy.com

Simplify your research with reliable products that **"Keep it easy!"**. Save time, expense, and handling steps while increasing convenience and minimizing stress.

"Keep it easy!" with cOmplete Protease Inhibitor Cocktail Tablets and cOmplete Lysis kits.

- **cOmplete convenience:** Simply drop a tablet into your lysis buffer.
- **cOmplete protection:** Reliably inhibit protease activity in lysates from animal and plant cells or tissues, yeast, and bacteria.
- **cOmplete flexibility:** Choose tablets with or without EDTA, for volumes of 10 ml or 50 ml.
- **cOmplete lysis:** Use kits that combine simple, rapid lysis of bacteria, mammalian, or yeast cells with cOmplete Tablets in *EASYpacks*.

Staying at the cutting edge of life science research is difficult. Cell lysis and protease inhibition don't have to be.

Keep it easy… Keep it Roche Applied Science.

Roche Diagnostics

Roche Diagnostics GmbH
Roche Applied Science
68298 Mannheim
Germany

YYePG Proudly Presents, Thx for Support

Donald Kennedy is Editor-in-Chief of *Science*.

Brooks Hanson is Deputy Editor for physical sciences at *Science*.

Ice and History

IF YOU PAUSED AT THE TABLE OF CONTENTS, YOU NOTICED THAT THERE IS A LOT ABOUT ICE IN this issue. Ice is important not only because we are losing it but also because it is an archive that has told us much about past climates. But the climate-change debate has focused perhaps too much on the past few hundred years. That baseline has told us much about what has been happening to global temperature lately, but it may not be the best baseline to use in exploring our future.

For that, the relationship between greenhouse gas levels and temperature, evident in data from ice cores, illuminates climates in the geological past and may be a more useful guide to the future. Fifty million years ago, CO_2 levels may have topped 1000 parts per million by volume (ppmv) and sea levels were about 50 meters higher than those today. CO_2 levels gradually decreased as marine organisms fixed carbon through photosynthesis and then buried it by sinking into the ocean basins. This reduction and a corresponding decrease in temperatures allowed ice sheets to develop in Antarctica starting 30 to 40 million years ago. By 3 to 4 million years ago, CO_2 levels probably dropped to or below the preindustrial level of about 290 ppmv, and permanent ice sheets appeared in the Northern Hemisphere. As subsequent glaciations came and went, CO_2 concentration and temperature were tightly linked. When both went down, ice sheets grew and sea levels sank, lower than today's by more than 100 meters. When both went up, there were relatively stable warm periods with high sea levels.

A central feature of this long baseline is this: At no time in at least the past 10 million years has the atmospheric concentration of CO_2 exceeded the present value of 380 ppmv. At this time in the Miocene, there were no major ice sheets in Greenland, sea level was several meters higher than today's (envision a very skinny Florida), and temperatures were several degrees higher. A more recent point of reference, and the subject of two papers in this issue, is the Eemian: the previous interglacial, about 130,000 to 120,000 years ago. This was a warm climate, comparable to our Holocene, during which sea levels were several meters higher than today's, even though CO_2 concentrations remained much lower than today's postindustrial level.

So what should the appropriate baseline be for estimating our present climate prospects? Is it the relatively recent evidence of climate change, or is it the developing knowledge from ice cores and the geologic record about past climate equilibria? The Holocene, over its 10,000-year life, has provided us with a comparatively stable period. Now we are changing an important parameter. Evidence presented in two papers, a News story, and two Perspectives in this issue demonstrates an accelerating decay of ice sheets in Greenland and Antarctica. Given the concurrent rapid recent rise in CO_2 concentration, history suggests that we should expect other changes. Will these changes return us to a climate like the Miocene or earlier? Or will we experience a repeat of the Eemian?

Nothing in the record suggests that an "equilibrium" climate model is the right standard of comparison. We are in the midst of a highly kinetic system, and in the past, dramatic climate changes have taken place in only a few decades. Our comfort in the Holocene may have heightened our sense of security, but the expectation that change is unlikely is not a reasonable position. The central question of today's climate policy discussions centers on whether the change in average global temperature over the past century represents the result of new climate forcing or instead simply reflects natural variation.

That question invites us to examine recent statistics on climate variation and then test the current excursion for significance. But if one is interested in risks and in preparing to meet them, the more interesting question is what the deep historical record can tell us about the circumstances under which climates have changed rapidly in the past and the severity of the consequences. Considered in that way, accelerated glacial melting and larger changes in sea level (for example) should be looked at as probable events, not as hypothetical possibilities. We don't have to abandon the short-term baseline, but the longer one may give a more realistic picture of our future.

– Donald Kennedy and Brooks Hanson

10.1126/science.1127485

TriFECTa™

IDT's winning Dicer-Substrate RNAi Kit

Why run behind with ordinary 21mer siRNA's? They only mimic Dicer products and bypass interaction with important components of the endogenous RNAi pathway.

Not so with our Dicer-Substrate RNAi. Published experiments show that 27mer siRNA duplex designs can yield up to a 100-fold increase in potency over first-generation 21mer designs [1]. Our RNAi duplexes are HPLC purified and backed by our functional knockdown guarantee.* Tri*FECTa*'s huge performance edge is based on our proprietary Dicer-Substrate technology#. Our unique Dicer cleavage design rules (free to you online) direct the dicing to get the specific results you want for maximum potency [2]. They're flat out winners!

Each Tri*FECTa*™ Dicer-Substrate RNAi kit contains:
3 Dicer-Substrate RNAi duplexes, ESI-MS QC and HPLC purification for each duplex, duplex resuspension buffer, negative and positive control duplexes, and a fluorescent, transfection control duplex.

Order or get the details now at www.idtdna.com.

*Using the IDT design service, IDT guarantees that at least 1 of the 3 duplexes will give a 70% knockdown of the target mRNA (when >90% transfection efficiency and >90% knockdown with positive control is demonstrated).
Patent Pending

References:

1. Kim, D.-H., Behlke, M.A., Rose, S.D., Chang, M.-S., Choi, S., and Rossi, J.J. (2005) Synthetic dsRNA dicer substrates enhance RNAi potency and efficacy. Nature Biotechnology, 23:222-226.

2. Rose, S.D., Kim, D.-H., Amarzguioui, M., Heidel, J.D., Collingwood, M.A., Davis, M.E., Rossi, J.J., and Behlke, M.A. (2005) Functional polarity is introduced by Dicer processing of short substrate RNAs. Nucleic Acids Res., 33:4140-4156.

Innovation and Precision in Nucleic Acid Synthesis

IDT
INTEGRATED DNA TECHNOLOGIES, INC.

1710 Commercial Park Coralville, IA 52241 USA
800.328.2661 www.idtdna.com

ISO 9001:2000
FM88954

EDITED BY GILBERT CHIN AND JAKE YESTON

The American robin.

HIGHLIGHTS OF THE RECENT LITERATURE

EPIDEMIOLOGY

Seasonal Tastes

The mosquito-borne West Nile virus (WNV) has caused repeated human epidemics in North America and is a zoonotic virus transmitted by *Culex* mosquitoes whose preferred host is the emblematic American robin (*Turdus migratorius*). Kilpatrick *et al.* have shown that the mosquitoes exhibit a shift in feeding behavior when the robins disperse after breeding. In early summer (May and June), about half of the mosquitoes' blood meals come from the robin, despite house sparrows (*Passer domesticus*) being common and susceptible to infection. In late summer (July to September), the robins disperse and the *Culex* shift to feeding on humans, again despite the ubiquity of house sparrows. Integrating available data into a model based on a shift in mosquito feeding preference leads to the prediction that the peak transmission of WNV to humans should occur by late July to mid-August and then decline in early October when cold weather hampers mosquito activity. Seasonal shifts in mosquito feeding behavior occur across the United States and appear to intensify epidemics of several avian zoonotic viruses, not only WNV but also Western equine encephalitis virus, St. Louis encephalitis virus , and possibly other vector-borne pathogens. — CA

PloS Biol. **4**, e82 (2006).

GEOPHYSICS

A Collapsing Umbrella

Observations of volcanic plumes have provided fundamental insight into volcanic processes, one notable instance being Pliny the Younger's descriptions of Vesuvius in 79 AD. Large eruptions, like nuclear explosions, often form an umbrella-shaped plume. The top of the umbrella forms when hot gases and particles in a central eruption column reach neutral bouyancy and mix with cold dense air that is being driven upward; this process helps to stabilize the umbrella, allowing ash to fall gradually. Most such plumes have a cauliflower-shaped outer surface.

Chakraborty *et al.* describe a more ordered umbrella that formed during the November 2002 eruption of Reventador in Ecuador. In this instance, the edge of the umbrella formed large regular undulations approximately every 0.7 km, producing a shape similar to the edge of a scallop. The authors ascribe this phenomenon to an instability that occurs when the outer rim of the umbrella becomes too dense to be neutrally buoyant, a plausible result of this relatively cool eruption. Such a loss of buoyancy could lead to collapse of the umbrella, which would produce another type of volcanic flow. — BH

Geophys. Res. Lett. **33**, L05313 (2006).

PSYCHOLOGY

Misjudging Priors

Mental models or simulations of future outcomes can be extremely helpful in planning and guiding our behavior, as when a forward model of a reaching movement is used to reduce the variance in the trajectory of the arm. In situations where several outcomes with associated likelihoods exist, there is a known tendency, referred to as hindsight bias, for the actual outcome to inflate our post-outcome estimates of the initial likelihoods.

One arena where this bias comes into play is in the forensic reconstructions of traffic accidents, and Roese *et al.* have examined whether using computerized simulations (versus text and diagram visual aids) elicits these overestimates. They find that animated sequences exacerbate hindsight bias and, more intriguingly, that the bias reverses when the post-outcome estimate is compared to one made just before the time of collision. This so-called propensity effect

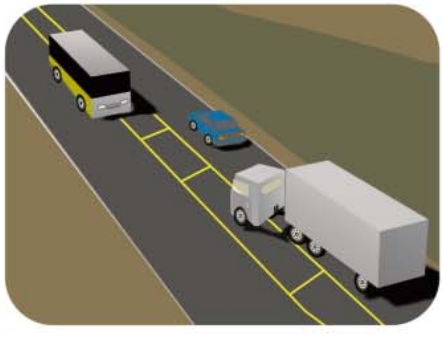

An accident about to happen . . . or not?

describes our sense that the collision is destined to occur before it takes place, something we are surprisingly less certain about after the collision has actually occurred. — GJC

Psychol. Sci. **17**, 305 (2006).

CHEMISTRY

Small-Scale Synergy

In metallic and semiconductor nanoparticles, the material properties can be tuned simply by changing the particle size. Shi *et al.* have explored the additional dimension of varying nanoparticle composition to incorporate multiple kinds of materials—specifically magnetic-metallic, magnetic-semiconducting, and semiconducting-metallic hybrids, as well as ternary combinations.

The synthetic strategy involved spontaneous epitaxial nucleation and growth of the second and third components onto seed particles in high-temperature organic solutions. For the magnetic-metallic particles (Fe_3O_4 grown on gold), solvent choice influenced the particle morphology, with good electron donors leading to core-shell geometries and poor electron donors yielding peanut-shaped fused particles. For Au-PbS particles, which combine a metal and a semiconductor, the choice of solvent did not influence the particle morphology, but the concentration of gold seed particles was critical. Finally, heating strategy and seed particle dimensions were the key variables for setting the ternary particle morphologies. The optical and magnetic properties of the particles were influenced by the hybrid interface. For example, the Au plasmon resonances were red-shifted in the hybrid particles; at the same time, the magnetization saturation field of the Fe_3O_4-Au particles was an order of magnitude greater than that of pure magnetite. — MSL

Nano Lett. **6**, 10.1021/nl0600833 (2006).

Continued on page 1677

Our new breed is the center of attention.

PfuUltra™ II enzyme for highest fidelity · Herculase® II enzyme for superior yield

Our next generation of high fidelity *Pfu*-based fusion enzymes sets a new standard in high fidelity PCR performance. Engineered for industry-leading fidelity *plus* 12x enhanced processivity, our new *PfuUltra*™ II Fusion HS DNA Polymerase and Herculase® II Fusion DNA Polymerase deliver superior yield, excellent reliability, and faster overall run times.

Our *PfuUltra*™ II Fusion HS DNA Polymerase offers the highest fidelity.
Error rates were determined by the *lac*I fidelity assay.

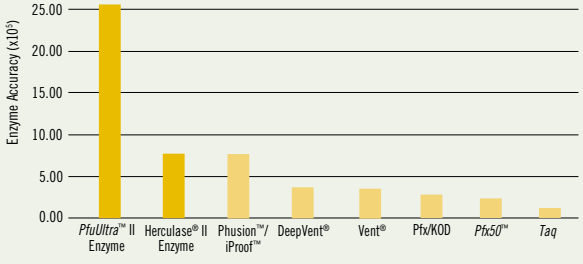

Our Herculase® II Fusion DNA Polymerase produces superior yield in as short as 15 second/kb extension time.

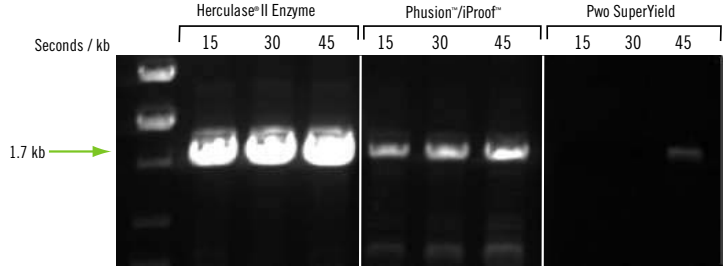

Need More Information? Give Us A Call:

Stratagene USA and Canada
Order: (800) 424-5444 x3
Technical Services: (800) 894-1304 x2

Stratagene Japan K.K.
Order: 03-5159-2060
Technical Services: 03-5159-2070

Stratagene Europe
Order: 00800-7000-7000
Technical Services: 00800-7400-7400

www.stratagene.com

Ask us about these great products:

***PfuUltra*™ II Fusion HS DNA Polymerase**	**40 rxn**	**600670**
Herculase® II Fusion DNA Polymerase	**40 rxn**	**600675**

STRATAGENE®

Continued from page 1675

CHEMISTRY

Switching Philicity

The immiscibility of organic and aqueous solutions (such as oil and vinegar) underlies a wide range of practical chemical separations. For versatility, liquid fluorocarbons have come into increasing use over the past decade as a third solvent phase, into which highly fluorinated solutes partition from both water and the more traditional organic solvents.

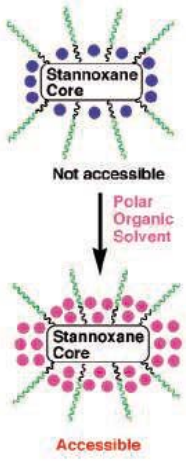

Displacement of water (blue) by ethyl acetate (pink) induces fluorophilicity.

Orita *et al.* were therefore surprised to find that a hydrated distannoxane complex bearing linear fluorocarbon tails—an Sn-O-Sn core with two $C_6F_{13}C_2H_4$ chains and a perfluorooctane sulfonate chain appended to each Sn—failed to dissolve in common fluorous solvents such as FC-72. The compound did dissolve in polar organic liquids (ethyl acetate, acetone, and tetrahydrofuran), and subsequently partitioned into the fluorous phase upon addition of FC-72 to the solution. The authors explain these observations by suggesting that the waters of hydration initially bound to the tin repel the fluorous solvent but can be displaced by polar organics, which in turn allows the fluorous liquid to approach. The compound proved useful as a homogenizing agent for fluorous and organic solvents, with 1.7 g nearly tripling the solubility of ethyl acetate in FC-72. — JSY

J. Am. Chem. Soc. **128**, 10.1021/ja058105v (2006).

DEVELOPMENT

More Is Bigger

Multicellular organisms can grow by making more cells or by making larger ones. The nematode *Caenorhabditis elegans* uses both methods: Cell proliferation drives worm growth until sexual maturity, whereas cell growth (mainly of epidermal cells) accounts for the twofold increase in size during adulthood. Growing adult cells also undergo endoreduplication, wherein genomic DNA is replicated repeatedly without cell division, resulting in each cell containing multiple copies of the genome (polyploidy) rather than just two.

Lozano *et al.* address the question of whether endoreduplication is directly responsible for adult growth in the worm. Blocking endoreduplication after the final larval molt results in dwarf worms that are roughly half the size of wild-type adults, whereas in a tetraploid strain, adult worms are roughly 40% larger than normal. Cyclin E is involved in the control of endoreduplication in a number of organisms, including *C. elegans*, and adult worms mutant for *cye-1* have both reduced epidermal ploidy and are dwarfed, often to less than half the size of comparable wild-type adults. Although it is clear that endoreduplication can account for the growth of polyploid somatic cells in worms, cells that remain diploid in the adult are presumably stimulated to grow by their polyploid neighbors. — GR

Curr. Biol. **16**, 493 (2006).

Science STKE AAAS

www.stke.org

<< Larger Pipe, Lower Resistance

The pathogenesis of hypertension—a risk factor for heart disease, kidney disease, and stroke—is complex and poorly understood. Zacchigna *et al*. find that mice lacking elastin microfibril interface-located protein 1 (Emilin1), a secreted extracellular matrix protein expressed in the cardiovascular system, had high blood pressure in conjunction with decreased blood vessel diameter and increased peripheral resistance. Emilin1 contains a cysteine-rich domain, as do other proteins involved in the regulation of growth factor signaling, leading the authors to investigate the relationship between Emilin1 and transforming growth factor–β (TGF-β), which plays a critical role in vascular development and pathophysiology. Emilin1 blocked TGF-β signaling upstream of receptor activation and did not interfere with ligand/receptor binding or signaling in response to mature TGF-β1. Rather, Emilin1 bound to proTGF-β1, preventing its proteolytic processing and the production of biologically active TGF-β1. TGF-β signaling was enhanced in the aortic wall of the mice lacking Emilin1, and inactivation of one *TGF-β1* allele in *Emilin1* knockout mice restored normal blood vessel diameter and blood pressure. Thus, the authors conclude that Emilin1 acts to regulate blood pressure by modulating TGF-β processing and thus the availability of the biologically active form. — EMA

Cell **124**, 929 (2006).

CREDIT: ORITA *ET AL., J. AM. CHEM. SOC.* **128**, 10.1021/JA058105V (2006)

"I think the dosage needs adjusting. I'm not nearly as happy as the people in the ads."

It's time for genetics.

What if you could use DNA to identify patients who respond well to your drug? You might use that knowledge to reach more patients and expand your market, or to get a drug to market faster. Either way – patients win. Perlegen is helping drug companies do just that – today.

Working with you, we can comprehensively analyze the DNA from hundreds of patients taking your drug. Out of the millions of genetic variations between patients, we help you identify the ones that are associated with strong efficacy, poor efficacy, or side effects. Perlegen's unparalleled coverage of the genome and experienced team of analysts mean you get clinically relevant answers, not just data, in a matter of months.

We partner with the top pharmaceutical companies around the world. We also license late-stage drugs. If you have a drug that can benefit from our approach, please contact us.

Patients are waiting.

genetics@perlegen.com
Mountain View, California • 650-625-4500
Tokyo, Japan • +81 (0)3 3444-6080
www.perlegen.com

Targeting today's drugs. Discovering tomorrow's.™

PERLEGEN SCIENCES®

www.sciencemag.org

Science

1200 New York Avenue, NW
Washington, DC 20005
Editorial: 202-326-6550, FAX 202-289-7562
News: 202-326-6500, FAX 202-371-9227

Bateman House, 82-88 Hills Road
Cambridge, UK CB2 1LQ
+44 (0) 1223 326500, FAX +44 (0) 1223 326501

Subscription Services For change of address, missing issues, new orders and renewals, and payment questions: 800-731-4939 or 202-326-6417, FAX 202-842-1065. Mailing addresses: AAAS, P.O. Box 1811, Danbury, CT 06813 or AAAS Member Services, 1200 New York Avenue, NW, Washington, DC 20005

Institutional Site Licences please call 202-326-6755 for any questions or information

Reprints: Author Inquiries 800-635-7181
Commercial Inquiries 803-359-4578
Corrections 202-326-6501

Permissions 202-326-7074, FAX 202-682-0816

Member Benefits Bookstore: AAAS/BarnesandNoble.com bookstore www.aaas.org/bn; Car purchase discount: Subaru VIP Program 202-326-6417; Credit Card: MBNA 800-847-7378; Car Rentals: Hertz 800-654-2200 CDP#343457, Dollar 800-800-4000 #AA1115; AAAS Travels: Betchart Expeditions 800-252-4910; Life Insurance: Seabury & Smith 800-424-9883; Other Benefits: AAAS Member Services 202-326-6417 or www.aaasmember.org.

science_editors@aaas.org	(for general editorial queries)
science_letters@aaas.org	(for queries about letters)
science_reviews@aaas.org	(for returning manuscript reviews)
science_bookrevs@aaas.org	(for book review queries)

Published by the American Association for the Advancement of Science (AAAS), *Science* serves its readers as a forum for the presentation and discussion of important issues related to the advancement of science, including the presentation of minority or conflicting points of view, rather than by publishing only material on which a consensus has been reached. Accordingly, all articles published in *Science*—including editorials, news and comment, and book reviews—are signed and reflect the individual views of the authors and not official points of view adopted by the AAAS or the institutions with which the authors are affiliated.

AAAS was founded in 1848 and incorporated in 1874. Its mission is to advance science and innovation throughout the world for the benefit of all people. The goals of the association are to: foster communication among scientists, engineers and the public; enhance international cooperation in science and its applications; promote the responsible conduct and use of science and technology; foster education in science and technology for everyone; enhance the science and technology workforce and infrastructure; increase public understanding and appreciation of science and technology; and strengthen support for the science and technology enterprise.

Information for Contributors

See pages 102 and 103 of the 6 January 2006 issue or access www.sciencemag.org/feature/contribinfo/home.shtml

PIERCE

The Protein People™

Western Blotting

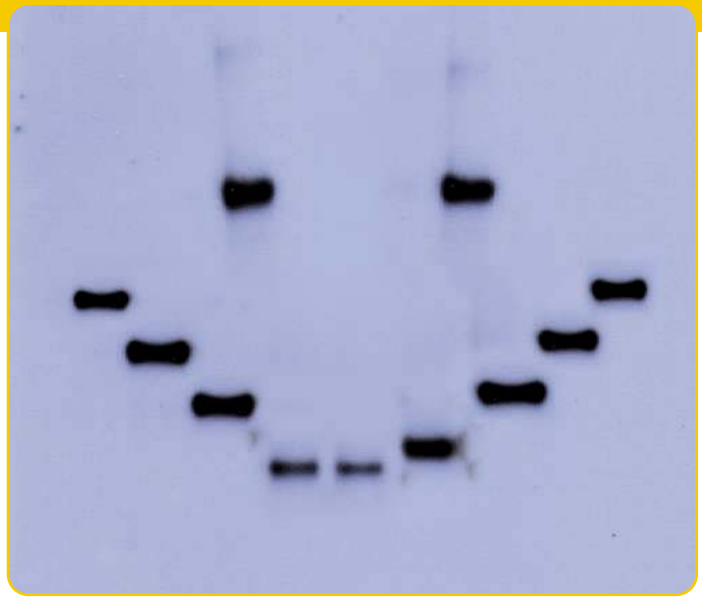

happy blotting.

Smile, and your blot smiles with you! A well-run Western blot with a strong signal-to-noise ratio will put a smile on any researcher's face. Pierce has ALL the products you need to achieve a happy Western blot.

SDS-PAGE

Precise™ Precast Gels & Ranger™ MW Markers

Membrane Treatment Products

MemCode™ Stains, Qentix™ Signal Enhancer & Miser™ Antibody Extender

Blocking Buffers

StartingBlock™, SuperBlock® & SEA BLOCK Buffers; Casein and BSA

Antibodies & Other Probes

Primary and secondary antibodies with fluorescent or enzymatic labels

Enzyme Substrates

Pierce SuperSignal®, ECL and 1-Step™ Substrates

Detection & Enhancement Products

Restore™ Stripping Buffer, Erase-It® Background Eliminator and CL-XPosure™ Film

FREE
8 Steps to Better Blotting! Log on to *www.piercenet.com* or call 800-874-3723 to request your FREE Western Blotting Handbook!

www.piercenet.com/imno22a

PIERCE

Tel: 815-968-0747 or 800-874-3723 • Fax: 815-968-7316
Technical Assistance E-mail: TA@piercenet.com • Customer Assistance E-mail: CS@piercenet.com

For distributors outside the U.S. and Europe, visit www.piercenet.com

For European offices and distributors, visit www.perbio.com

PERBIO

Inositol Phospholipids

for cell signalling research

Phosphatidylinositols

PtdIns-(1,2-dioctanoyl)
PtdIns-(1,2-dipalmitoyl)
PtdIns-(3)-P_1 (1,2-dipalmitoyl)
PtdIns-(3)-P_1 (1,2-dipalmitoyl)-d_{62}
PtdIns-(4)-P_1 (1,2-dihexanoyl)
PtdIns-(4)-P_1 (1,2-dioctanoyl)
PtdIns-(4)-P_1 (1,2-dipalmitoyl)
PtdIns-(5)-P_1 (1,2-dihexanoyl)
PtdIns-(5)-P_1 (1,2-dioctanoyl)
PtdIns-(5)-P_1 (1,2-dipalmitoyl)
PtdIns-(3,4)-P_2 (1,2-dihexanoyl)
PtdIns-(3,4)-P_2 (1,2-dipalmitoyl)
PtdIns-(3,5)-P_2 (1,2-dioctanoyl)
PtdIns-(4,5)-P_2 (1,2-dihexanoyl)
PtdIns-(4,5)-P_2 (1,2-dioctanoyl))
PtdIns-(4,5)-P_2 (1,2-dipalmitoyl)
PtdIns-(4,5)-P_2 (1,2-dipalmitoyl)
PtdIns-(4,5)-P_2 (1,2-dipamitoyl)-d_{62}
PtdIns-(3,4,5)-P_3 (1,2-dioctanoyl)
PtdIns-(3,4,5)-P_3 (1,2-dipalmitoyl)
PtdIns-(3,4,5)-P_3 (1-stearoyl, 2-arachidonoyl)

PLC-Thio PIP2 *A novel chromogenic substrate for PLC*

Inositol Phosphates

D-*myo*-Inositol-1-phosphate
D-*myo*-Inositol-3-phosphate
D-*myo*-Inositol-1,2,6-triphosphate
D-*myo*-Inositol-1,3,4-triphosphate
D-*myo*-Inositol-1,3,5-triphosphate
D-*myo*-Inositol-1,4,5-triphosphate
D-*myo*-Inositol-1,4,5-triphosphate
D-*myo*-Inositol-2,4,5-triphosphate
D-*myo*-Inositol-1,3,4,5-tetraphosphate
D-*myo*-Inositol-1,4,5,6-tetraphosphate
D-*myo*-Inositol-3,4,5,6-tetraphosphate
D-*myo*-Inositol-1,3,4,5,6-pentaphosphate

Cayman CHEMICAL

800.364.9897
www.caymanchem.com

Polymorphism Resequencing • Whole Genome Methylation Analysis •

DNA Methylation Sequencing • Microarray SNP Genotyping •

Expression Analysis • Custom Gene Silencing Constructs

SeqWright
DNA Technology Services

Phone: 800-720-4363 • Email: sales@seqwright.com
2575 West Bellfort, Houston, TX 77054-5025

www.seqwright.com

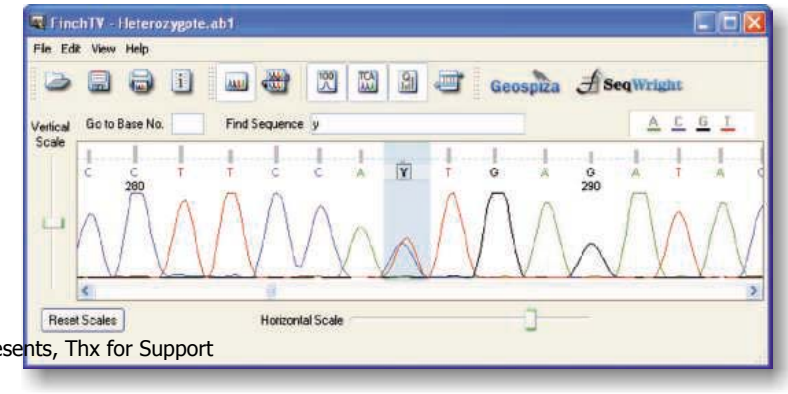

LOPAC[1280]

Defined Biology. Diverse Chemistry.

Predictable Activities and Proven Scaffolds from Sigma-RBI

You can rely on the power and convenience of the known actives in the Sigma-Aldrich **Library of Pharmacologically Active Compounds.** This comprehensive collection of small molecule modulators and approved drugs impacts most cellular processes and covers all major drug target classes.

When you think about what bioactives you want in your library, see for yourself why researchers worldwide trust what we have in ours.

1,280 high-purity, bioactive small organic molecules with well-documented activities

- *Antiproliferatives*
- *Enzyme inhibitors*
- *Antibiotics*
- *Cell cycle regulators*
- *Apoptosis inducers*
- *GPCR ligands*

The Sigma-RBI Handbook of Receptor Classification and Signal Transduction, 5th Edition

Now available as an eHandbook at

sigma-aldrich.com/rbihandbook

To request more information on ***LOPAC[1280]*** *or browse the* ***LOPAC[1280] Navigator****, please visit:* ***sigma-aldrich.com/lopac***

SIGMA®
RBI®

sigma-aldrich.com/cellsignaling

LEADERSHIP IN LIFE SCIENCE, HIGH TECHNOLOGY AND SERVICE

SIGMA-ALDRICH CORPORATION • 3050 SPRUCE STREET • ST. LOUIS • MISSOURI 63178 • USA

DATABASE

MOLD CODES

At this new microbial database from Virginia Polytechnic Institute and State University in Blacksburg, researchers can compare the genomes of two pathogens that irk farmers and foresters. Both are funguslike water molds from the genus *Phytophthora*. *P. sojae* (above) plagues soybeans and other crops, and *P. ramorum* blights oaks and other trees along the U.S. West Coast. Using tools on the site, researchers can identify genes that are diverging rapidly and that might enable the pathogens to victimize different hosts, says co-curator and molecular biologist Brett Tyler. Genomes from two other microbial pests are coming by the end of the year. >> phytophthora.vbi.vt.edu

DATABASE

Reading the Reeds

Modern parents will recognize the sulky tone in a letter from a 2nd century C.E. Egyptian responding to a scolding from his mother and sister. The writer, Ptolemaios, first swears "by all the gods that I have done nothing of what has been said," then pouts that his family ignored him even though he "was kicked by a horse and was in danger of losing my foot [or even] my life." That's one tidbit from the Advanced Papyrological Information System, a master catalog of more than 23,000 papyri—texts inscribed on paper made from flattened reeds—and other ancient writings. The artifacts reside at 10 institutions, including Columbia University and the State Hermitage Museum in Russia. Scrawled in 13 languages on everything from wooden tablets to banana leaves, the texts date back as far as the 2nd millennium B.C.E. More than half of them have digital images, and about one-fourth provide English translations. You can browse official and private documents such as trial transcripts and contracts—complete with fine print. >> www.columbia.edu/cu/lweb/projects/digital/apis

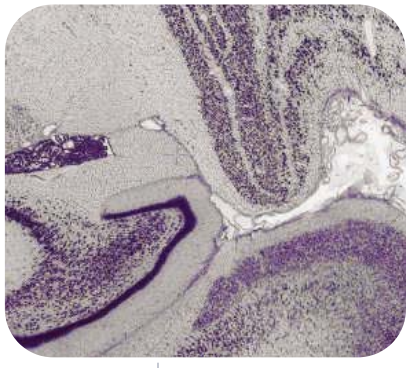

IMAGES

Mars Jaunt

Google can already steer you through the Internet and send you soaring over Earth. The company's latest release, Google Mars, lets armchair astronauts browse the surface of the Red Planet. With a click you can pinpoint craters, sand dunes, spacecraft landing sites, and other notable features on a relief map. Many of the landmarks link to eye-catching close-ups from the Mars Odyssey and Mars Express missions. >> www.google.com/mars

RESOURCE

Disease in the Wild

A threat is stalking North America's deer and elk—chronic wasting disease (CWD). Triggered by the infectious proteins called prions, the brain-devastating ailment has attacked wild and captive animals in 14 U.S. states and Canadian provinces since the late 1960s (at right, a sick doe). Find out more about CWD and other wildlife illnesses at this online clearinghouse from the U.S. Geological Survey's National Wildlife Health Center.

Aimed at resource managers, researchers, and the public, the site's nine major sections describe maladies that afflict North American animals in nature, including several such as plague and West Nile fever that can jump to humans. Each section offers fact sheets, abstracts of recent papers, links to news updates, and other resources. For instance, you can check out the latest map of CWD's spread and learn more about its risks to humans. Other mapping features allow you to, say, chart 50 years' worth of avian cholera outbreaks. >> wildlifedisease.nbii.gov

IMAGES

<< Scoping Out the Brain

Unlike glass microscope slides, the virtual slides at BrainMaps can't chip or break, and you can see details without squinting through an eyepiece. The atlas from neuroanatomist Edward Jones of the University of California, Davis, and colleagues displays hundreds of thin brain sections from healthy rhesus monkeys, mice, humans, and cats. You can browse the collection by species or by structure. Then zoom in on particular cells, rotate the image, or pan to find other features. The slice at left from a monkey brain shows the junction between the hippocampus (lower left), cerebral cortex (lower right), and lateral geniculate body. >> www.brainmaps.org

Send site suggestions to >> netwatch@aaas.org
Archive: www.sciencemag.org/netwatch

CREDITS (TOP TO BOTTOM): ELIZABETH BUSH/VIRGINIA TECH; ASSOCIATED PRESS; EDWARD JONES/UC DAVIS

Unlock the Potential
within a Single Cell

GenomePlex® Single Cell Whole Genome Amplification Kit

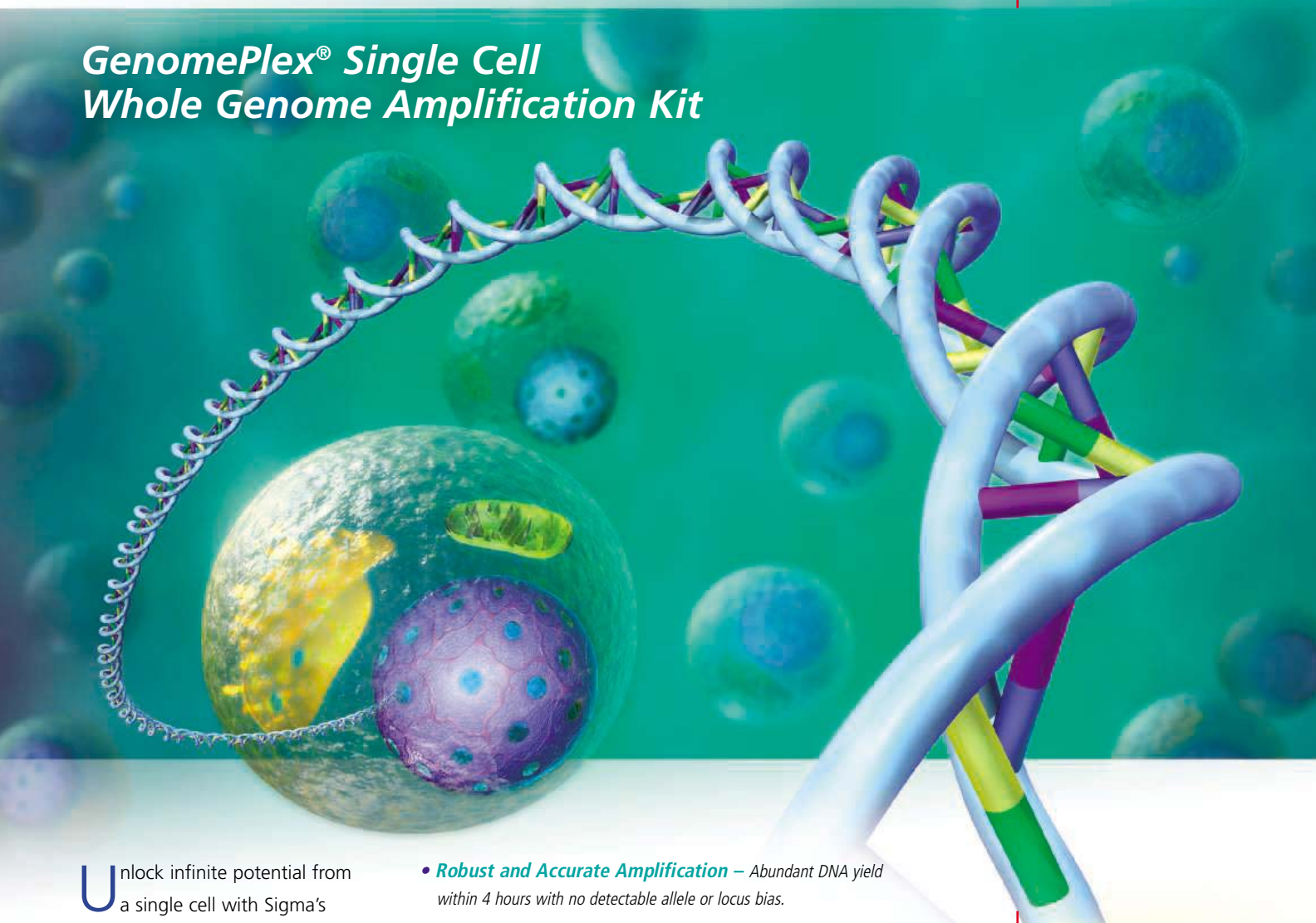

Unlock infinite potential from a single cell with Sigma's **GenomePlex® Single Cell Whole Genome Amplification Kit.** This rapid and straightforward method provides million-fold amplification yielding microgram quantities of genomic DNA from a single cell.

- ***Robust and Accurate Amplification –*** *Abundant DNA yield within 4 hours with no detectable allele or locus bias.*
- ***Maximum Flexibility –*** *Amplify DNA from any source including lymphocytes, cancer cells, epithelial cells, fibroblast amniotic cells, polycarbonate fixed cells, and plant cells.*
- ***Unlimited Genetic Analysis –*** *GenomePlex Single Cell WGA DNA is suitable for use with downstream applications including gel electrophoresis, QPCR, CGH microarray, STR analysis, and SNP analysis.*

Catalog No.	Description
WGA4	GenomePlex Single Cell WGA Kit
RELATED PRODUCTS	
WGA1	GenomePlex WGA Kit
WGA2	GenomePlex Complete WGA Kit
WGA3	GenomePlex WGA Reamplification Kit

*For more information on this and other Whole Genome Amplification Kits call **800-325-3010** or visit us on the Web at **sigma-aldrich.com/wga4***

sigma-aldrich.com

LEADERSHIP IN LIFE SCIENCE, HIGH TECHNOLOGY AND SERVICE
SIGMA-ALDRICH CORPORATION • BOX 14508 • ST. LOUIS • MISSOURI 63178 • USA

SIGMA-ALDRICH

THE WORLD OF WATER

Close to 1 billion people lack access to fresh water, according to the second triennial *World Water Development Report* from the United Nations. The report, presented this week at the World Water Forum in Mexico City, is a panoramic view of world water problems. It includes photographs such as this one above of nomad women drawing water in Mauritania; case studies, such as water-management plans for the Danube watershed and for the greater Tokyo area; and illuminating charts, including one showing how U.S. sales of agricultural products to Japan make Japan a huge importer of "virtual water."

Journals Winging It On Good Conduct

You're a journal editor looking at a paper whose authors have drug company ties. Or you suspect the paper has already been published in Norwegian. How do you make sure it's on the level? Many journals may be at a loss, a new survey finds, because they lack policies to deal with such situations.

The U.K.-based Committee on Publication Ethics (COPE) surveyed its 346 member biomedical journals. About one-third responded. "So many journals had weak or nonexistent policies" for authors, says COPE chair Harvey Marcovitch, a pediatrician. Some 13% lack a procedure for handling conflict of interest, and 28% have no system to ensure that a paper has gone through an ethics approval. Feedback mechanisms are also weak: 60% had no complaint procedure for authors, and 9% did not publish letters to the editor, which COPE considers an important postpublication peer-review mechanism. And 64% of journals have no policy for dealing with a potential case of research misconduct. Even when journals tried to get to the bottom of an allegation, one in five cases ended in a stalemate. (See the report at www.publicationethics.org.uk/reports/2005.)

Baby blues.

BLUER IS BETTER >>

Many species of birds lay blue-green eggs, but what the color signifies has stumped biologists. One theory is that it serves as a signal of quality to males, as the shell pigment, biliverdin, is expensive to produce.

To test whether blueness is an indicator of reproductive benefits, a team led by Juan Moreno, an ornithologist at the National Museum of Natural Sciences in Madrid, measured the color intensity of the eggs of pied flycatchers. The researchers also measured the amount of antibody proteins within each egg and the survival rate of the chicks.

The bluer the better, it turns out. Bluer eggs contained more maternal antibodies—the first line of immunological defense for freshly hatched chicks. Chicks from such eggs also were more likely to survive their first 2 weeks, the researchers reported online 15 March in *Biology Letters*. As a bonus, biologists can now use egg color as a quick guide to the health of such bird populations.

These results firm up the "signal theory" of egg color, says Lynn Siefferman, an ornithologist at Auburn University in Alabama. The next step, she says, is for researchers to artificially color eggs and see if males invest more care in bluer ones.

Sentenced to Remember

Proust, move over. A woman known as "AJ" remembers every day of her life since she was 14. So unusual is she that neuroscientists have coined a new term—"hyperthymestic syndrome"—for someone in whom "remembering dominates her life."

AJ, now in her early 40s, caught the attention of neuroscientist James McGaugh of the University of California, Irvine, in 2000 when she sent him an e-mail saying "since I was eleven, I have had this unbelievable ability to recall my past." The memories, she wrote, are "nonstop, uncontrollable, and totally exhausting."

Over the next 5 years, McGaugh and colleagues gave her various tests. Once, for example, they asked her to recall the previous 24 Easters. In 10 minutes, she came up with the dates as well as details of her activities. Every date but one was accurate. "She sort of has a vacuum cleaner sucking up all of the personal experiences and storing them away so that they're available," says McGaugh.

The researchers say AJ differs from other cases of extraordinary memory because hers is all about her own life—unlike autistic savants who can recall vast amounts of irrelevant information or calculate dates far in the future. Tests do show that AJ may have impairment in the left frontal lobe, like people with autism or obsessive-compulsive disorder. But AJ, who has average intelligence, has managed to graduate from college, hold jobs, and get married, researchers report in the February issue of *Neurocase*.

Some researchers are skeptical that AJ's abilities are all that unusual. Cognitive neuropsychologist Stephen Christman of the University of Toledo in Ohio says they may result from a combination of natural retentiveness and a tendency to obsess over her memories for hours every day. McGaugh says the team plans to do brain scans to see whether areas involved in memory [illegible] different in AJ.

CREDITS (TOP TO BOTTOM): FAO/22404/R. FAIDUTTI; JUAN MORENO/MNCN; CHAD BAKER/PHOTODISC GREEN

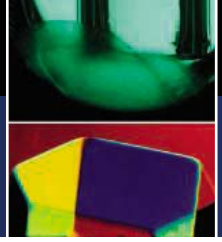

Supersolid sightings repeated 1693

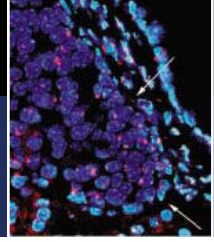

Diabetes finding doesn't hold up 1694

DRUG TRIALS

Violent Reaction to Monoclonal Antibody Therapy Remains a Mystery

CAMBRIDGE, U.K.—It took only minutes to realize that something had gone seriously wrong. On 13 March, six healthy volunteers in a clinical trial were injected with a "superagonist," a drug meant to boost a type of T cell in the immune system, and soon all of them became violently ill. According to relatives and friends last week, the six vomited, collapsed, and passed out; one became bloated "like the Elephant Man," his girlfriend told the press. Two additional participants who had received a placebo showed no ill effects.

The volunteers were paid to participate in the trial (according to one, about $3460), the first human tests of a drug aimed at treating leukemia and autoimmune diseases such as multiple sclerosis and rheumatoid arthritis. They were given a synthetic (monoclonal) antibody called TGN1412, designed by TeGenero in Würzburg, Germany, and manufactured by Boehringer Ingelheim. In animal tests, the molecule triggered the production of so-called regulatory T cells, which keep the immune system in check. But something went amiss. The worst-affected volunteers were kept alive with mechanical life support and large doses of steroids to reduce inflammation. After 5 days, a doctor at Northwick Park Hospital near London said four were improving and three had been removed from machines. But the two worst affected remained in critical condition early this week.

Exactly what triggered the reaction is not known. It seemed at first that an error in drug dosing or manufacture may have been to blame, says Simon Gregor, spokesperson for the U.K. Medicines and Healthcare Regulatory Authority (MHRA), which approved the trial. Managers at Northwick Park were so surprised that they even called in the police to check for evidence of a crime. But as MHRA and other investigators analyze materials and swarm over the private, 36-bed ward where the test took place, no crime or technical error has come to light. Suspicion is focusing instead on TGN1412 itself.

MHRA, TeGenero, and the company that managed the trial, Parexel in Boston, Massachusetts, say that their procedures still look watertight. The volunteers' reactions were unforeseeable, they maintain. TeGenero's chief scientific officer Thomas Hanke expressed "shock" in a statement on 17 March: "Extensive preclinical tests showed no sign of any risk."

Hanke told *Science* that a rodent version of the molecule was tested extensively at high doses in rats and mice, with no ill effects; TGN1412 itself was given to 20 cynomolgus monkeys in an unpublished study—after it was shown that their T cells were activated in the same way as human cells—with no significant adverse effects other than a short-lived increase in lymph node size. MHRA's Gregor says, "We have gone back [to the files] this week, and there is nothing in the documentation that would cause us to think there is a concern here."

But some independent observers have suggested that the trial was moving too aggressively. It was "a mad concept" to give a potent drug never tested in humans to six people at once, says medicines policy expert Joe Collier of St. George's Hospital Medical School in London. It would have been better to do one test and pause, he says. Monoclonal cancer vaccine researcher Angus Dalgleish of St. George's agrees that the procedure looks "bizarre," because the results of T cell activation are notoriously hard to predict.

Hanke responds that the trial's approach was "fairly common," reflecting "current practice in biopharmaceutical development." He adds: "We did not have any evidence to suspect that this drug would be unsafe at the dosage we applied," which was, at 0.1 milligram per kilogram of weight, one-500th that given as a safe dose in animals.

Some also question TeGenero's decision to move into human testing without a better developed—or at least a more publicly documented—rationale for how TGN1412 could up the count of regulatory T cells without turning on other, destructive responses. TeGenero's co-founder and scientific adviser Thomas Hünig of Würzburg University says that research since 1997 has shown that TGN1412 and analogous antibodies bind to the CD28 receptor on T cells, triggering a powerful expansion of cells dominated by regulatory T cells. Even at "horrific" doses in rats and mice, he says, regulatory cells dominated, giving credence to the view that these cells' damping effect would swamp out the more harmful effects of conventional T cells, also activated by TGN1412. The monkey study supported this ▶

Roulette. Six healthy volunteers injected with a test drug had to be rushed into critical care at Northwick Park Hospital; two others injected with a placebo weren't affected.

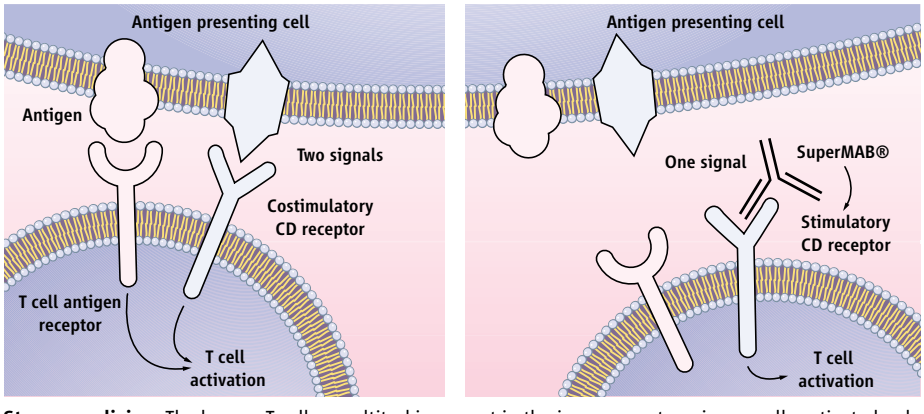

Strong medicine. The human T cell, a multitasking agent in the immune system, is normally activated only when two receptors are stimulated (*left*). But the "superagonist" used in a London clinical trial can activate T cells by stimulating a single receptor (*right*).

CREDITS (TOP TO BOTTOM): KIRSTY WIGGLESWORTH/AP PHOTO; (ILLUSTRATION) C. BICKEL/*SCIENCE*

FOCUS

confidence, says Hanke: "We saw no drug-related adverse events."

Some experts in monoclonal antibodies—including Dalgleish and Arlene Sharpe and David Hafler of Harvard Medical School in Boston, as well as John Isaacs of the University of Newcastle, U.K.—say that without having seen the relevant monkey data or results from tests with human cells in vitro, it's difficult to evaluate the argument that TGN1412 would likely have the same selective, benign effect in humans as in test animals. But they say they would not be surprised to find that TGN1412 stimulates harmful as well as beneficial effects. "A lot of cells" carry the CD28 receptor and might be activated, Hafler notes, adding, however, that "I wouldn't have thought [an accident like this] could happen."

Johannes Löwer, president of the Paul Ehrlich Institute in Langen, Germany, says his center was also approached by TeGenero to assess the TGN1412 trial. "We reviewed it very carefully" and reached the same conclusion as the U.K. group: The trial was safe and should proceed. Löwer offers two lessons for the future. Research is needed to define better animal models of the human response to CD28 agonists, he says. And he recommends that extra precaution be taken when antibodies are used to stimulate rather than neutralize components of the immune system.

–ELIOT MARSHALL

With reporting by Gretchen Vogel in Berlin.

COSMOLOGY

Long-Awaited Data Sharpen Picture of Universe's Birth

If good things come to those who wait, astrophysicists and cosmologists are reaping a well-deserved reward. Last week—a year later than originally planned—researchers working with NASA's Wilkinson Microwave Anisotropy Probe (WMAP) satellite released their second batch of data. The new measurements pinpoint the emergence of the first stars and tighten the screws on theories of how the infant universe expanded from the size of a marble to billions of light-years across in 10^{-35} seconds.

"The new WMAP results are extremely important," says Andrew Lange, an astrophysicist at the California Institute of Technology in Pasadena. "They usher in a whole new phase of cosmological research."

Launched in 2001, WMAP detects light from the big bang, which has cooled and stretched to longer wavelengths, leaving a pervasive haze of microwaves with a temperature of 2.7 kelvin. Three years ago, WMAP researchers used data collected in the satellite's first year in space to chart the faint variations in the temperature of the microwaves across the sky (*Science*, 14 February 2003, p. 991).

Scrutinizing the fluctuations, the team hammered down the cosmos's vital statistics to unprecedented precision. The universe is 13.7 billion years old; is "flat" (curved neither inward like a gigantic sphere nor outward like a gigantic potato chip); and consists of a smattering of ordinary matter, much more unseen dark matter, and a whopping amount of space-stretching "dark energy."

Now, WMAP researchers have analyzed data collected during the second and third years of the satellite's mission. The microwaves coming from different places in the sky can point in different directions, like wind-speed arrows on a weather map, and the new work tracks how that polarization varies across the sky. The data give researchers another window into the infant universe, team leader Charles Bennett, an astrophysicist at Johns Hopkins University in Baltimore, Maryland, said Friday in a telephone press conference at Princeton University.

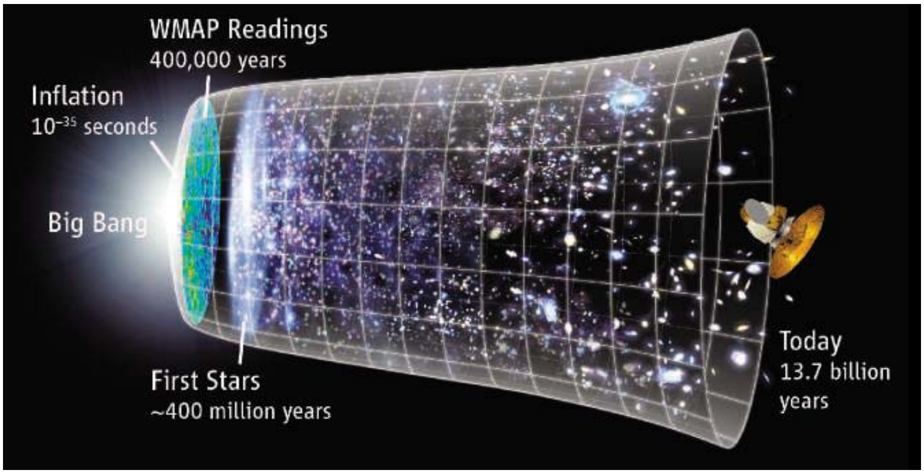

Lights on. New data from NASA's WMAP satellite show that stars emerged 400 million years after the big bang and limit theories of how the newborn universe inflated at faster-than-light speed.

CREDIT: NASA/WMAP SCIENCE TEAM

The polarization arose when photons in the big bang afterglow collided with free electrons whizzing through the youthful universe. And the electrons popped out of neutral atoms when the atoms were illuminated by the light of the first stars. So by studying the polarization, the researchers could tell that the first stars emerged about 400 million years after the big bang, says David Spergel, a theoretical astrophysicist at Princeton University and member of the WMAP team.

Knowing when the stars turned on and the fog of electrons emerged, researchers refined their analysis of the temperature variations, which are also affected by the electrons. The results rule out certain models of inflation, the mind-boggling expansion that took place in the universe's first split second, Spergel says. "This is a powerful step toward winnowing the field of contenders of how inflation took place," says Brian Greene, a theoretical physicist at Columbia University.

The polarization fluctuations are only a hundredth as pronounced as the temperature variations, and checking and rechecking the analysis took longer than researchers expected, Bennett says. "It wasn't anything fundamental that was difficult, but a lot of little things that had to be done right," he says.

Next, researchers hope to detect tiny swirls in the microwave background, which would be a sign of gravity waves from the big bang itself. But those swirls should be fainter still and may fall to WMAP's successor, Europe's Planck satellite, scheduled for launch in 2007.

–ADRIAN CHO

Unravel the complexities of cancer pathology.
Accelerating the discovery and validation of therapeutic targets and biomarkers is critical for advancing research and patient care. Affymetrix leads the way with the most powerful portfolio of solutions for understanding the complex genomic processes in cancer. Analyze copy number alterations, transcription quantitation and regulation, alternative splicing and somatic mutations – all on the proven GeneChip® platform. Be the 1 to find the biomarkers that lead to the breakthrough.

www.affymetrix.com/genechip/cancer • 1-888-DNA-CHIP (362-2447)
Europe: +44 (0) 1628 552550 • Japan: +81-(0)3-5730-8200

The Way Ahead™

AFFYMETRIX®

ORGANIC ELECTRONICS

Plastics Break the Speed Barrier

Conducting plastics have long been a bit of a tease. Depending on their makeup, they can carry a current freely like metals or switch on and off like semiconductors. But when it comes to making transistors and other electronic devices, semiconducting plastics have been slowpokes. Even amorphous silicon, the low-grade silicon used to make the transistor arrays that drive liquid crystal displays, whisks electrical charges along almost an order of magnitude faster than semiconducting plastics do. That's a major reason plastics haven't dethroned amorphous silicon in large-scale applications. But new work from researchers in the United Kingdom and the United States could change all that.

In a paper published online this week by *Nature Materials*, researchers led by Iain McCulloch, a polymer chemist at Merck KGaA in Southampton, U.K., report making plastic-based transistors that ferry electrical charges at nearly the same speed as amorphous silicon, a sixfold improvement over the previous generation of materials. "That's a very significant improvement" and could give plastic electronics a major push into electronics applications, says Zhenan Bao, a plastic electronics expert at Stanford University in California, who helped develop a previous record holder.

The speed boost could finally help plastic electronics take advantage of their other selling points. Chief among these is their ease of fabrication. Unlike amorphous silicon, which must be grown in a vacuum chamber, plastics can be laid down from solution. That opens the door to patterning huge arrays of devices with what amounts to an ink-jet printer or other simple and cheap technologies. Plastic electronics researchers have been doing just that for over a decade. But when researchers first started laying down plastic conductors and semiconductors from solution in the early 1990s, the molecules in their films formed a jumble, like straw strewn on the ground. That disorder made it hard for conducting electrical charges to hop from one molecule to another in their devices, slowing their speed to a crawl.

Bao and her colleagues, then at Lucent Technologies' Bell Laboratories, improved matters in 1996 when they came up with new semiconducting polymers known as regioregular polyhexylthiophenes. These plastics contained a series of ring structures in the polymer backbone with hydrocarbon arms that hung off the sides. Because the rings on neighboring molecules preferred to lie flat atop one another, the polymers automatically stacked themselves into perfectly ordered 20-to-50-nanometer crystals. On surfaces, the crystals packed side by side like bricks in a patio, forming a continuous sheet. Thanks to that orderly pattern, electrical charges jogged through the films at 0.1 centimeters squared per volt per second ($cm^2/V\text{-}s$)—a respectable speed, but still only 1/10 as fast as in the best amorphous silicon films. The charges, it turned out, still ran into speed bumps each time they tried to hop from one tiny crystal in the sheet to the next.

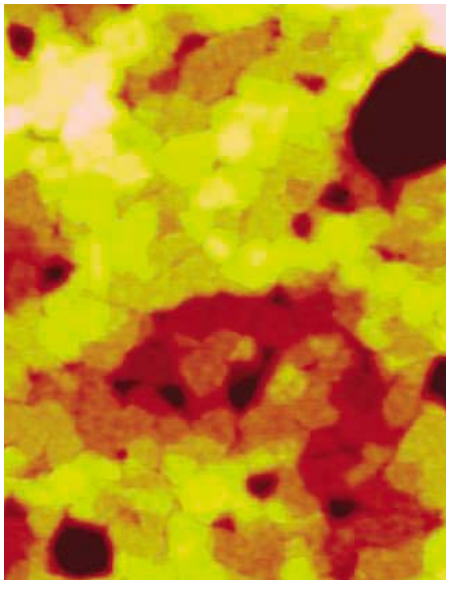

Crystal power. New semiconducting plastics form large crystals that help whisk electrical charges at higher speeds than ever before.

CREDIT: IAIN MCCULLOCH *ET AL.*, *NATURE MATERIALS* (19 MARCH 2006)

McCulloch and his colleagues at the Palo Alto Research Center in California and Stanford decided to remove some of those speed bumps by growing larger crystals. They started with regioregular polythiophenes and fused a pair of neighboring rings at regular intervals along the polymer backbone. The rings locked the arms into a flatter shape and made it energetically even easier for neighboring molecules to stack side by side. As a result, crystallites in their film grew larger, to about 200 nanometers across, and the speed of charges in their devices ultimately reached 0.6 $cm^2/V\text{-}s$. As a bonus, McCulloch says, the fused rings also are harder for oxygen atoms to break apart, making the plastics more resistant to degradation when exposed to air or water, another common problem with conducting plastics.

McCulloch says the new plastics still need improvements before they can replace amorphous silicon. For one, because the materials are still prone to degradation, researchers must find ways to hide them from air. If they succeed, perhaps plastic electronics will stop teasing and get down to business. –ROBERT F. SERVICE

Boehlert Bids Bye-Bye

It's hard out there for a term-limited chariman. Forced by House rules to step down at the end of the year as chair of the science committee, Representative Sherwood Boehlert (R–NY) last week announced he would not run for a 13th term in November. He's the fifth Republican who has chosen to leave Congress instead of returning without a leadership post after reaching the 6-year limit. His retirement, coming in his 70th year and 2 years after he had successful heart bypass surgery, will also deprive science of one of its staunchest supporters.

"The scientific community will never know or appreciate the extent to which he has been their advocate," says Representative Vernon Ehlers (R–MI), a former college physics professor and a colleague on the committee. "He's been indefatigable in arguing and fighting for science." Ehlers would like to succeed Boehlert, if the Republicans retain control of the House this fall, but Representative Ralph Hall (R–TX) has the most seniority on the panel. Representative Bart Gordon (D–TN) has the inside track if the Democrats prevail in November.

–JEFFREY MERVIS

Travel Rules Rile Researchers

A controversial Bush Administration decision to cap the number of government researchers allowed to attend meetings outside the country apparently doesn't apply when the United States is the host—even if the meeting is across the ocean (*Science*, 24 February, p. 1086). AIDS scientists are scratching their heads over the logic behind a 50-person limit for the International AIDS Conference in Toronto in August when none exists for a similar meeting this June in Durban, South Africa, sponsored by the Office of the U.S. Global AIDS Coordinator in the State Department.

Mark Wainberg, co-chair of the Canadian conference, says the goals of the two meetings "overlap to a considerable extent," and that the Toronto location was chosen largely for its proximity to the United States. The bill for travel to Durban "could have sent a lot of people to Toronto," he says.

State Department spokesperson Kristin Pugh contends that the 50-person limit, adopted last year by Congress, "doesn't apply" because the Durban meeting is sponsored by the U.S. government. No such exemption exists in the legislation, which refers only to any "international conference occurring outside the United States." But Pugh says the department's policy will "comply with U.S. law." –JON COHEN

U.S. SCIENCE POLICY

Cancer Institute Director Tapped for FDA

The National Cancer Institute (NCI) will be getting a new leader following the nomination last week of its controversial director Andrew von Eschenbach to head the U.S. Food and Drug Administration (FDA). As *Science* went to press, federal officials said von Eschenbach would step down "soon."

The $4.8 billion NCI is the National Institutes of Health's (NIH's) largest institute and the only one whose director is appointed by the president. A urologic surgeon and three-time cancer survivor, von Eschenbach arrived 4 years ago from the University of Texas M. D. Anderson Cancer Center in Houston, where he became friends with former president George H. W. Bush and his family. Von Eschenbach's tenure at NCI has been rocky, not least of all because he set the contentious goal of eliminating suffering and death from cancer by 2015. He also launched initiatives in nanomedicine, proteomics, and other areas at the same time success rates have dropped for investigator-initiated grant proposals.

Von Eschenbach was named acting FDA commissioner last fall after the surprise resignation of Lester Crawford (*Science*NOW, 26 September 2005, sciencenow.sciencemag.org/cgi/content/full/2005/926/1). After lawmakers protested that the two jobs posed a conflict of interest and too heavy a workload, von Eschenbach turned over day-to-day operations at NCI to John Niederhuber, a former University of Wisconsin surgical oncologist who joined NCI as a deputy director last fall.

Rolling along. NCI's Andrew von Eschenbach, shown promoting a drug company–sponsored bicycle tour to fight cancer, is headed to FDA.

A fight over FDA's handling of Plan B, the "morning after" pill, will likely slow von Eschenbach's confirmation in the Senate. Hillary Clinton (D–NY) and Patty Murray (D–WA) want the agency first to rule on whether the drug, now sold by prescription, should be made available over the counter, as many scientists and FDA officials have advocated. In August, Crawford announced he was putting off a decision indefinitely.

Von Eschenbach's nomination is also likely to face some opposition. Citing the 2015 goal, Sidney Wolfe of the Washington, D.C.–based consumer activist group Public Citizen says von Eschenbach "continues to exhibit extraordinarily bad judgment" at NCI and is "a very bad choice to head this critical agency [FDA]."

Two days after von Eschenbach was nominated, Niederhuber notified NCI staff that he would continue overseeing day-to-day operations until an acting director is announced. Several prominent cancer researchers told *Science* they hope the White House will launch a national search for von Eschenbach's successor. "Let's look for the very best person in the United States who's willing to take this job on," says John Mendelsohn, president of M. D. Anderson. Applicants may be scared away, however, by the prospects of a declining NCI budget, a lame-duck Administration, and tight new conflict-of-interest rules for NIH senior officials.

–JOCELYN KAISER AND JENNIFER COUZIN

AVIAN INFLUENZA

Studies Suggest Why Few Humans Catch the H5N1 Virus

This week, two research groups are independently reporting results that help explain why the H5N1 avian influenza virus is so lethal to humans but so difficult to spread. Unlike human influenza viruses, the teams report, H5N1 preferentially infects cells in the lower respiratory tract. Residing deep in the airways, the virus is not easily expelled by coughing and sneezing, the usual route of spread. The results "explain a lot of the mysteries" surrounding H5N1, says K. Y. Yuen, a virologist at the University of Hong Kong.

A better understanding of the virus couldn't be more timely. Endemic in much of Asia, H5N1 has recently spread through Europe and to Africa. It has killed 98 of the 177 humans it has infected. Flu experts worry that if the virus mutates into a form that could be easily passed among humans, it could spark a pandemic. The two reports, which used different strategies but reached the same conclusion, suggest just what sort of mutation would be needed.

One team, led by Yoshihiro Kawaoka of the University of Wisconsin, Madison, tested various tissues of the human respiratory tract for receptors to which the virus can bind. Human flu viruses preferentially bind to what are known as α 2,6 galactose receptors, which populate the human respiratory tract from the nose to the lungs. Avian viruses prefer α 2,3 galactose receptors, which are common in birds but were thought to be nearly absent in humans. Using marker molecules that bind to one receptor or the other, the team found that humans also have α 2,3 galactose receptors, but only in and around the alveoli, structures deep in the lungs where oxygen is passed to the blood. They describe their findings in the 23 March issue of *Nature*.

The second team, led by pathologist Thijs Kuiken of Erasmus University in Rotterdam, the Netherlands, used a more direct technique to show that H5N1 readily binds to alveoli but not to tissues higher up in the respiratory tract. Kuiken, whose team publishes its findings online this week in *Science* (www.sciencemag.org/cgi/content/abstract/1125548), notes that only patients with severe

autopsies that have shown heavy damage to the lungs but little involvement of the upper respiratory tract. Among experimental animals, the team reports, cats and ferrets more closely match the human pattern of infection than do mice and macaques. "This is an important factor to consider when planning experiments" to understand the pathology of H5N1, says Yuen.

Yuen notes that the findings also explain clinical anomalies such as why nasal swabs of H5N1 patients are less reliable than throat swabs in detecting the virus. And they suggest that clinicians need to exercise particular care when performing procedures, such as intubation, that might give the virus a route out of a patient's lungs.

The risk of a pandemic would ratchet up substantially should the virus acquire the ability to bind to receptors in the upper respiratory tract, Kuiken warns. But just how difficult that mutation is to acquire "is something this research did not address," he says.

–DENNIS NORMILE

CONDENSED-MATTER PHYSICS

Free-Flowing Supersolid Confirmed, But Origins Remain Murky

BALTIMORE, MARYLAND—Two years ago, a team of physicists created a stir by reporting that solid helium could flow without resistance, like a liquid devoid of viscosity. Now, three other groups have reproduced the bizarre effect. But data presented here last week at the March meeting of the American Physical Society also suggest that the "supersolid" flow occurs only in crystals riddled with defects.

"The more perfect the crystal, the less supersolid there is," says Ann Sophie Rittner of Cornell University. That observation suggests the flow is not an intrinsic property of crystalline helium, as the most exotic explanation would have it.

The first signs of supersolidity were spotted by Eunseong Kim and Moses Chan of Pennsylvania State University in State College in a tiny can filled with pressurized solid helium-4, the heavier isotope of helium (*Science*, 1 July 2005, p. 38). When they set the can twisting atop a thin shaft and cooled it below 0.2 kelvin, the frequency of the twisting suddenly shot up.

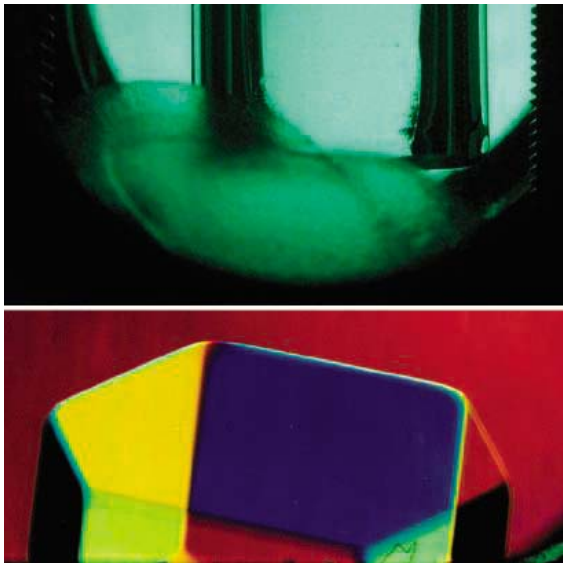

Defective. New data suggest supersolid flow can occur in a defect-riddled helium crystal (*top*), but not in an orderly one.

CREDITS (TOP TO BOTTOM): R. ISHIGURO, F. CAUPIN, H. J. MARIS, AND S. BALIBAR; PHOTO BY S. BALIBAR, E. ROLLEY, C. GUTHMANN/ENS-PARIS (1994)

The jump indicated that about 1% of the helium had let go of the can and was standing still as the rest of the helium crystal continued to gyrate. And that implied the solid helium flowed freely through itself. Theorists disagree on how that might occur, however, or whether it's possible in a perfect crystal. And until now experimenters hadn't reproduced the spectacular results.

New experiments also reveal the helium letting go, says Keiya Shirahama of Keio University in Yokohama, Japan. "We have confirmed the Kim and Chan observation," Shirahama says. Minoru Kubota and colleagues at the University of Tokyo have obtained similar results, as have Rittner and John Reppy of Cornell. But Rittner and Reppy say the flow vanishes when they heat the crystal to just below its melting temperature and slowly cool it, a process called annealing that eliminates defects.

Chan says he sees no such effect, but Rittner and Reppy's data suggest that supersolidity is not an inherent feature of crystalline helium-4. Other experiments seem to support that conclusion. Kim, now at the Korea Advanced Institute of Science and Technology in Daejeon, and Chan have found that the supersolid signal reaches its maximum when their helium-4 contains several parts per million of the lighter isotope helium-3. It shrinks steadily as the helium-3 concentration falls to the lowest achieved level of a part in a billion.

Chan's group also sees no clear spike in the specific heat—the amount of heat needed to raise the temperature a fixed amount—which ought to accompany the onset of superflow in a crystal. And Yuki Aoki and Haruo Kojima of Rutgers University in Piscataway, New Jersey, have yet to spot a telltale type of sound caused by the free-flowing portion of the helium sloshing back and forth.

The new results still leave physicists debating how the flow occurs. Some had argued that it might arise when many helium atoms crowd into a single quantum wave in a phenomenon called Bose-Einstein condensation. That weird effect enables liquid helium-4 to flow without resistance, but some theorists argue that it is impossible in a well-ordered crystal. The new data make Bose-Einstein condensation in the solid "very unlikely," says David Ceperley, a theorist at the University of Illinois, Urbana-Champaign.

Others aren't so sure. Boris Svistunov of the University of Massachusetts, Amherst, and colleagues argue that the helium may jumble together to form a kind of glass. The atoms in the disorderly solid might undergo Bose-Einstein condensation, Svistunov says. That would make it a glass more than half-full with physics.

–ADRIAN CHO

Senate Boosts NIH Budget Hopes

Biomedical researchers cheered last week after the Senate agreed that health and education programs should get $7 billion more next year. Although the number is part of a nonbinding budget resolution, the vote makes it more likely that the National Institutes of Health (NIH) will receive an increase rather than the level $28.6 billion budget that President George W. Bush requested for 2007. Many thousands of scientists sent letters supporting the resolution, according to the Federation of American Societies for Experimental Biology. The next move is up to twin congressional spending committees. Scientists may once again have to take up their pens, however, as the House has been less generous toward NIH in recent years than has the Senate.

–JOCELYN KAISER

French Researchers Hear Promises, Promises

PARIS—Scientists are dismayed by what's missing from a reform of the national research agenda that was expected to be passed this week by the French legislature.

The biggest problem, according to Edouard Brézin, president of the French Academy of Sciences, is a broken promise to index research funding to inflation (*Science*, 10 March, p. 1371). This omission would create a funding gap of roughly $500 million a year, Brézin claims. While research minister François Goulard has promised to adopt such indexing if his Conservative Party is reelected in 2007, the Socialist opposition has pledged to raise research spending by 10%.

–BARBARA CASASSUS

Russia Probes Defense Scientist

The Russian security services are investigating a well-known Siberian physical chemist on suspicion of divulging state secrets. Oleg P. Korobeinichev, 65, who heads a research laboratory at the Institute of Chemical Kinetics and Combustion in Novosibirsk, has not been formally charged, but he has been ordered not to leave the country. Neither the government nor Korobeinichev is commenting on the case.

Korobeinichev's lab specializes in the structure of flames of gaseous and condensed systems, work that has had applications to the weapons and space industries. Its more recent efforts to develop technology for the disposal of chemical weapons involve collaborations with Cornell University, Sandia National Laboratories, and the National Institute of Standards and Technology, according to its Web site.

–BRYON MACWILLIAMS

IMMUNOLOGY

Diabetes Studies Conflict on Power of Spleen Cells

Three separate attempts have failed to replicate promising results that electrified the diabetes community 2 years ago. The outcome severely weakens the theory that the spleen cradles stem cells with curative powers against mouse diabetes. But some researchers, including the leader of the original studies, haven't given up on the idea.

"An experimental result is not a valid one until it's been repeated," says Diane Mathis of the Joslin Diabetes Center in Boston, Massachusetts. That's one reason her team and two others set out to duplicate startling findings published more than 2 years ago. Both the original and the recent studies reversed diabetes in ailing mice. But the recent studies attribute that reversal to a therapy that's too toxic for humans, although it has previously been used to prevent, and occasionally treat, mouse diabetes.

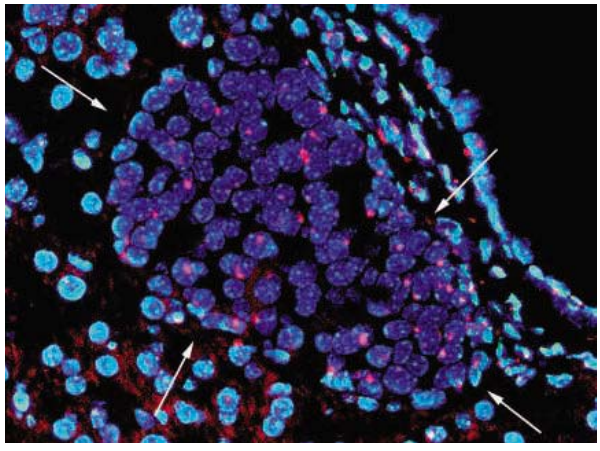

Inconsistent observation. A 2003 *Science* paper reported that donor spleen cells (labeled in pink) could morph into pancreatic islets in a diabetic mouse. But other scientists have seen no hint of donor cells in their experiments.

The story began in 2001, when Denise Faustman of Massachusetts General Hospital in Boston and her colleagues described in *The Journal of Clinical Investigation* a combination of standard and novel strategies for treating diabetic mice. Her team gave diabetic animals an immune-modulating agent along with donor spleen cells. As is fairly common in such studies, the mice also got a temporary transplant of new islets, which include insulin-producing beta cells; the islets weren't curative, but they normalized the animals' blood sugar to give the other treatments a chance to take effect.

When the sugar-stabilizing islets were removed, Faustman reported, 78% of the mice maintained normal blood sugar. Publishing more detailed work in *Science* in 2003, the team obtained cure rates as high as 90%. Furthermore, Faustman and her colleagues detected donor spleen cells that had morphed into beta cells and shown up in the animals' pancreases.

The work engendered special hope. Unlike traditional islets, which must be culled from cadaver pancreases in short supply, "here you would have the possibility of collecting spleens" that people "don't really need," says Louis Philipson of the University of Chicago, Illinois. "That promise … demanded that there be some sort of replication." Starting on page 1774, the three groups—Joslin's Mathis, Christophe Benoist, and their colleagues; Philipson, Anita Chong, and their colleagues at Chicago; and Emil Unanue, Anish Suri, and colleagues at Washington University in St. Louis, Missouri—describe efforts to do just that.

Following the Faustman protocol, the three injected between 22 and 53 diabetic animals with the immune modulator, called complete Freund's adjuvant (CFA). Containing killed bacteria that cause tuberculosis, CFA provokes a massive immune response and protects the pancreas from attack. It has previously been found to prevent and, sometimes, cure mouse diabetes. The immune reaction it triggers, however, is considered too hazardous for humans.

> "That promise [of the earlier experiment] … **demanded that there be some sort of replication."**
>
> —Louis Philipson, University of Chicago

Along with a CFA shot, the mice received injections of spleen cells from donor animals. Functioning islets were also wedged under their kidney capsules for 120 days to keep animals healthy during treatment.

"The [spleen] injections did not take," says Unanue. No group detected donor spleen cells in the blood, pancreas, or mice's kidneys.

beta cells in the pancreas, suggesting that the immune system had destroyed them.

However, like Faustman and her colleagues, all the groups successfully treated a subset of animals, although their "cure" rates were lower, roughly 10% to 25%. These animals, as well as some others that weren't cured, were found to have some beta cells in their pancreases, suggesting that mice can retain or perhaps regenerate the cells after diabetes develops. This finding is consistent with earlier mouse work and is increasingly suspected to apply to humans with newly diagnosed diabetes. But because the three groups could not detect spleen-derived beta cells, and because treatment with CFA and islets alone yielded the same results as when spleen cells were added to the mix, the groups attribute these cures to CFA and temporary islets.

"It's hard to know what to say," admits Kevan Herold, an endocrinologist at Columbia University. The groups "went to extremes" to replicate the spleen cell findings and were unable to do so.

Faustman disagrees with this interpretation on several levels. The important point, she says, is that in every experiment mice were cured, an outcome she calls "fantastic." The spleen cells, she adds, were "a minor point" in her paper. Still, she says she is certain that spleen cells can become beta cells and suggests that the groups used techniques too weak to detect them.

Neuroanatomist Éva Mezey of the National Institute of Dental and Craniofacial Research in Bethesda, Maryland, endorses the idea that in mice, spleen cells can be a powerful mediator of autoimmune disease. With help from the Faustman lab, she has successfully tested CFA and spleen cells against the autoimmune disease Sjögren's syndrome in a handful of mice; the work is not yet published. In diabetes, another autoimmune disease, Mezey believes that CFA can jump-start residual beta cells, and that spleen cells can create new ones if none remain naturally.

But most diabetes experts consider the spleen question settled. The problem now, says George Eisenbarth, executive director of the Barbara Davis Center for Childhood Diabetes at the University of Colorado Health Sciences Center in Denver, is that using CFA to cure mice is probably not relevant to humans. CFA's effects on mice have been studied for years, and a related but less toxic substance, the tuberculosis vaccine BCG, has failed to counter human diabetes. Faustman is raising money through the Iacocca Foundation to test BCG again (*Science*, 27 August 2004, p. 1237). Diabetes experts disagree whether, in light of these new findings, additional experiments with BCG should be considered.

–JENNIFER COUZIN

CREDIT: S. KODAMA *ET AL.*, *SCIENCE* **302**, 1223 (2003)

SCIENTIFIC PUBLISHING

Turmoil Threatens to Sink Canadian Journal

TORONTO—Canada's premier journal of medical science continues to implode in the wake of allegations of censorship by its publisher, the Canadian Medical Association (CMA). The 20 February firing of Editor John Hoey and Deputy Editor Anne Marie Todkill (*Science*, 3 March, p. 1226) has prompted the resignations of 14 of 19 board members and a succession of senior and intermediate *CMA Journal* editors, as well as calls for a boycott. Researchers fear the loss of an important outlet for Canadian science.

"The *CMAJ* no longer exists as we knew it," says Amir Attaran, an associate professor of health law at the University of Ottawa, who wants researchers and reviewers to boycott the journal unless CMA reinstates Hoey and Todkill or explains more fully why it dismissed them. "It would be sad if such action were to lead to the *CMAJ*'s demise, but it would still be preferable to accepting anything less than a fully free journal."

CMA officials say Hoey and Todkill were fired without notice because a "fresh approach" was required. But most observers believe it was the final step in a series of clashes over articles and editorials Hoey published during his 10-year reign and his commissioning of an outside panel that last month issued a scathing report of CMA's behavior. Hoey has declined comment due to a confidentiality agreement he and other editors signed with the CMA last year.

The Ottawa-based journal is now under its third acting editor, and only three of nine section editors remain on staff. Noni MacDonald, a pediatrician and medical professor in Halifax, Nova Scotia, says she stepped in as editor after the CMA promised to investigate how the journal is managed and adopt guidelines employed by the *Journal of the American Medical Association* to protect editorial independence. MacDonald was a member of the journal's Oversight Committee, which departing editorial board members say failed to preserve the journal's editorial independence.

In the meantime, MacDonald warns, a boycott could be fatal. "What's the goal there?" she asks. "To kill the journal, so we have no voice for national research issues?"

CMAJ's influence has been rising, say scientists, according to both quantifiable measures such as impact factor and anecdotal evidence. "Ten years ago, this journal was just another throwaway publication produced by the doctors' association," says Jacques Pepin, a microbiologist at the University of Sherbrooke in Quebec. "Under Hoey and Todkill, it has become an interesting journal for clinicians."

In August 2004, for example, *CMAJ* published Pepin's analysis of an outbreak of *Clostridium difficile* bacterial infections that had killed 200 patients in Quebec hospitals. Pepin says the paper alerted authorities in other countries about the difficulty of controlling the infection, which subsequently showed up in the United States. "For 18 months or so, the *CMAJ* was the only international journal with new research [on the outbreaks]," he says.

Retired Canadian Supreme Court judge Antonio Lamer is leading a review of governance issues at the journal. But Pepin and others are worried that their recommendations may not go far enough. "The CMA seems not to have carefully planned any of its actions," Pepin says. "We are worried the *CMAJ* may be headed back to throwaway status."

–PAUL WEBSTER

Paul Webster writes from Toronto, Canada.

RESEARCH MISCONDUCT

Seoul National University Dismisses Hwang

SEOUL—Seoul National University's (SNU's) disciplinary committee announced on 20 March that it would dismiss disgraced cloner Woo Suk Hwang, a professor at its Veterinary College, for his involvement in fabricating data. Six other professors and co-authors on the two papers on embryonic stem cell cloning, which were published in 2004 and 2005 and later retracted from *Science*, received lighter sentences.

At a press conference, Chang Ku Byun, dean of academic affairs, said dismissal is the harshest punishment the committee could impose. Hwang will be banned from working in a public position for 5 years after his dismissal and will receive only half of his retirement money.

According to Byun, Hwang said that he would take all responsibility for the fabrication because he was the leader of the cloning project. In particular, Hwang admitted to ordering a junior researcher to take photographs of two stem cell lines in the 2005 article so that it would look as if the team had created 11 customized stem cell lines.

The committee also suspended four other professors and cut the wages of two. Shin Yong Moon and Sung Keun Kang were both suspended for 3 months; Byung Cheon Lee and Curie Ahn were suspended for 2 months. They all will receive one-third of their wages during the suspension period and are not eligible for promotions for an additional 18 months. Chang Gyu Lee and Sun Ha Baek will have their wages deducted by one-third for 1 month.

CREDIT: AHN YOUNG-JOON/AP PHOTO

Fired. SNU's disciplinary committee has dismissed Hwang for fabricating data.

"The professors fundamentally went back on the values of integrity and honesty that should have been kept as an academic and professor of a national university," Byun said. The committee imposed comparatively harsher punishment on Moon and Kang because Moon was a co-author of the 2004 paper and Kang was working in the same lab as Hwang and was deeply involved in the data manipulation. Lee and Baek were listed as co-authors but did not make any contributions to the paper, Byun added.

Meanwhile, the special investigative team of Seoul Central Prosecutors' Office said, also on 20 March, that the initial contamination of stem cells in January last year was not deliberate, as they had previously thought, but arose from "accidents" by the researchers. The prosecutors are still investigating whether stem cells from Hwang's project were intentionally switched with those of MizMedi Hospital, which collaborated with Hwang on the research. The prosecutors, who are also examining how Hwang spent state funds and private donations, hope to conclude their investigations early next month.

–YVETTE WOHN

Yvette Wohn is a reporter in Seoul.

microRNA

Labelling - Array - Bioinformatics

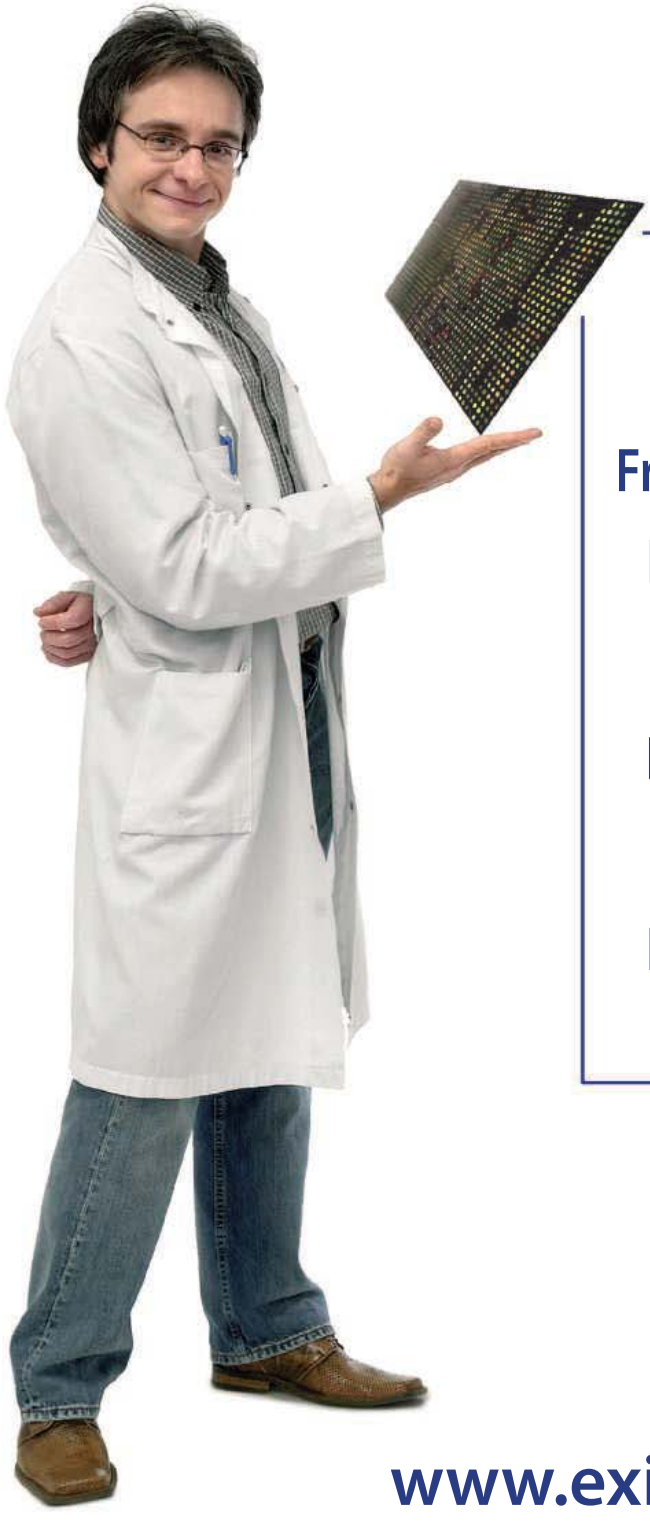

miRCURY™ Array

From sample to results in 24 h

- **Use less sample**
  - *Works on <1 µg total RNA*
  - *Highly sensitive LNA™ capture probes*
- **Save time**
  - *No miRNA enrichment required*
  - *1 hour labelling protocol*
- **Get instant target prediction**
  - *Free online miRNA Resource Center*

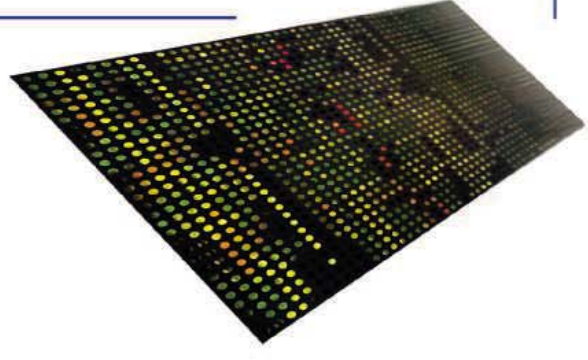

www.exiqon.com

EXIQON

THE HOME OF LNA™

MICROBIAL ECOLOGY

How a Marine Bacterium Adapts To Multiple Environments

Ahab chased a giant sperm whale through the seas for years. Sallie Chisholm has spent much of her professional career tracking far smaller denizens of the ocean: photosynthetic bacteria called *Prochlorococcus*. A marine microbiologist at the Massachusetts Institute of Technology (MIT), Chisholm helped discover these microbes 20 years ago. Now, she and her colleagues have charted the distribution of *Prochlorococcus* across the Atlantic Ocean and found that various strains congregate at different depths and places.

In a Research Article on page 1737 of this issue of *Science*, Chisholm's team describes how water temperature and other environmental factors determine which strains thrive at particular places. And in a Report on page 1768, she and her colleagues reveal newly discovered "guest" genes in two strains that may help each strain survive in particular ocean environments. The studies "give us a rare glimpse into the population genetics of a native population," says Stephen Giovannoni, a marine microbiologist at Oregon State University in Corvallis.

With 1700 genes, *Prochlorococcus* has the smallest genome known for a free-living, photosynthetic organism. Yet, in low-nutrient environments typical of deep oceans, it outnumbers all other marine microbes and can account for up to 48% of net primary production there. Moreover, although all *Prochlorococcus* strains are quite closely related—at least according to traditional comparisons of their ribosomal RNA gene—Chisholm and her colleagues found a diversity of physiologically distinct strains, or ecotypes. For example, some grow best in dim light, whereas others require four times as much sunshine as their low-light–adapted peers.

In 2003, Zackary Johnson, Chisholm's postdoctoral fellow, surveyed the ocean distribution of these ecotypes during a research cruise from Europe to the tip of South America. He and another postdoc, Erik Zinser, used the polymerase chain reaction to identify which ecotypes lived where. They also measured the biomass of *Prochlorococcus* and the amount of photosynthesis at specific depths at each sampling site. "This is the first [extensive] study about *Prochlorococcus* distributions at the ecotype level," says Jakob Pernthaler, a microbial ecologist at the University of Zurich, Switzerland. "It's an impressive data set."

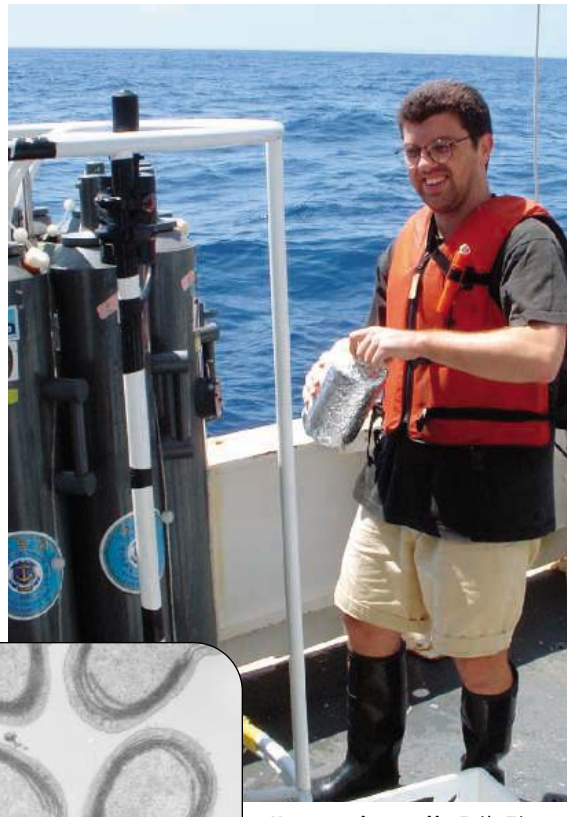

Hot on the trail. Erik Zinser searches for the cyanobacterium *Prochlorococcus* (*inset*).

CREDITS: ZACKARY JOHNSON/MIT; (INSET) CLAIRE C. TING/WILLIAMS COLLEGE

On the trip, water temperatures ranged from 5°C to 29°C, and nitrate, phosphate, silicate, and other nutrients utilized by *Prochlorococcus* were more abundant in the southern reaches. At certain sampling sites, two of the light-loving strains populated the surface in about equal numbers. And at depths of 50 meters, a low-light–adapted strain typically appeared, its abundance increasing with depth until about 75 meters down. Deeper down, a second low-light–adapted strain would take over. However, these distributions varied by latitude. Close to the equator, one low-light–adapted strain was as common at the surface as a high-light–adapted one. Together, these data provide "an ocean snapshot of *Prochlorococcus* biogeography" that will aid the understanding of this organism's ecology and role in the environment, says Eugene Madsen, a microbial ecologist at Cornell University.

Edward DeLong, a microbiologist at MIT, also recently found stratification of the *Prochlorococcus* strains, but through a slightly less robust method (*Science*, 2 January, p. 496). His team, which included Chisholm and her postdoc Matthew Sullivan, sampled all the DNA in a water column from 10 meters to 4000 meters down, at a monitoring station off Hawaii. They then used a sophisticated computer program to assemble the bits of DNA into sequences large enough to identify genes and to get a read on which organisms were present. For example, that work showed that genes from high-light–adapted and low-light–adapted *Prochlorococcus* strains had different abundances at various depths.

DeLong's group also discovered high concentrations of bacterial viruses called phages at ocean depths where *Prochlorococcus* lives; the greatest concentrations were at a depth of 70 m. The second study by Chisholm's team indicates that such phages are key to the adaptability of *Prochlorococcus*. Chisholm says that the viruses have inserted "islands" of genes into this bacterium, helping to create the various ecotypes she and others have found. In each strain, the islands are located in about the same place on the bacteria's chromosome, but the genes they contain vary from strain to strain. "These are hot spots in the genomes that appear to be very dynamic," says Chisholm.

When Chisholm's graduate student Maureen Coleman looked at these islands in two high-light–adapted strains growing in the lab, she found genes important for photosynthesis and for proteins for coping with stress, such as phosphorus deficiencies. Some of the islands' genes were the same in all strains. But not always: *Prochlorococcus* collected from the Mediterranean had a gene likely to be important for nitrogen scavenging, but this gene was lacking in another strain. Thus, the island genes may enable various strains to thrive at particular depths, light intensities, nutrient content, and temperatures. "The case is very strong that the islands and their variations play a role in [*Prochlorococcus*] evolution," says Madsen.

Pathogenic bacteria often have phage-delivered islands of DNA that contain genes for increased virulence or drug resistance, so it's not unexpected that similar islands enhance *Prochlorococcus*'s survival, says Xabier Irigoyen of AZTI-Tecnalia in Pasaia, Spain. Nonetheless, Pernthaler notes, "it's a great piece of science that will inspire follow-up for other marine bacteria."

–ELIZABETH PENNISI

Startling amounts of ice slipping into the sea have taken glaciologists by surprise; now they fear that this century's greenhouse emissions could be committing the world to a catastrophic sea-level rise

A Worrying Trend of Less Ice, Higher Seas

HAVE AN URGE LATELY TO RUN FOR higher ground? That would be understandable, given all the talk about the world's ice melting into the sea. Kilimanjaro's ice cloak is soon to disappear, the summertime Arctic Ocean could be ice-free by century's end, 11,000-year-old ice shelves around Antarctica are breaking up over the course of weeks, and glaciers there and in Greenland have begun galloping into the sea. All true. And the speeding glaciers, at least, are surely driving up sea level and pushing shorelines inland.

Scientists may not be heading for the hills just yet, but they're increasingly worried. Not about their beach houses being inundated anytime soon; they're worried about what they've missed. Some of the glaciers draining the great ice sheets of Antarctica and Greenland have sped up dramatically, driving up sea level and catching scientists unawares. They don't fully understand what is happening. And if they don't understand what a little warming is doing to the ice sheets today, they reason, what can they say about ice's fate and rising seas in the greenhouse world of the next century or two?

That uncertainty is unsettling. Climatologists know that, as the world warmed in the past, "by some process, ice sheets got smaller," says glaciologist Robert Bindschadler of NASA's Goddard Space Flight Center (GSFC) in Greenbelt, Maryland. But "we didn't know the process; I think we're seeing it now. And it's not gradual." Adds geoscientist Michael Oppenheimer of Princeton University, "The time scale for future loss of most of an ice sheet may not be millennia," as glacier models have suggested, "but centuries."

The apparent sensitivity of ice sheets to a warmer world could prove disastrous. The greenhouse gases that people are spewing into the atmosphere this century might guarantee enough warming to destroy the West Antarctic and Greenland ice sheets, says Oppenheimer, possibly as quickly as within several centuries. That would drive up sea level 5 to 10 meters at rates not seen since the end of the last ice age. New Orleans would flood, for good, as would most of South Florida and much of the Netherlands. Rising seas would push half a billion people inland. "This is not an experiment you get to run twice," says Oppenheimer. "I find this all very disturbing."

A rush to the sea

Much of the world's ice may be shrinking under the growing warmth of the past several decades, but some ice losses will have more dramatic effects on sea level than others. Glaciologists worried about rising sea level are keying on the glaciers draining the world's two dominant ice reservoirs, Greenland and Antarctica. Summertime Arctic Ocean ice may be on its way out, but its melting does nothing to increase the volume of ocean water; that ice is already floating on the ocean. The same goes for floating ice shelves around Antarctic. The meltwater from receding mountain glaciers and ice caps is certainly raising sea level, but not much.

The truly disturbing ice news of late is word that some of the ice oozing from the 3-kilometer-thick pile on Greenland has doubled its speed in just the past few years. In the 17 February issue of *Science*, for example, radar scientists Eric Rignot of the Jet Propulsion Laboratory in Pasadena, California, and Pannir Kanagaratnam of the University of Kansas, Lawrence, analyzed observations made between 1996 and 2005 by four satellite-borne radars. These synthetic aperture radars measure the distance to the surface during successive passes over a glacier. The changing distance can then be extracted by letting successive observations form interference patterns. The changing distance, in turn, translates to a velocity of the ice toward the sea.

In central east Greenland, Kangerdlugssuaq Glacier more than doubled its speed from 2000 to 2005, Rignot and Kanagaratnam found, from 6 kilometers per year to 13 kilometers per year. That made it the fastest in Greenland. To the south, Helheim Glacier accelerated 60%. And on the west of Greenland, Jakobshavn Isbrae almost doubled its speed between 1996 and 2005. The accelerations are "actually quite surprising," says glaciologist Julian Dowdeswell of the University of Cambridge in the United

CREDIT: RICHARD ALLEY

Going. Greenland glaciers like those dumping into Sondre Sermilik Fjord have sped up and retreated.

Kingdom. Even at its slower speed, Jakobshavn had ranked as one of the fastest-flowing glaciers in the world, perhaps the fastest; now it's just one of the pack.

As glaciers draining the Greenland Ice Sheet are picking up speed, researchers are realizing that nothing has made up for the increased loss of ice. Greenland's pile of ice is getting smaller. How much smaller is still being debated, if only because of the vast scope of an ice sheet. What goes out through glaciers is just one part of the equation: Ice sheets also lose mass by melting and gain it from snowfall. To gauge those gains and losses, Rignot and Kanagaratnam used previously published estimates of how the warming climate over Greenland has increased meltwater losses and slightly increased snowfall, making for a growing net loss in addition to the glacier flow. All told, the scientists find that the loss of mass from Greenland doubled from 1996 to 2005, reaching 224 ± 41 cubic kilometers per year. Los Angeles uses 1 cubic kilometer of water per year.

In another approach to estimating mass balance, researchers sketch the changing shape and therefore volume of the ice sheet. In a paper just out in the *Journal of Glaciology*, glaciologist Jay Zwally of GSFC and colleagues use satellite radars to measure the height of the Greenland Ice Sheet's broad plateau and airborne laser altimeters to monitor the height of glaciers draining to the coast, which are too small for satellite radars to see reliably. "We have strong evidence the ice sheet was near balance [during] the last decade of the 20th century," says Zwally. "Our measures show a slight positive gain of 11 [cubic kilometers] per year" between 1992 and 2002.

Global warming contrarians have already taken up Zwally's result as evidence that nothing much is happening with the ice sheet, so there's nothing to worry about. Zwally disagrees. "There's no question there's been an acceleration of some of Greenland's glaciers over the last 5 years," after his surveys were completed, he says. "I would say that right now the current loss is 30 to 40 [cubic kilometers] per year," he says, based on his gut feeling about the most recent radar and laser observations.

That's getting close to the mass loss reported last fall using a third approach: repeatedly weighing the ice sheet. Geophysicists Isabella Velicogna and John Wahr of the University of Colorado, Boulder, reported in *Geophysical Research Letters* how the two satellites of the Gravity Recovery and Climate Experiment (GRACE), flying in tandem, gauge the mass beneath them. They precisely measure the changing distance between them caused by the gravitational pull of the passing ice. Between 2002 and 2004, GRACE found a loss of about 82 cubic kilometers of ice per year.

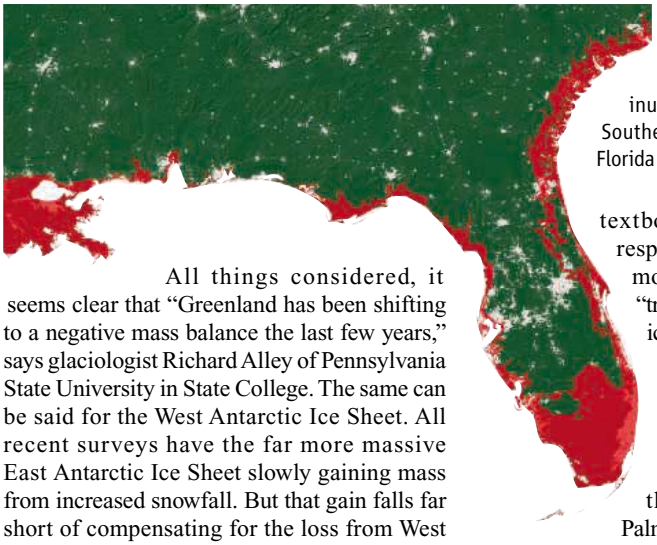

Going under? Global warming might trigger a 6-meter rise in sea level that would inundate coasts (red) worldwide. Southern Louisiana (*left*) and South Florida (*lower right*) would be hard hit.

All things considered, it seems clear that "Greenland has been shifting to a negative mass balance the last few years," says glaciologist Richard Alley of Pennsylvania State University in State College. The same can be said for the West Antarctic Ice Sheet. All recent surveys have the far more massive East Antarctic Ice Sheet slowly gaining mass from increased snowfall. But that gain falls far short of compensating for the loss from West Antarctica. There, Zwally's analysis has the ice shrinking by about 47 cubic kilometers per year. And Velicogna and Wahr, writing in this week's issue of *Science* (p. 1754), report a GRACE-estimated loss of about 148 cubic kilometers per year. In West Antarctica, as in Greenland, the culprit is the acceleration of outlet glaciers in recent years (*Science*, 24 September 2004, p. 1897).

Why the rush?

The recent proliferation of galloping glaciers caught researchers unawares. "None of the models [of glacier flow] predict there should be such rapid change," says glaciologist Ian Joughin of the University of Washington, Seattle (see Perspective on p. 1719). "If you look at a textbook, you'll see an ice sheet response time of 1000 years or more." That's because models "treat ice sheets as a big lump of ice," he says. They melt, or they don't melt.

In the case of West Antarctica, there is tentative agreement about what is triggering the acceleration of the glaciers. Around the Palmer Peninsula that juts northward from West Antarctica, the world's strongest regional warming of the past 50 years first puddled the surface of ice shelves with meltwater. The meltwater then drove into the ice along growing cracks, breaking up shelves over a few weeks. Without the shelves to hold them back, apparently, the glaciers feeding them sped up (*Science*, 30 August 2002, p. 1494). To the south, where it's still far too cold for surface melting, a third-of-a-degree warming of the ocean seems to have eaten away at the shelves jutting into the Amundsen Sea. That in turn sped up Pine Island Glacier and its neighbors.

Around Greenland, however, both surface melting and shelf-bottom melting seem to be happening to some extent. Surface melting around the ice sheet's periphery has increased

Off to sea. The acceleration of glaciers draining both the Greenland and Antarctic ice sheets has meant more icebergs and ... world.

CREDITS (TOP TO BOTTOM): IMAGE BY JEREMY L. WEISS AND JONATHAN T. OVERPECK/UNIVERSITY OF ARIZONA; FRANK LUKASSECK/ZEFA/CORBIS

EndNote. Where millions of researchers, librarians and students begin.

Learn about new tools for your research and publishing—

Onfolio™
Organize RSS feeds and Web research

RefViz™
Visualize references

sciPROOF™
Proof your manuscript

800-722-1227 • 760-438-5526
Fax: 760-438-5573
rs.info@thomson.com

EndNote, used by millions of researchers, students, professors, librarians and writers worldwide, is known for introducing innovative features such as the ability to search online bibliographic databases, organize references and images, and create instant bibliographies. With EndNote 9, you can work faster with increased performance, connect to more data sources worldwide, and share customized libraries with colleagues easily. EndNote is easy to use, easy to learn and is seamlessly compatible with Microsoft® Word for Windows® and Mac® OSX. There simply is no better way to manage your references and build instant bibliographies.

Download your Free demo or buy online today.
www.endnote.com

in recent years. Some of the meltwater plunges into open crevasses, where Zwally has shown that it can lubricate the bottom of the ice and accelerate ice flow. But, as Bindschadler argues on page 1720 of this issue of *Science*, the accelerating Greenland glaciers all flow through deep troughs that expose the ice to any warming ocean water, and all lost their buttressing ice shelves before or during acceleration. So both mechanisms are plausible drivers of glacier acceleration, but glaciologists cannot agree on their relative importance.

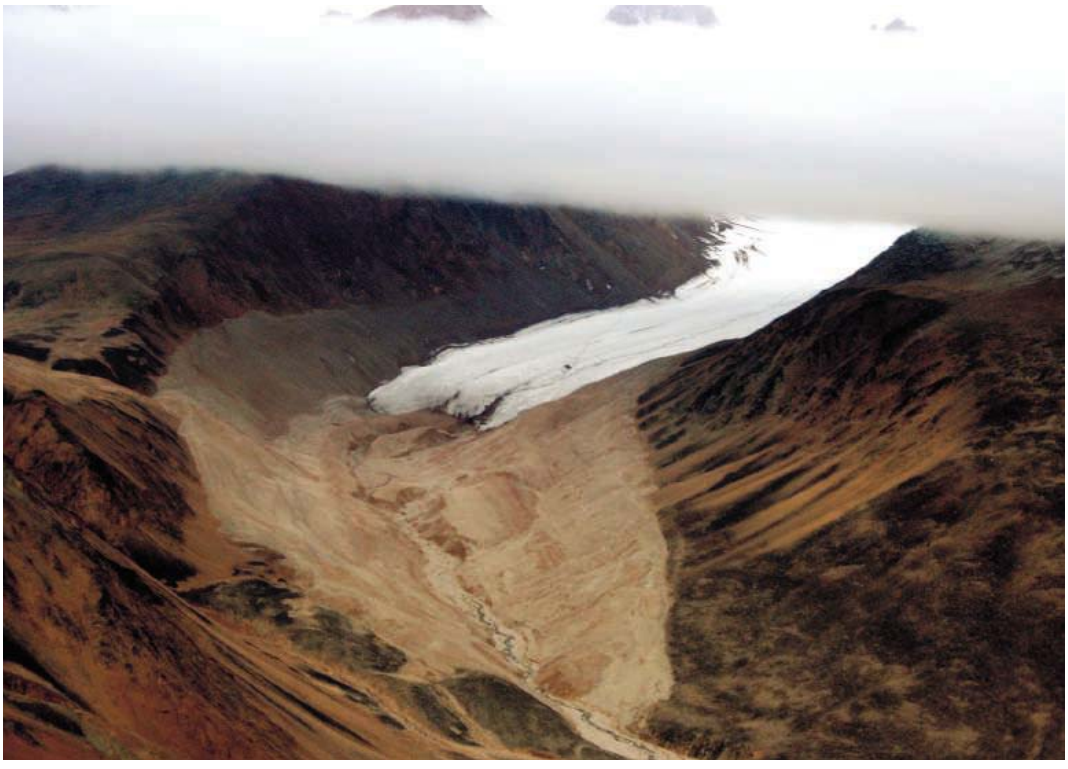

Not just the heat. Greenland glaciers retreat (tan area) when warming increases melting, but they can also accelerate when warmer ocean water destroys their lower reaches or added meltwater lubricates their undersides.

CREDIT: RICHARD ALLEY

Whither the world's ice

If the recent behavior of ice sheets is not fully understood, their future is largely a blank. "We don't actually understand what's driving these higher velocities," says Dowdeswell, so "it's difficult to say whether that's going to continue," or spread.

At the moment, ice loss from Greenland and West Antarctica combined is contributing less than half of the ongoing 2-millimeters-per-year rise in sea level; the rest comes from melting mountain glaciers and the simple thermal expansion of seawater. If the recent surge of ice to the sea continues, sea level might reach something like half a meter higher by 2100. That would be substantial but not catastrophic. To produce really scary rises really fast (say, a meter or more per century), the air and water will have to continue warming in the right—or wrong—places. The temperature rise will have to spread northward around Greenland and in the south around West Antarctica, reaching the big ice shelves where most of that ice sheet drains. And glacier accelerations triggered near the sea must propagate far inland to draw on the bulk of an ice sheet.

Faced with uncertainty about the present, paleoclimatologists look to the past. About 130,000 years ago, between the last two ice ages, the poles may have warmed as much as they will with only a couple of degrees of global warming. But sea level was considerably higher then, something like 3 to 4 meters higher. In two articles in this issue of *Science*, paleoclimatologist Jonathan Overpeck of the University of Arizona, Tucson (p. 1747), paleoclimate modeler Bette Otto-Bliesner of the National Center for Atmospheric Research in Boulder (p. 1751), and their colleagues consider whether the greenhouse world of a century hence might be as warm—and thus as destructive of ice—as during the previous interglacial.

First they simulated the climate of 130,000 years ago. Back then, Earth was tilted slightly more on its axis, so more solar radiation hit the high northern latitudes, driving warming there. Because the model included that added radiation, it had Greenland warming by about 3°C in the interglacial period. When that warming was put into a model of the ice sheet, the ice melted away slowly (because the model lacked any acceleration mechanisms) until about half remained. That produced enough meltwater to raise sea level 2 to 3 meters. Overpeck and colleagues suggest that another couple of meters of sea level rise could have come from West Antarctica; it was not as warm there, but much of the ice sheet lies below sea level, making it inherently unstable.

When the climate model simulates the next 140 years of rising greenhouse gases, Greenland warms as much by 2100 as it did in the previous interglacial and would thus—eventually—melt as much. "Ice sheets have contributed meters above modern sea level in response to modest warming," Overpeck and his colleagues conclude, and "a threshold triggering many meters of sea-level rise could be crossed well before the end of this century."

The paleoclimate argument for large, imminent ice losses "is fascinating and scary at the same time," says Oppenheimer. "Paleoclimate always has a large amount of uncertainty, [but] we should take this as a serious warning sign. You could lock in a dangerous warming during this century."

An icy conundrum

The ice sheet problem today very much resembles the ozone problem of the early 1980s, before researchers recognized the Antarctic ozone hole, Oppenheimer and Alley have written. The stakes are high in both cases, and the uncertainties are large. Chemists had shown that chlorine gas would, in theory, destroy ozone, but no ozone destruction had yet been seen in the atmosphere. While the magnitude of the problem remained uncertain, only a few countries restricted the use of chlorofluorocarbons, mainly by banning their use in aerosol sprays.

But then the ozone hole showed up, and scientists soon realized a second, far more powerful loss mechanism was operating in the stratosphere; the solid surfaces of ice cloud particles were accelerating the destruction of ozone by chlorine. Far more drastic measures than banning aerosols would be required to handle the problem.

Now glaciologists have a second mechanism for the loss of ice: accelerated flow of the ice itself, not just its meltwater, to the sea. "In the end, ice dynamics is going to win out" over simple, slower melting, says Bindschadler. Is glacier acceleration the ozone hole of sea level rise? No one knows. No one knows whether the exceptionally strong warmings around the ice will continue apace, whether the ice accelerations of recent years will slow as the ice sheets adjust to the new warmth, or whether more glaciers will fall prey to the warmth. No one knows, yet.

–RICHARD A. KERR

Along the Road From Kyoto

Global greenhouse gas emissions keep rising

2006 marks a key year for climate policy around the world. Participants at a U.N.–sponsored meeting in Nairobi in November will debate what should happen after the 1997 Kyoto Treaty expires in 2012. Meanwhile, the 34 countries that have agreed to specific cuts under the accords are gearing up for 2008, when the enforcement clock starts ticking.

A number of nations have already moved to cut emissions. Emissions in Germany, for example, are down by nearly a fifth compared with 1990 levels. At the same time, emissions have risen substantially in Canada and Japan despite their promise to achieve a 6% reduction over 1990 levels. As a result, government officials in both nations are debating tough measures to reverse that trend.

In contrast, the United States and Australia, two major nonratifying nations, insist that long-term investment in technology and voluntary reductions are a better approach; their emissions have grown steadily since 1990. And developing nations not bound by Kyoto targets, in particular China and India, are beginning to emit carbon at absolute rates that match those of more industrialized nations.

The following graphics depict the state of greenhouse gas emissions for 10 key countries, and where the planet is headed.

–ELI KINTISCH (TEXT) AND KELLY BUCKHEIT (DESIGN)

CONTRIBUTING FACTORS TO CO_2 CHANGE

The World Resources Institute has identified four factors that drove changes in a country's greenhouse gas emissions from 1990 to 2002. The numbers represent the relative contributions of each factor, and the contributions sum to the overall increase or decrease in that country's emissions. In the case of China, for example, 122% of its growth in emissions resulted from a per capita rise in GDP, while a shift in energy intensity reduced emissions growth by 96%.

GDP per Capita
Increasing wealth tends to mean rising carbon emissions.

Population
More people usually boosts emissions, but it need not.

Energy Intensity
Energy consumed per unit of GDP. Intensity declines as a country shifts from an industrial to a service economy or uses its resources more efficiently.

Fuel Mix
Carbon content of energy source. Coal produces many more greenhouse gases than hydropower per unit of energy created.

GLOBAL EMISSIONS PROJECTIONS

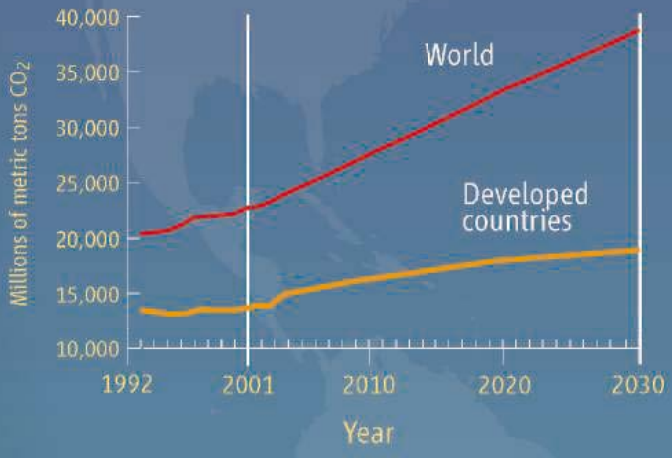

Worldwide problem. The sharp rise in global emissions is fueled increasingly by the energy demands of the developing world. Future levels are based on projections for business-as-usual growth.

SOURCE: WORLD RESOURCES INSTITUTE/INTERNATIONAL ENERGY AGENCY

Science

CHINA +49%

BRAZIL +57%

UNITED STATES +18%

GDP per capita: +23

Population: +16

Energy intensity: –20

Fuel mix: –1

RUSSIA –23%

GDP per capita: –5

Population: –3

Energy intensity: –12

Fuel mix: –3

CANADA +20%

GDP per capita: +24

Population: +13

Energy intensity: –18

Fuel mix: 0

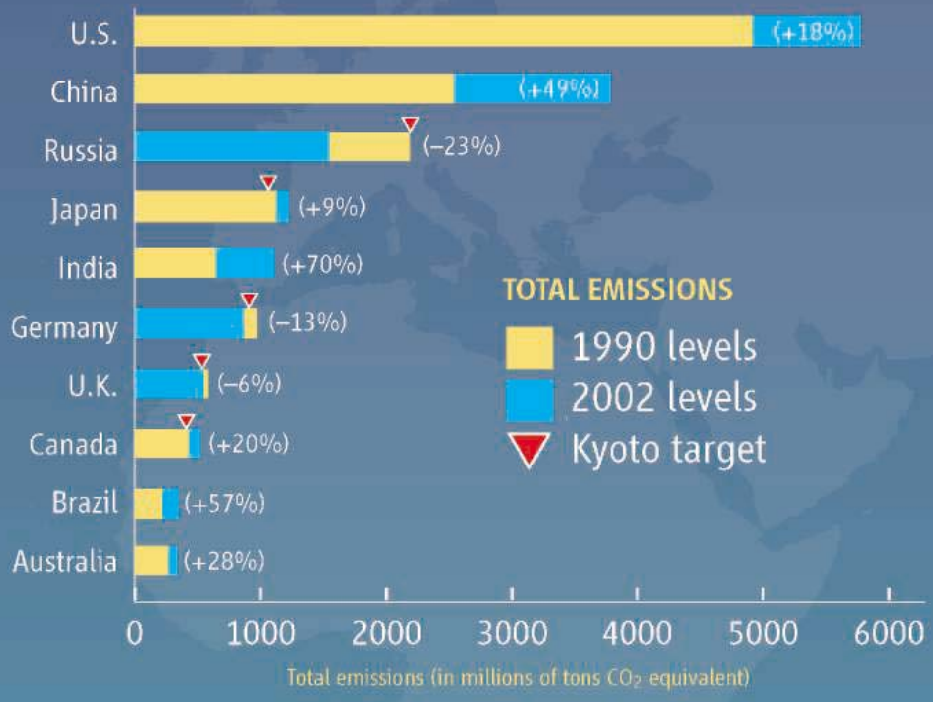

Follow the carbon. The United States and China, with no obligation to meet Kyoto targets, have stretched their lead as the world's biggest carbon emitters. Among Kyoto ratifiers listed here, Russia and Germany have cut total emissions and exceeded Kyoto targets, whereas Japan and Canada face daunting challenges to meet their targets. The percentages in parentheses reflect changes in emissions from 1990 to 2002.

SOURCE: CLIMATE ANALYSIS INDICATORS TOOL; WORLD RESOURCES INSTITUTE; UNITED NATIONS

GERMANY –13%

GDP per capita: +15

Population: +4

Energy intensity: –21

Fuel mix: –10

INDIA +70%

GDP per capita: +55

Population: +28

Energy intensity: –31

Fuel mix: +19

AUSTRALIA +28%

GDP per capita: +31

Population: +16

Energy intensity: –19

Fuel mix: –1

JAPAN +9%

GDP per capita: +12

Population: +3

Energy intensity: 0

Fuel mix: –7

UNITED KINGDOM –6%

GDP per capita: +24

Population: +3

Energy intensity: –20

Fuel mix: –13

A Clearer View of Macular Degeneration

Genes tied to age-related macular degeneration confirm the notion that inflammation helps destroy the central area of the retina in this vision disorder

More than 10 million people in the United States and an estimated 50 million worldwide suffer from age-related macular degeneration (AMD). This deterioration of the retina wipes out their central vision, robbing them of the ability to perform essential activities such as reading or driving a car. Until recently, researchers had few clues to what causes AMD. But a series of recent gene discoveries has gone a long way toward solving the mystery.

The work has shown that variations in two genes encoding proteins in the so-called complement cascade account for most of the risk of developing AMD. This complex molecular pathway is the body's first line of defense against invading bacteria, but if overactive, the pathway can produce tissue-damaging inflammation.

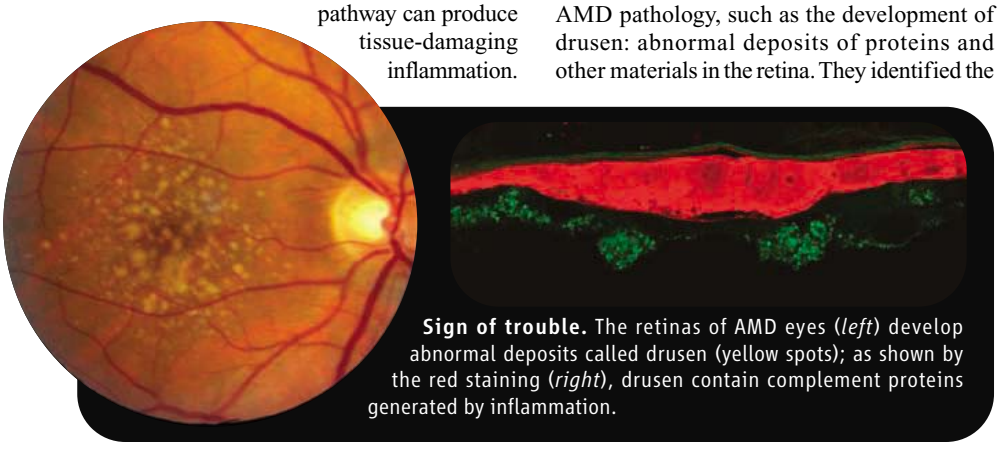

Sign of trouble. The retinas of AMD eyes (*left*) develop abnormal deposits called drusen (yellow spots); as shown by the red staining (*right*), drusen contain complement proteins generated by inflammation.

The new links between AMD and the complement genes suggest that excessive inflammation resulting from uncontrolled complement activity underlies the vision-destroying changes that particularly strike the macula, the central region of the retina. Indeed, such inflammation-promoting gene variants contribute to the development of perhaps as many as 75% of AMD cases. Several other genes have also been implicated recently, including one of as-yet-unknown function that may also make a substantial contribution to AMD risk.

At long last, say researchers, they have the kind of information needed to find ways to prevent or treat AMD. "I think we're headed for a period of time when we're going to come up with possible therapies," says AMD researcher Michael Gorin of the University of Pittsburgh School of Medicine in Pennsylvania. This might be accomplished, for example, by finding ways to inhibit complement activity in the eye.

A tough disease to crack

The causes of AMD have been hard to pin down partly because the disease develops late in life, usually after age 60. In addition, AMD is a complex disease, caused by an interaction between multiple genes and environmental factors such as diet and smoking. That's made it hard to do studies aimed at tying particular gene variants to the disease. "Until last year, we just didn't have a clue about the etiology [of AMD]. It's been very frustrating," says Gregory Hageman of the University of Iowa in Iowa City, one of the field's pioneers.

In their search for clues, researchers have looked at hereditary eye diseases that develop early in life and mimic some features of AMD pathology, such as the development of drusen: abnormal deposits of proteins and other materials in the retina. They identified the genes at fault in some of these early developing diseases and for a time hoped that the same genes might also be major contributors to AMD. "It turns out that for the most part that idea was wrong," says Gorin.

About 15 years ago, Hageman began pursuing a different tack, collecting donated eyes from both people afflicted with AMD and those who were not. His analyses of those eyes suggested that inflammation is a key player in the etiology of AMD.

For example, working with Iowa colleague Robert Mullins and Don Anderson and Lincoln Johnson of the University of California, Santa Barbara, Hageman found that proteins associated with immune system activity are located in or near the drusen in eyes with AMD. These proteins included various activated components of the complement system, such as the membrane attack complex, which is the business end of the complement cascade. It destroys pathogenic bacteria or viruses by poking holes in their membranes, but it can also damage normal cells if not controlled.

Based on these and other results, Hageman and his colleagues proposed about 5 years ago that drusen growth begins when some as-yet-unknown insult damages cells in the retina. The leftover cell debris provides the seed for drusen formation and triggers complement activation and local inflammation. Over time, the drusen grow as they accumulate inflammatory proteins and other materials, and the inflammation persists, causing additional damage to the retina and, in the worst cases, blindness.

At the time, this idea "was not met with a lot of positivity," Hageman wryly recalls. "He pushed the hypothesis for many years, and nobody believed him," says Rando Allikmets of Columbia University, a recent collaborator. Allikmets notes that he, like many other AMD researchers, acknowledged that there could be an inflammatory component in AMD but "thought this was secondary or tertiary" to whatever was actually causing the retinal damage.

A genetic link to inflammation

The turning point in the inflammation story came just over a year ago, thanks mainly to new gene-hunting tools, including the human genome sequence as well as the growing library of human single-nucleotide polymorphisms (SNPs), subtle DNA sequence changes that can be used to pin down the gene variants at fault in a disease. Over the past few years, researchers have used these SNPs to identify several chromosomal regions likely to contain genes that influence the risk of getting AMD and then zeroed in on the genes themselves.

Last March, three independent groups—led by Josephine Hoh of Yale University School of Medicine; Margaret Pericak-Vance of Duke University Medical Center in Durham, North Carolina; and Albert Edwards of the University of Texas Southwestern Medical Center in Dallas and Lindsay Farrer of Boston University School of Medicine—reported online in *Science* that they had uncovered a gene on chromosome 1 that greatly increases the risk of getting AMD. The gene encodes a protein called complement factor H that helps keep the complement system under tight control so that it doesn't attack the body's normal cells. The researchers found that people bearing a particular variant of the factor H gene were much more likely to get AMD than were people with other variants (*Science*, 15 April 2005, pp. 362, 385, 419, and 421). Their calculations showed that the high-risk variant could explain up to 50% of the cases, presumably because the protein product of that gene is less effective in inhibiting the complement pathway.

Hageman describes this confirmation of complement involvement in AMD as "pretty

Proudly Presented by Yale IT Services. Thank You for Support

CREDITS (LEFT TO RIGHT): GREGORY HAGEMAN; DON H. ANDERSON/CENTER FOR THE STUDY OF MACULAR DEGENERATION, UNIVERSITY OF CALIFORNIA, SANTA BARBARA

Missing faces. As illustrated by the simulated picture at right, AMD robs its victims of their central vision and can leave them legally blind even though a rim of peripheral vision may remain.

wonderful"—even though the other teams got their work into print before his own. In the 17 May 2005 *Proceedings of the National Academy of Sciences*, Allikmets and Hageman, working with Bert Gold and Michael Dean of the National Cancer Institute in Bethesda, Maryland, and colleagues reported that they, too, had linked the same high-risk variant of the factor H gene to AMD and also identified other variants that appeared protective. In addition, they showed that factor H is made in the macula and is present in drusen. In other words, it's right where it should be to influence AMD development.

The case for a link between complement activity and AMD risk got another major boost earlier this month. In the March issue of *Nature Genetics*, Allikmets, Hageman, Gold, Dean, and their colleagues report linking the gene for a second component of the complement cascade to the eye disease. This gene, located on chromosome 6, produces a protein called factor B involved in complement activation; the researchers again found both high-risk and protective variants.

The earlier factor H studies showed that some people with healthy eyes also carry the AMD-predisposing variant, although it is present in more AMD patients. Allikmets says that the existence of protective variants of the factor H and B genes can help explain why some people with the "bad" variants don't get AMD. By looking at the variants of both genes that people have, he says, "you get a much clearer picture. Seventy-four percent of the patients had no protective [gene variants], while 56% of the controls had at least one."

Still unclear, however, is the nature of the initial trigger that touches off complement activation. An infection is one possibility. About a year ago, Joan Miller of Harvard Medical School in Boston and her colleagues reported evidence indicating that the eyes of patients with the so-called wet form of AMD, characterized by blood vessel growth in the macula, had been infected by the bacterium *Chlamydia pneumoniae*. A causative link between *Chlamydia* infection and AMD needs to be confirmed, however.

More AMD genes

A third gene recently tied to AMD doesn't fall neatly into the complement story. In work published last summer in the *American Journal of Human Genetics*, Gorin and his colleagues followed up on previous studies placing an AMD gene on chromosome 10. Gorin says that his group's analysis homed in on two tightly linked genes (designated *PLEKHA1* and *LOC387715*) but couldn't discern which is the culprit. However, in a paper that appeared a few months later in *Human Molecular Genetics*, a team led by Bernhard Weber of the University of Regensburg, Germany, reported that the strongest AMD risk seemed to be associated with a single amino acid change in the protein predicted to be encoded by *LOC387715*. In work published online early this month in the *American Journal of Human Genetics* (*AJHG*), Pericak-Vance and her colleagues confirmed that conclusion.

The genetic analyses indicate that *LOC387715*'s effect on AMD is independent of that of the factor H gene but is almost as strong, contributing to perhaps 40% of AMD cases. Still, the function of the gene's protein is a mystery. "Until one knows what it does, you can't really say it's the gene," Gorin cautions.

In their *AJHG* paper, Pericak-Vance and her colleagues also point out an intriguing connection between the high-risk variant of *LOC387715* and cigarette smoking, one of the strongest environmental risk factors for AMD. The researchers found that the combined risk of smoking and carrying the AMD-promoting gene variant was more than the sum of the risk of the two individually. This indicates, Pericak-Vance says, that the two factors interact to foster AMD development.

Pioneer. Despite early skepticism from his colleagues, Gregory Hageman's view that inflammation plays a causal role in AMD is proving correct.

The factor H and B genes and *LOC387715* are likely not the only ones that affect AMD risk. For example, in a study published in January in *Investigative Ophthalmology and Visual Science*, Pericak-Vance's team looked at eight candidate genes that were suspected of involvement in AMD. Their analysis implicated three of them, including the *VEGF* gene and two involved in lipid metabolism. The product of the *VEGF* gene stimulates blood vessel growth, suggesting it might be involved in wet AMD, which is the most severe form.

But the complement genes and *LOC387715* are certainly the major contributors to AMD risk, and establishing that, Hageman says, is good news for people who might develop AMD. Having to look at just a few genes could make it easier to identify high-risk individuals, who could then take preventive steps such as avoiding smoking, decreasing their fat intake, and increasing their intake of antioxidants and carotenoids. Many of these steps, suggested by epidemiology studies, are the same ones prescribed to reduce a person's risk of heart attack and stroke. "There is a very similar risk profile for cardiovascular disease and AMD," says epidemiologist Johanna Seddon of Harvard Medical School.

If just a few genes account for almost all of the risk of getting AMD, that should also help in devising therapies that can slow or prevent vision loss in people with the disease. "If each gene contributed just 4% or 5%, developing a therapy [based on those genes] would be pretty much impossible," Hageman says. However, the new studies suggest a much brighter outlook for efforts to beat this devastating disease.

–JEAN MARX

CREDITS (TOP TO BOTTOM): NATIONAL EYE INSTITUTE, NATIONAL INSTITUTES OF HEALTH; ED HEFFRON

EDITED BY KELLI WHITLOCK BURTON

TV Tales

NO SURVIVOR. Former shuttle astronaut and biomedical engineer Dan Barry's run on the popular television series *Survivor* ended earlier this month when he failed to solve a crucial puzzle. That flop meant his team had to vote off one member, and he was chosen.

Barry, 52, who flew on the space shuttle three times and founded Denbar Robotics, says he was slotted to be "the nice old man with lots of integrity." He came across as a classy, standup guy who broke with reality-show tradition by taking responsibility for his team's defeat.

Barry says his time on the show, in which contestants live in the wild and compete for $1 million, was a useful exercise in group dynamics and adaptation to extreme environments with potential lessons for astronauts in stressful situations. But after enduring 15 days with little food, he says that it's lucky that the iguanas on the island are protected by the Panamanian government.

WINNERS

WADING INTO SCIENCE. For 6 months, Shannon Babb (below) arose before dawn to monitor water quality at a river near her home in Highland, Utah. Yesterday she collected a reward for those early-morning jaunts: first place in the annual Intel Science Talent Search and a $100,000 college scholarship.

Babb, a senior at American Fork High School, found low levels of dissolved oxygen, pill bugs, and traces of fertilizer runoff—all signs of an unhealthy river. Humans are the main culprit, says Babb, 18, who began monitoring water quality in area rivers when she was 13. Chemist Philip DeShong of the University of Maryland, College Park, who helped judge the 40 finalists, says that the longitudinal aspect of Babb's project was particularly notable: "She'd done it for 5 years, and she had gotten more and more complex every year." Yi Sun, 17, of the Harker School in San Jose, California, and Yuan "Chelsea" Zhang, 17, of Montgomery Blair High School in Silver Spring, Maryland, finished second and third, respectively.

PIONEERS

NEUROSCIENCE IN ECUADOR. A spouse often influences the other spouse's career. German neuroscientist Winfried Wojtenek's may influence science in an entire country.

Wojtenek was a postdoc at the University of Marburg in Germany when he received two job offers. One was from the University of Hawaii. With a sidelong glance at his wife, an Ecuadorian scientist, Wojtenek instead chose to start Ecuador's first neuroscience program.

Now, 2 years later, the undergraduate minor in neuroscience Wojtenek created at the Universidad San Francisco de Quito is on its way to becoming a master's-level program. Despite being what he calls "a First World country without money," Ecuador has a rich diversity of model organisms that makes for some interesting science. "We [have] the most fascinating ecosystems on Earth," he says.

MOVERS

HIGH TIDE. Japanese civil engineer Kuniyoshi Takeuchi has been named director of a new international center to study water-related disasters. Supported by UNESCO, the International Centre for Water Hazard and Risk Management (ICHARM) was inaugurated this month in Tsukuba, Japan.

"Studying hydrology in Japan, it was impossible to avoid the subject of water-related disasters," says Takeuchi, a professor of civil engineering at Yamanashi University in Kofu who's been involved with the center since it was first proposed 3 years ago.

ICHARM will develop inundation models and distribute them to countries to help forecast and mitigate damage. The center also will train researchers from developing countries to create flood-hazard maps.

Got a tip for this page? E-mail people@aaas.org

Three Q's >>

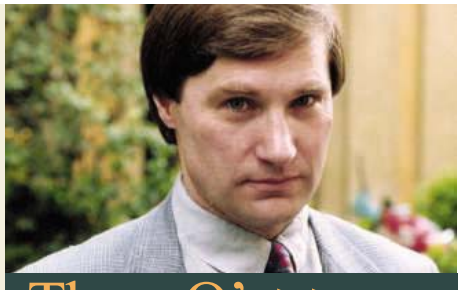

This year's Templeton Prize goes to John Barrow, a 53-year-old cosmologist at the University of Cambridge, U.K. The $1.4 million prize, awarded for "progress toward research or discoveries about spiritual realities," recognizes Barrow's musings on the anthropic principle, the idea that the universe has physical constants finely tuned to human existence because we could not otherwise be here to observe them.

Q: Some scientists argue that accepting the Templeton Prize is tantamount to blurring the line between science and religion. Did you have any qualms about accepting the prize?
No qualms. The prize has been going on for a long time, and there is a wide range of views about it. But if you look at the panel that selects the winner, there's no obvious pattern.

Q: What do you think scientists misunderstand most about religion?
Some scientists may think that religion equals creationism or Islamic fundamentalism, which would be a misunderstanding. Others may think, almost by definition, that religion is antiscience or that science and religion supply mutually exclusive explanations.

Q: What do you think is needed to bridge the gap between science and religion?
What's needed is mutual engagement. Seminaries should teach their students some science, and scientists need to make efforts to engage in discussions on subjects of common interest.

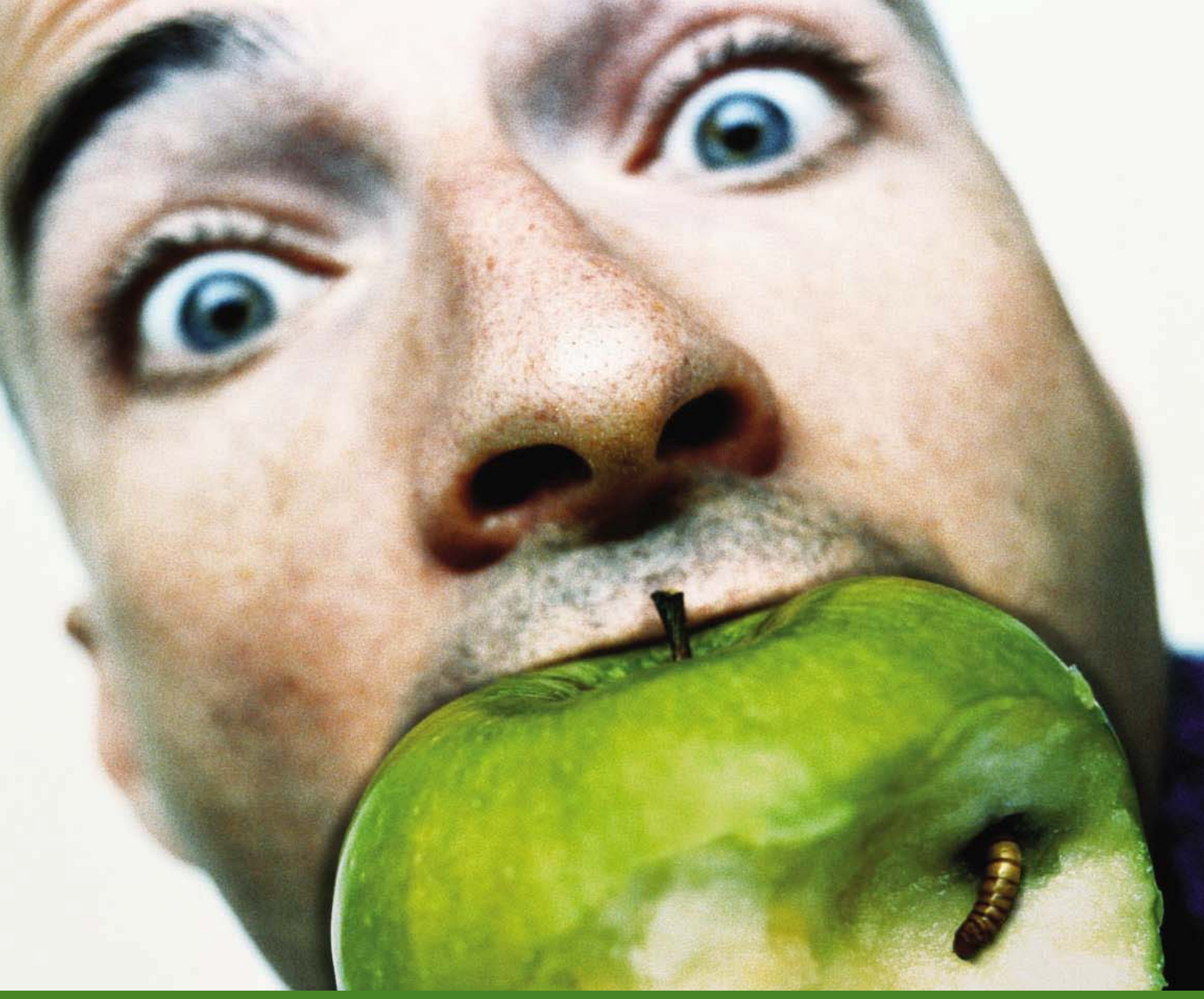

Is unexpected DNA worming its way into your RNA?

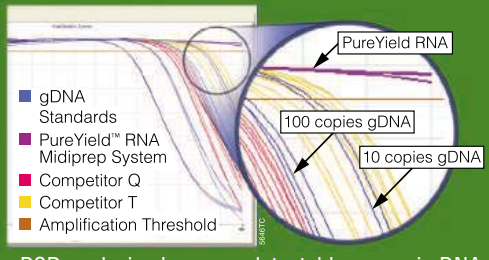

qPCR analysis shows no detectable genomic DNA contamination in PureYield™ RNA samples.

The PureYield™ RNA Midiprep System uses a novel, non-DNase method to remove genomic DNA prior to RNA isolation. PureYield reduces your chances of inaccurate results by eliminating DNA from your RNA preps. You get pure, total RNA with no detectable genomic DNA contamination. No surprises. No starting over.

Request a FREE sample* at: **www.promega.com/rna**

*Samples to qualified customers where available, while supplies last.

PROMEGA CORPORATION • www.promega.com

Promega

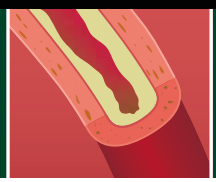

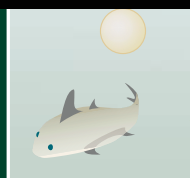

LETTERS

edited by Etta Kavanagh

How Many New Genes Are There?

IN THEIR REPORT "THE TRANSCRIPTIONAL LANDSCAPE OF THE MAMMALIAN GENOME" (2 SEPT. 2005, p. 1559), the RIKEN Genome Exploration Research Group and Genome Science Group (Genome Network Project Core Group) and the FANTOM Consortium claim to have found 5154 new proteins in the mouse genome not encoded by previously known mRNA sequences, which could potentially correspond to a considerable number of new protein-coding genes (4311, following clustering) (*1*). This claim contrasts dramatically with the view of the International Human Genome Sequencing Consortium (*2*), which estimated that there are 20,000 to 25,000 protein-coding genes. Since there are already 22,287 genes in the Ensembl 34d catalog, this implies 0 to 2713 new genes. RIKEN/FANTOM's estimate contrasts even more strikingly with our results using exon microarrays (*3*), in which the number of new multi-exon protein-coding genes was estimated to be at most in the hundreds. We analyzed the putative new FANTOM proteins (*4*), first by comparing their sequences with RefSeq release 13 from NCBI, NIH, and including only those transcripts that are linked to a reference published no later than 1 May 2005, thus excluding all the new FANTOM proteins. Restricting our analysis to the transcripts that have strong experimental evidence (labeled Provisional, Validated, or Reviewed), we found that 2917 (56.6%) of the FANTOM proteins are in fact splice isoforms of known RefSeq transcripts, with the majority of them (2716) corresponding to exon-skipping events. By then including predicted RefSeq transcripts (labeled Genome Annotation, Inferred, Model, Predicted) in our analysis, 3568 (69.2%) were found to be splice isoforms of known transcripts. By including GenBank mRNAs linked to publications before 1 May 2005, we found an extra 303 splice isoforms, bringing the total of already-annotated genes to 3871 (75.1%). Moreover, of the 5154 FANTOM proteins, our microarray analysis detected 2293 (by two or more exons), 144 of which are among the remaining 1283 FANTOM proteins and most (131) of which are associated with known genes. We next asked whether the remaining 1193 putative proteins could be accounted for as false detections. The median open reading frame (ORF) size in this set is 119 amino acids (aa), significantly shorter than that of all the FANTOM proteins (330 aa). Although many real proteins have a length less than 119 aa, we hypothesized that such a short ORF length can arise in noncoding transcripts by chance. The FANTOM Consortium identified 23,218 nonoverlapping, noncoding transcripts, so to test this hypothesis we generated a set of 20,000 random cDNAs of 2000 bases (typical gene length) and found that 1247 of them had ORFs of 119 aa or more. Therefore, it is possible that a large portion of the remaining 1193 putative proteins arose at random from noncoding transcripts and may not encode functional polypeptides. On the basis of this analysis, the number of completely new protein-coding genes discovered by the FANTOM Consortium is at most in the hundreds, consistent with current estimates based on both sequence and microarray analysis (*2*, *3*).

> **"...the number of completely new protein-coding genes discovered by the FANTOM Consortium is at most in the hundreds..."**
>
> —Lee *et al.*

LEO J. LEE,[1] TIMOTHY R. HUGHES,[2] BRENDAN J. FREY[1]

[1]Department of Electrical and Computer Engineering and [2]Banting and Best Department of Medical Research, University of Toronto, 10 King's College Road, Toronto, ON M5S 3G4, Canada.

References and Notes

1. FANTOM3 cDNA sequences are not provided, but the protein sequences can be downloaded from http://fantom3.gsc.riken.jp/.
2. International Human Genome Sequencing Consortium, *Nature* **431**, 931 (2004).
3. B. J. Frey *et al.*, *Nat. Genet.* **37**, 991 (2005).
4. See www.psi.toronto.edu/TransLand for details.

Response

LEE *ET AL.* POINT OUT THAT THE NUMBER OF reported protein sequences in FANTOM3 that map to new positions on the genome appears to be too large. We are grateful to them for highlighting this discrepancy, which we investigated and thus discovered an error. For a detailed description of the correction, see the Corrections and Clarifications section in this issue. The effect of the error is somewhat less than suggested by Lee *et al.* In particular, our estimate of the number of new protein-coding genes found by us has been revised from 5154 to 2222, a reduction of more than half, but much less than the order of magnitude suggested by Lee *et al*. As correctly pointed out, the rest of the 5154 cDNAs are mainly alternatively spliced isoforms.

Lee *et al.* present three forms of evidence: sequence similarity, exon microarray data, and ORF size. (i) The sequence homology data largely reflect the revision to the number that we mention above, except that Lee *et al.* used a recent RefSeq database, whereas we used Genbank (7 January 2004). There is no evidence that all RefSeq sequences correspond to real transcribed RNAs because they often include ab initio predicted exons (*1*). Our strategy was to construct the transcriptional frameworks entirely based on real RNA transcripts, rather than in silico reconstruction of putative gene structures. (ii) The exon microarray data concern less than 3% of the number

> **"...the number of new protein-coding genes found by us has been revised from 5154 to 2222..."**
>
> —FANTOM Consortium

of discussed proteins and do not have any impact on the global message of a project of the scale of FANTOM3. Despite Frey *et al.*'s impressive computational reconstruction of gene structure by analyzing expression patterns of ab initio predicted exons (*2*), we argue that this does not prove the physical structure of each mRNA and the complexity of the transcriptome with the same resolution achieved by sequencing libraries derived from mRNAs. In fact, our data show that "genes" have multiple starting and termination sites: We have conservatively identified at least 181,000 different RNA transcripts. Additionally, Frey *et al.* (*2*) used only computationally predicted exons. Rare, newly discovered transcripts are unlikely to have been in the training sets of ab initio exon identification tools, and their sensitivity to predict rare transcriptional events is not obvious. (iii) As for ORF size, 119 amino acids is a perfectly respectable size for a protein and within the bounds of statistical variation we expect. In this regard, we have further identified in the FANTOM3 dataset at least 1100 proteins shorter than 100 amino acids (*3*). Also, all of the novel FANTOM3 transcripts have been manually curated by individual researchers to distinguish them from novel noncoding RNAs. In any case, our final understanding of the number of protein-coding mRNAs will derive from experimental validation with full-length cDNA clones (*3*) rather than computational inferences. We direct interested parties to the relevant section of the FANTOM3 Web site (http://fantom.gsc.riken.jp) where the updated files are available, and we thank Lee *et al.* for helping us to improve and update our analysis.

PIERO CARNINCI,[1,2] JULIAN GOUGH,[1] TAKEYA KASUKAWA,[1,3] YOSHIHIDE HAYASHIZAKI[1,2]

[1]Laboratory for Genome Exploration Research Group, RIKEN Genomic Sciences Center (GSC), RIKEN Yokohama Institute, 1-7-22 Suehiro-cho, Tsurumi-ku, Yokohama, Kanagawa, 230-0045, Japan. [2]Genome Science Laboratory, Discovery and Research Institute, RIKEN Wako Institute, 2-1 Hirosawa, Wako, Saitama, 351-0198, Japan.[3]NTT Software Corporation, Teisan Kannai Building 209, Yamashita-cho, Naka-ku, Yokohama, Kanagawa, 231-8551, Japan.

References

1. X. Pruitt *et al.*, *Nucleic Acids Res.* **33,** D501 (2005).
2. B. Frey *et al.*, *Nat. Genet.* **37**, 991 (2005).
3. M. Frith *et al.*, *Plos Genet.*, in press.

Why Suicide Rates Are High in China

WE READ WITH INTEREST G. MILLER'S ARTICLE describing a discrepancy between Chinese rates of suicide and depression ("China: healing the metaphorical heart," News Focus, 27 Jan., p. 462). However, we feel that Miller, by concentrating on fatal self-harm rather than all acts of self-harm, misses an opportunity to understand the discrepancy he notes.

High rates of suicide and low rates of depression are not restricted to China. Many countries of the Asian "suicide belt" have suicide rates higher than those of China (*1*, *2*).

Suicide rates result from the incidence of self-harm and the resulting fatality rate among those individuals. Our research in Sri Lanka indicates that high rates of suicide from self-poisoning are due to a high fatality rate rather than a high incidence of self-harm itself (*3*). A useful contrast can be made with the UK.

Self-poisoning in the UK is very common, with an annual incidence of presentation to hospital of around 300 per 100,000. However, self-poisoning is rarely lethal, with a fatality rate per 1000 incidents normally less than 0.5% (*4*). Self-poisoning is also common in Sri Lanka, with an estimated incidence of around 363 per 100,000 in one rural district. However, the fatality rate is significantly higher at ~7.4%—at least 15 times higher than in the UK (*3*). The reason for this higher fatality rate in Sri Lanka, as in China, is the common use of highly toxic poisons such as pesticides. Sri

Lankan self-poisoners are not more keen to die—they simply have easier access to pesticides than do the residents of the UK (*5*).

The high suicide rate in Sri Lanka and China is not due to higher levels of mental illness or rates of self-harm, but to a higher lethality of self-harm acts. Concentrating solely on rates of mental illness in Asia will not explain the high rate of suicide in this region.

MICHAEL EDDLESTON[1]* AND DAVID GUNNELL[2]

[1]Centre for Tropical Medicine, Nuffield Department of Clinical Medicine, University of Oxford, Oxford OX3 9DU, UK. [2]Department of Social Medicine, University of Bristol, Bristol BS8 2PR, UK.

*To whom correspondence should be addressed. E-mail: eddlestonm@eureka.lk

References

1. P. Brown, *New Sci.*, 22 Mar. 1997, p. 34.
2. A. Joseph *et al.*, *Br. Med. J.* **326**, 1121 (2003).
3. M. Eddleston *et al.*, *Bull. World Health Org.*, in press.
4. D. Gunnell, D. D. Ho, V. Murray, *Emergency Med. J.* **21**, 35 (2004).
5. M. Eddleston *et al.*, *Clin. Toxicol.*, in press.

CORRECTIONS AND CLARIFICATIONS

BOOKS *ET AL.*: "Humanity usurps nature" by B. Chameides (10 Mar., p. 1379). The affiliation information is incorrect. Bill Chameides is at Environmental Defense, 257 Park Avenue South, New York, NY 10010, USA. E-mail: BChameides@environmentaldefense.org

REPORTS: "The transcriptional landscape of the mammalian genome" by the FANTOM Consortium *et al.* (2 Sept., p. 1559). On page 1561, column 3, lines 40–46 should read: "In the FANTOM3 data set, 11,559 protein sequences are newly described. Their splice variants were grouped together into 7445 TKs (transcriptional frameworks). For 5453 of these, a previously known sequence maps to the same TK (locus), but 1992 clusters (2222 different proteins) map to new TKs (see SOM text 3)."

NEWS FOCUS: "With energy to spare, an engineer makes the case for basic research" by E. Kintisch (10 Mar., p. 1369). The National Superconducting Cyclotron Laboratory at Michigan State University was incorrectly identified as being supported by the Department of Energy. The NSCL is a campus-based national user facility funded by the National Science Foundation.

TECHNICAL COMMENT ABSTRACTS

Comment on "Changes in Tropical Cyclone Number, Duration, and Intensity in a Warming Environment"

Johnny C. L. Chan

Analyses of tropical cyclone records from the western North Pacific reveal that the recent increase in occurrence of intense typhoons reported by Webster *et al*. (Reports, 16 September 2005, p. 1844) is not a trend. Rather, it is likely a part of the large interdecadal variations in the number of intense typhoons related to similar temporal fluctuations in the atmospheric environment.

Full text at www.sciencemag.org/cgi/content/full/311/5768/1713b

Response to Comment on "Changes in Tropical Cyclone Number, Duration, and Intensity in a Warming Environment"

P. J. Webster, J. A. Curry, J. Liu, G. J. Holland

Although Chan makes several valid points, his analysis confuses relationships associated with the long-term variations with those associated with shorter term variability (interannual and decadal). We present an analysis that clarifies the observations from the western North Pacific.

Full text at www.sciencemag.org/cgi/content/full/311/5768/1713c

Letters to the Editor

Letters (~300 words) discuss material published in *Science* in the previous 6 months or issues of general interest. They can be submitted through the Web (www.submit2science.org) or by regular mail (1200 New York Ave., NW, Washington, DC 20005, USA). Letters are not acknowledged upon receipt, nor are authors generally consulted before publication. Whether published in full or in part, letters are subject to editing for clarity and space.

MOVIES: PRIMATOLOGY

The Greatest of Apes

Guy Cowlishaw

Among our closest cousins, there is no ape more famous than King Kong. Since his first appearance in Merian C. Cooper and Ernest B. Schoedsack's classic 1933 film (RKO Pictures), King Kong has roamed widely in our cultural conscience, making innumerable appearances in movies, books, cartoons, toys, and video games and so becoming a household name. Kong's extraordinary success has made him one of the most powerful of modern myths, veritably "the eighth wonder of the world."

King Kong
by Peter Jackson
Universal Pictures, Universal City, CA, 2005. 187 minutes.
www.kingkongmovie.com

New Zealander Peter Jackson, the Oscar-winning director of the *Lord of the Rings* trilogy, has taken the story of King Kong and lovingly retold it for contemporary audiences. The film revolves around music-hall performer Ann Darrow (Naomi Watts), playwright Jack Driscoll (Adrien Brody), and obsessive film director Carl Denham (Jack Black). Denham hires Darrow and Driscoll and charters a ship that, with the aid of an old map, takes them to the location of his next movie, Skull Island: an uncharted landmass west of Sumatra and the primal rainforest kingdom of Kong. The discovery of a giant gorilla on such a remote island is not quite as far fetched as it might seem (although, admittedly, Skull Island's biogeographic position suggests that a giant orangutan would have been more likely). Island gigantism is a well-documented phenomenon, exemplified by species such as the moa and komodo dragon, and giant island primates have existed until quite recently. One genus of extinct lemur, *Archaeoindris*, exceeded the size of modern-day gorillas and only disappeared a thousand years ago, after people first arrived on Madagascar.

Once ashore, the film crew is savagely attacked by the islanders, and Darrow is subsequently kidnapped and sacrificed to Kong. Initially, as the giant gorilla claims his prize, we only catch him in glimpses. But then, at last, we see Kong in all his glory. And he is magnificent. Digitally animated from an inspired performance by actor Andy Serkis (Gollum in *The Lord of the Rings*), Kong's character and moods are richly created through vocalization, facial expression, and body language. Kong becomes obsessed with Darrow, and their relationship becomes the centerpiece of the film's narrative. In a delicious twist of irony, the roles were reversed during Serkis's research at London Zoo: a female gorilla called Zaire became infatuated with him, and when his wife visited him at work, Zaire threw a jealous tantrum.

As Darrow attempts to escape from Kong, and the film crew and sailors endeavor to rescue her, we come face-to-face with some of the other denizens of Skull Island. Cooper envisaged Kong as a survivor from prehistoric times. (In this, he anticipated the 1935 discovery of fossils of the largest ape known to have ever lived, *Gigantopithecus blacki*. Somewhat smaller than Kong, it too ranged in the tropical forests of Asia, in coexistence with *Homo erectus*.) Other ancient creatures also escaped extinction on Skull Island, and dinosaurs play a prominent role in an ensuing series of jaw-dropping—quite literally for Darrow—sequences. Nevertheless, the movie's most gruesome moment comes in a gorge filled with giant cockroaches and carnivorous worms. Several of the rescue party come to a grisly end in this terrifying episode, which was also filmed for but then cut from the 1933 original due to its harrowing content.

Kong keeps Darrow alive, and a strong bond of affection grows between them. But eventually she is rescued by Driscoll, and Kong is brutally captured. Denham takes him to New York and exhibits him in a flamboyantly tasteless music hall show. Kong escapes and runs amok until he is reunited with Darrow. Finally, in search of the solitude of the high mountain crags of Skull Island, Kong climbs with Darrow to the summit of the Empire State Building. There, as the first rays of dawn rake across the skyline, the peace is broken by the whine of approaching biplanes….

What is it about King Kong that makes the giant gorilla so memorable? Our reverence for primates is not a new phenomenon. Thousands of years ago, the Nazca people inscribed a vast monkey on the desert plains of Peru, and in early Egypt the baboon was venerated as a sacred animal. Some ancient traditions still flourish today: Hanuman the Hindu monkey god and the Monkey King of Chinese legend (both of whom, like Kong, epitomize strength and courage) are popular living heroes. A modern folklore also persists about mysterious undiscovered apes (the yeti, sasquatch, and orang pendek). Perhaps Kong shares roots with all these traditions, which may in turn reflect the close kinship between ourselves and other primates.

But King Kong is a monster as well, and our fascination with monsters is also an ancient one. Kong exhibits a winning combination of monster traits—large, ferocious, and unknown—so it is perhaps no surprise that we should find him so unforgettable. Yet why should monsters have this allure in the first place? One likely explanation is that it is because we obtain a sense of relief and elation when they are defeated. However, this does not account for the appeal of Kong, who is an altogether different beast. Although a monster, Kong is not evil but an innocent, and we empathize with his tragic plight. Monsters like Kong, which are rich in pathos, therefore give us the opportunity to express our own humanity. Such compassion may also help us to avoid a grim Nietzschean fate: that in the process of overcoming and destroying monsters, we might otherwise become monsters ourselves.

CREDIT: UNIVERSAL/WING NUT FILMS/THE KOBAL COLLECTION

Jackson's *King Kong* is a moving story of a terrible but majestic beast that is tamed and ultimately killed by a "civilized" society. But this is not all. The director has also given us a powerful modern fable about the ferocity and beauty of wild nature and our destructive exploitation of it. King Kong dies, but in the end it is clear that we too are the losers. The importance of this message cannot be understated at a time when, through habitat destruction and hunting, we are in the process of destroying the very animals that are so valuable to us, that inspire us and enrich our lives.

The reviewer is at the Institute of Zoology, Zoological Society of London, Regent's Park, London NW1 4RY, UK. E-mail: guy.cowlishaw@ioz.ac.uk

10.1126/science.1125822

BOTANY

Conservation Lessons from Herbaria

Mike Maunder

The great natural history museums are indeed alive, and they are actively demonstrating their roles in conservation and sustainable development. This is particularly the case for herbaria, reference collections of preserved plants. In terms of fundamental infrastructure, this often overlooked set of facilities would still be recognizable to the 16th-century Italian physician and botanist Luca Ghini, who is credited as the inventor of the herbarium. While the dried plant specimens still sit in folders within cabinets, the use and value of those specimens have changed beyond recognition over the past 20 or 30 years. Ghini did not need to worry about extinctions and the destruction of the plant resources that underpin sustainable development—problems that are the focus of *Plant Conservation: A Natural History Approach*, edited by Gary A. Krupnick and W. John Kress.

Plant Conservation
A Natural History Approach

Gary A. Krupnick and W. John Kress, Eds.

University of Chicago Press, Chicago, 2005. 380 pp. $75, £47.50. ISBN 0-226-45512-2. Paper, $30, £21. ISBN 0-226-45513-0.

The editors are curators in the Department of Botany at the Smithsonian Institution's National Museum of Natural History. They have assembled a team of colleagues (from the Smithsonian) and collaborators (from other U.S. institutions, Germany, Britain, Venezuela, and Brazil) to produce a useful, authoritative, and highly readable review of issues affecting the conservation of botanical diversity. In the foreword, Dan Janzen sets the tone through positioning the urgency of real-world conservation problems against the need to make botanical information both readily available and relevant. Chapters in the first two of the volume's four sections take this challenge forward through placing botanical diversity in its geological and geographic contexts. Particularly interesting are the short natural history essays in which contributors review case studies of selected tropical and subtropical habitats (e.g., the Ecuadorian Andes, oceanic islands in the Pacific, and mountains in southwest China) and taxonomic groups (e.g., dinoflagellates, lichens, mosses, grasses, and African violets). In the third section, the authors consider the causes of contemporary extinctions of plants. These chapters offer a series of geographical case studies of habitat degradation and fragmentation as well as brief overviews of aspects of invasive species, climate change, and population genetics. I found the contributions on the diversity, ecology, and conservation of marine plants such as coral reef algae and kelp communities especially welcome.

The fourth part of the book examines biodiversity assessments, management strategies, and conservation actions. Sadly, the chapter on the mapping of biological diversity manages to underplay the expertise resident in the Smithsonian. Readers looking for practical guidance on conserving plant diversity will be disappointed with the review of conservation responses, because the topics of species conservation and recovery management are poorly covered. This section would have benefited from some case studies illustrating the value of museum collections to conservation (e.g., protected areas planning based on museum records or the application of DNA technology to species conservation).

Written predominantly by systematists and taxonomists, the volume offers a very useful perspective on the complex issues of plant conservation and the debates over what must be done to preserve botanical diversity. Many readers will find the early chapters on the evolutionary context of plant diversity especially informative and the geographic and taxonomic case studies fascinating. For example, we finally learn whether or not the endemics Al Gentry found on western Ecuador's Centinela Ridge before its nearly complete deforestation are extinct: "a number of the seemingly site-specific plants have now turned up in surrounding areas." Krupnick, Kress, and the contributors have produced an excellent overview that will serve as both a reference for conservation professionals and a great resource for university teaching. I hope the volume is regularly updated. One clear message from *Plant Conservation* is that although natural history museums and taxonomic institutions may not actually be implementing front-line practical conservation, they are the custodians and translators of vast reservoirs of essential information that will guide the work of conservationists. That important point is too often forgotten.

10.1126/science.1125541

Lost diversity. *Watsonia distans*, an endemic species from the western Cape region of South Africa, can now be found only in herbaria.

CREDIT: COURTESY U.S. NATIONAL HERBARIUM, SMITHSONIAN INSTITUTION

The reviewer is at the Fairchild Tropical Botanic Garden, 10901 Old Cutler Road, Coral Gables, FL 33156, USA. E-mail: mmaunder@fairchildgarden.org

BROWSING

Ice. The Nature, the History, and the Uses of an Astonishing Substance. Mariana Gosnell. Knopf, New York, 2005. 578 pp. $30, C$42. ISBN 0-679-42608-6.
Early in this comprehensive exploration of the world of ice, Gosnell explains what separates her subject from snow. On the ground, snow is permeated by continuous chanels of air, whereas in ice the air is restricted to unconnected bubbles. Much further along, she discusses snow among the various kinds of ice that "materialize out of the sky" (along with freezing rain, sleet, rime, hail, and frost). Packed with facts, the book combines engaging descriptions of technical material (e.g., nucleation process of freezing water, melting, humans' physiological responses to cold, and icing of airplane wings), literary snippets (from books, poems, and films), and human-interest stories (e.g., ice sports, the sinking of the *Titanic*, and adventures clearing ice roads over frozen waterways). There are accounts of ices I through XII, potential losses of ice due to global warming, and 18 words Newfoundlanders have for ice. The author organizes her material into categories on ice in lakes, rivers, glaciers, icebergs, plants, animals, recreation, the atmosphere, and space. Nonetheless, readers who do not share her obsession with frozen water may prefer to use the index to pick and choose from this encyclopedic treatment.

SCIENCE AND LAW

Intellectual Property and Human Embryonic Stem Cell Research

The history of U.S. stem cell patents illuminates their potential as research barriers and possible vulnerabilities.

Jeanne F. Loring and Cathryn Campbell

On 9 August 2001, U.S. President George W. Bush directed that federal funding could be used for human embryonic stem (HES) cell research, but only for the small number of ES cell lines then in existence (listed on the National Institutes of Health Stem Cell Registry) (*1*). In reaction to the limitations, individual states and private foundations are designating funds to support research on the much larger number of HES lines that were derived after the President's deadline. Although these funding sources sidestep the strictures of the President's order, they do not remove what may ultimately prove a more daunting barrier to progress in this field: the intellectual property rights for HES cells. This commentary describes two fundamental patents that cover HES cells in the United States and highlights their implications for HES cell research.

What are the patents on HES cells? Three years before the presidential directive, the U.S. Patent and Trademark Office (PTO) issued a broad patent claiming primate (including human) ES cells, entitled "Primate Embryonic Stem Cells" (Patent 5,843,780). On 13 March 2001, a second patent (6,200,806), with the same title but focused on HES cells, issued from a "divisional application" (*2*).

These two patents have considerable consequence for HES cell research in the United States, because they have claims to ES cells themselves, not just a method of deriving them. The claims give the patent owner, the Wisconsin Alumni Research Foundation (WARF) the legal right to exclude everyone else in the United States from making, using, selling, offering for sale, or importing any HES cells covered by the claims until 2015. The right of exclusivity is rooted in the U.S. Constitution (*3*) and was intended to benefit society by encouraging innovation while discouraging secrecy on the part of inventors.

No other country has allowed HES cells to be so broadly patented, and although the U.S. patent rights can only be enforced within the United States, HES cells made in another country become subject to U.S. patent law if they are imported into the United States. Although a patent application with the same claims was filed in other countries, the claims have issued as a patent only in the United States. This may be in part because the United States has a 1-year grace period to file after an invention has been publicly disclosed. This means that a newspaper article that appeared in November 1994 in the *Milwaukee Journal*, was considered to be prior art by non–U.S. patent filings, but not for the U.S. patent application. Another factor is whether the European Patent Convention prohibition on patenting human embryos covers HES cells, an issue currently before the Board of Appeals of the European Patent Office (*4*).

What is protected? The most important part of a patent is a list of claims, which are carefully crafted descriptions of the invention that define the limits of patent protection. The broadest claim of both the 1998 and 2001 patents is claim 1, which claims the "composition of matter" of ES cells. The 1998 patent (*2*) reads as follows:

"We claim: 1. A purified preparation of primate embryonic stem cells which (i) is capable of proliferation in an in vitro culture for over one year, (ii) maintains a karyotype in which all the chromosomes characteristic of the primate species are present and not noticeably altered through prolonged culture, (iii) maintains the potential to differentiate into derivatives of endoderm, mesoderm and ectoderm tissues throughout the culture, and (iv) will not differentiate when cultured on a fibroblast feeder layer." Composition of matter claims are generally more powerful than method claims because they cover the matter itself, regardless of how it is made or used. As the characteristics listed in claim 1 in the 1998 patent describe the essence of ES cells, the patent effectively covers all ES cell lines regardless of who makes them or how they are generated. How is it possible to claim ES cells when they are products of nature rather than of manufacture? The U.S. patent law allows claims to a "form" not found in nature, so claims for an "isolated" or "purified" preparation are acceptable.

How did HES cells become patented? To the nonlawyer, the process that led to patenting HES cells is an intriguing primer in how the U.S. patent system works. On 20 January 1995, WARF filed a patent application for primate ES cells on behalf of James Thomson, an assistant professor at the University of Wisconsin Primate Center. The application described work that was submitted for publication 3 days later and published today (*5*). A separate application may contain the same data as a scientific manuscript, but the patent application uses the data to support claims that are much broader than the actual results. In this case, on the basis of experiments deriving ES cells from only two species of nonhuman primates, the application claimed ES cells that derived from a larger group of primate species, including humans.

At the PTO, an examiner was assigned to determine whether patenting was justified. A year later, on 17 January 1996, the examiner rejected all 11 of the original claims, explaining that there was ample earlier published literature that made the claims obvious (*6*–*8*). Such rejections are a routine part of the discourse between the applicant and the PTO, and WARF responded with arguments that the claims were novel. However, just 1 day after the claims were rejected, the WARF attorneys filed a second U.S. patent application with the identical title and claims as the one undergoing examination. This application was filed as "a continuation in part" (CIP) of the earlier application (*9*). The CIP was assigned to a different examiner, so for another 2 years while attorneys continued to argue for patentability of both applications, two different PTO examiners were examining the same claims in separate applications.

The examiner for the original parent application continued to reject the claims and the original application was abandoned in December 1997. However, in March 1998, the second examiner determined that the identical claims were allowable. Before the patent was issued, however, there was one more hiccup in the procedure. On 18 November 1998, John Doll, who was then director of the examining group responsible for the application (he is now commissioner of patents), sent a memorandum to the patent publication office to stop the issuance procedure. But the memo did not reach the publication office in time, and, with the claims intact, the PTO issued the patent on 1 December 1998.

A separate (but highly related) patent application was undergoing examination at the same time. On 26 June 1998, WARF had filed a "divisional" (*10*) application, which was also entitled "Primate Embryonic Stem Cells." The claims were virtually identical to the pending patent, but with the term "human" substituted for "primate." This application went relatively smoothly through the examination process, and the patent was issued on 13 March 2001 (Patent

J. F. Loring is at the Burnham Institute for Medical Research, La Jolla, CA 92037, USA. C. Campbell is with McDermott Will & Emery, LLP, Washington, DC 90005, USA. E-mail: jloring@burnham.org (J.F.L.) and ccampbell@mwe.com (C.C.).

6,200,806). This heterogeneity in handling reflects the realities of the U.S. PTO. The existence of two (or more) issued patents with the same title is not unusual, but it can be confusing; the important information to keep in mind is that the claims in the 1998 patent cover both nonhuman primate and human primate ES cells, whereas the similar claims in the 2001 patent apply only to human cells. Since 2001, there have been four more continuations of the original application filed with the PTO, all entitled "Primate Embryonic Stem Cells" (*11*).

How do fundamental HES cell patents affect scientific research? Although many patent holders choose to license others to practice the patented invention in exchange for royalties, in the United States, licensing is not compulsory; patent holders can choose to license on their own terms or not to license at all. Because WARF controls the rights to HES cells, researchers who wish to use these cells must be aware of their obligations to the patent owners under U.S. law. The NIH took steps to engage WARF's cooperation shortly after the presidential announcement, signing a memorandum of understanding (MOU) with WARF. The NIH retains rights to the 1998 (-780) patent, because the work was supported by federal grants (*12*). This MOU gave researchers employed by the NIH, the Food and Drug Administration, and the Centers for Disease Control and Prevention a license to use HES cells for research. Also, WARF agreed that it would not impose more restrictive terms for any other not-for-profit institutions. In early 2002, the NIH made similar MOU agreements with other groups that had made lines that were eligible for funding, including the University of California at San Francisco, Mizmedi (Korea), BresaGen (Australia), Technion (Israel), Cellartis (Sweden), and ES Cell International (Singapore). These institutions received Infrastructure grants from the NIH of about $200,000 to $500,000 a year (*13*) to facilitate the distribution of their own HES cell lines under a license from WARF, and were limited by the MOU to charge no more than $5000 (or $6000 for foreign shipping to the United States) per cell line.

Currently, WARF requires a license agreement for distribution of any HES cell lines in the United States, whether or not they are on the NIH registry. The Harvard HES cell material transfer agreement (MTA) (*14*), for example, requires that the recipient of their cell lines acknowledges WARF's patent rights. Only the institutions that have MOUs with the NIH have price regulations; other suppliers of HES cells can charge as much or as little as they wish for the cells. Harvard charges nothing for its lines. However, because the WARF patents are only valid in the United States, non–U.S.-based HES researchers do not need a license unless they import the cells into the United States.

As a result of an NIH contract to serve as the main distribution center for HES cells in the United States, WARF recently reduced the price of cells to $500 for academic investigators, and opened the possibility of rebates for investigators who had paid $5000 before the contract went into effect (*15*). Although the academic price is now less onerous, the situation for commercial biotechnology and pharmaceutical companies remains difficult. First, because the biotechnology company Geron funded the patented HES cell derivations, they received an exclusive license for broad therapeutic use in the United States of HES cell–derived cardiac, nervous system, and pancreatic cells. This means that if a company wishes to develop therapies in these areas, they must negotiate with Geron for fees and royalties. But what if a company simply wants to use the ES cells for basic research? Even if the company's research is noncommercial, WARF still requires a commercial license, which costs an upfront fee (typically $125,000), with $40,000 annual maintenance fees to retain the license. This fee gives commercial entities the same research freedom as academic researchers, and, with negotiated royalty payments, they may commercialize reagents for research. Two companies, Becton-Dickinson and Chemicon, announced that they have obtained research licenses from WARF.

The research license cost has complicated the situation for start-up biotechnology companies that want to obtain NIH funding for HES cell research. Small companies may find themselves in what we call the "SBIR paradox." The NIH is willing to fund HES cell research through its Small Business Innovative Research (SBIR) program, but the company is not allowed to use NIH money, usually $100,000 for a phase 1 SBIR (R43), to pay WARF for a commercial research license. Therefore, the company must come up with separate funding of perhaps $125,000 for a license to do the NIH-funded research with the cells. As a result of discussions with the NIH, WARF has offered to take equity instead of cash for a license in some cases.

Are the WARF patents enforceable? When a U.S. patent is issued, it is presumed to be valid. However, if the patent holder sues another entity for allegedly infringing their patent, the defendant often raises the issue of the patent's validity. The court gives some degree of deference to the decision of the PTO, but the courts can and do sometimes find that a patent is invalid. The WARF patents have not yet been tested in court.

There are also procedures that can be raised against a patent through the PTO itself. When more than one party files patents claiming the same subject matter, the U.S. patent laws specify that the rights to a patent will be awarded to "first to invent." This contrasts with virtually all other countries, which give rights to an invention to the party that was the first to file a patent application. When an issued patent and another pending application claim the same subject matter, the applicant of the pending application can seek to provoke an "interference," which is a PTO procedure to determine who was the first to invent.

In December of 2003, a request for interference was filed against the claims to purified stem cell preparations in both the 1998 and 2001 WARF patents. Two patents that are licensed to Plurion (U.S. Patent 5,690,926 and 5,670,372) have issued from a 1992 application claiming methods of deriving pluripotent cells. A pending application with the same priority date claims the isolated pluripotent stem cells themselves. When the PTO indicated that the Plurion composition of matter claims were allowable, the applicant filed a request for interference, asserting that these claims overlap (and predate) the WARF pluripotent stem cell claims. Although no interference has yet been declared, the outcome of this case may have important consequences for ES cell researchers, funding agencies, and companies.

References and Notes

1. Registry (http://stemcells.nih.gov/research/registry/).
2. The patents and all of the official correspondence and documents (called File Wrappers) can be found at this PTO site: (www.uspto.gov).
3. U.S. Constitution, Article 1, Section 8, "the Congress shall have the power [t]o promote the Progress of Science and useful Arts, by securing for limited Times to Authors and Inventors the exclusive Right to their respective Writings and Discoveries."
4. G. Vogel, *Science* **305**, 1887 (2004).
5. J. A. Thomson *et al*., *Proc. Natl. Acad. Sci. U.S.A.* **92**, 7844 (1995).
6. The examiner noted a newspaper article that predated the application (*7*), and cited several scientific publications, most notably Bongso *et al*. (*8*).
7. P. Raeburn, "Embryonic monkey cells isolated," Associated Press, *Milwaukee Journal*, 4 November 1994.
8. A. Bongso, C. V. Fong, S. C. Ng, S. Ratnam, *Hum. Reprod.* **9**, 2110 (1994).
9. For a continuation in part application, material from the original application ("the parent") was given the benefit of the original filing date, while additional information that may have been provided was given the priority date of the new application.
10. A divisional application is a later application for a distinct invention that claims only a portion of the subject matter disclosed in the parent application. In this case, among the primates, only the human was claimed.
11. Patents 09/982,637, filed 10/18/2001; 10/430,496, filed 5/06/2003; 11/033,335, filed 1/11/2005; 11/036,245, filed 1/14/2005.
12. The patent states: "This invention was made with United States government support awarded by NIH NCRR Grant No. RR00167. The United States government has certain rights in this invention." The principal investigator on this grant was John P. Hearn, the Director of the NIH Regional Primate Research Center.
13. Data from NIH Center for Scientific Review: (http://grants1.nih.gov/grants/award/state/state.htm).
14. (www.mcb.harvard.edu/melton/hues/HUES_request.html).
15. (http://stemcells.nih.gov).

10.1126/science.1120953

ENDOGEN® SEARCHLIGHT®

SearchLight® Analysis Service

Put SearchLight® Technology to Work for You

With Our Multiplex Protein Analysis Service

- Design your own array from a menu of over 200 protein biomarkers
- Ship serum, plasma, culture supernatant, BAL, CSF, amniotic fluid, tissue homogenates, and other noninfectious samples overnight on dry ice
- Receive quantitative data in 5 to 10 business days

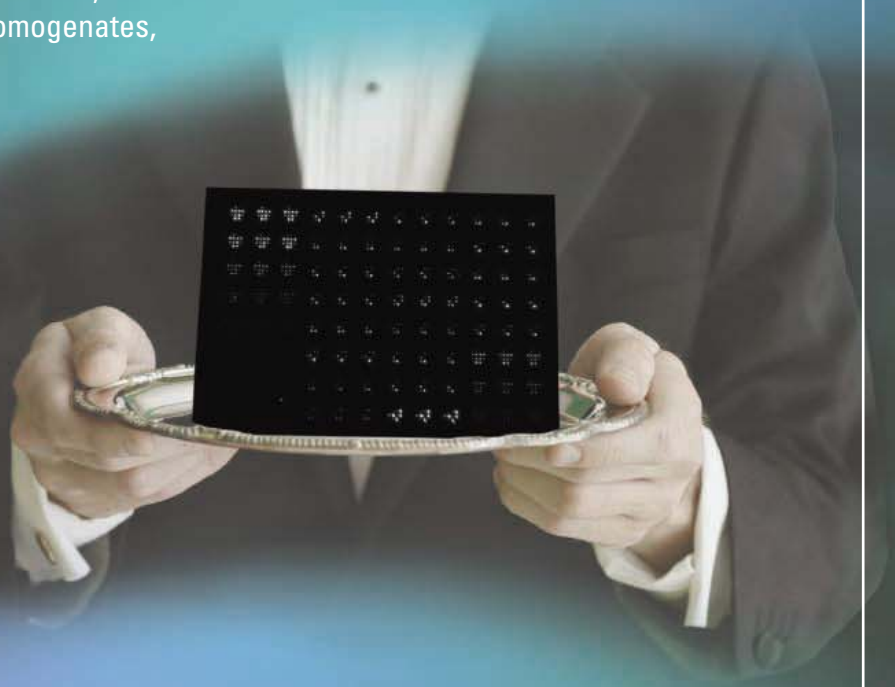

The SearchLight® Service Offers...

- **Sensitive**, chemiluminescent detection (sensitivity of <0.8 pg/ml for many analytes)
- **Accurate,** quantitative data based on testing in duplicate at a minimum of two sample dilutions
- **Specificity** testing on each new antibody combination
- Over five years of **experience** testing thousands of samples
- **Competitive** pricing with a minimum order of only 10 samples

www.endogen.com/searchlight

ENDOGEN®

Tel: 815-968-0747 or 800-874-3723 • Fax: 815-968-7316
Customer Assistance E-mail: CS@endogen.com

For distributors outside the U.S. and Europe, visit www.endogen.com

For European offices and distributors, visit www.perbio.com

PERBIO

CLIMATE CHANGE

Greenland Rumbles Louder as Glaciers Accelerate

Flow rates of many large glaciers in Greenland and Antarctica have accelerated recently. Greenland earthquakes produced from glacier motion and calving have also increased dramatically.

Ian Joughin

Ice sheets are often assumed to respond slowly to climate change, with dynamic response times measured in centuries to millennia. On page 1756 of this issue, however, Ekström *et al.* (*1*) describe a dramatic increase in glacial seismicity over the past several years, which coincides with the acceleration of many of Greenland's major outlet glaciers (*2–4*). The rapidity of these changes counters the view of a sluggishly responding ice sheet and indicates that outlet glacier dynamics can respond swiftly to climate change with consequent increases in sea level. Over the past decade alone, glacier acceleration has increased Greenland's contribution to sea-level rise by more than 0.3 mm year^{-1} (*2*).

Using teleseismic data from 1999 and 2000, Ekström *et al.* (*5*) previously identified earthquakes associated with glacial flow—"glacialquakes." Their more-recent observations cover more than a decade (1993 to 2005) and reveal a seasonal signal, with summer seismicity nearly five times greater than in winter. They also found a modest increase in seismicity in the late 1990s that was followed by a rapid increase from 2002 onwards, with 2005 producing nearly as many events as the combined total for 1993 through 1996.

The glacialquake magnitudes range from 4.6 to 5.1, yielding products of the displaced mass and slip of 0.1 × 10^{14} to 2.0 × 10^{14} kg m. This means that the Hellheim Glacier's 26 glacialquakes each resulted from roughly 0.16 to 3.7 m of slip if the displacement occurred along the full 14-km length of its fast-moving trunk, which has a mass of ~6.1 × 10^{13} kg (*6*) and flows at a rate of ~20 m day^{-1}. This finding suggests that the glacialquakes make up only a small fraction of glacial motion.

The glacialquakes all originated on fast-moving (>2 km year^{-1}) glaciers, with Greenland's three largest glaciers—Kangerdlugssuaq, Jakobshavn Isbrae, and Helheim—accounting for 72% of the events. Few glacialquakes were detected from Antarctica (*5*), possibly because the larger spatial extents of Antarctic ice streams produce slower events, with periods well beyond the 150-s detection threshold. For example, much of the Whillans Ice Stream moves primarily during twice-daily 0.5-m slip events lasting several minutes, with mass-slip products of roughly 3 × 10^{15} kg m (*7*).

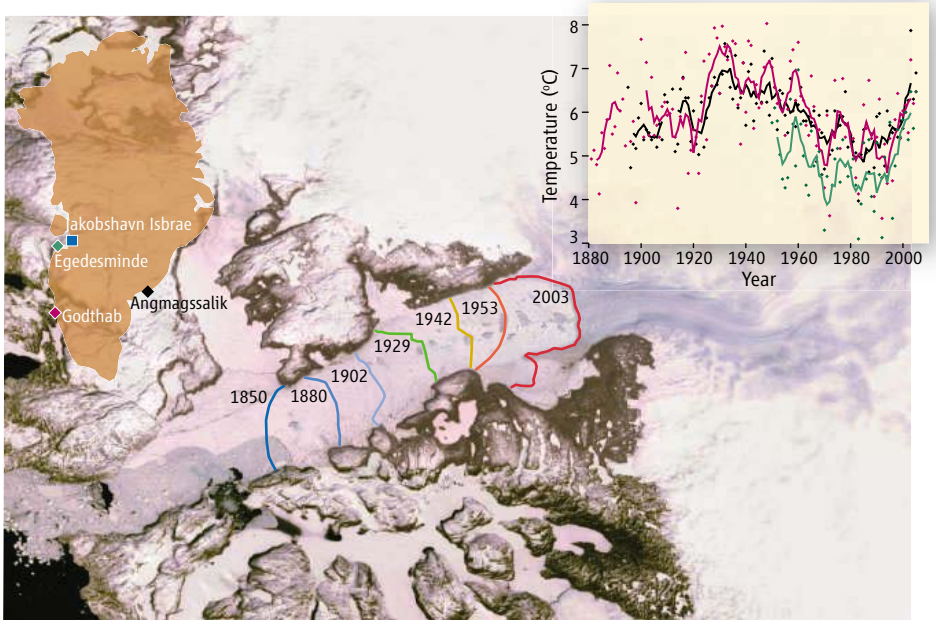

On the move. Retreat of Jakobshavn Isbrae since the Little Ice Age (*10*) marked by colored lines at different yearly intervals. (**Inset graph**) Summer (June, July, and August) temperatures (points) at several coastal stations shown in the silhouette map (*9, 11*). The solid lines are 5-year averages; color indicates measurement station.

The Kangerdlugssuaq, Jakobshavn Isbrae, and Helheim glaciers all accelerated by more than 50% over the period of increased seismicity, as have many of Greenland's smaller glaciers (*2–4*). The cause, seasonality, and the relation of the glacialquakes to these recent accelerations are not yet clear. Ekström *et al.* note that the drainage of summer melt to the bed through moulins (glacial conduits) may enhance lubrication at the bed to produce slip events. Other explanations may relate to the seasonal variation in calving, which for Jakobshavn Isbrae demonstrates an annual variability similar to that of the glacialquakes (*8*). Large calving events alone might yield mass displacements sufficient to produce glacialquakes. Alternatively, changes in glacier geometry after a calving event introduce a force imbalance, which may yield a slip event as a new force balance is established. Finally, the glacialquakes may be produced by stick-slip events that occur in the normal course of glacier sliding, with only brief (hours) periods of stick required to build enough elastic strain to produce detectable (magnitude >4.6) slip events.

The increased seismicity may be directly associated with the glacier accelerations if, for example, they are related to large calving events, which appear to precede acceleration (*4*). Alternatively, the increased incidence of glacialquakes may be a consequence of acceleration if seismicity scales with glacier speed. In either case, the ability to detect these events with teleseismic data provides a powerful new means for monitoring glacial activity. Furthermore, a new network of seismometers around Greenland might allow the detection of events on smaller glaciers, which may produce glacialquakes below the current detection threshold.

Although the reasons for increased incidence of glacialquakes and glacier acceleration are not clear, warming temperatures may be the underlying cause. Greenland undergoes regional warming and cooling (see the figure) on multidecadal times scales, with variability that exceeds global temperature trends (*9*). Summer temperatures from the late 1960s through mid-1990s tended to be cooler than average, which may have promoted glacier stability. For example, after decades of retreat, Jakobshavn Isbrae's calving front maintained its position during this cool period (*8*). Starting in about 1995, mean summer temperatures began to rise at coastal stations (*9*), reaching near-centurial highs. The correspondence between the rapid rise in temperature and the increased glacial activity (*1–4*) suggests that warming has a nearly immediate influence on glacier speeds. Although the duration of the recent warming is too short to determine

The author is at the Polar Science Center, Applied Physics Laboratory, University of Washington, 1013 NE 40th Street, Seattle, WA 98105, USA. E-mail: ian@apl.washington.edu

whether it is an anthropogenic effect or natural variability, in either case, the data suggest that modest (~1°C) changes in temperature can lead to large changes in discharge of glacial ice to the ocean. This sensitivity is not currently represented in ice-sheet models, which largely account for direct melt in response to climate change. Consequently, any further temperature increases may increase Greenland's contribution to sea level much more than anticipated.

References and Notes

1. G. Ekström, M. Nettles, V. C. Tsai, *Science* **311**, 1756 (2006).
2. E. Rignot, P. Kanagaratnam, *Science* **311**, 986 (2006).
3. I. Joughin, W. Abdalati, M. Fahnestock, *Nature* **432**, 608 (2004).
4. I. M. Howat, I. Joughin, S. Tulaczyk, S. Gogineni, *Geophys. Res. Lett.* **32** L22502, (2005).
5. G. Ekstrom, M. Nettles, G. A. Abers, *Science* **302**, 622 (2003).
6. These quantities are derived assuming width × thickness × length × density = 6 km × 800 m × 14 km × 910 kg m^{-3} = 6.1 × 10^{13} kg.
7. R. A. Bindschadler, M. A. King, R. B. Alley, S. Anandakrishnan, L. Padman, *Science* **301**, 1087 (2003).
8. H. G. Sohn, K. C. Jezek, C. J. van der Veen, *Geophys. Res. Lett.* **25**, 2699 (1998).
9. P. Chylek, J. E. Box, G. Lesins, *Climatic Change* **63**, 201 (2004).
10. A. Weidick, *U.S. Geol. Soc. Prof. Pap. 1386-C* (1995).
11. The temperature data is from www.giss.nasa.gov and the image is from the NASA Goddard Space Flight Center Scientific Visualization Studio.

12. I.J. acknowledges support from NSF through grant ARC0531270.

10.1126/science.1124496

CLIMATE CHANGE

Hitting the Ice Sheets Where It Hurts

In both hemispheres, glacier discharge to the sea has increased markedly in recent years as warm water from intermediate depths is melting the floating ends of glaciers from below, accelerating them.

Robert Bindschadler

Several large tidewater outlet glaciers of the Greenland and Antarctic ice sheets now appear to exhibit a nearly universal signature of recent increased discharge to the ocean. That this increase is occurring in the Northern and Southern hemispheres suggests a common cause. The culprit may be additional heat delivered by subsurface waters melting the submarine bases of these glaciers. This scenario would explain the observations and at the same time provide evidence that warmer subsurface waters are reaching the Earth's polar latitudes. Moreover, it indicates that the ocean plays a more critical role than the atmosphere in determining near-term glaciological contributions to changes in sea level.

The acceleration, thinning, and retreat of Pine Island Glacier in West Antarctica in the mid-1990s sparked an awareness of increased activity at the margin of the Antarctic ice sheet (*1*, *2*). Other glaciers discharging directly into the Amundsen Sea were soon discovered to be accelerating and thinning (*3*, *4*). Airborne ice-sounding measurements have established that these glaciers are deep, with bases hundreds of meters below sea level (*5*). These observations, along with modeling that predicted rapid upstream propagation of thinning, led to a claim that oceanic forcing was at work (*6*, *7*). Elsewhere around the continent, the Cook Ice Shelf in East Antarctica is fed by ice that is thinning and accelerating at comparable rates (*8*). This area drains the largest portion of the East Antarctic ice sheet grounded on a submarine bed, making it most like the Amundsen Sea sector of West Antarctica in behavior as well as setting (*9*).

Nearly half a world away, similar behavior has been reported for outlet glaciers draining the southern half of the Greenland Ice Sheet. On the west coast, the largest outlet glacier, Jakobshavns Isbrae, has been thinning at 15 m $year^{-1}$ since 1997, whereas on the east coast the major outlets of Kangerdlugssuaq and Helheim glaciers began thinning in 2003 at rates of 40 and 25 m $year^{-1}$, respectively (*10*, *11*). These glaciers also occupy deep submarine channels.

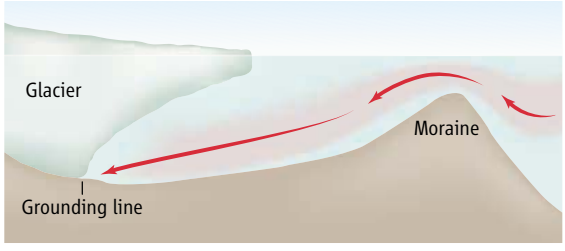

Oceanic low blows. Schematic representing warm intermediate-depth water breaching a submarine sill and sinking in a water cavity beneath the ice shelf to access the grounding line of an outlet glacier.

A recent assessment of changes in speed and mass balance around Greenland identifies these three large glaciers as among the most active recently, with accelerations up to 210% (*12*). The activity on Kangerdlugssuaq and Helheim glaciers has been confirmed by analysis of optical imagery on slightly different time intervals (*13*). Smaller glaciers along the southeast and southwest Greenland coasts are also accelerating (*12*).

Searching for a common cause of the most dramatic changes in the dynamics of the largest outlet glaciers in both Antarctica and Greenland leads one to consider the oceans (*6*, *7*). Melting at the base of a tidewater glacier causes it to accelerate by reducing basal friction and by reducing the buttressing resistance of any floating ice shelf (*14*). However, there remain questions of whether this warmer water exists, especially given the absence of any indication of increasing sea surface temperature in high latitudes, and how it could be conveyed to these glaciers.

Only about half of Earth's present radiation imbalance has been detected in rising atmospheric temperatures, and it has been suggested that the remainder is being stored in the world's oceans (*15*). Analyzing observations from buoys and ships, Levitus *et al.* demonstrated that the tropical and mid-latitude oceans have been warming in recent decades (*16*). They observed that because regional subsurface warming predated the expression of increased regional sea surface temperatures, the additional heat was being transported below the surface. Most of the warming was limited to the upper 1000 m, with the single exception of the North Atlantic where deep convection carried increased heat to greater depths.

The warmest water in polar oceans is neither at the surface (where summer melting of sea ice provides a surface layer of fresher water) nor at the bottom (where dense water from winter freezing of sea ice sinks to the ocean floor). In the Amundsen Sea, the warmest water is concentrated at 600-m depth (*17*). However, additional warmth in the ocean arriving from lower latitudes would raise the temperature of this intermediate water a fraction of a degree, hardly enough to initiate a sudden glacier acceleration.

That the deeper tidewater glaciers have proven most vulnerable to recent changes hints that the answer to recent acceleration lies in the manner in which this warmer intermediate-depth water can access the deep grounding lines of these glaciers, where the ice first floats free from the bed. These glaciers flow out to the ocean in deep channels with bases well below sea level and in short, floating ice shelves a few hundred meters thick. Extensive bathymetry data are rare beneath and immediately in front of these glaciers. Jakobshavns Isbrae in Greenland

The author is at the Hydrospheric and Biospheric Science Laboratory, NASA Goddard Space Flight Center, Greenbelt, MD 20771, USA. E-mail: robert.a.bindschadler@nasa.gov

and Pine Island Glacier in Antarctica, the two glaciers with the earliest recorded accelerations, are among the deepest outlets with grounding lines over 1000 m below sea level. It is likely that the large outlet glaciers such as these have eroded deeper basins than the smaller adjacent glaciers that have accelerated more recently.

In this context, a key characteristic of troughs eroded by tidewater glaciers is that they end with a shallower terminal moraine at the site of their maximum glacial cycle extent. In warmer climates, they retreat from this advanced position, leaving this moraine, or sill, as a barrier that prevents deeper water seaward of the sill from reaching the deep grounding line (see the figure). Once breached, however, the warm, salty water will sink in the cold, fresh water behind the sill and reach ice at the grounding line. Increased pressure at these greater depths lowers the melting point of this ice, increasing the melting efficiency of the warmer water. Rapid melting results. This process has been modeled for the observed sill geometry in front of and beneath Pine Island Glacier (*18*).

Surface meltwater cannot explain this common behavior. Penetration of surface meltwater to the glacial bed in Greenland can lead to seasonal flow acceleration (*19*), but the annually averaged increase in speed is only a few percent. In the case of Helheim Glacier, the relative intensities of warm summers were not associated with the observed changes in glacier speed (*20*). And surface melting is uncommon for any of the Antarctic glaciers cited here.

Outlet glacier acceleration will probably continue. As sea ice growth and decay diminish, warmer waters will reach shallower depths and access shallower tidewater glaciers, as well as move northward along Greenland's coasts. This will lead to increasing discharge of grounded ice and accelerating sea level rise. Increased discharge could encourage longer ice shelves, helping to protect the grounding lines, but this has not been observed because ice shelves have failed to grow in front of accelerating glaciers and retreat is exceeding historical bounds. Retreating glaciers lengthen the distance warmer water must travel from any sill to the grounding line, and eventually tidewater glaciers retreat to beds above sea level. This might limit the retreat in Greenland but will save neither West Antarctica, nor the equally large subglacial basin in East Antarctica where submarine beds extend to the center of the ice sheet.

References and Notes

1. E. Rignot, *Science* **281**, 549 (1998).
2. A. Shepherd, D. J. Wingham, J. A. D. Mansley, H. F. J. Corr, *Science* **291**, 862 (2001).
3. A. Shepherd, D. J. Wingham, J. A. D. Mansley, *Geophys. Res. Lett.* **29**, 1364 (2002).
4. E. Rignot, D. G. Vaughan, M. Schmeltz, T. Dupont, D. MacAyeal, *Ann. Glaciol.* **34**, 189 (2002).
5. R. Thomas *et al.*, *Science* **306,** 255 (2004).
6. A. J. Payne, A. Vieli, A. P. Shepherd, D. J. Wingham, E. Rignot, *Geophys. Res. Lett.* **31**, L23401 (2004).
7. A. Shepherd, D. J. Wingham, E. Rignot, *Geophys. Res. Lett.* **31**, L23402 (2004).
8. A. Shepherd, paper presented at the Royal Society meeting on "The Dynamics of the Antarctic and Greenland Ice Sheets: Combining Earth Observation and Modeling", London, 17 to 18 October 2005.
9. M. B. Lythe, D. G. Vaughan, BEDMAP Consortium, *J. Geophys. Res.* **106**, 11335 (2001).
10. W. Krabill *et al.*, *Science* **283**, 1522 (1999).
11. W. Krabill, paper presented at the Fall 2005 meeting of the American Geophysical Union, San Francisco, CA, 5 to 9 December 2005.
12. E. Rignot, P. Kanagaratnam, *Science* **311**, 986 (2006).
13. L. A. Stearns and G. S. Hamilton, paper presented at the Fall 2005 meeting of the American Geophysical Union, San Francisco, CA, 5 to 9 December 2005.
14. R. H. Thomas, E. Rignot, P. Kanagaratnam, W. Krabill, G. Casassa, *Ann. Glaciol.* **39**, 133 (2004).
15. J. Hansen *et al.*, *Science* **308**, 1431 (2005).
16. S. Levitus, J. I. Antonov, T. P. Boyer, C. Stephens, *Science* **287**, 2225 (2000).
17. S. S. Jacobs, H. H. Hellmer, A. Jenkins, *Geophys. Res. Lett.* **23**, 957 (1996).
18. D. M. Holland, A. Jenkins, S. S. Jacobs, in preparation; see also http://efdl.cims.nyu.edu/project_oisi/realistic/pig/overview.html.
19. H. J. Zwally *et al.*, *Science* **297**, 218 (2002).
20. R. DeLange, T. Murray, A. Luckman and E. Hanna, paper presented at the Fall 2005 meeting of the American Geophysical Union, San Francisco, CA, 5 to 9 December 2005.

21. I thank D. Holland for assistance in preparation of the manuscript.

10.1126/science.1125226

BIOMEDICINE

Lowering LDL—Not Only How Low, But How Long?

People with a mutation in a proteolytic enzyme are at a substantially lower risk for coronary heart disease because of their lifelong reduction of plasma low-density lipoprotein.

Michael S. Brown and Joseph L. Goldstein

The causal relation between plasma low-density lipoprotein (LDL) cholesterol (LDL-C) levels and coronary heart disease is well established. Compelling evidence from between-country comparisons shows that large and lifelong diet-related differences in LDL-C levels are associated with 10-fold differences in coronary mortality (*1*) (see the figure). Strong support comes from observations on genetic diseases such as heterozygous familial hypercholesterolemia, in which mutations in the LDL receptor gene double LDL-C levels throughout life and increase the risk of early heart attack by more than 10-fold (*2*). So, it has been somewhat disappointing that treatment with cholesterol-lowering statins for 5 years reduces the incidence of heart attacks by only 40%, even when LDL-C concentration is reduced by 80 mg/dl (*3*), a reduction that should give much more protection based on the population studies. A likely explanation is provided by Cohen, Hobbs, and their colleagues in this week's issue of the *New England Journal of Medicine* (*4*). In lowering LDL levels, the appropriate consideration may be not only how low, but also how long.

Cohen *et al.* studied middle-aged Americans with lifelong low LDL levels, owing to loss-of-function mutations in the gene encoding PCSK9, a secreted enzyme of the serine protease family. In a small number of subjects with severe nonsense mutations, the concentration of LDL-C was reduced by 38 mg/dl, and the prevalence of coronary heart disease declined by a remarkable 88%. In a larger number of subjects with a less severe missense mutation, LDL-C concentration was reduced by only 21 mg/dl, yet coronary heart disease decreased by 47%.

What is the function of PCSK9, and how do mutations in the *PCSK9* gene lower the concentration of LDL? Experiments in mice showed that overproduction of PCSK9 in liver and cultured hepatocytes severely reduces the number of LDL receptors (*5*, *6*). The simplest hypothesis is that PCSK9 directly catalyzes the breakdown of LDL receptors, but this has not been demonstrated experimentally. Inasmuch as LDL receptors mediate high-efficiency removal of LDL from plasma, a reduction in the number of LDL receptors causes LDL to accumulate. Ablation of the *PCSK9* gene in mice through gene-knockout technology increased the number of LDL receptors in liver and enhanced the clearance of LDL from the plasma (*7*). This striking finding indicates that PCSK9 functions tonically in mice to keep LDL receptor number lower and plasma LDL concentration higher than they would be otherwise.

PCSK9 appears to have the same effect on LDL in humans. A role for PCSK9 was first rec-

The authors are in the Department of Molecular Genetics, University of Texas Southwestern Medical Center, 5323 Harry Hines Boulevard, Dallas, TX 75390–9046, USA. E-mail: mike.brown@utsouthwestern.edu, joe.goldstein@utsouthwestern.edu

ognized in families with autosomal dominant hypercholesterolemia, owing to amino acid substitutions in PCSK9 that are postulated to increase its function (*8–10*). As expected, affected individuals suffered from premature heart attacks. Cohen *et al.* have now demonstrated the opposite effect—namely, that loss-of-function mutations in PCSK9 lower LDL levels and reduce the incidence of heart attacks.

In a previous study, Cohen *et al.* (*11*) sequenced *PCSK9* in a population-based study designed to reflect the ethnic diversity of Dallas, Texas. Among 1802 individuals of African descent, 2% carried one of two loss-of-function nonsense mutations in *PCSK9.* Individuals harboring either of these mutations had plasma LDL levels averaging 40% lower than those without them. These mutations were rare (0.1%) in Americans of European ancestry (Caucasians) (*11*).

Cohen *et al.* (*4*) now demonstrate the cardioprotective effect of the LDL-lowering mutations in *PCSK9*. They analyzed data from a prospective study of 15,792 Caucasians and African-Americans from four U.S. communities that was initiated in 1987 (*12*). These randomly selected individuals averaged 53 years of age at entry, and have been followed for 15 years. Among the 3278 African-American individuals without a *PCSK9* mutation, LDL-C levels averaged 138 mg/dl, and 319 of these individuals developed symptomatic coronary heart disease for an incidence of 9.7%. Among the 85 African-American individuals with a *PCSK9* nonsense mutation, LDL-C concentration was reduced by 38 mg/dl (to 100 mg/dl). Remarkably, only one of these 85 people (1.2%) developed coronary heart disease, an 88% reduction. In these protected individuals, coronary heart disease was rare despite a high prevalence of hypertension (37%) and diabetes (13%). Although the number of subjects is small, the extremely low incidence of coronary heart disease in African-Americans with *PCSK9* nonsense mutations is consistent with other studies (see the figure) that show an extremely low incidence of coronary heart disease in populations with lifelong low cholesterol levels (*1*, *13*). Among Caucasians in the same study, 301 individuals (3.2%) had a missense mutation that lowered LDL-C levels by only 21 mg/dl, yet reduced coronary heart disease incidence by 47%.

Why does lowering of LDL-C concentration by 40 mg/dl by a *PCSK9* mutation reduce coronary heart disease incidence by 88%, whereas a 40-mg/dl lowering with a statin reduces coronary heart disease prevalence by only 23% on average (*3*)? The most likely answer is duration. People with nonsense mutations in *PCSK9* likely have maintained relatively low LDL levels throughout their lives. People in statin trials have had their LDL levels lowered for only 5 years. Atherosclerosis is a chronic disease that begins in the teenage years (*14*). In a statin trial, an individual destined to have a heart attack within the 5-year observation period must have had advanced atherosclerosis when entering the trial. Indeed, the degree of protection in statin trials increases with duration (*3*, *15*).

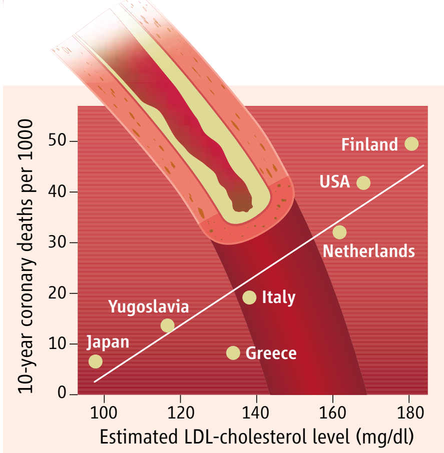

Where high cholesterol and coronary death meet. Beginning in 1952, Keys and colleagues measured the levels of total plasma cholesterol in 12,763 men aged 40 to 59 from selected population groups from seven countries, with wide variation in fat intake and plasma cholesterol levels (*1*). The men were followed for 10 years, and the number of fatal coronary events was measured. Inasmuch as the study did not measure plasma lipoprotein concentrations, we estimated the LDL-C levels based on the data for total cholesterol levels. For each country, we averaged the data from the populations that were studied. Coronary mortality between countries varied by 10-fold.

The lesson of PCSK9 is clear. If we are to attain an 88% reduction in the incidence of coronary heart disease, we must lower LDL levels well before atherosclerosis has become advanced. If we start early enough, it may be sufficient to lower LDL-C concentration only to 100 mg/dl, a goal that should be attainable for most people. These individuals must be prepared for lifetime treatment. Early intervention is designed to prevent a heart attack that might not occur for many years.

The physiological means to lower LDL concentration is through a stringent diet that is low in cholesterol and saturated fat. If this fails, drugs can be used. These include statins, cholesterol-absorption inhibitors, and bile acid–binding resins, all of which function by depleting the liver of cholesterol and increasing the number of hepatic LDL receptors. Statins inhibit 3-hydroxy-3-methylglutaryl coenzyme A reductase, the rate-controlling enzyme in cholesterol synthesis (*16*). This action depletes liver cholesterol and activates a transcription factor called SREBP (sterol regulatory element–binding protein), which increases the expression of mRNA encoding LDL receptor (*17*). The increased numbers of LDL receptors produce a selective fall in LDL concentration (*18*). Statins have been in widespread use for 20 years, and placebo-controlled studies in 90,056 patients have shown a very low incidence of side effects, primarily rare muscle necrosis and occasional increases in circulating liver enzymes (*3*).

The use of cholesterol-lowering drugs has been restricted to individuals suspected to be at high risk for myocardial infarction. Treatment is usually initiated at ages in which the atherosclerotic process is likely to have already advanced. One objection to earlier use has been cost. This objection may be overcome by the availability of low-cost generic statins. Generic statins are an option for relatively young individuals with LDL-C levels that are "normal" for the U.S. population, but are above the levels that offer protection from heart attacks. Selection of individuals for preventive treatment would improve if we had reliable noninvasive methods to diagnose early atherosclerosis.

Current data justify initiating more aggressive drug therapy at the first sign of hypertension or diabetes, even when blood pressure and glucose levels can be controlled. Current guidelines of the U.S. National Institutes of Health–sponsored Cholesterol Education Treatment Panel (*19*) recommend lowering plasma LDL-C concentration to 70 mg/dl in people at high risk for early heart attack. Concern over whether these recommended levels are too low should be tempered by the reality that the average level of plasma LDL-C in newborn infants throughout the world is only 50 to 70 mg/dl (*20*) and that LDL-C levels remain at or below 100 mg/dl on average throughout life in populations that consume low-fat diets (*13*).

Although studies of PCSK9 are still in their infancy, they suggest a new approach to enhancing the effectiveness of statins and other drugs that deplete cholesterol in the liver and raise LDL receptor number. Mouse experiments indicate that SREBP, the transcription factor that increases the expression of LDL receptors, also increases the production of PCSK9 (*21*, *22*). Depletion of liver cholesterol activates SREBPs, thereby increasing LDL receptor numbers (*17*), but also increasing PCSK9 levels (*23*). The PCSK9 destroys some of the LDL receptors, thereby partially negating the LDL-lowering effect. A PCSK9 inhibitor should synergize with cholesterol-depletion therapy in raising LDL receptor number and lowering plasma LDL concentration (*7*).

Admittedly, our knowledge of the pathogenesis of atherosclerosis is incomplete, and more research is needed. We do not know precisely how LDL particles cause the inflammatory and proliferative lesions of the atherosclerotic plaque. Although we measure LDL by its cholesterol content, the most toxic component may be its fatty acids or phospholipids. Also, we cannot be certain that the atherogenic effect of PCSK9 is due solely to its LDL-elevating action. It is possible that PCSK9 also exerts a direct toxic effect on the arterial wall and that loss-of-function mutations reduce atheroscle-

rosis by avoiding this toxicity as well as by lowering LDL levels. Despite these unanswered questions, the data on PCSK9 are consistent with the extensive genetic, epidemiologic, experimental, and therapeutic data that justify an aggressive public health program aimed at lowering LDL levels before the atherosclerotic process has become advanced. Early intervention may well put an end to the epidemic of coronary heart disease that ravaged Western populations in the 20th century.

References and Notes

1. A. Keys, *Seven Countries: A Multivariate Analysis of Death and Coronary Heart Disease* (Harvard Univ. Press, Cambridge, MA, 1980).
2. J. L. Goldstein, H. H. Hobbs, M. S. Brown, in *The Metabolic and Molecular Bases of Inherited Disease*, C. R. Scriver, A. L. Beaudet, W. S. Sly, D. Valle, Eds. (McGraw-Hill, New York, 2001), chap. 120, pp. 2863–2913.
3. Cholesterol Treatment Trialists' (CTT) Collaborators, *Lancet* **366**, 1267 (2005).
4. J. C. Cohen, E. Boerwinkle Jr., T. H. Moseley, H. H. Hobbs, *N. Engl. J. Med*. **354,** 1264 (2006).
5. K. N. Maxwell, J. L. Breslow, *Proc. Natl. Acad. Sci. U.S.A.* **101**, 7100 (2004).
6. S. W. Park, Y.-A. Moon, J. D. Horton, *J. Biol. Chem*. **279**, 50630 (2004).
7. S. Rashid *et al*., *Proc. Natl. Acad. Sci. U.S.A.* **102**, 5374 (2005).
8. M. Abifadel *et al*., *Nat. Genet.* **34**, 154 (2003).
9. K. M. Timms *et al*., *Hum. Genet*. **114**, 349 (2004).
10. T. Lerens, *Clin. Genet.* **65,** 419 (2004).
11. J. Cohen, A. Pertsemlidis, I. K. Kotowski, R. G. C. K. Graham, H. H. Hobbs, *Nat. Genet.* **37**, 161 (2005).
12. ARIC Investigators., *Am. J. Epidemiol*. **129**, 687 (1989).
13. Z. Chen *et al*., *Brit. Med. J*. **303**, 276 (1991).
14. W. F. Enos, R. H. Holmes, J. Beyer, *J. Am. Med. Assoc*. **152**, 1090 (1953).
15. M. R. Law, N. J. Wald, A. R. Rudnicka, *Brit. Med. J.* **326**, 1423 (2003).
16. M. S. Brown, J. L. Goldstein, *Atherosclerosis Suppl*. **5**, 13 (2004).
17. J. D. Horton, J. L. Goldstein, M. S. Brown, *J. Clin. Invest*. **109**, 1125 (2002).
18. C. J. Vaughan, A. M. Gotto, *Circulation* **110**, 886 (2004).
19. S. M. Grundy *et al.*, *Circulation* **110**, *227* (2004).
20. N. Bansal, J. K. Cruickshank, P. McElduff, P. N. Durrington, *Curr. Opin. Lipidol*. **16**, 400 (2005).
21. J. D. Horton *et al*., *Proc. Natl. Acad. Sci. U.S.A.* **100**, 12027 (2003).
22. K. N. Maxwell *et al., J. Lipid Res.* **44**, 2109 (2003)
23. G. Dubuc *et al.*, *Arterioscler. Thromb. Vasc. Biol*. **24**, 1454 (2004).
24. M.S.B. holds shares of stock in Merck and Pfizer, two companies that discovered and market cholesterol-lowering drugs. He is on the board of directors of Pfizer. J.L.G. holds shares in five companies that discovered and market cholesterol-lowering drugs (Astra Zeneca, Bristol-Myers-Squibb, Merck, Pfizer, and Schering-Plough). Since 2003, he has received consulting fees from two companies that develop drugs and related strategies to lower cholesterol (Schering-Plough and Amgen). The authors do not have planned, pending, or awarded patents related to the work discussed here, nor do they have relationships with companies that market generic drugs. Authors receive research support from the NIH and the Perot Family Foundation.

10.1126/science.1125884

CHEMISTRY

Dissolved Natural Organic Matter as a Microreactor

Organic matter dissolved in rivers and oceans undergoes poorly understood complex reactions, including the light-induced formation of a highly reactive form of oxygen that can subsequently react with pollutants and water contaminants.

John P. Hassett

Almost all organic molecules dissolved in fresh and marine waters come from natural sources, ultimately derived from decay of algae and higher plants. These molecules form a very complex mixture whose underlying molecular structures are poorly characterized (*1*). Consequently, they are often referred to in aggregate as dissolved organic matter (DOM) and quantified as dissolved organic carbon (DOC). They are also referred to as aquatic humic substances, in recognition of a similarity between freshwater DOM and soil organic matter. Although chemical characterization of DOM is elusive, properties of DOM that influence the physical and chemical behavior of natural and pollutant ions and molecules in water have often been investigated. On page 1743 of this issue, Latch and McNeill (*2*) present a striking study of how DOM can enhance the reactivity of a hydrophobic molecule by bringing it into close association with a photochemically produced, short-lived reactant, singlet oxygen.

Enhanced online at www.sciencemag.org/cgi/content/full/311/5768/1723

Hydrophobic contaminants in water are a major concern. Those that are chemically and biologically stable, such as the insecticide DDT, accumulate in aquatic food chains and can reach levels that threaten fish-eating organisms such as humans and predatory birds. Some, such as 2,3,7,8-tetrachlorodibenzodioxin (TCDD), are very toxic. Others, such as natural and synthetic steroid hormones, can disrupt endocrine functions in aquatic organisms. DOM has both hydrophobic and hydrophilic groups, giving it micelle-like properties. Therefore, it is able to bind other molecules by hydrophobic interactions. Hydrophobes in apparent solution in natural waters may thus exist in two states: one that is truly dissolved and one that is bound to DOM (see the figure). This binding decreases a hydrophobe's apparent volatility, bioavailability, and attachment to particles and increases its apparent solubility. Binding also brings a hydrophobe into a chemical environment that is distinct from water, and so can affect its reactivity.

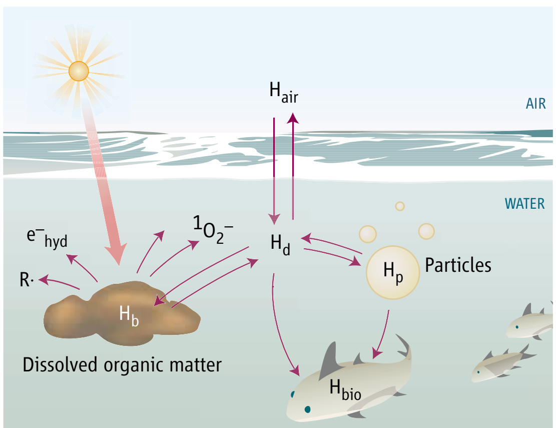

Hydrophobe-DOM interactions. Truly dissolved hydrophobic molecules (H_d) can be bound (H_b) to dissolved organic matter, decreasing their ability to be captured by particles (H_p), taken up by organisms (H_{bio}), or escape into the atmosphere (H_{air}). When bound to DOM, they are more likely to encounter photochemically produced, short-lived reactants such as singlet oxygen ($^1O_2$), superoxide (O_2^-), organic radicals (R·), or hydrated electron (e^-_{hyd}).

DOM contains groups (chromophores) that absorb sunlight. Absorbance is strongest in the ultraviolet but often extends into the visible portion of the spectrum, giving the brown color often associated with water from wetlands (bogs, peatlands, and swamps). Absorption of light by this chromophoric DOM (CDOM) can lead to formation of short-lived reactive products such as singlet oxygen ($^1O_2$). Although many of these products can react with hydrophobic compounds in water, their concentrations as measured with hydrophilic probes (furfuryl alcohol in the case of singlet oxygen) are too low to be important even at diffusion-controlled rates. However, Blough (*3*) and Burns *et al.* (*4*) have demonstrated that ions or molecules associated with DOM encounter higher concentrations of short-lived reac-

The author is in the Chemistry Department, State University of New York, College of Environmental Science and Forestry, 1 Forestry Drive, Syracuse, NY 13210–2726, USA. E-mail jphasset@syr.edu

tants and react faster than expected on the basis of bulk solution concentrations of the reactants. Thus, CDOM is a microreactor that enhances the reactivity of a molecule by bringing it into close association with a very reactive intermediate.

Latch and McNeill now demonstrate that hydrophobic molecules bound to CDOM encounter much higher concentrations of singlet oxygen produced photochemically from CDOM by light in the solar spectrum. A probe that is essentially completely bound to CDOM reports a $^1O_2$ activity that is more than 100 times the average concentration encountered by hydrophilic furfuryl alcohol. The environmental significance of this finding is that a hydrophobic molecule that is only 10% bound to CDOM will still encounter a $^1O_2$ activity that is 10 times the average concentration in the whole solution. Therefore, the potential for degradation of compounds susceptible to reaction with $^1O_2$ is much greater than expected on the basis of experiments with furfuryl alcohol. Latch and McNeill introduce a model for distribution of $^1O_2$ and find that it is limited to the CDOM matrix and to a "corona" that extends out a few nanometers from each CDOM molecule. Thus, it appears that most of the solution contains essentially no $^1O_2$. The concept of a corona predicts enhanced reactivity not only of hydrophobic compounds but also of cations such as protonated amines attracted to the net negative charge of DOM. Blough (*3*) in fact observed this to be the case for cationic nitroxides reacting with photochemically produced radicals.

The localized nature of these reactions leads to quantitative differences from results expected for a homogeneous solution. Hydrophilic scavengers of $^1O_2$ or other reactive intermediates have little affinity for the DOM matrix and therefore have a low probability of being present where $^1O_2$ is formed. Thus, they are much less effective at interfering with the reaction of a hydrophobic molecule than would be expected in a homogeneous water solution. Latch and McNeill demonstrate this for azide ion, which has little quenching effect on the intra-DOM reaction, and also for D_2O, which promotes reaction in homogeneous solution by stabilizing $^1O_2$ but has no promotional effect on the intra-DOM reaction. Conversely, a hydrophobic scavenger (β-carotene in this case) is much more effective than expected. However, molar concentrations of hydrophobic compounds in natural waters tend to be much lower than the concentrations of DOM, leaving most of the DOM molecules unoccupied. Consequently, substantial quenching of intra-DOM reactions by hydrophilic or hydrophobic scavengers is unlikely under normal environmental conditions.

Latch and McNeill use custom-made probe molecules that are ideal for these types of studies. Hydrophobic molecules are difficult to work with in water solution because of their low solubility and tendency to attach to surfaces. By measuring the chemiluminescence of the reaction product, the authors are able to achieve very low detection limits on small subsamples. This helps to minimize spurious results from molecules attached to the container wall that might be included if the entire solution was extracted. They are also able to observe production of a product rather than disappearance of a reactant, which greatly aids monitoring slow reactions that can still be important in the environment.

Intra-DOM reactions have received little attention, but as the present work demonstrates, they may be important photochemical mechanisms for transformation of organic chemicals in the environment. This has recently been shown to be true for intra-DOM reaction of the insecticide mirex in Lake Ontario (*5*), and is likely to be so for other compounds and other systems as well.

References

1. R. Sutton, G. Sposito, *Environ. Sci. Technol.* **39**, 9009 (2005).
2. D. E. Latch, K. McNeill, *Science* **311**, 1743 (2006); published online 23 February 2006 (10.1126/science.1121636).
3. N. V. Blough, *Environ. Sci. Technol.* **22**, 77 (1988).
4. S. E. Burns, J. P. Hassett, M. V. Rossi, *Environ. Sci. Technol.* **31**, 1365 (1997).
5. K. L. Lambrych, J. P. Hassett, *Environ. Sci. Technol.* **40**, 858 (2006).

10.1126/science.1123389

EVOLUTION

Tracing Oxygen's Imprint on Earth's Metabolic Evolution

As oxygen built up in Earth's atmosphere during the Precambrian, organisms evolved more complex biochemical networks. This expansion made feasible oxygen-dependent metabolisms that coopted parts of preexisting anaerobic ones.

Paul G. Falkowski

Life on Earth created, and is dependent on, nonequilibrium cycles of electron transfers involving primarily five elements: hydrogen, carbon, nitrogen, oxygen, and sulfur (*1*). Although biophysical and biochemical reactions catalyze specific electron transfers at a local, molecular level, the metabolic consequences are global. Through opportunity and selection, metabolic pathways evolved to form an interdependent, planetary "electron market" where reductants and oxidants are traded across the globe. The exchanges are made on a planetary scale because gases, produced by all organisms, can be transported around Earth's surface by the ocean and atmosphere. Exactly how these five elements came to form an electron market place remains largely unresolved, however. On page 1764 of this issue, Raymond and Segrè (*2*) use an ingenious bioinformatics approach to reveal the evolution of metabolic pathways. Their analysis elegantly reveals not only the profound role that molecular oxygen (O_2) has played in shaping the electron market place, but also the evolutionary constraints on, and trajectories of, the ensemble of electron traders.

Before the evolution of free O_2 ~2.3 billion years ago (*3*, *4*), there was a glut of reducing equivalents on Earth's surface. The first traders consumed electrons from the large populations of potential donors, including H_2, H_2S, and CH_4 (*5*). These electrons, extracted either with the release of energy or with the aid of low-energy (infrared) solar photons, were sold at relatively low energy prices to acceptors such as CO_2 and, to a lesser extent, SO_4. Although there was a very large pool of an alternative electron acceptor, N_2, considerable metabolic energy is required to reduce the gas to NH_3 and biologically appropriate compounds. Over the first 2 billion years of Earth's history, the electron market evolved to produce a well-structured set of metabolic pathways distributed among groups of interconnected anaerobic microbes, each selected to conduct one, or at most a small subset, of redox reactions. Because of the relatively large investment in energy to oxidize water, the biggest electron-donor pool, H_2O, remained biologically inaccessible.

When and how the first photosynthetic organisms evolved that were capable of oxidizing water to oxygen remains one of the great mysteries in the evolution of life on Earth (*6*). However, between ~3.2 and 2.4 billion years ago, either through progressive gene duplication events and selection, or by massive lateral transfer of genes, or both (*7*, *8*), an organism emerged that was capable of extracting four electrons from two molecules of water to form free O_2 as a metabolic waste product. This waste product proved not only highly useful as an electron acceptor, but also potentially damaging to the intricate metabolic

The author is with the Environmental Biophysics and Molecular Ecology Program, Institute of Marine and Coastal Sciences and Department of Geological Sciences, Rutgers University, New Brunswick, NJ 08901, USA. E-mail: falko@imcs.rutgers.edu

networks that had evolved over the first 2 billion years of Earth's history. The oxidation of water requires 1.2 V per electron. The only viable source of energy to sustain this reaction is higher energy (visible) solar radiation (*9*). Hence, oxygenic photosynthesis was confined to a thin film of sunlit water on the surface of the planet. Over a relatively short period of geological time (~100 million years), O_2 built up in Earth's atmosphere, such that by 2.2 billion years ago, the old electron market place, which had operated so smoothly for so long, was in danger of becoming a historical relic, to be supplanted by a new, high-powered machine that used the latest, most complex, energy-transducing process (*10*). The core machinery for this process evolved only once on Earth, and because of protein-protein, protein-cofactor, and protein-lipid interactions, the fundamental design became an immutable, "frozen" metabolic accident, encoded by a set of highly conserved genes (*11*). But with the appearance of this new technology, the electron traders, which had evolved under anaerobic conditions, had to accommodate the new oxidant, go into hiding, or become extinct.

Over the next 1.5 billion years, the oxidation of the atmosphere and, ultimately, oceans depleted Earth's surface of many of the reductants that were so abundant in the first half of the planet's history. Most of the anaerobic machinery in these organisms was corralled by the oxidizing conditions into relatively small, fragile, hypoxic or anaerobic reserves. However, some microbes broke free and either modified parts of their metabolic machinery, or formed symbiotic associations that permitted them to couple the oxidation of organic matter to the reduction of O_2 back to water. This supercharged respiratory pathway yielded four times as much energy per molecule of glucose oxidized than any of the ancient anaerobic pathways, but it came at a price. The triplet ground state of O_2 is highly reactive, and one misstep in an electron transfer can yield peroxides, superoxide, and/or hydroxyl anion radicals, collectively called reactive oxygen species. Reactive oxygen species can be highly destructive, oxidizing membrane lipids, ripping cofactors from proteins, and even oxidizing polymeric molecules such as proteins and nucleic acids (*12*). Rather than abandon O_2, selection salvaged and remodeled parts of the old, anaerobic machinery. This gave rise to both enzymatic and nonenzymatic mechanisms to protect the genetic investment in the core metabolic pathways that drive the "water-water" cycle upon which most life on Earth would come to depend. The protective pathways evolved in turn from gene duplication and lateral gene-transfer processes to spread across all three domains of life, but were absolutely essential to the evolution of eukaryotic organisms, from which all animals and plants descend (*13*, *14*).

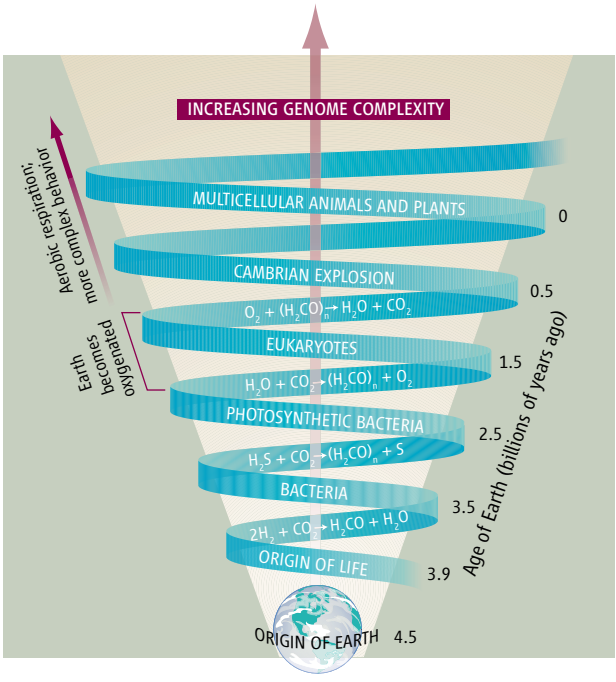

The evolution of genomic complexity and metabolic pathways during Earth's history. The earliest origin of life is not known. However, assuming a single last universal common ancestor evolved in mid-Proterozoic, there is evidence of microbial life. When oxygenic photosynthesis evolved is not clear, but geochemical data suggest that between ~2.3 and 2.2.billion years ago, there was sufficient oxygen in the atmosphere to permit an ozone layer to form. That singular event appears to have precipitated a massive increase in genome and metabolic complexity, culminating in the rise of metazoans around 600 million years ago, and the rise of terrestrial plants around 430 million years ago. The feedbacks in the evolutionary trajectory have led to increasing genomic and metabolic complexity.

But the influence of O_2 did not stop there. Novel secondary gene products, including sterols (and their derivatives), indoles and alkaloids, several antibiotics (including penicillins), and some detoxifying pathways, evolved to become obligately oxygen dependent. Indeed, as Raymond and Segré enumerate in their meta-metabolomic analysis of 70 genomes [from the Kyoto Encyclopedia of Genes and Genomes (*15*)], O_2 is predicted to be either directly involved in, or indirectly associated with, more than 10^3 metabolic reactions not found in anaerobes. Hence, the evolution of O_2 not only created redox energy couples that would allow complex animal life to evolve in the Ediacarian and Cambrian periods (approximately 630 to 490 million years ago), but also precipitated an evolutionary explosion of unpredictable, alternative, as well as novel pathways that gave rise to a wide variety of secondary gene products that increased fitness through regulation of gene expression, modification of behavior, and protection against competitors. The metagenomic analysis reveals how the rise of O_2 forced a selection of parts of anaerobic metabolic pathways from ancestral genes and, through processes not yet fully understood, appropriated the salvaged bits and pieces to construct an expanding galaxy of interdependent, and increasingly complex, metabolic pathways that became dependent on O_2. This is the biological equivalent of grabbing the most valuable possessions (including pictures of your ancestors) when your house is on fire, so that you may be able to start life anew after the catastrophe.

We still have a long way to go to understand how life evolved and how singular events (such as the rise of oxygen) altered evolutionary trajectories on Earth. The study by Raymond and Segré reinforces profoundly the notion that we are nonlinear and, over time, create "emergent" properties, which, by definition, cannot be predicted by reductive analyses. Ironically, bioinformatics itself is an emergent property of technology. The very tools used by Raymond and Segré to find the patterns of metabolic relationships were made possible by sequencing and annotation technologies developed primarily for the human genome project, by computer scientists searching for algorithms to organize and find relationships within the sea of data produced by genome sequencing, and by organismal microbial ecologists, who painstakingly isolate and grow individual organisms, study their metabolic pathways, and extract and purify their DNA so that the sequences obtained can be assembled into genomes. Although it is difficult to predict the emergent tools from present investments in science or technology, it is certain they will allow us to better understand the pathways that led to the connectivity and complexity in the electron market we observe on the planet today.

We thank Profully Presents, Inc., for support.

References

1. P. Falkowski, in *Encyclopedia of Biodiversity*, S. Levin, Ed. (Academic Press, New York, 2001), vol. 1, pp. 437–453.
2. J. Raymond, D. Segrè, *Science* **311**, 1764 (2006).
3. A. Bekker *et al.*, *Nature* **427**, 117 (2004).
4. J. Farquhar, H. Bao, M. Thiemens, *Science* **289**, 756 (2000).
5. K. H. Nealson, P. G. Conrad, *Philos. Trans. R. Soc. London B* **354**, 1923 (1999).
6. P. G. Falkowski, A. H. Knoll, Eds., *Evolution of Aquatic Photoautotrophs* (Academic Press, New York, 2006).
7. R. E. Blankenship, *Trends Plant Sci.* **6**, 4 (2001).
8. J. Xiong, K. Inoue, C. E. Bauer, *Proc. Natl. Acad. Sci. U.S.A.* **95**, 14851 (1998).
9. D. Mauzerall, *Photosynthesis Res.* **33**, 163 (1992).
10. P. G. Falkowski, J. A. Raven, *Aquatic Photosynthesis* (Blackwell Scientific, Oxford, 1997).
11. T. Shi, T. S. Bibby, L. Jiang, A. J. Irwin, P. Falkowsk, *Mol. Biol. Evol.* **22**, 2179 (2005).
12. N. Lane, *Oxygen: The Molecule that Made the World* (Oxford Univ. Press, Oxford, 2004).
13. A. H. Knoll, *Life on a Young Planet: The First Three Billion Years of Evolution on Earth* (Princeton Univ. Press, Princeton, NJ, 2003).
14. S. L. Baldauf, *Science* **300**, 1703 (2003).
15. M. Kanehisa, S. Goto, *Nucleic Acids Res.* **28**, 27 (2000).

10.1126/science.1125937

CREDIT: P. HUEY/*SCIENCE*

Mutation Pressure and the Evolution of Organelle Genomic Architecture

Michael Lynch,† Britt Koskella,* Sarah Schaack*

The nuclear genomes of multicellular animals and plants contain large amounts of noncoding DNA, the disadvantages of which can be too weak to be effectively countered by selection in lineages with reduced effective population sizes. In contrast, the organelle genomes of these two lineages evolved to opposite ends of the spectrum of genomic complexity, despite similar effective population sizes. This pattern and other puzzling aspects of organelle evolution appear to be consequences of differences in organelle mutation rates. These observations provide support for the hypothesis that the fundamental features of genome evolution are largely defined by the relative power of two nonadaptive forces: random genetic drift and mutation pressure.

The evolution of eukaryotes, and subsequently of multicellularity, was accompanied by dramatic changes in the nuclear genome, including expansions in sizes and numbers of introns, proliferation of mobile elements, and increases in lengths of intergenic regions. The continuity in scaling of these architectural features with genome size across major phylogenetic groups suggests that cellular and developmental features are not the primary driving forces in genome evolution, and the hypothesis has been raised that expansions in genome complexity are largely driven by two nonadaptive processes, random genetic drift and mutation (*1*, *2*). If this hypothesis is correct, it ought to apply to all genomic regions.

However, in contrast to the shared patterns of evolution in the nuclear genomes of animals and plants, the organelle genomes of these lineages have evolved in radically different directions. Animal mitochondrial genomes are highly streamlined, whereas plant mitochondrial genomes contain large amounts of noncoding DNA. Is the theory less general than supposed, or do unique features of various organelle lineages encourage different evolutionary trajectories? Here we argue that when differences in mutation rates are accounted for, patterns of variation in organelle genome architecture support the theory that multiple aspects of genomic complexity owe their origins to nonadaptive processes.

Scaling of Mitochondrial Genome Content

Over the range of eukaryotic diversity, the scaling of mitochondrial genome content with genome size is quite similar to that in nuclear genomes (*1*, *2*). The largest genome-size expansions are only weakly associated with gene number and primarily reflect increases in intronic and intergenic DNA [Fig. 1 and (*3*)]. However, in contrast to the situation with nuclear genomes, animals and plants occupy positions at the opposite ends of this gradient. The diminutive mitochondrial genomes of animals generally fall in the range of 14 to 20 kb, whereas plant mitochondrial genome sizes range from ~180 to 600 kb. Most unicellular species have intermediate aspects of mitochondrial genomic architecture and contain many genes absent from animal mitochondria (*4*). Thus, mitochondrial genomic architecture does not show overlap between animals and plants; this incongruity appears to be a consequence of contrasting evolutionary pressures unique to each lineage, with a strong ancestral component.

To put these results in a broader perspective, the average fractions of intergenic DNA in the nuclear genomes of vertebrates [0.65 (SEM = 0.05)], invertebrates [0.64 (0.03)], and plants [0.68 (0.10)] (*1*) are comparable to that for plant mitochondria, 0.72 (0.07). In contrast, the fraction of noncoding DNA in most animal mitochondria is just 0.05 to 0.10, less than that in any eukaryotic nuclear genome, and even below the average for prokaryotes, 0.12 (0.01) (*1*).

Mutation Rate

The two primary nonadaptive forces influencing genomic evolution are mutation, which defines the excess vulnerability of genes with complex structural features, and random genetic drift, which defines the magnitude of stochasticity in the evolutionary process (*1*). Any attempt to explain organelle genome diversity must address these issues. Comparative analysis of mitochondrial protein-coding genes implies substantial mutation-rate differences among major phylogenetic groups (Table 1). Rates of silent-site divergence range from 15 to 34 substitutions per site per billion years for all bilaterian-animal groups, whereas the average for plants is just 1/100th as much. In contrast, mutation rates are fairly similar in animal and plant nuclear genomes (*1*, *5*). Mitochondrial mutation-rate estimates in bilaterians are ~9 to 25 times those for the nuclear genomes in the same lineages, whereas the rates for most plants are ~0.05 times the nuclear rate (Table 1). This estimated disparity in mitochondrial mutation rates may be downwardly biased, as the only direct measures of the mitochondrial rate in animals are ~10 times the phylogenetically derived estimates, possibly because silent sites are not entirely neutral (*6*, *7*).

The fact that unicellular eukaryotes have similar mitochondrial and nuclear mutation rates (Table 1) suggests that animal and plant mitochondria, respectively, acquired higher and lower mutation rates, rather than one of these lineages retaining the ancestral condition. At least three factors may promote elevated mutation rates in animal mitochondria. First, mitochondria generate free oxygen radicals, producing an internal environment with an exceptionally high mutagenic potential (*8*). Second, in contrast to nuclear DNA, mitochondrial DNA (mtDNA) is continuously replicated within nondividing cells, and the base-misincorporation rate (before proofreading) is $\sim 10^3$ to 10^4 times that in the nuclear genome (*9*). Third, few mitochondrial genomes encode DNA repair proteins, although some mitochondrial repair genes were apparently transferred to the nucleus during the establishment of the primordial mitochondrion. Mitochondrial nucleotide-excision repair may have been entirely lost, and mismatch repair is greatly curtailed in mammalian cells relative to yeast (*10*). Less clear are the reasons for the dramatic reduction in plant mitochondrial mutation rates, although this feature is not entirely invariant (*11*).

Genetic Effective Population Size

The genetic effective size of a population (N_e), which defines the power of random genetic drift, is a function of the absolute number of individuals in the population, the mating system, the degree of genetic linkage, and the background mutation rate (*1*, *12*). Although there is substantial variation within lineages, the average N_e for nuclear genomes is substantially reduced in multicellular species; it is $\sim 10^7$ for unicellular eukaryotes, $\sim 10^6$ for invertebrates and annual plants, and $\sim 10^4$ for vertebrates and trees (*1*). Thus, from the standpoint of drift, the population-genetic environments of animal and plant nuclear genomes are quite similar. Does this conclusion extend to organelles?

It is commonly argued that haploidy and uniparental inheritance reduce the effective number of organelle genes per locus (N_g) in a diploid population to about one-quarter that for nuclear genes (*13*). (N_g equals the effective number of segregating units at the population level $2N_e$ for a nuclear locus and is approximately the effective number of females for a maternally inherited organelle.) This argument overlooks

Department of Biology, Indiana University, Bloomington, IN 47405, USA.

*These authors contributed equally to the gathering of data.

†To whom correspondence should be addressed. E-mail: milynch@indiana.edu

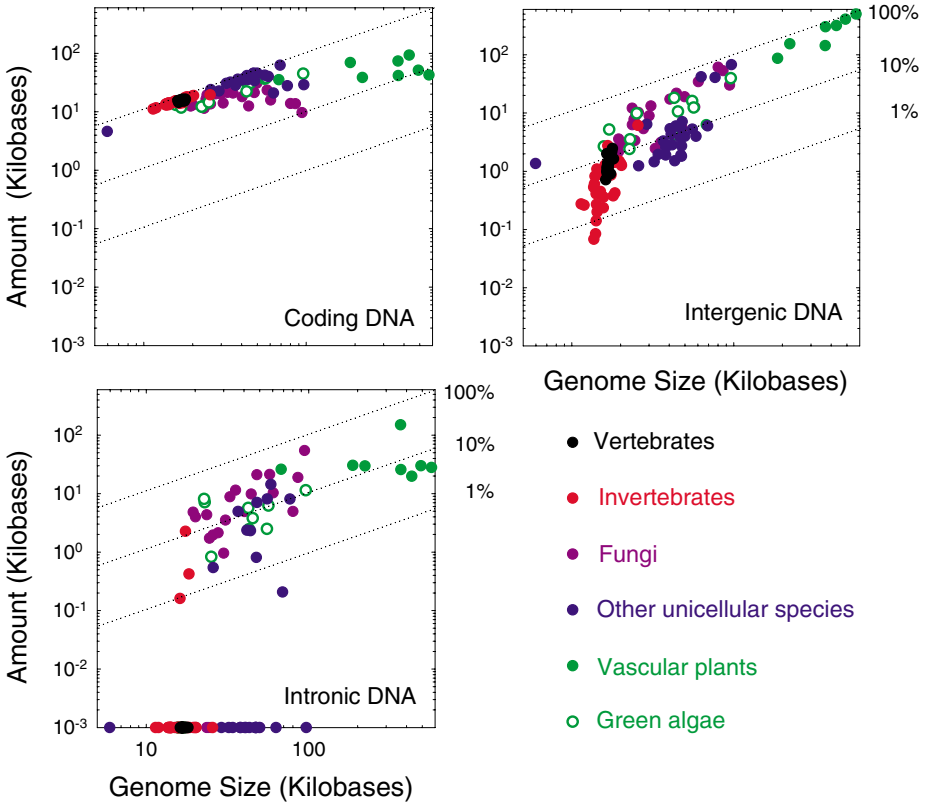

Fig. 1. Scaling of genome content with mitochondrial genome size, color coded according to major organismal groups (*3*). Diagonal lines denote points of constant fractional genomic contributions. Data points at the base of the graph (i.e., 10^{-3}) denote zero content.

Table 1. Rates of mutation per nucleotide site in mitochondria estimated from phylogenetic comparisons under the assumption of neutral silent sites (u_m, in units of 10^{-9} base substitutions per site per year), and ratios of mutation rates (μ_m/μ_n) and effective number of genes (N_{gm}/N_{gn}) in mitochondrial (*m*) versus nuclear (*n*) genomes (*3*). Plants are defined to be multicellular members of the chlorophyte lineage. SEM in parentheses, a convention used throughout the paper.

Phylogenetic group	u_m	μ_m/μ_n	N_{gm}/N_{gn}
Mammals	33.88 (6.11)	24.60 (5.80)	1.27 (0.43)
Birds	17.34 (4.88)	13.72 (2.86)	
Reptiles/amphibians	15.43 (3.70)	24.68 (8.12)	2.18 (0.37)
Fish		23.11 (12.70)	
Bilaterian invertebrates	16.86 (8.70)	8.84 (3.17)	0.31 (0.14)
Plants	0.34 (0.07)	0.05 (0.01)	
Uni/oligocellular species		1.58 (0.48)	0.49 (0.16)

two key issues. First, the "one-quarter rule" assumes an identical level of selective interference in nuclear- and organelle-housed genes. The absence of recombination in animal mitochondria is one reason why this might not be true [e.g., (*14*)], but there are other complicating factors: Nuclear chromosomes contain many more potential targets for selective sweeps; the distributions of mutational effects driving selective interference may differ between the two types of genomes; and the organelle genomes of some unicellular species and plants do recombine (*15*). Second, the one-quarter rule assumes that males and females are equivalent with respect to progeny production. In principle, a low ratio of male to female participants in mating (common in animals) can reduce the effective number of nuclear genes below that of maternally inherited organelle genes (*16*). Given these complexities, the degree to which the population-genetic environment differs among organelle and nuclear genes can only be resolved by empirical study.

From observations on mutation rates (Table 1) and within-population silent-site variation for mitochondrial versus nuclear genes (π_{sm} versus π_{sn}), the ratio of N_g for mitochondrial versus nuclear loci can be estimated (*3*). The average ratios for invertebrates and unicellular species are not significantly different from 0.25, consistent with the "one-quarter" rule, whereas N_{gm} in vertebrates is generally one to two times N_{gn}. For plant mitochondrial genes, within-population polymorphisms are usually almost entirely absent, so few attempts have been made to estimate π_{sm}. However, if we take 0.001 to be a conservative upper bound (*3*), and note that the range of π_{sn} for plant nuclear genes is ~0.003 to 0.04 (*1*), then N_{gm}/N_{gn} is <0.5 and <6.6, respectively. All of these results imply that N_{gm} and N_{gn} within species are generally within a factor of 4 or so from each other. Thus, given the similarity of N_{gn} in animals and plants, the altered patterns of mitochondrial genome evolution in these lineages do not appear to be a consequence of a radical change in the power of random genetic drift. This leaves mutation as the likely determinant.

The Mutational Barrier to Organelle Genome Evolution

A key determinant of many aspects of genomic evolution is the ratio of the per-generation rate of mutation per nucleotide site (μ) to the power of random genetic drift ($1/N_g$), i.e., $N_g\mu$ (*1*), and it is useful that the within-population sequence divergence at silent sites (π_s) has an expected value equal to twice this quantity under drift-mutation equilibrium. In the nuclear genome, π_s is generally <0.01 in animals and plants and severalfold higher in unicellular species with elevated N_g (*1*). In contrast, π_s for animal mitochondrial genomes is generally higher than that in unicellular lineages and >100 times that in plants (Table 2), in accordance with the reduction in μ in the latter. These mutation-rate driven differences in $N_g\mu$ provide a potentially unifying explanation for several previously unexplained and disconnected observations on organelle genomes.

Noncoding DNA is a genomic liability from the standpoint of mutational vulnerability. For example, introns increase the mutational target size of their host genes, which must maintain specific nucleotide sequences for splice-site recognition during mRNA processing (*17*). Likewise, intergenic DNA is a mutational substrate for the appearance of inappropriate transcription factor–binding sites, core promoters, premature initiation codons, etc. (*18*, *19*). Theory suggests that significant intron proliferation requires $2N_g\mu n < 1$, where n is the number of nucleotides reserved for splice-site recognition (*17*), or equivalently $\pi_s < 1/n$. For nuclear spliceosomal introns, $n > 20$ implies a threshold π_s for intron proliferation of ~0.05, which is consistent with the disparities in intron abundance between multicellular and unicellular species (*1*, *2*). Because organelle introns are self-splicing (i.e., do not rely on an external spliceosome), they must retain a larger number of nucleotides critical to proper splicing, implying a threshold π_s for organelle intron proliferation lower than 0.05 by a factor of perhaps 3 to 5. Consistent with the theory, this condition is generally violated in

Table 2. Average silent-site nucleotide diversity (π_s), in units of numbers of substitutions per site between random pairs of sequences. The sample size (n) denotes the number of pooled genera from which the averages were computed (*3*). Nuclear data are from (*1*).

Phylogenetic group	Mitochondrion	*n*	Nucleus	*n*
Mammals	0.0406 (0.0087)	12	0.0036 (0.0010)	10
Birds	0.0169 (0.0053)	4	0.0060 (0.0012)	4
Reptiles/amphibians	0.0516 (0.0128)	5	0.0013 (0.0008)	2
Fish	0.0362 (0.0150)	6	0.0046 (0.0012)	5
Arthropods	0.0276 (0.0056)	17	0.0292 (0.0060)	8
Molluscs	0.0135 (0.0068)	6	0.0229 (0.0132)	2
Nematodes	0.0677 (0.0084)	8	0.0272 (0.0168)	2
Fungi	0.0120 (0.0046)	3	0.0507 (0.0202)	12
Plants	<0.0004 (0.0004)	4	0.0152 (0.0027)	24

intron-free animal mitochondria but easily met in intron-rich plant mitochondria (Table 2).

Two additional observations support the hypothesis that high $N_g\mu$ imposes a barrier to organelle intron colonization. First, the only animal mitochondria known to harbor introns are those of cnidarians (*20*, *21*), which, like plant mitochondria, have such low mutation rates that within-species nucleotide polymorphisms are essentially unobservable, i.e., $\pi_s < 0.001$ (*22*). Second, in contrast to land-plant mitochondria, which generally contain 20 to 30 group II introns, all observed green-algal mitochondria have 0 to 8 mitochondrial introns (Fig. 1) (*3*). It is not known whether the per-generation rate of mutation per nucleotide site for green algae is similar to that for vascular plants, but an elevated N_g in the former is expected to promote a less permissive environment for intron proliferation.

Another unexplained aspect of mitochondrial genome evolution concerns the genetic code. Whereas the mitochondria of most unicellular lineages have experienced no more than two mitochondrial code changes, those of all bilaterians have between 3 and 5, with at least 12 unique changes occurring throughout the bilaterian phylogeny (*23*). In contrast, no reassignments have been found in plant mitochondria, and just one has been found in a cnidarian. Thus, there is an apparent association between the incidence of genetic-code alterations and the mutation rate.

The key first step in genetic-code evolution is a transient period during which a codon is entirely unused (*24*). The likelihood of such an event is miniscule in nuclear genomes with thousands of genes, but nontrivial in organelle genomes, ~70% of which completely lack one or more codons (*25*). There are still substantial impediments to genetic-code alterations in diminutive organelle genomes, but a central point is that codon reassignments must involve a series of fortuitous mutational events in the same linked genome, including modifications of transiently unassigned transfer RNAs (tRNAs) and reappearance of lost codons. Thus, the inverse scaling between the mutation rate and the waiting time for multiple mutations provides a reasonable explanation for the uneven incidence of mitochondrial genetic-code changes in animals, unicellular species, and plants.

A third peculiar feature of organelle genome evolution is the phylogenetic distribution of mRNA editing (*26*). Although a few animals use editing to restore mismatches in mitochondrial tRNA stems [e.g., (*27*)], mRNA editing appears to be absent from animal mitochondria. In contrast, plant mitochondria use mRNA editing extensively. For example, 441 editing sites are present in *Arabidopsis* mitochondria (*28*), and similar levels of mitochondrial editing are found in other plants (*29*). The absence of mRNA editing from the organelles of green algae suggests a dramatic expansion of editing after the origin of multicellular plants (*29*).

The vast majority of mRNA editing in plant organelles ensures the maintenance of amino acids at sites that are conserved across distantly related species (*30*). Although this observation motivates the idea that editing provides a genomic buffer against the accumulation of deleterious mutations (*26*), three observations raise doubts about this interpretation. First, there appear to be no phylogenetic barriers to editing (*26*), and yet under the buffering hypothesis, editing is expected to be most common in genomes with high mutation rates, contrary to the pattern seen with animals and plants. Second, the buffering hypothesis ignores the complex requirements of the editing process itself. Plant mitochondrial mRNA editing relies on cis-binding sites for trans-acting editing-site–specific proteins encoded in the nucleus (*31*, *32*). It is difficult to imagine a net advantage to editing if the processing of each site depends on numerous cis and trans sequences. Third, editing in plant organelles produces a heterogeneous pool of transcripts, some incompletely edited and others containing erroneous changes (*33*). Finally, mutations that restore the proper nucleotide at a previously edited site should accumulate at the neutral rate under the buffering hypothesis, but actually occur at four times the rate of silent-site substitution, which suggests a selective disadvantage to editing (*34*).

The mutation-pressure hypothesis helps explain these paradoxical observations by postulating that the maintenance of proper editosome recognition sites imposes a mutational burden on an allele. The minimal mutational disadvantage of an editing site is approximated by the total mutation rate over the nucleotide sites reserved for editing-site recognition, >23 for plants (*31*, *32*), which implies a threshold $\pi_s < 0.04$ for the maintenance of editing sites. Thus, the absence of mRNA editing in animal mitochondria is in accordance with the hypothesis that the mutation-associated disadvantages are simply too great to allow its establishment, whereas π_s for plant mitochondria is well below the barrier to the accumulation of editing sites.

These observations on the attributes of mitochondrial genomes, combined with prior analyses of nuclear genomes (*1*, *2*), lend generality to the conclusion that the primary factors driving genome architectural evolution are nonadaptive in nature. Although analyses spanning all of eukaryotes leave little room for independent hypothesis testing, a third opportunity is provided by the more phylogenetically limited chloroplast lineage. Studies of silent-site divergence in plants suggest that chloroplast mutation rates are about two to four times those in mitochondria and about 1/10th those in nuclei (*35*, *36*), and the limited data for species with silent-site diversities measured jointly in chloroplast and nuclear genomes (*3*) suggest a ratio of N_g of 1.03 (0.45). In addition, the average π_s for plant chloroplasts, 0.0037 (0.0011) (*3*), is >10 times that for plant mitochondria but about 1/10th of that for animal mitochondria (Table 1). These observations suggest that, although the power of random genetic drift is roughly comparable in all three compartments of the plant genome, the efficiency of selection in the chloroplast is intermediate to that for animal and plant mitochondria, although much closer to the latter.

In accordance with the mutation-pressure hypothesis, intron densities per protein-coding gene and fractional contributions of intergenic DNA in plant chloroplasts are about one-third those in plant mitochondria (*3*). In addition, plant chloroplasts have experienced no genetic-code changes, and although editing is much less extensive than in plant mitochondria, there are still ~25 to 30 editing sites per genome (*30*). With the exception of euglenoids, which may be obligately asexual and highly vulnerable to selective interference, the chloroplast genomes of the main algal groups (with presumably larger N_g than plants) are completely lacking in introns or nearly so and also tend to have much lower levels of intergenic DNA (green algae being exceptions) (*3*).

Concluding Comments

Because mutation and random drift are universal genetic forces, before invoking natural selection as the underlying determinant of an observed pattern of biodiversity, an evaluation of the expectations under a purely nonadaptive scenario is desirable. Natural selection is clearly

a significant force on organelle gene-sequence evolution (*37*, *38*), but selective arguments for the architectural features of organelle genomes have remained elusive. Although it has been suggested that an intracellular "race to replication" is responsible for the streamlining of animal mitochondrial genomes (*38*), it is unclear whether broader phylogenetic patterns in organelle evolution can be explained by variation in intracellular competition. Perhaps differential metabolic demands and/or organelle turnover rates are involved, but this remains to be demonstrated. The arguments presented above help explain not just the phylogenetic variation in noncoding organelle DNA, but also the peculiar distribution of genetic code changes and mRNA editing. Thus, while serving as a useful null model, the hypothesis that genome evolution is strongly influenced by nonadaptive forces appears to have broad explanatory power, with variation in nuclear-genome architecture being primarily driven by variation in N_e (*1*, *2*), and differences in μ making a major contribution to organelle evolution.

References and Notes

1. M. Lynch, *Mol. Biol. Evol.* **23**, 450 (2006).
2. M. Lynch, J. S. Conery, *Science* **302**, 1401 (2003).
3. Materials and methods are available as supporting material on *Science* Online.
4. M. W. Gray *et al.*, *Nucleic Acids Res.* **26**, 865 (1998).
5. W.-H. Li, *Molecular Evolution* (Sinauer Associates, Sunderland, MA, 1997).
6. D. R. Denver, K. Morris, M. Lynch, L. L. Vassilieva, W. K. Thomas, *Science* **289**, 2342 (2000).
7. N. Howell *et al.*, *Am. J. Hum. Genet.* **72**, 659 (2003).
8. R. S. Balaban, S. Nemoto, T. Finkel, *Cell* **120**, 483 (2005).
9. A. A. Johnson, K. A. Johnson, *J. Biol. Chem.* **276**, 38097 (2001).
10. P. A. Mason, R. N. Lightowlers, *FEBS Lett.* **554**, 6 (2003).
11. Y. Cho, J. P. Mower, Y. L. Qiu, J. D. Palmer, *Proc. Natl. Acad. Sci. U.S.A.* **101**, 17741 (2004).
12. J. H. Gillespie, *Genetics* **155**, 909 (2000).
13. S. R. Palumbi, F. Cipriano, M. P. Hare, *Evol. Int. J. Org. Evol.* **55**, 859 (2001).
14. S. Berlin, H. Ellegren, *Nature* **413**, 37 (2001).
15. N. W. Gillham, *Organelle Genes and Genomes* (Oxford Univ. Press, Oxford, UK, 1994).
16. C. W. Birky Jr., T. Maruyama, P. M. Fuerst, *Genetics* **103**, 513 (1983).
17. M. Lynch, *Proc. Natl. Acad. Sci. U.S.A.* **99**, 6118 (2002).
18. M. W. Hahn, J. E. Stajich, G. A. Wray, *Mol. Biol. Evol.* **20**, 901 (2003).
19. M. Lynch, D. G. Scofield, X. Hong, *Mol. Biol. Evol.* **22**, 1137 (2005).
20. M. J. H. van Oppen *et al.*, *J. Mol. Evol.* **55**, 1 (2002).
21. G. Pont-Kingdon *et al.*, *J. Mol. Evol.* **46**, 419 (1998).
22. T. L. Shearer, M. J. H. van Oppen, S. L. Romano, G. Worheide, *Mol. Ecol.* **11**, 2475 (2002).
23. R. D. Knight, S. J. Freeland, L. F. Landweber, *Nat. Rev. Genet.* **2**, 49 (2001).
24. T. H. Jukes, S. Osawa, *Comp. Biochem. Physiol. B* **106**, 489 (1993).
25. J. Swire, O. P. Judson, A. Burt, *J. Mol. Evol.* **60**, 128 (2005).
26. T. L. Horton, L. F. Landweber, *Curr. Opin. Microbiol.* **5**, 620 (2002).
27. D. V. Lavrov, W. M. Brown, J. L. Boore, *Proc. Natl. Acad. Sci. U.S.A.* **97**, 13738 (2000).
28. P. Giegé, A. Brennicke, *Proc. Natl. Acad. Sci. U.S.A.* **96**, 15324 (1999).
29. R. Hiesel, B. Combettes, A. Brennicke, *Proc. Natl. Acad. Sci. U.S.A.* **91**, 629 (1994).
30. T. Tsudzuki, T. Wakasugi, M. Sugiura, *J. Mol. Evol.* **53**, 327 (2001).
31. T. Miyamoto, J. Obokata, M. Sugiura, *Proc. Natl. Acad. Sci. U.S.A.* **101**, 48 (2004).
32. E. Kotera, M. Tasaka, T. Shikanai, *Nature* **433**, 326 (2005).
33. C. G. Phreaner, M. A. Williams, R. M. Mulligan, *Plant Cell* **8**, 107 (1996).
34. D. C. Shields, K. H. Wolfe, *Mol. Biol. Evol.* **14**, 344 (1997).
35. K. H. Wolfe, W. H. Li, P. M. Sharp, *Proc. Natl. Acad. Sci. U.S.A.* **84**, 9054 (1987).
36. B. S. Gaut, B. R. Morton, B. C. McCaig, M. T. Clegg, *Proc. Natl. Acad. Sci. U.S.A.* **93**, 10274 (1996).
37. M. Lynch, *Mol. Biol. Evol.* **14**, 914 (1997).
38. D. M. Rand, *Annu. Rev. Ecol. Syst.* **32**, 415 (2001).

39. Supported by grants from the NIH and NSF to M.L., an NSF predoctoral fellowship to B.K., and an NSF Integrative Graduate Education and Research Traineeship Program (IGERT) fellowship to S.S. Some key comments from J. Palmer led us to pursue this work. We are grateful to M. Neiman, J. Palmer, A. Richardson, and the reviewers for helpful comments.

Supporting Online Material

www.sciencemag.org/cgi/content/full/311/5768/1727/DC1
SOM Text
Fig. S1
Tables S1 to S5
References

10.1126/science.1118884

The Nature and Dynamics of Bacterial Genomes

Howard Ochman* and Liliana M. Davalos

Though generally small and gene rich, bacterial genomes are constantly subjected to both mutational and population-level processes that operate to increase amounts of functionless DNA. As a result, the coding potential of bacterial genomes can be substantially lower than originally predicted. Whereas only a single pseudogene was included in the original annotation of the bacterium *Escherichia coli*, we estimate that this genome harbors hundreds of inactivated and otherwise functionless genes. Such regions will never yield a detectable phenotype, but their identification is vital to efforts to elucidate the biological role of all the proteins within the cell.

The organization of bacterial genomes is simple and elegant. These genomes are small, ranging from 500 to 10,000 kb, and are tightly packed with genes and other functional elements. The coding regions themselves are intronless and short, averaging a scant 1 kb, and are aligned almost contiguously along the chromosome. The common view is that the streamlining of bacterial genomes is the result of selection acting on replication efficiency and growth rates. Although this idea is warranted by the relatively low ceiling on bacterial genome size, there is no clear association between chromosome length and cell division rates either within or across bacterial species, implying that factors other than selection on overall chromosome size contribute to the compactness of bacterial genomes (*1*).

The elucidation of complete sequences has helped define the forces that shape bacterial genomes. Early research showed bacterial genomes to be tightly packed with functional elements, but unprecedented discoveries from genome analyses have shown that the genetic information encoded within bacterial genomes decays over evolutionary time scales (*2*–*4*). At first, this feature seems at odds with the high gene density observed in most bacterial genomes, but it is actually one of the primary determinants of their streamlined organization. All organisms accumulate mutations that can disrupt and degrade functional regions, but in bacteria (as well as in several eukaryotes) there is a mutational bias toward deletions over insertions (*1*, *5*–*7*). When disruptions occur in genes that are no longer required, the nonfunctional regions can be maintained in the genome for some time, but they gradually erode and are eventually eliminated, as is evident from comparisons of bacterial pseudogenes with their functional counterparts. In this manner, bacterial genomes maintain high densities of functional genes.

The primary force countering the erosion of genomes is natural selection, which serves to maintain the functional regions. The degree of selection varies along a continuum depending on the role of a gene in cell survival and replication: Genes with little contribution to fitness are more susceptible to inactivating and deletional mutations, whereas those that are critical will resist such mutation. Moreover, the degree of selection acting on any particular gene can change over time and according to a specific ecological context. For example, the inactivation or loss of one or more genes can increase the value of others, and changes in bacterial ecology or lifestyle might render some genes redundant (*8*).

As important as the intensity of selection is the effectiveness of selection, which depends on population size and structure. In very large populations, deleterious mutations in beneficial genes are not likely to become fixed by chance; but in small populations, even useful genes can

Department of Biochemistry and Molecular Biophysics, University of Arizona, Tucson, AZ 85721, USA.

*To whom correspondence should be addressed. E-mail: hochman@email.arizona.edu

be inactivated and deleted. Population-level processes operate on all genomes, and their effects are even observed in the functional regions of the human genome (*9*). Thus, organisms with small population sizes are more prone to gene decay and loss, even for genes that are usually considered beneficial. This is the case for pathogens, which typically require only small inocula to infect each new host, resulting in a reduction in the effective size of their populations.

The impact of these factors is evident from the contents and organization of sequenced bacterial genomes. When compared with their free-living relatives, facultative bacterial pathogens are seen to harbor substantial numbers of pseudogenes (*5*, *10*) and a population structure that promotes the maintenance of deleterious mutations (*1*, *11*, *12*). Such pathogens represent an intermediate stage of genome erosion relative to the obligately host-associated lineages, whose genomes are highly reduced, having undergone massive inactivation and loss of nonessential genes (Fig. 1). When considering all bacterial genomes, there appears to be a set of only 50 to 100 genes that are universally maintained. The losses observed in degraded and reduced genomes include not only those genes that are clearly superfluous but also many that are beneficial but not essential, such as those involved in DNA repair (*2*, *13*, *14*).

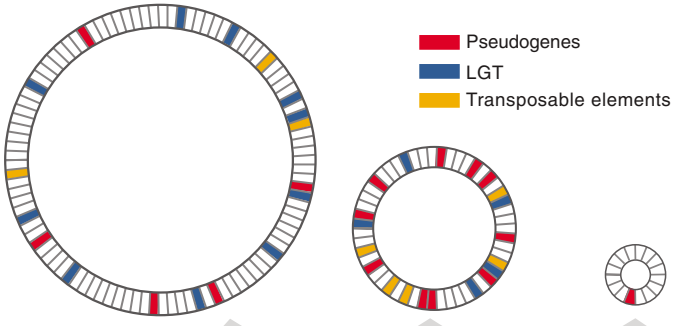

	Free-living	Recent or facultative pathogen	Obligate symbiont or pathogen
Genome size	Large (5-10 MB)	Intermediate (2-5 MB)	Small (0.5-1.5 MB)
Number of pseudogenes	Few	Many	Rare
Incidence of LGT	Frequent	Frequent to rare	Rare to none
Selfish genetic elements	Few	Common	Rare
Genome organization	Stable or unstable	Unstable	Stable
Effective population size	Large	Small	Small

Fig. 1. Trends in the size and contents of bacterial genomes. Upon classifying bacteria according to their degree of association or dependence on a eukaryotic host, several general features emerge (*8*). Because of their relatively large population sizes, selection operates most effectively in free-living species—i.e., those that replicate in the environment independently of a host. Because selection is effective in removing deleterious sequences, these species usually possess large genomes containing relatively few pseudogenes (red) or mobile genetic elements (yellow). In recently derived pathogens, the availability of host-supplied nutrients combined with decreases in effective population sizes allows for the accumulation of pseudogenes and of transposable elements. In long-term host-dependent species, the ongoing mutational bias toward deletions has removed all superfluous sequences, resulting in a highly reduced genome containing few, if any, pseudogenes or transposable elements. LGT, lateral gene transfer.

Redundant Regions in Bacterial Genomes

Some fraction of genes in each bacterial genome will not be functional because of ongoing mutational and population-level processes. Most genome annotations carry in them the implicit assumption that all predicted coding DNA sequences (CDSs) confer some (although often unspecified, hypothetical, or putative) function (*15*–*18*), but the critical task of identifying inactivated genes has been largely ignored.

To understand the functional status of a genome, we need to recognize the pseudogenes within it. Unfortunately, there are inconsistencies in the methods by which pseudogenes are defined (*19*, *20*). Hence, the assignment of pseudogenes must be based on some a priori assumptions about the spectrum of alterations in a gene that will abolish the function of its encoded protein. For example, genes in adenine + thymine (A + T)–rich genomes are often shorter than their homologs in other genomes, owing to their propensity toward mutations that form stop codons (*21*, *22*). Such truncations cannot automatically be taken to reflect a global inactivation of genes. Wherever possible, predicted pseudogenes should also be appraised in light of the physiological features of the cell. For example, the bacterial pathogen *Yersinia pestis*, unlike its sister taxon *Y. pseudotuberculosis*, requires exogenous methionine and phenylalanine for growth because it contains disabled versions of the *metB* and *pheA* genes (*4*, *20*).

Finding Pseudogenes

The availability of genome sequences from closely related organisms has considerably altered the way that genes are recognized and annotated, but just how useful and accurate are genome annotations for the downstream analyses of microbial systems? Their reliability can be best assessed in *E. coli* K-12, which, owing to its long history as an experimental organism, has the highest proportion of genes for which functions have been determined directly (*23*–*25*). Furthermore, many genomic features first discovered in *E. coli* (such as gene and operon structure, occurrence of mobile elements, mutational patterns, and rates of gene exchange and acquisition) subsequently have been found to be characteristic of other bacterial groups.

Early molecular genetic analyses gave little indication that *E. coli*, or any other bacterial genome, might harbor substantial numbers of nonfunctional genes. The original annotation of the *E. coli* K-12 reported only a single pseudogene among its 4288 coding regions. Because this genome is expected to possess all of the hallmarks of free-living bacteria (Fig. 1), we set out to identify the inactivated and nonfunctional portion of the *E. coli* K-12 genome and to assess the number and authenticity of pseudogenes predicted by several analytical approaches.

Genes and Proteins with Structural Alterations

We searched the annotated genome of *E. coli* K-12 (*26*) for genes that differed substantially in length from their homologs in the genome sequences of close relatives (i.e., enteropathogenic *E. coli* EDL933, uropathogenic *E. coli* CFT073, and *Shigella flexneri* 2a, which is more closely related to K-12 than either of the other two *E. coli* strains). As a consequence, more than 160 putative coding regions in *E. coli* K-12 were predicted to be pseudogenes (*27*, *28*). Contained within intergenic regions, there were 47 additional pseudogenes that were not recognized as such in the original annotation.

Although the criteria for distinguishing pseudogenes differ among studies, the overall rationale is the same: The predicted protein must be altered to a degree that abolishes its function. Such thresholds should derive from the known size and organization of functional domains within proteins, the observed length variation within individual gene families conserved across bacteria, and available information on experimentally disrupted proteins. In general, we classed as pseudogenes those cases

Table 1. Predicted pseudogenes in the *E. coli* K-12 genome. Functional categories, obtained from the 1 July 2004 annotation deposited in GenBank, are as follows: Hypothetical genes are CDSs of no known function; putative genes are CDSs with homology-derived functions; functional genes have an experimentally confirmed function. Essential genes are those determined experimentally to be required for aerobic growth in nutrient-rich conditions, as assayed in (*29*), with numbers of genes of annotated (known) and hypothetical (unknown) functions shown. Dashes denote the cases where CDSs predicted to be pseudogenes were not tested or yielded ambiguous results in (*29*). Ten genes of known function remain annotated as a "hypothetical" in GenBank. Conversely, there are 23 instances in which the GenBank annotation assigned named functions to CDSs based solely on sequence homology, whereas they should be classified as "putative." Gene names, identification numbers, genomic coordinates, strand orientations, and functional assignments of annotated CDSs in each category of predicted pseudogenes are available in tables S1 to S5.

	Method of recognizing pseudogenes				
	Disruption		K_a/K_s	SIFT‡	Not expressed
	2002§	2004¶			
Total number detected*	95	68	4	5	62
Intergenic†		47			
Hypothetical	56	59‖	4	1	16
Putative	27	14‖	0	2	17
Functional	11	15	0	2	28
Essential (known/hypothetical)	0/5	2/4	–/–	–/–	0/6

*Numbers of CDSs in the original genome annotation of *E. coli* K-12 that are putative pseudogenes. Matches to intergenic regions not included. †Intergenic pseudogenes are disrupted copies of CDSs in other *E. coli* genomes but do not match any annotated CDS in the *E. coli* K-12 genome. Some entries are blank because the methods only apply to annotated CDSs. ‡SIFT (*35*) searches for amino acid replacements predicted to disrupt protein function. §Data from (*27*). ¶Data from (*28*). Pseudogenes considered in this column do not overlap with those reported in (*27*). ‖Includes matches of CDSs and intergenic regions to named genes in other *E. coli* genomes.

in which a stop codon or deletion has resulted in an encoded protein that is less than 80% of the length of its counterpart in the contrasted genome and those cases in which a frameshift or insertion has altered more than 20% of the amino acid sequence (*28*).

Because pseudogenes have no role in cellular processes, their status has to be supported by the lack of any direct evidence indicating a function. While such validations are conditional and do not prove that a region is inert, authentic pseudogenes are expected to be among those CDSs with functions that have not been (and can never be) resolved (Table 1). Despite the extensive biochemical, physiological, and molecular genetic characterization of *E. coli*, no functions have been uncovered for more than 90% of the 207 disrupted CDSs we found, bolstering their designation as pseudogenes. Most of these predicted pseudogenes are annotated as "hypothetical," although some (those designated "putative" in Table 1) have been assigned a provisional name or function based solely on their similarity to sequences already characterized in other organisms. Pseudogenes that are generated from genes of known function are among the most biologically interesting portions of a genome, because they disclose which specific functions are vulnerable to loss during the process of genome decay. Although it has been hypothesized that disrupted regions might take on a new role after their initial inactivation (*19*), there are as yet no verified cases in bacteria in which a pseudogene has assumed a function.

Extending this analysis to the other sequenced members of the *E. coli*/*Shigella* clade has resolved similarly high numbers of pseudogenes within each genome. Among these strains, the genome of the human pathogen *S. flexneri* displayed the highest level of genome erosion and degradation, containing more than 400 truncated or inactivated genes, as well as substantial numbers of translocatable insertion sequences (ISs) (*9*, *28*). Although the sequenced strains within the *E. coli*/*Shigella* clade are very closely related (averaging only 1% in sequence divergence), the set of disrupted genes harbored by each strain is distinct. The lack of pseudogenes shared among multiple strains indicates that pseudogenes are generated continually, but older pseudogenes are eliminated and only rarely persist in bacterial genomes.

Functions have been specified for 15 of the *E. coli* K-12 pseudogenes we recognized (Table 1), including two found to be essential for growth in nutrient-rich conditions (*29*). Sequencing errors resulted in incorrect assignment as pseudogenes, which have since been corrected; the other cases, which represent less than 3% of the total sample, are likely to be false positives.

Unconstrained Substitutions

The most widely used method for identifying nonfunctional genes has been the K_a/K_s test, which compares nucleotide substitution rates at synonymous sites (K_s) to those at nonsynonymous sites (K_a) (*30*). Regions that are unfettered by functional constraints, such as pseudogenes, are expected to have K_a/K_s ratios that do not differ significantly from one. We searched for pseudogenes by estimating the K_a/K_s ratio for each of nearly 1500 coding regions shared between *E. coli* K-12 and *Salmonella enterica* serovar Typhimurium strain LT2. We first excluded genes subject to extreme codon-usage bias as well as short leader peptides, which have been shown to give the appearance of neutral evolution (*30–32*), and then we applied a likelihood ratio test for detecting selection (*33*) to genes in the top 5% of the distribution ($K_a/K_s > 0.104$).

The K_a/K_s ratio test exposed only four of the *E. coli/Salmonella* homologs as pseudogenes (Table 1). If most pseudogenes in the *E. coli* genome are newly derived (and strain specific), most of the evolutionary divergence between the *E. coli/Salmonella* homologs must have occurred while both copies were intact and undergoing purifying selection. There has simply not been sufficient time since the inactivation event for new mutations to equilibrate the levels of divergence at synonymous and nonsynonymous sites (*28*), resulting in K_a/K_s ratios much less than one.

The K_a/K_s test, although commonly used for detecting nonfunctional regions in eukaryotic genomes, is of limited value for uncovering pseudogenes in bacterial genomes, where most pseudogenes are of recent origin (*34*). Nonetheless, this method is robust and those few bacterial pseudogenes uncovered in this manner are likely to be authentic. As expected, no functions have been ascribed to any of the four high K_a/K_s genes in the *E. coli* K-12 genome.

Radical Amino Acid Replacements

Owing to the high gene density of bacterial genomes, the majority of point mutations result in amino acid replacements that can potentially alter protein function. To search for pseudogenes caused by missense mutations, we used a homology-based tool [termed Sorting Intolerant from Tolerant (SIFT)] (*35*) that sorts intolerant from tolerant substitutions. SIFT reveals differences in the primary structure of an *E. coli* protein that were sufficient to disrupt protein function when compared with orthologs present in at least three other sequenced members of the Gammaproteobacteria. The method examines all possible amino acid substitutions with a set of proteins and predicts those that are likely to be deleterious. SIFT identified only five genes with encoded proteins that contained potentially deleterious amino acid replacements (Table 1), suggesting that the proportion of single amino acid substitutions that completely abolishes protein function and generates a pseudogene is low.

Transcriptional Pseudogenes

In addition to those encoding nonfunctional proteins, pseudogenes can arise when tran-

scription is permanently obstructed such that no protein is produced. To identify genes that are transcriptionally inactivated, we analyzed the results of studies of global gene expression in *E. coli* MG1655 (*36*–*38*), searching for genes that produce no detectable transcripts. There were 62 *E. coli* K-12 genes for which no transcripts were detected under any of the tested conditions, but for nearly half of these genes a function had been assigned. Because our analyses were limited to the three studies that used identical methods (and reflected a narrow range of growth conditions), it is likely that we overlooked the particular contexts under which many genes are expressed. By including an additional experiment that used similar but not identical methods (*39*), the occurrence of completely silenced genes was reduced to one (the putative acetyltransferase *ycdJ*). The low number of transcriptional pseudogenes reflects the evidence that the sequences regulating gene expression span much shorter regions than do the coding sequences within bacterial genomes, thereby providing a smaller target for inactivating mutations that silence genes.

The Functional Component of Bacterial Genomes

By relying solely on comparisons of full genome sequences, we estimate that nearly 1 in 20 of the annotated coding regions in the *E. coli* K-12 genome are pseudogenes and that they tend to occur among genes of unknown function. Because *E. coli* K-12 has one of the smallest genomes of any *E. coli* strain (*40*), it is usually considered to have a relatively compact genome; however, the number of nonfunctional genes is likely to be higher than we predict.

There are also hundreds of genes in the *E. coli* K-12 genome whose functional status cannot be assessed by comparative approaches because they have no counterparts in closely related genomes. These include 104 known prophage- and IS element–associated genes, which may encode functional proteins but are generally assumed to be dispensable for host-cell survival and fitness, as well as numerous sequences acquired from distant sources.

Although it is not possible to specify which of the acquired genes are still functional on the basis of their sequence characteristics, the proportion that will be retained might be estimated by examining their incidence throughout the history of the *E. coli* lineage. Assuming that rates of gene transfer and loss have remained relatively constant over evolutionary time scales, we calculate that an additional 77 K-12 genes are expendable and could be removed from the genome (*41*). When combined with the 172 putative pseudogenes and the 104 phage- and IS-associated genes, this brings the total number of inactivated, nonfunctional, and expendable genes in the *E. coli* K-12 genome to 353, constituting 8% of the annotated coding regions.

Cumulatively, these analyses demonstrate that the coding potential of *E. coli* K-12 is less than that expected from the high density of predicted CDSs. However, the functional component of a genome is not confined to protein coding regions. There are not only transfer and ribosomal RNAs that operate in translation but also numerous small noncoding RNAs (sRNAs), with roles in regulation, as well as in RNA processing, stability, and degradation that have been detected in the intergenic regions of the *E. coli* genome. The numbers of predicted sRNAs in *E. coli* vary by an order of magnitude, depending on the particular procedure used to search the genome (*42*–*45*). However, more than a dozen sRNAs have been functionally characterized in *E. coli*, and there is strong support for at least 50 others (*46*, *47*).

The ultimate objective of genomics is to elucidate the biological role and phenotypic consequence of every nucleotide within a genome. Given that most bacterial lineages experience a massive turnover of genes through acquisition of foreign DNA and loss of existing sequences, any given genome will possess the "debris" generated by these dynamics. Delineating these sites and regions must be a central goal if we are to attain a comprehensive understanding of genomes.

E. coli K-12, and indeed most other bacteria, contains fewer functional protein-coding regions than anticipated, but many functional elements may lay hidden in the noncoding portion of genomes. Such insights alter our expectations about the contents and organization of bacterial genomes. We now recognize that many apparent coding regions might never surrender a meaningful phenotype, no matter how sensitive the assay. Alternatively, those genomic regions not regularly surveyed are likely to control many phenotypes.

References and Notes

1. A. Mira, H. Ochman, N. A. Moran, *Trends Genet.* **17**, 589 (2001).
2. S. G. E. Andersson *et al.*, *Nature* **396**, 133 (1998).
3. S. T. Cole *et al.*, *Nature* **409**, 1007 (2001).
4. J. Parkhill *et al.*, *Nature* **413**, 523 (2001).
5. J. O. Andersson, S. G. E. Andersson, *Curr. Opin. Genet. Dev.* **9**, 664 (1999).
6. J. O. Andersson, S. G. E. Andersson, *Mol. Biol. Evol.* **18**, 829 (2001).
7. D. A. Petrov, D. L. Hartl, *J. Hered.* **91**, 221 (2000).
8. N. A. Moran, G. R. Plague, *Curr. Opin. Genet. Dev.* **14**, 627 (2004).
9. P. D. Keightley, M. J. Lercher, A. Eyre-Walker, *PLoS Biol.* **3**, e42 (2005).
10. Q. Jin *et al.*, *Nucleic Acids Res.* **30**, 4432 (2002).
11. D. I. Andersson, D. Hughes, *Proc. Natl. Acad. Sci. U.S.A.* **93**, 906 (1996).
12. V. S. Cooper, R. E. Lenski, *Nature* **407**, 736 (2000).
13. C. M. Fraser *et al.*, *Science* **270**, 397 (1995).
14. N. A. Moran, J. J. Wernegreen, *Trends Ecol. Evol.* **15**, 321 (2000).
15. P. Bork, *Genome Res.* **10**, 398 (2000).
16. S. Bocs, A. Danchin, C. Medigue, *BMC Bioinformatics* **3**, 5 (2002).
17. D. W. Ussery, P. F. Hallin, *Microbiology* **150**, 2015 (2004).
18. E. Kolker *et al.*, *Nucleic Acids Res.* **32**, 2353 (2004).
19. H. Ogata *et al.*, *Science* **293**, 2093 (2001).
20. P. S. Chain *et al.*, *Proc. Natl. Acad. Sci. U.S.A.* **101**, 13826 (2004).
21. J. L. Oliver, A. Marin, *J. Mol. Evol.* **43**, 216 (1996).
22. H. Charles, D. Mouchiroud, J. Lobry, I. Goncalves, Y. Rahbe, *Mol. Biol. Evol.* **16**, 1820 (1999).
23. M. H. Serres, S. Goswami, M. Riley, *Nucleic Acids Res.* **32**, D300 (2004).
24. I. M. Keseler *et al.*, *Nucleic Acids Res.* **33**, D334 (2005).
25. R. V. Misra, R. S. Horler, W. Reindl, I. I. Goryanin, G. H. Thomas, *Nucleic Acids Res.* **33**, D329 (2005).
26. F. R. Blattner *et al.*, *Science* **277**, 1453 (1997).
27. K. Homma, S. Fukuchi, T. Kawabata, M. Ota, K. Nishikawa, *Gene* **294**, 25 (2002).
28. E. Lerat, H. Ochman, *Genome Res.* **14**, 2273 (2004).
29. S. Y. Gerdes *et al.*, *J. Bacteriol.* **185**, 5673 (2003).
30. M. Nei, S. Kumar, *Molecular Evolution and Phylogenetics* (Oxford Univ. Press, New York, 2000).
31. H. Ochman, *Trends Genet.* **18**, 335 (2002).
32. J. G. Lawrence, *Trends Genet.* **19**, 131 (2003).
33. Z. Yang, *Mol. Biol. Evol.* **15**, 568 (1998).
34. E. Lerat, H. Ochman, *Nucleic Acids Res.* **33**, 3125 (2005).
35. P. C. Ng, S. Henikoff, *Nucleic Acids Res.* **31**, 3812 (2003).
36. A. Lobner-Olesen, M. G. Marinus, F. G. Hansen, *Proc. Natl. Acad. Sci. U.S.A.* **100**, 4672 (2003).
37. R. W. Corbin *et al.*, *Proc. Natl. Acad. Sci. U.S.A.* **100**, 9232 (2003).
38. S. J. Arends, D. S. Weiss, *J. Bacteriol.* **186**, 880 (2004).
39. D. W. Selinger *et al.*, *Nat. Biotechnol.* **18**, 1262 (2000).
40. U. Bergthorsson, H. Ochman, *Mol. Biol. Evol.* **15**, 6 (1998).
41. The fraction of acquired genes that becomes dispensable is estimated by comparing the absolute numbers of acquired genes that are unique to *E. coli* K-12 to those shared among *E. coli* strains. Since its split from *Salmonella*, the *E. coli* lineage leading to strain K-12 acquired 394 genes, of which 91 are restricted to the genome of the K-12 strain (*48*). These 91 genes accumulated over a period spanning just under 5% of the history of the lineage, with the disproportionate representation of recent acquisitions attributable to the loss of older arrivals. If the acquisition rate has been relatively constant, only 303 genes remain from a total of 2093 that were introduced up to the time when K-12 diverged from other *E. coli* strains. Because most pseudogenes are of recent origin, the attrition rate of 85% can be applied to the 91 genes unique to *E. coli* K-12, yielding 77 expendable genes. In this regard, it is noteworthy that M. Taoka *et al*. (*49*) found that only a small fraction (~10%) of genes mapping to *E. coli* regions specific to K-12 are translated into proteins.
42. L. Argaman *et al.*, *Curr. Biol.* **11**, 941 (2001).
43. R. J. Carter, I. Dubchak, S. R. Holbrook, *Nucleic Acids Res.* **29**, 3928 (2001).
44. E. Rivas, R. J. Klein, T. A. Jones, S. R. Eddy, *Curr. Biol.* **11**, 1369 (2001).
45. K. M. Wassarman, F. Repoila, C. Rosenow, G. Storz, S. Gottesman, *Genes Dev.* **15**, 1637 (2001).
46. R. Hershberg, S. Altuvia, H. Margalit, *Nucleic Acids Res.* **31**, 1813 (2003).
47. J. Vogel *et al.*, *Nucleic Acids Res.* **31**, 6435 (2003).
48. V. Daubin, H. Ochman, *Genome Res.* **14**, 1036 (2004).
49. M. Taoka *et al.*, *Mol. Cell. Proteomics* **3**, 780 (2004).

50. Funded by NIH grant GM56120 to H.O. We thank N. Moran, A. Corthals, E. Groisman, and the three anonymous reviewers for their comments on the manuscript; E. Lerat for providing information about *E. coli* pseudogenes; P. Ng for assistance with SIFT; and S. Miller and B. Nankivell for technical support. The GenBank accession number for the *E. coli* MG1655 genome is U00096. Gene designations in tables S1 to S5 follow those in the most recent release (obtained from www.genome.wisc.edu/sequencing/updating.htm).

Supporting Online Material

www.sciencemag.org/cgi/content/full/311/5768/1730/DC1
Tables S1 to S5

10.1126/science.1119966

An Integrated Logic Circuit Assembled on a Single Carbon Nanotube

Zhihong Chen,[1] Joerg Appenzeller,[1]* Yu-Ming Lin,[1] Jennifer Sippel-Oakley,[2] Andrew G. Rinzler,[2] Jinyao Tang,[3] Shalom J. Wind,[4] Paul M. Solomon,[1] Phaedon Avouris[1]*

The excellent electrical properties of single-walled carbon nanotubes (SWCNTs) make them the most promising candidate for creating transistors on a scale smaller than can be achieved with silicon. A field-effect transistor (FET), which is the basic component of present computer circuitry, has been demonstrated based on individual SWCNTs (*1*, *2*). An important next step would be the construction of integrated circuits along a single SWCNT. This achievement would demonstrate that SWCNTs can be used as a basis for electronics, similar to the way silicon wafers are currently used. A ring oscillator is the ultimate test for new materials in high-frequency ac applications and for evaluating their compatibility with conventional circuit architectures. Here we demonstrate a complementary metal-oxide semiconductor (CMOS)–type ring oscillator built entirely on one 18-μm-long SWCNT (Fig. 1A).

In a CMOS inverter, both an n-type FET (electron carrier) and a p-type FET (hole carrier) are needed to realize a basic logic function. In order to obtain both p- and n-type FETs on the same SWCNT, we controlled the polarities of the FETs by using metals with different work functions as the gates. We chose Pd as the metal gate for the p-FET and Al for the n-FET. The difference in the work functions of these two metals effectively shifts the SWCNT FET characteristics to form a p/n-FET pair (Fig. 1B). In each logic cycle, ideally only one of the two FETs is active, with only a very small current passing through the inverter; therefore, CMOS logic involves almost no static power dissipation. By arranging five inverters (10 FETs) side by side on one SWCNT, we successfully applied the CMOS architecture onto a single molecule to realize a ring oscillator circuit. An extra inverter stage (two FETs), which eliminates interference between the measurement setup and the oscillator operation, follows the ring oscillator portion to allow for the signal to be read by a spectrum analyzer. The inverter characteristics (Fig. 1C) show that the gain is greater than one. Signal propagation in a ring oscillator requires all five inverters to be stable throughout the oscillation cycles, and its robustness can be judged from the area of the "eye" (Fig. 1C, shaded area).

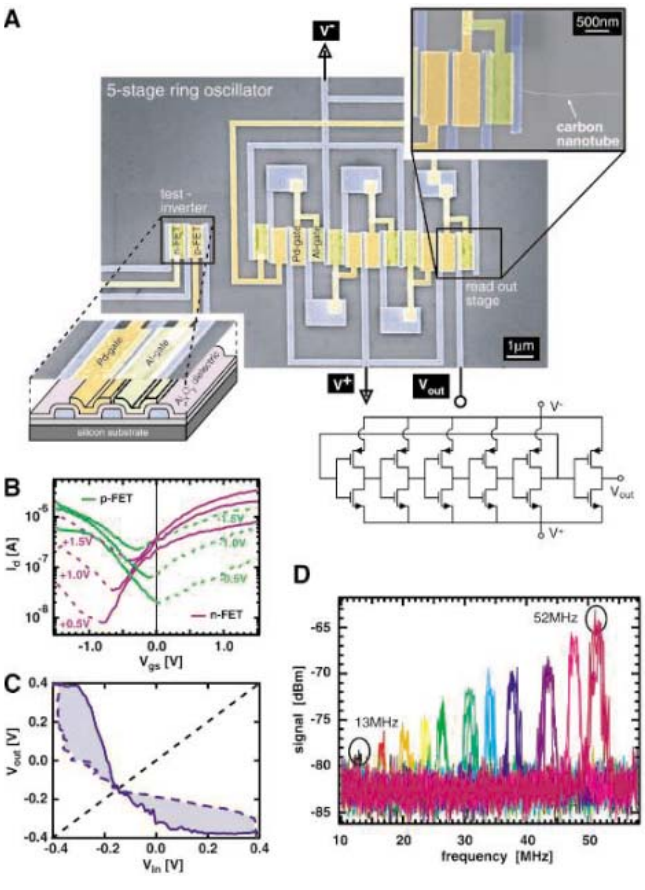

Fig. 1. (**A**) Scanning electron microscope image of a SWCNT ring oscillator consisting of five CMOS inverter stages. A test inverter was added to determine the parameter set for the actual measurement. (**B**) Characteristics for the p-type FET with Pd metal gate and n-type FET with Al gate. (**C**) Inverter characteristics and its mirrored curve. (**D**) Voltage-dependent frequency spectra. From the left to the right, the respective supply voltages are as follows: V_{dd} = 0.5 V and 0.56 V to 0.92 V (in 0.4-V increments).

The output signal of the ring oscillator was measured as a function of the supply voltage (Fig. 1D). A resonance occurs at 13 MHz for supply voltage V_{dd} = 0.5 V. The frequency increases with the voltage and reaches 52 MHz at V_{dd} = 0.92 V, with a corresponding stage-delay time of 1.9 ns. This behavior, which is a result of the increasing drain current I_d in the individual FETs with increasing gate/drain voltage, agrees with the anticipated operation of the ring oscillator. The measured frequencies are limited by the parasitics rather than by the intrinsic nanotube properties (*3*). Compared with previous ring oscillators fabricated on multiple nanotubes with external wiring (*4*, *5*), our ring oscillator shows a five– to six–orders of magnitude greater frequency response. Between V_{dd} = 0.5 V and V_{dd} = 0.92 V, the signal height detected by the spectrum analyzer changed from –79 dB m to –64 dB m, again as a consequence of the I_d–V_{dd} dependence. Because of the impedance mismatch between the output of the ring oscillator (~1 × 10^6 ohm) and the input of the spectrum analyzer (50 ohm), the circuit signal is attenuated by approximately four orders of magnitude, resulting in signal heights of 25 to 140 μV rather than the applied V_{dd}.

The demonstrated intramolecular ring oscillator is a useful tool to characterize the suitability of SWCNTs for ac applications. It enables the detailed study of the performance-limiting aspects in SWCNTs and offers a way to evaluate their potential as a platform for future nanoelectronics applications. The central goal is to ultimately benefit from the expected intrinsic switching speed in SWCNT FETs, which is predicted to allow for terahertz applications.

References and Notes

1. S. J. Tans, A. R. M. Verschueren, C. Dekker, *Nature* **393**, 49 (1998).
2. R. Martel, T. Schmidt, H. R. Shea, T. Hertel, P. Avouris, *Appl. Phys. Lett.* **73**, 2447 (1998).
3. Supporting materials are available on *Science* Online.
4. A. Bachtold, P. Hadley, T. Nakanishi, C. Dekker, *Science* **294**, 1317 (2001).
5. A. Javey, Q. Wang, A. Ural, Y. Li, H. Dai, *Nano Lett.* **2**, 929 (2002).

6. S.J.W. and J.T. acknowledge support under NSF Award CHE-0117752 and New York State Office of Science, Technology, and Academic Research.

Supporting Online Material

www.sciencemag.org/cgi/content/full/311/5768/1735/DC1
SOM Text
References and Notes

18 November 2005; accepted 8 February 2006
10.1126/science.1122797

[1]IBM Thomas J. Watson Research Center, Yorktown Heights, NY 10598, USA. [2]Department of Physics, University of Florida, Gainesville, FL 32611, USA. [3]Department of Chemistry and [4]Department of Applied Physics and Applied Mathematics, Columbia University, New York, NY 10027, USA.

*To whom correspondence should be addressed. E-mail: joerga@us.ibm.com (J.A.); avouris@us.ibm.com (P.A.)

Niche Partitioning Among *Prochlorococcus* Ecotypes Along Ocean-Scale Environmental Gradients

Zackary I. Johnson,[1,2]* Erik R. Zinser,[1,3]* Allison Coe,[1] Nathan P. McNulty,[1] E. Malcolm S. Woodward,[4] Sallie W. Chisholm[1]†

Prochlorococcus is the numerically dominant phytoplankter in the oligotrophic oceans, accounting for up to half of the photosynthetic biomass and production in some regions. Here, we describe how the abundance of six known ecotypes, which have small subunit ribosomal RNA sequences that differ by less than 3%, changed along local and basin-wide environmental gradients in the Atlantic Ocean. Temperature was significantly correlated with shifts in ecotype abundance, and laboratory experiments confirmed different temperature optima and tolerance ranges for cultured strains. Light, nutrients, and competitor abundances also appeared to play a role in shaping different distributions.

The marine cyanobacterium genus *Prochlorococcus* (*1*) is the numerically dominant phytoplankter in tropical and subtropical oceans (*2*–*5*). It is distributed throughout the illuminated surface waters from about 40°N to 40°S, can be found as deep as 200 m, and sometimes reaches abundances greater than 10^5 cells per ml (*2*). *Prochlorococcus* can account for 21 to 43% of the photosynthetic biomass in oligotrophic oceans and 13 to 48% of the net primary production (*4*–*6*). As such, its abundance and dynamics have a substantial impact on open ocean ecosystems and global biochemical cycles.

In the tropical and subtropical Atlantic Ocean, *Prochlorococcus* maintains its numerical dominance throughout most of the year, despite 10-fold changes in depth-integrated abundance (*3*, *6*). It reaches its maximum (*6*, *7*) when surface waters are highly stratified and devoid of major nutrients (*8*) and its minimum during deep winter mixing when blooms of *Synechococcus* and larger eukaryotic phytoplankton occur (*3*, *6*, *7*). *Prochlorococcus* abundance falls off sharply at higher latitudes, suggesting that temperature, or some related variable, is an important factor in shaping its global distributions (*2*).

Phylogenetic trees constructed with several marker genes, including small subunit (SSU) ribosomal RNA (rRNA), the rRNA internal transcribed spacer (ITS) regions, *psbB*, *petB/D*, and *rpoC1*, as well as whole-genome analyses, show that flow-cytometrically defined (*9*) *Prochlorococcus* is a genetically diverse group with several distinct clades, which have SSU rRNA gene sequences that differ by less than 3% (*10*–*14*). Cultured strains belonging to different clades have different pigmentation, maximum growth rates, metal tolerances, nutrient utilization, and photophysiological characteristics, and thus these clades have been called ecotypes (*15*–*17*). The ecotypes have recently been named after type strains with the prefix "e" (*18*, *19*). Cells belonging to different ecotypes are distributed differently along environmental gradients. For example, high light–adapted ecotypes [sensu (*12*)] such as eMIT9312 and eMED4 are more abundant near the surface than low light–adapted ecotypes such as eSS120, eMIT9313, eNATL2A, and eMIT9211 (*18*–*20*), which are typically most abundant in the deeper waters.

To better understand the drivers of ecotypic differentiation between *Prochlorococcus* clades, we measured, by using quantitative polymerase chain reaction (qPCR), the abundance of cells belonging to the six known ecotypes (fig. S1) as a function of depth along a meridional transect in the Atlantic Ocean (AMT) (*21*) (Fig. 1A). We then analyzed the distribution and abundance of ecotypes in the context of relevant environmental variables and the physiological properties of type strains.

The AMT transect covered a broad range of biogeochemical provinces (*22*), with surface temperatures ranging from 5°C to 29°C (Fig. 1A). The availability of major phytoplankton nutrients, including nitrate, nitrite, ammonium, phosphate, and silicate, also varied, reaching maxima in the south, near the coastal Canary Current upwelling system, and around the equatorial upwelling region (Fig. 1D and fig. S2). For all locations, nitrate, phosphate, and silicate concentrations were correlated (r^2 = 0.9), following near Redfield ratios (15 N/1 P/1 to 10 Si), whereas nitrite and ammonium were localized to specific regions and depths and did not follow strict relationships with other nutrients (figs. S2 and S3). Consistent with these nutrient patterns, surface chlorophyll fluorescence, an indicator of autotrophic biomass, was elevated at high latitudes and in the Canary Current upwelling system but remained low in the severely nutrient-limited subtropical gyres (Fig. 1A).

Ecotype distributions. The depth distributions of *Prochlorococcus* ecotypes at three stations representing different biogeochemical provinces revealed distinctly different patterns (Fig. 1B). Although total *Prochlorococcus* abundance (which was measured independently by using flow cytometry) was maximal at the surface and decreased with depth at each station, the ecotypes comprising this total had different distributions. In well-stratified waters (1°N and 25°N in Fig. 1B), ecotype depth distributions had a stacked nature typical of these environmental conditions (*18*, *19*). The high light–adapted clades eMIT9312 or eMED4 dominated near the surface (~0 to 50 m), and low light–adapted eNATL2A increased in abundance at middepths (~75 m), followed by eMIT9313, another low-light clade. Closer examination of the patterns at these two stations, however, revealed subtle differences that suggest that light adaptation was not the only variable shaping distributions. At 1°N, for example, eNATL2A and eMED4, low and high light–adapted clades, respectively, were roughly equal in abundance at the surface, whereas at 25°N eNATL2A was orders of magnitude less abundant than eMED4 near the surface. At high latitudes such as 48°N (Fig. 1B), one of the high light–adapted clades, eMED4, outnumbered the other, eMIT9312, by orders of magnitude in surface waters. Furthermore, the low light–adapted clade eMIT9313, which displayed deep subsurface maxima (~100 m) at low and midlatitudes, was so reduced in numbers at high latitudes that it was near the limit of detection. As has been previously reported (*18*, *19*), two of the clades, eMIT9211 and eSS120, were present at low concentrations (<50 cells per ml) in all samples and thus were not included in this part of our analysis (fig. S4).

Similar shifts in ecotype dominance were also revealed by ecotype depth-integrated abundances along the entire transect (Fig. 1C), despite relatively constant (~1×10^7 to 2×10^7 cells per mm^2) total *Prochlorococcus* concentrations. Overall, high light–adapted eMIT9312 was the dominant ecotype, exceeding the abundance of other ecotypes by two orders of magnitude between 15°N and 15°S. Low light–adapted ecotypes eNATL2A and eMIT9313 had roughly equal abundance in this part of the transect, and high light–adapted

[1]Department of Civil and Environmental Engineering, Massachusetts Institute of Technology, 15 Vassar Street 48-419, Cambridge, MA 02139, USA. [2]Department of Oceanography, University of Hawaii, 1000 Pope Road MSB614, Honolulu, HI 96822, USA. [3]Department of Microbiology, University of Tennessee, M409 WLS, Knoxville, TN 37996, USA. [4]Plymouth Marine Laboratory, Prospect Place, The Hoe, Plymouth PL1 3DH, UK.

*These authors contributed equally to this work.
†To whom correspondence should be addressed. E-mail: chisholm@mit.edu

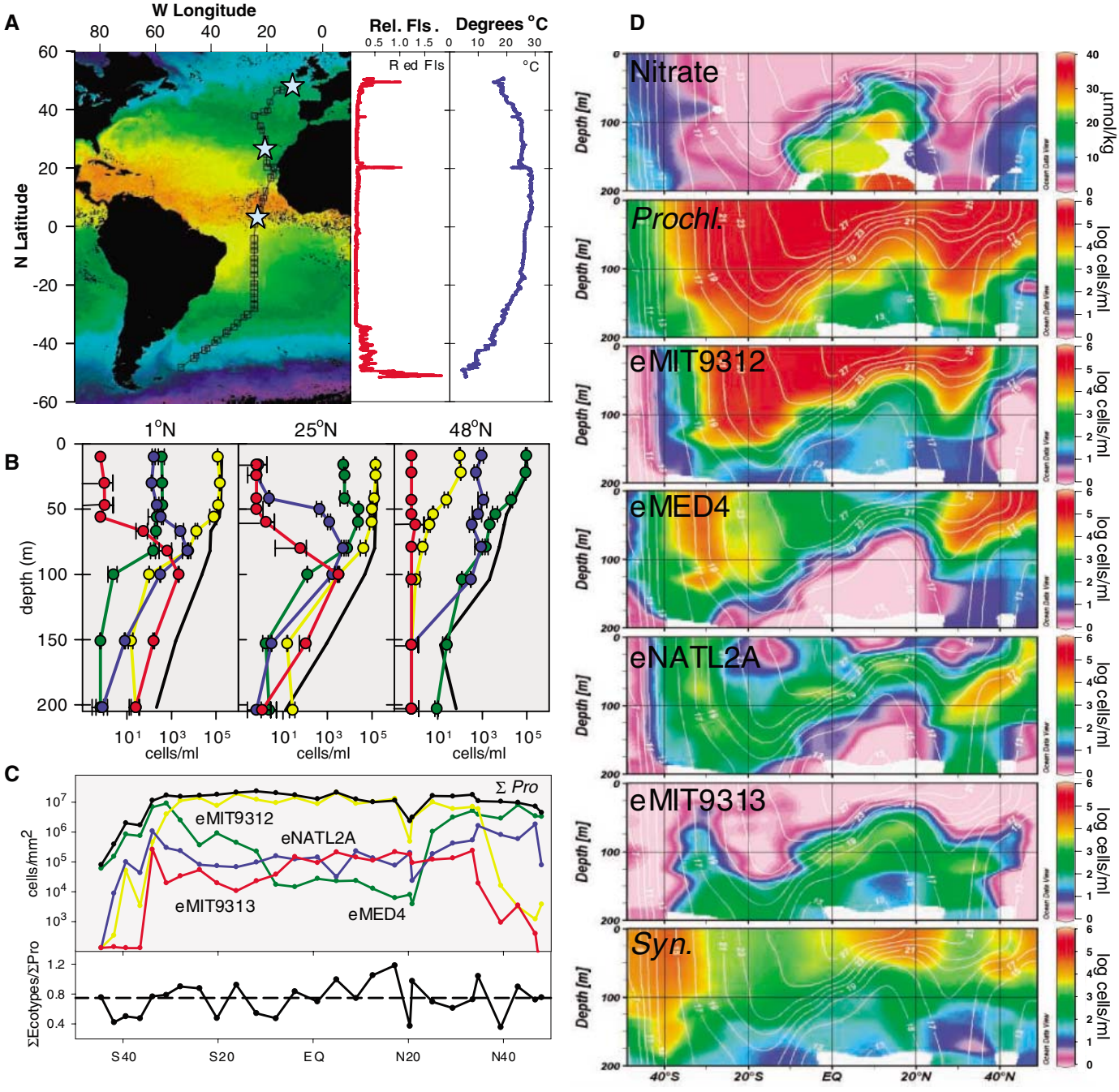

Fig. 1. (**A**) False-color image of sea surface temperature during the Atlantic Ocean meridional transect cruise (AMT13) from September to October 2003, overlaid with cruise track and sampled stations (boxes). Reds are warm temperatures; blues are cold temperatures. (Right) In situ measured surface red fluorescence (relative) (Rel. Fls), indicative of chlorophyll concentrations and temperature. The cruise track goes through the coastal Canary Current upwelling feature around 20°N. (**B**) Depth profiles of the abundance of four dominant *Prochlorococcus* ecotypes (red, eMIT9313; blue, eNATL2A; green, eMED4; and yellow, eMIT9312) and total *Prochlorococcus* cell concentrations (solid black) from three representative stations [stars in (A)]. The 1°N station is typical of equatorial region stations, 25°N is typical of stratified subtropical stations, and 48°N is typical of high-latitude (not polar) stations. Note that the abundance scale is logarithmic. Error bars indicate one standard deviation of the mean. (**C**) (Top) Depth-integrated (0 to 200 m) ecotype abundance and total *Prochlorococcus* abundance over the transect. (Bottom) Meridional distribution of the ratio of the summed ecotype abundances measured by qPCR and total *Prochlorococcus* abundance determined by flow cytometry. (**D**) Cross sections along the transect (upper 200 m) of nitrate concentration (µmol kg^{-1}); total *Prochlorococcus* (log cells per ml); dominant ecotype clade abundances (log cells per ml) for eMIT9312, eMED4, eNATL2A, and eMIT9313; and *Synechococcus* (log cells per ml). Temperature contour lines are shown in white.

eMED4 was the least abundant. By contrast, in cooler, well-mixed, nutrient-rich, high-latitude waters where eMED4 achieved numerical dominance, eMIT9313 disappeared, and eNATL2A achieved the second highest abundance. eMIT9312, the most abundant clade in the tropical and subtropical oceans, was below the detection limit at latitudes above 42°S. Our qPCR primers, designed from sequences of cultured isolates, captured on average ~75% (range from 35 to 118%) of the total *Prochlorococcus* population counted by using flow cytometry (Fig. 1C),

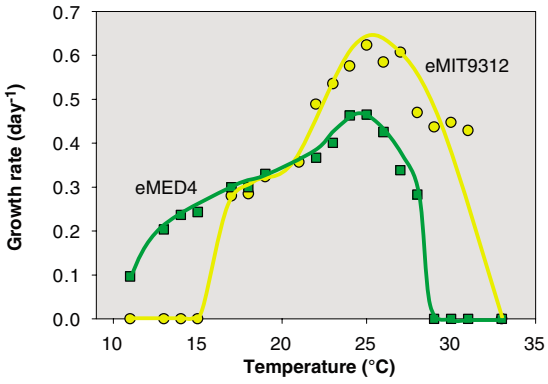

Fig. 2. Maximum growth rate as a function of temperature derived from the analysis of cultured strains belonging to the eMIT9312 clade (yellow) and the eMED4 clade (green), the two dominant near-surface ecotypes. (Specific strain data are shown in fig. S5.)

indicating that there are likely additional members not quantified in this study. However, there was no pattern to the residuals, suggesting that our observations were not greatly affected by culture bias (*23*).

Environmental factors and ecotype abundance. By using nitrate concentration to represent a suite of covarying nutrients (figs. S2 and S3), depth as related to light intensity, and plotting temperature contours on a slice through the upper 200 m along the transect, we visualized how ecotype abundances map on to environmental gradients (Fig. 1D). As expected, total *Prochlorococcus* cell concentrations were typically highest at or near the surface and decreased with depth. They were also highest in warm waters, which here are defined as waters above the 17°C isotherm, except below 150 m, where populations were likely limited by light availability. Lastly, total *Prochlorococcus* abundances were highest where nutrients were lowest, consistent with findings in other tropical and subtropical oligotrophic regions (*4*, *6*, *7*, *24*).

These patterns of total *Prochlorococcus* abundance emerge from the distributions of ecotypes, which display more complex behavior when viewed individually. For example, the relative abundances of the high light–adapted ecotypes (eMIT9312 and eMED4) depended on latitude and closely followed nutrient and temperature contours (Fig. 1D). eMIT9312 dominated at low and midlatitudes but was progressively replaced by eMED4 at latitudes above 30°. Thus, these two ecotypes, which differ in their SSU rRNA sequences by less than 1% (*12*), had overlapping but distinct niches in the Atlantic Ocean and comprised the majority (93%) of the *Prochlorococcus* cells over the transect.

Ecotypes eMIT9313 and eNATL2A had more restricted distributions. eNATL2A was most prevalent along the trailing edge of the eMIT9312 abundance contour and was most abundant in waters between the 15°C and 23°C isotherms. This distribution started at the surface waters of 45°N, meandered in the water column in mid- and low latitudes, and reached higher abundances again at the surface waters near 30°S. eNATL2A only reached high concentrations in deeper waters, where eMIT9312 and eMED4 numbers were reduced. Similarly, eMIT9313's distribution was more patchy and localized to specific latitudes or depths, closely following the vertical gradients of eMIT9312 and eMED4, and was maximal where total *Prochlorococcus* abundance decreased the most sharply with depth. Thus, although eNATL2A and eMIT9313 were minor contributors to overall *Prochlorococcus* numbers in the Atlantic Ocean, they dominated at certain depths and latitudes.

Regression analysis. The geographic patterns of *Prochlorococcus* and its ecotypes suggest causal relationships with environmental variables (Fig. 1D). We used stepwise regression analyses to investigate relationships with temperature, light, nitrate, nitrite, ammonia, phosphate, and *Synechococcus* (a potential competitor) (table S1). As has been observed previously (*25*), a significant fraction (26%, $P < 0.01$) of the variability in the total *Prochlorococcus* population could be explained by temperature, which was largely driven by significant correlations between the numerically dominant ecotype, eMIT9312, and temperature (56%, $P < 0.01$). By using laboratory isolates belonging to the two dominant (and high light–adapted) ecotypes, we found that, although both had similar temperature optima for growth, members of eMIT9312 grew faster at this temperature (25°C) and could tolerate warmer temperatures than eMED4. The latter could grow at temperatures below 15°C, however, whereas eMIT9312 could not (Fig. 2 and fig. S5), thus confirming the importance of temperature in defining ecotype niche space.

Prochlorococcus ecotype abundances are related to other variables as well. For example, eMED4 was correlated (9%, $P < 0.01$) with light, which is consistent with its adaptations to high light (*16*). Nutrient relationships were complex (often being anticorrelated with ecotypes) (table S1) and were generally not consistent with the ability of strains to use nutrient sources (*17*, *26*), suggesting that colinear variables not measured here were responsible for these relationships. Integrated abundances of *Synechococcus* (Fig. 1D), which unlike *Prochlorococcus* can use nitrate (*17*), were also inversely related to *Prochlorococcus* (fig. S6). This relationship has been found before for seasonal cycles in the Atlantic Ocean (*3*, *6*) and implies that at high nutrient levels *Synechococcus* and larger phytoplankton may exclude *Prochlorococcus*. But this relationship with *Synechococcus* was complex: eMIT9313 was anticorrelated (22% of the variability), eMED4 (18%) and eMIT9312 (10%) were correlated, and the abundance of eNATL2A was uncorrelated.

The stepwise regressions, which had varying degrees of success in explaining the overall abundance patterns, also demonstrated that there were additional factors that were important in determining *Prochlorococcus* ecotype abundance. This complexity is likely governed by differential susceptibility to viruses (*27*) and protozoan grazers (*28*) as well as other factors, such as metal tolerances (*15*).

The relationships we have established here represent only a broad-brush assessment, to be refined as we learn more about *Prochlorococcus* microdiversity. By design, multiple ribotypes (based on ITS sequences) are represented in the ecotype populations that are enumerated by our qPCR primers (*18*), and it is likely that each of these is a physiological and genomic variant. This prompts the question: If one designed primers to enumerate ribotypes within the ecotype clusters, what would their distributions look like along these gradients? Would they be more similar to each other than to those belonging to other clades? Furthermore, although the four dominant ecotypes account for the majority of the total *Prochlorococcus* population, our analyses (Fig. 1), as well as evidence from clone libraries (*18*) and Sargasso Sea shotgun sequencing (*29*), reveal the existence of additional genotypes that do not group with any of the six defined genetic clades and thus would not be captured by our approach. These additional clades likely account for the difference between the total *Prochlorococcus* population measured by flow cytometry and the summed clades measured by qPCR (Fig. 1C), particularly in the deeper waters (Fig. 1B).

References and Notes

1. S. W. Chisholm *et al.*, *Nature* **334**, 340 (1988).
2. F. Partensky *et al.*, *Microbiol. Mol. Biol. Rev.* **63**, 106 (1999).
3. R. J. Olson *et al.*, *Deep-Sea Res. Part I Oceanogr. Res. Pap.* **37**, 1033 (1990).
4. L. Campbell *et al.*, *Deep-Sea Res. Part I Oceanogr. Res. Pap.* **44**, 167 (1997).
5. D. Vaulot, D. Marie, R. J. Olson, S. W. Chisholm, *Science* **268**, 1480 (1995).
6. M. D. DuRand *et al.*, *Deep-Sea Res. Part II Top. Stud. Oceanogr.* **48**, 1983 (2001).
7. M. V. Zubkov *et al.*, *Prog. Oceanogr.* **45**, 369 (2000).
8. Z. Johnson, P. Howd, *Deep-Sea Res. Part I Oceanogr. Res. Pap.* **47**, 1485 (2000).
9. L. R. Moore *et al.*, *Nature* **393**, 464 (1998).
10. E. Urbach *et al.*, *J. Mol. Evol.* **46**, 188 (1998).
11. E. Urbach, S. W. Chisholm, *Limnol. Oceanogr.* **43**, 1615 (1998).
12. G. Rocap *et al.*, *Appl. Environ. Microbiol.* **68**, 1180 (2002).
13. G. Rocap *et al.*, *Nature* **424**, 1042 (2003).
14. B. Palenik, R. Haselkorn, *Nature* **355**, 265 (1992).
15. E. L. Mann *et al.*, *Limnol. Oceanogr.* **47**, 976 (2002).

16. L. R. Moore, S. W. Chisholm, *Limnol. Oceanogr.* **44**, 628 (1999).
17. L. R. Moore *et al.*, *Limnol. Oceanogr.* **47**, 989 (2002).
18. E. Zinser *et al.*, *Appl. Environ. Microbiol.* **72**, 723 (2006).
19. N. Ahlgren *et al.*, *Environ. Microbiol.* **8**, 441 (2006).
20. N. J. West, D. J. Scanlan, *Appl. Environ. Microbiol.* **65**, 2585 (1999).
21. J. Aiken *et al.*, *Prog. Oceanogr.* **45**, 257 (2000).
22. S. B. Hooker *et al.*, *Prog. Oceanogr.* **45**, 313 (2000).
23. M. S. Rappe, S. J. Giovannoni, *Annu. Rev. Microbiol.* **57**, 369 (2003).
24. L. Campbell *et al.*, *Deep-Sea Res. Part II Top. Stud. Oceanogr.* **45**, 2301 (1998).
25. K. K. Cavender-Bares *et al.*, *Deep-Sea Res. Part I Oceanogr. Res. Pap.* **48**, 2373 (2001).
26. L. R. Moore *et al.*, *Aquat. Microb. Ecol.* **39**, 257 (2005).
27. M. B. Sullivan *et al.*, *Nature* **424**, 1047 (2003).
28. B. C. Monger *et al.*, *Limnol. Oceanogr.* **44**, 1917 (1999).
29. J. C. Venter *et al.*, *Science* **304**, 66 (2004).
30. The authors acknowledge C. Robinson and the captain and crew of Royal Research Ship *James Clark Ross* for our participation in the AMT cruise and D. Veneziano for guidance with the statistical analysis. This work was funded in part by the Gordon and Betty Moore Foundation, the Seaver Foundation, NSF Biological Oceanography Division (to S.W.C.), and U.S. Department of Energy (to S.W.C.), NOAA and the University of Hawaii (to Z.I.J.), and NSF and the University of Tennessee (to E.R.Z.). It was also supported by the UK Natural Environment Research Council through the AMT consortium (NER/O/S/2001/00680). This is School of Ocean and Earth Science and Technology contribution no. 6686 and AMT contribution no. 107.

Supporting Online Material
www.sciencemag.org/cgi/content/full/311/5768/1737/DC1
Materials and Methods
Figs. S1 to S6

27 July 2005; accepted 11 January 2006
10.1126/science.1118052

REPORTS

General Strategies for Nanoparticle Dispersion

Michael E. Mackay,[1,2]* Anish Tuteja,[1] Phillip M. Duxbury,[2] Craig J. Hawker,[3,4] Brooke Van Horn,[4] Zhibin Guan,[5] Guanghui Chen,[5] R. S. Krishnan[1]

Traditionally the dispersion of particles in polymeric materials has proven difficult and frequently results in phase separation and agglomeration. We show that thermodynamically stable dispersion of nanoparticles into a polymeric liquid is enhanced for systems where the radius of gyration of the linear polymer is greater than the radius of the nanoparticle. Dispersed nanoparticles swell the linear polymer chains, resulting in a polymer radius of gyration that grows with the nanoparticle volume fraction. It is proposed that this entropically unfavorable process is offset by an enthalpy gain due to an increase in molecular contacts at dispersed nanoparticle surfaces as compared with the surfaces of phase-separated nanoparticles. Even when the dispersed state is thermodynamically stable, it may be inaccessible unless the correct processing strategy is adopted, which is particularly important for the case of fullerene dispersion into linear polymers.

Polymer phase stability in solution (*1*) or with another polymer (*2*) has been studied for over 50 years and found to be a delicate balance of entropic and enthalpic contributions to the total free energy. For example, it is possible to fractionate a polymer by size with a small change in solvent quality (*3*) and to control miscibility of chemically identical polymers whose only difference is architecture (branching) (*4*). More recently, the phase stability of nanoparticle-polymer blends has attracted intense scrutiny (*5*) and is challenging to predict because of computational difficulty in accessing the relevant length and time scales. Flory theories, density functional theories, and molecular dynamics methods provide essential guidance, although accurate calculations are restricted to two or at most a few nanoparticles in the relevant size regime (*6*, *7*). Despite these difficulties, a vast array of applications are emerging that require nanoparticle dispersion, such as in the use of fullerenes to enhance the efficiency of polymer-based photovoltaic devices (*8*, *9*) and in the control of polymer viscosity using nanoparticles (*10*).

We demonstrate strategies for control of nanoparticle dispersion in linear polymer melts. We start with discussion of processing procedures that enable stable dispersion of fullerenes and then present an experimental characterization of the parameters that control the phase boundary between the dispersed and phase-segregated states of carefully considered nanoparticle-polymer mixtures. Moreover, it has been proven possible to disperse polyethylene nanoparticles in polystyrene despite the fact that linear polyethylene–linear polystyrene is a classic phase-separating blend, which implies that nanoparticle morphology may actually enhance dispersion. This hypothesis is tested by using a system composed of polystyrene nanoparticles dispersed in linear polystyrene, because the monomer-monomer contacts in this system are the same for all of its constituents. An enthalpic mechanism that arises from nanoparticle packing effects operates at the nanoscale and is necessary in order to understand dispersion in this size regime. A Flory theory, which includes this enthalpic contribution as well as chain stretching caused by nanoparticle dispersion and the standard mixing entropy, is used to reconcile the experimental observations and emphasize the importance of the nanoparticle-to-polymer size ratio in controlling nanoparticle dispersion.

First we discuss the dispersion of fullerenes into polystyrene, motivated by earlier work that suggested that fullerene dispersion in polymers (*11*) is poor, limiting their utility, for example, in solar cells (*8*, *9*). For a polymer blend, the insertion energy of a linear polymer chain with another controls dispersion and grows with the number of monomers in the chain. So, the insertion enthalpy of a chain of N monomers is proportional to $N\chi$, where χ is the Flory mixing parameter and is the primary cause of phase separation in incompatible blends. Nanoparticles have an insertion enthalpy that grows in proportion to the surface area of the nanoparticle, yielding an insertion enthalpy of $s \sim A\chi$, where $A = 4\pi a^2$ for a nanoparticle of radius a. Although this enhancement is not as strong as for polymer blends, dispersion of nanoparticles still depends critically on χ. We observed experimentally that it is possible to disperse up to a concentration of 2 volume % of C_{60} in linear, monodisperse polystyrene. At small nanoparticle concentration, Flory theory (*1*) gives a binodal or phase stability volume frac-

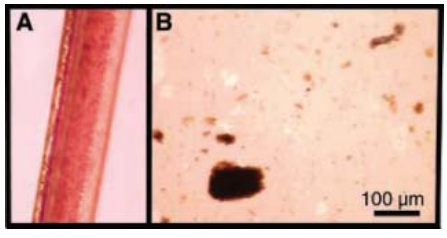

Fig. 1. (**A**) Rapid precipitation of fullerene-polystyrene blends, followed by drying and melt processing, allows manufacture of fibers. The fibers contains 1 wt % C_{60} fullerenes that were melt spun into long fibers with a diameter of circa 1 mm. (**B**) Fullerene (1 wt %)-polystyrene blends developed through regular solvent evaporation produce large, phase-separated domains, which are not apparent in the fiber.

[1]Department of Chemical Engineering and Materials Science, [2]Department of Physics and Astronomy, Michigan State University, East Lansing, MI 48824, USA. [3]Materials Research Laboratory, University of California, Santa Barbara, CA 93106, USA. [4]IBM Almaden Research Center, 650 Harry Road, San Jose, CA 95120, USA. [5]Department of Chemistry, University of California, Irvine, CA 92697, USA.

*To whom correspondence should be addressed. E-mail: mackay@msu.edu

tion (ϕ_B) of $\phi_B \approx \exp[-(1 + s)]$, assuming the phase-separated fullerenes form a pure nanoparticle phase. The use of the experimental value of $\phi_B = 0.02$ yields an insertion enthalpy per fullerene on the order of $s \approx 3$. The molecular insertion energy per monomer (ε) is given by $s = z\varepsilon/k_BT$, where z is the coordination number; k_B, the Boltzmann constant; and T, the temperature; yielding an insertion energy of $\varepsilon \approx 0.02$ eV for fullerenes in polystyrene. This relatively small energy may be rationalized by the fact that favorable molecular contacts between the aromatic rings on polystyrene and the hexagons on the surface of C_{60} may occur.

Fullerene dispersion is enabled by using our technique of rapidly precipitating the components in a mutual nonsolvent (*10*, *12*) to arrive at a dried powder that is then thermally aged, allowing melt processing and fiber spinning (Fig. 1A). It is known that fullerenes have limited solubility in organic solvents (*13*) on the order of 5 to 10 mg/ml. Solvent evaporation from a fullerene-polymer solution will lead to a fullerene supersaturated state at low overall concentration and likely phase separation (Fig. 1B). Thus, to reach the thermodynamically favored state, we had to carefully control the processing procedure for nanoparticle dispersion to avoid a kinetically trapped condition.

A more surprising result is that we observed dispersion of large branched polyethylene nanoparticles (*14*, *15*) in polystyrene (Fig. 2 and SOM). This is surprising because linear polystyrene–linear polyethylene blends (*2*) have an unfavorable mixing enthalpy and are a classic phase-separating system, with complete phase separation occurring at molecular weights typical of those used here. We have taken transmission electron microscope (TEM) images and collected small angle neutron scattering (SANS) data for a wide variety of mixtures. The TEM image (Fig. 2B) illustrates the dispersion of dendritic polyethylene nanoparticles in 393-kD linear polystyrene, from which a nanoparticle radius of 10 to 15 nm can be extracted. Moreover, a Guinier analysis of SANS data (*16*, *17*) from polyethylene nanoparticles in dilute solution yields a polyethylene-nanoparticle radius of 12.8 ± 0.1 nm, which is consistent with the TEM measurement. Neutron-scattering data for the same nanoparticles blended with linear polystyrene melts with different molecular weights are also presented (Fig. 2C). Architecture and size both make a clear difference in the miscibility of this system, because the dendritic polyethylene nanoparticles are miscible with 393-kD linear polystyrene [radius of gyration (R_g) = 17.3 nm], as evidenced by the nonfractal SANS results at small wave vector (*16*, *17*). However, miscibility does not occur when the same polyethylene nanoparticles are blended with either 155-kD (deuterated) linear polystyrene (R_g = 10.5 nm) or a smaller protonated 75-kD polystyrene (R_g = 7.5 nm), as shown (Fig. 2C). The latter experiment demonstrates that the isotope effect (*18*) is not causing phase separation; rather, the relative size of the nanoparticle and polymer is key (*19*–*21*).

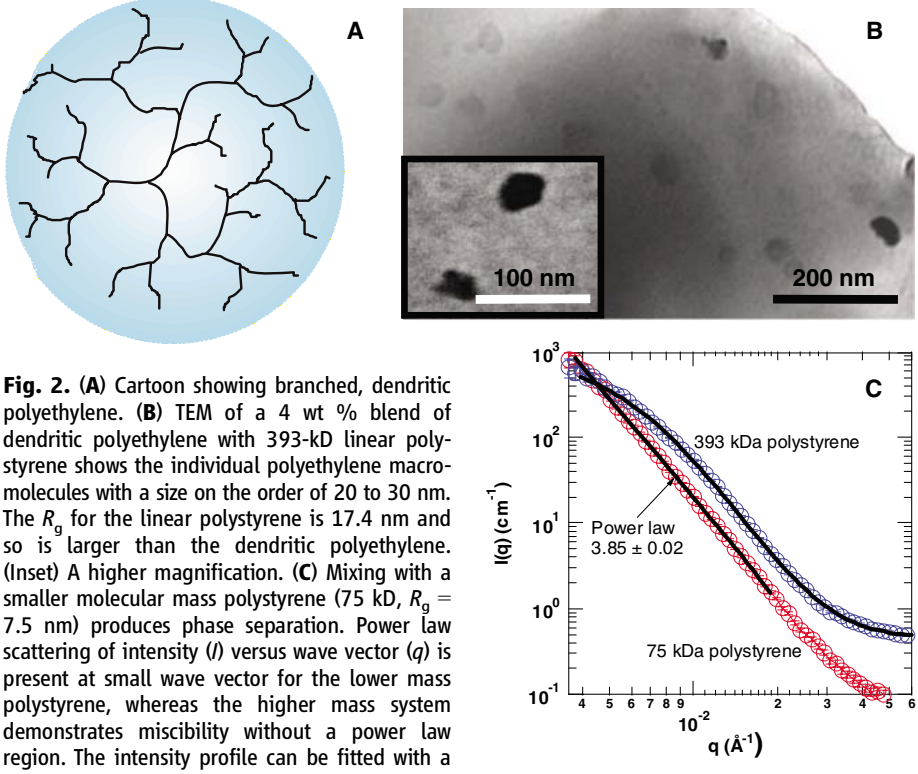

Fig. 2. (**A**) Cartoon showing branched, dendritic polyethylene. (**B**) TEM of a 4 wt % blend of dendritic polyethylene with 393-kD linear polystyrene shows the individual polyethylene macromolecules with a size on the order of 20 to 30 nm. The R_g for the linear polystyrene is 17.4 nm and so is larger than the dendritic polyethylene. (Inset) A higher magnification. (**C**) Mixing with a smaller molecular mass polystyrene (75 kD, R_g = 7.5 nm) produces phase separation. Power law scattering of intensity (I) versus wave vector (q) is present at small wave vector for the lower mass polystyrene, whereas the higher mass system demonstrates miscibility without a power law region. The intensity profile can be fitted with a polydisperse sphere model, yielding a mean radius (11.0 nm) for the dendritic polyethylene that agrees well with the TEM images.

A particularly clear illustration of the importance of the ratio a/R_g on nanoparticle dispersion is provided by a mixture consisting of cross-linked polystyrene nanoparticles (*22*) blended with linear polystyrene. We observed phase separation when the nanoparticle size was greater than the polymer radius of gyration in a manner similar to that observed in the case of polyethylene nanoparticle mixtures discussed above.

Tightly cross-linked polystyrene nanoparticles, where every fifth monomer unit is potentially cross-linked (*22*), were blended with linear polystyrene (*10*). This system produces a stable blend even when the interparticle gap reaches surprisingly small distances, suggesting the linear polystyrene molecule is highly distorted (*10*). The distortion was directly measured through a SANS Guinier analysis from a sample in which 2 weight (wt) % deuterated linear polystyrene was blended with protonated linear polystyrene of similar molecular weight and various concentrations of protonated polystyrene nanoparticles (Fig. 3A). The radius of gyration for the linear polystyrene increases with nanoparticle concentration, and the linear chains remain globular in nature, as determined through careful analysis using models that distinguish between sphere-like, rod-like, and disk-like shapes (*23*).

Chain stretching has been observed in some Monte Carlo simulations (*24*), although in many others chain contraction has been noted (*25*). Both chain expansion and chain contraction have been observed in neutron scattering from isotopically labeled polydimethylsiloxane (PDMS) blends containing silica particles (*26*). In this system, nanoparticles of radius ~ 1 nm were blended with linear polymers with a similar R_g value of ~3 to 10 nm. The polymer mixtures with smaller R_g values experienced chain contraction upon nanoparticle addition, whereas the polymer mixtures with larger R_g values experienced chain expansion with nanoparticle addition. In our system, the linear polymer R_g value was varied between 4 and 11 nm, the nanoparticle radius was about 3 nm, and we observed chain expansion in all cases (Fig. 3A). Moreover, excluded volume does not fully account for the radius increase, because, if it is assumed that the individual polymer and nanoparticle densities do not change on mixing, then the radius of gyration relative to that without nanoparticle incorporation (R_g/R_{g0}) is expected to vary as $(1 + \phi)^{1/5}$. The chain stretching is larger than the amount suggested by this relationship and is empirically close to $1 + c\phi$, with c about 1.

Despite the linear polymer distortion, we found that a large miscible region exists for cross-linked polystyrene nanoparticles blended with linear polystyrene (Fig. 3B). The data were determined from SANS through presence or absence of fractal-like scattering at small wave vector and at nanoparticle concentrations of 2 wt %. Fractal-like behavior is indicative of a non-equilibrium state consisting of irregular phase-separated aggregates, which exist on many length

scales, despite the fact that the phase separation is driven by a gain in equilibrium free energy. Data from the fullerene–linear polystyrene and polyethylene nanoparticle–linear polystyrene systems are also included in this phase diagram, indicating that this graph provides a useful guide for a range of nanocomposite systems. The experimental data demonstrate that if the linear polymer R_g is larger than the nanoparticle radius then miscibility is promoted. Note that both the polymer R_g and nanoparticle radius were experimentally determined via SANS.

To experimentally determine the Flory χ parameter, we found the second virial coefficient for 211-kD tightly cross-linked polystyrene nanoparticles dissolved in 473-kD deuterated linear polystyrene to be $5.3 \times 10^{-5} \pm 3.4 \times 10^{-5}$ cc-mol/g^2 at 127°C and $2.4 \times 10^{-5} \pm 0.6 \times 10^{-5}$ cc-mol/g^2 at 170°C by using SANS data and a Zimm analysis (*16*, *17*). A standard analysis, strictly valid for linear-linear architecture blends (*27*, *28*), yields Flory parameters of χ equal to -2.7×10^{-3} (at 127°C) and -1.2×10^{-3} (at 170°C), demonstrating that mixing is favored at both temperatures. Bates and Wignall (*18*) found χ to be $\sim 10^{-4}$ for deuterated polystyrene blends, indicating that the negative mixing enthalpy is not due to isotopic substitution. Furthermore, the χ parameter is found to follow $\sim +0.01 - 6/T$ (in K), confirming that favorable enthalpic interactions, which are geometric in origin, are responsible for the phase stability.

This unusual behavior is explained by considering the number of molecular contacts between monomers in the isolated nanoparticle state compared to that of a nanoparticle in the dispersed state, as illustrated in the idealized model (Fig. 3C). The energy gain of a monomer-monomer contact is taken to be ε_{np}. However, the van der Waals force operates over an effective distance (δ) so that only a fraction of the nanoparticle area $(A_C) = (z\delta/4a) \times A$ has this favorable molecular contact. Here, z is the average coordination number of the nanoparticle aggregate. The remaining uncovered surface area of the nanoparticle ($A_U \equiv A - A_C$) does not profit from favorable contacts with other nanoparticles. Nanoparticles may thus gain enthalpically favorable monomer-monomer contacts by dispersion in the polymer melt, as has been noted in recent polymer reference interaction site model (PRISM) calculations (*7*). Smaller nanoparticles do not experience this enthalpic driving force because A_C tends toward A in this limit, confirming that C_{60} fullerenes are miscible solely through a favorable mixing entropy.

The mixing enthalpy of a nanoparticle, s, can be related to the Flory parameter via $s = A_C\chi + A_U(\chi - \varepsilon_{np}/k_BT) \equiv s_0 - s_1$. Here $s_0 = A\chi$ is the insertion enthalpy in the absence of geometric effects due to uncovered area, and $s_1 = A_U \times \varepsilon_{np}/k_BT$ is the reduction in enthalpy within the pure nanoparticle phase due to uncovered area. The areas are expressed in lattice site dimensions and so are dimensionless, with s_0 representing the insertion energy per nanoparticle and χ that of a monomer unit. Although the uncovered area can be quite small on a given nanoparticle, the enthalpy gain via dispersion can be substantial because of their large numbers, given by ϕ/v_{np} with v_{np} being the nanoparticle volume ($^4/_3\pi a^3$). So, the expected enthalpic stabilization is given by $\phi/v_{np} \times s_1$, which exhibits a maximum at a nanoparticle radius of $z\delta/2$. This is truly a nanoscopic effect because δ is on the order of 1 nm and z is on the order of 6 for random packing (*29*), making the optimum radius for dispersion on the order of 3 nm, the size scale we have used in the present study. If the nanoparticles are too small, then solubility suffers from too little or no uncovered area to achieve sufficient enthalpic gain, similar to that experienced by the fullerenes, whereas a system containing larger particles has a reduced mixing enthalpy by a reduction in nanoparticle number for a given volume fraction.

The above argument hinges on uncovered area developed by rigid particles (Fig. 3C) and is related to an increase in the cohesive energy of a material from its pure state. The dendritic polyethylene nanoparticle system is a liquid at room temperature, and so application of the cartoon to this system is suspect. However, by using SANS of thermally annealed samples we measured the virial coefficient for this molecule dissolved in 393-kD linear polystyrene to be $2.1 \times 10^{-5} \pm 1.7 \times 10^{-5}$ cm^3 mol/g^2 at room temperature, yielding $\chi = -1.7 \times 10^{-3} \pm 1.3 \times 10^{-3}$. Again a negative mixing enthalpy is found. This result is rationalized first by noting the density of this material was determined to be quite small, 0.81 ± 0.02 g/cm^3, compared with the linear polyethylene amorphous density extrapolated to room temperature (*30*), 0.86 to 0.89 g/cm^3. Secondly, the melt surface tension (*31*, *32*) at 160°C was measured and found to be ≈30% lower than that for polyethylene of similar molecular weight (mass of 236 kD). Both these results point to a reduced internal energy in the isolated nanoparticle melt by using the semi-empirical relation between the surface tension (ST) and the cohesive energy density (CED, internal energy per unit volume); ST is about CED$^{2/3}$ (*33*) and is consistent with the enthalpy gain on mixing discussed above (i.e., negative χ).

We generalized our observations by using a Flory lattice theory that has proven useful in

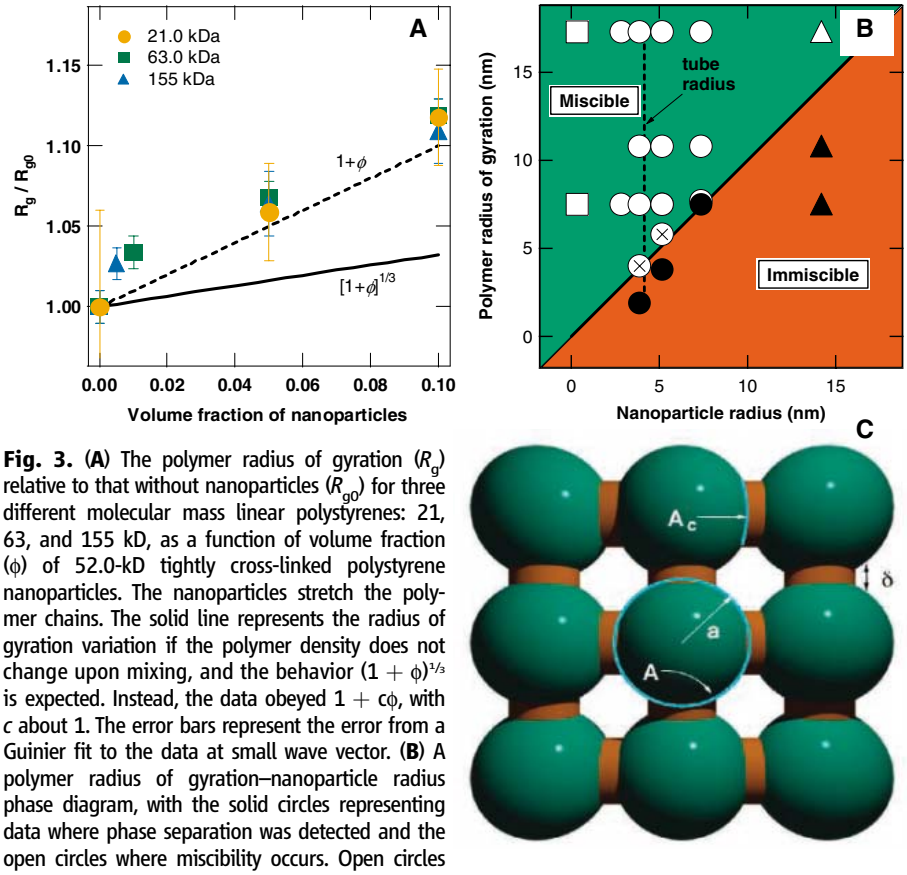

Fig. 3. (**A**) The polymer radius of gyration (R_g) relative to that without nanoparticles (R_{g0}) for three different molecular mass linear polystyrenes: 21, 63, and 155 kD, as a function of volume fraction (ϕ) of 52.0-kD tightly cross-linked polystyrene nanoparticles. The nanoparticles stretch the polymer chains. The solid line represents the radius of gyration variation if the polymer density does not change upon mixing, and the behavior $(1 + \phi)^{1/3}$ is expected. Instead, the data obeyed $1 + c\phi$, with c about 1. The error bars represent the error from a Guinier fit to the data at small wave vector. (**B**) A polymer radius of gyration–nanoparticle radius phase diagram, with the solid circles representing data where phase separation was detected and the open circles where miscibility occurs. Open circles with an × represent conditions where some agglomeration was detected by SANS yet large-scale phase separation was not observed. Squares are the C_{60}-polystyrene system; circles, the polystyrene nanoparticle–polystyrene system; and triangles, the dendritic polyethylene–polystyrene system. The dashed line represents the reptation tube radius, suggesting phase stability does not depend on the entanglement structure. The nanoparticle fraction used to generate each data point was 2 wt %. (**C**) Cartoon illustrating that the attraction between pure nanoparticles is effective only over a fraction (A_C) of the available surface area (A) because of the limited range (δ) over which dispersion forces operate.

interpreting the phase morphology of complex systems such as nanoparticle dispersion in polymer blends, where reasonable agreement with lattice density functional theory has been demonstrated (*19*). The first free energy term considered is the mixing entropy described by $F_m/Vk_BT = [\phi\log(\phi)]/v_{vp} + [(1-\phi)\log(1-\phi)]/N$, where F_m is the entropic gain due to mixing; N, the number of monomers in the linear polymer; and V, the sample volume. Polymer chain expansion (Fig. 3A) yields a loss of entropy, and so a "stretching" free energy cost (F_s) for each molecule (*34*, *35*) is included and approximated by $F_s/Vk_BT = {}^3/_2(1-\phi)(R_g{}^2/R_{g0}{}^2 - 1)/N$. Previous work (*21*, *36*) has used a chain stretching term that has its basis in the analysis of polymer brushes, which does not show as large an R_g variation with ϕ as we see experimentally. Combining the above terms, including the enthalpy of mixing discussed above, we find that

$$v_{np}F/Vk_BT = s\phi(1-\phi) + \phi\log(\phi) + t(1-\phi)\log(1-\phi) + {}^3/_2t(1-\phi)(R_g{}^2/R_{g0}{}^2 - 1) \quad (1)$$

where $t = v_{np}/N$, which in terms of experimentally accessible parameters is $t = (a/R_{g0})^3\rho/\rho_0$, where ρ is the bulk density of the linear polystyrene melt, and ρ_0 is the density associated with one chain in the bulk polystyrene melt (i.e., the density of a single chain based on its R_g and molecular weight). The fact that t increases as the cube of the size ratio a/R_{g0} implies that the stretching term is very unfavorable for $a > R_{g0}$, which is the basic reason why large nanoparticles do not disperse, although this may not be generalized to colloidal systems where other physics comes into play (*37*).

For the case of polystyrene nanoparticles in a linear polystyrene melt, we estimate the effect of the linear polymer stretch, the third term in Eq. 1, by using the data of Fig. 3A approximated by $R_g/R_{g0} \approx 1 + c\phi$. By setting the first and second derivatives of Eq. 1 with respect to ϕ to zero, one finds the binodal at $\phi_B = \exp\{-[1 + s + (3c-1)t]\} = \exp\{-[1 + s + (3c-1)(\rho/\rho_1)(a/R_{g0})^3]\}$ and the spinodal at $\phi_s = 1/[2s + (6c - 3c^2 - 1)t]$ for small ϕ. In Ginzburg's work (*21*), an addition nonideal term, the Carnahan-Starling term, is used to assess interaction effects between nanoparticles that do not alter the binodal at small concentration. Validity of the model is confirmed by calculating s from the predicted binodal concentration, assuming c is 1 (Fig. 3A). Further, letting a/R_{g0} be 1 to delineate the phase boundary (Fig. 3B) and calculating $\rho/\rho_0 (= 1.7 \times \sqrt{M})$ for polystyrene (M is molecular mass in kD), then s values of –15 and –64 for molecular masses of 30 kD (R_{g0} = 5 nm) and 320 kD (R_{g0} = 15 nm), respectively, are determined. Dividing these values by the nanoparticle area results in χ on the order of -3×10^{-3}, in good agreement with the values determined above via neutron scattering.

References and Notes

1. P. J. Flory, *Principles of Polymer Chemistry* (Cornell Univ. Press, Ithaca, NY, 1953), p. 672.
2. L. A. Utracki, *Polymer Alloys and Blends* (Hanser, New York, 1990), p. 356.
3. L. H. Cragg, H. Hammerschlag, *Chem. Rev.* **39**, 79 (1946).
4. L. A. Utracki, B. Schlund, *Polym. Eng. Sci.* **27**, 1512 (1987).
5. Y. Lin *et al.*, *Nature* **434**, 55 (2005).
6. J. B. Hooper, K. S. Schweizer, T. G. Desai, R. Koshy, P. Keblinski, *J. Chem. Phys.* **121**, 6986 (2004).
7. J. B. Hooper, K. S. Schweizer, *Macromolecules* **38**, 8858 (2005).
8. N. S. Sariciftci, L. Smilowitz, A. J. Heeger, F. Wudl, *Science* **258**, 1474 (1992).
9. N. S. Sariciftci, A. J. Heeger, *Synth. Met.* **70**, 1349 (1995).
10. M. E. Mackay *et al.*, *Nat. Mater.* **2**, 762 (2003).
11. D. Weng *et al.*, *Eur. Polym. J.* **35**, 867 (1999).
12. F. M. Du, J. E. Fischer, K. I. Winey, *J. Poly Sci. Part B* **41**, 3333 (2003).
13. V. N. Bezmel'nitsyn, A. V. Eletskii, *Usp. Fiz. Nauk* **41**, 1091 (1998).
14. Z. Guan, P. M. Cotts, E. F. McCord, S. J. McLain, *Science* **283**, 2059 (1999).
15. Z. B. Guan, *J. Poly Sci. Part A* **41**, 3680 (2003).
16. S. M. King, in *Modern Techniques for Polymer Characterisation*, R. A. Pethrick, J. V. Dawkins, Eds. (Wiley, New York, 1999).
17. J. S. Higgins, H. C. Benoît, *Polymers and Neutron Scattering* (Clarendon Press, Oxford, 2002), p. 436.
18. F. S. Bates, G. D. Wignall, *Phys. Rev. Lett.* **57**, 1429 (1986).
19. V. Lauter-Pasyuk *et al.*, *Physica B* (Amsterdam) **248**, 243 (1998).
20. R. B. Thompson, V. V. Ginzburg, M. W. Matsen, A. C. Balazs, *Science* **292**, 2469 (2001).
21. V. V. Ginzburg, *Macromolecules* **38**, 2362 (2005).
22. E. Harth *et al.*, *J. Am. Chem. Soc.* **124**, 8653 (2002).
23. J. M. Gallas, K. C. Littrell, S. Seifert, G. W. Zajac, P. Thiyagarajan, *Biophys. J.* **77**, 1135 (1999).
24. M. A. Sharaf, J. E. Mark, *Polymer* **45**, 3943 (2004).
25. M. Vacatello, *Macromolecules* **35**, 8191 (2002).
26. A. I. Nakatani, W. Chen, R. G. Schmidt, G. V. Gordon, C. C. Han, *Polymer* **42**, 3713 (2001).
27. W. A. Kruse, R. G. Kirste, J. Haas, B. J. Schmitt, D. J. Stein, *Makrom. Chem.* **177**, 1145 (1976).
28. T. P. Russell, R. S. Stein, *J. Poly Sci.* **20**, 1593 (1982).
29. C. S. O'Hern, L. E. Silbert, A. J. Liu, S. R. Nagel, *Phys. Rev. E* **68**, 011306 (2003).
30. P. Zoller, D. J. Walsh, *Standard Pressure-Volume-Temperature Data for Polymers* (Technomic, Lancaster, PA, 1995), p. 412.
31. G. T. Dee, B. B. Sauer, *J. Colloid Inter. Sci.* **152**, 85 (1992).
32. M. E. Mackay, G. Carmezini, B. B. Sauer, W. Kampert, *Langmuir* **17**, 1708 (2001).
33. D. W. van Krevelen, *Properties of Polymers, Their Estimation and Correlation with Chemical Structure* (Elsevier, New York, ed. 2, 1976), p. 620.
34. G. Marrucci, *Trans. Soc. Rheol.* **16**, 321 (1972).
35. S. Y. Park, C. J. Barrett, M. F. Rubner, A. M. Mayes, *Macromolecules* **34**, 3384 (2001).
36. J. Huh, V. V. Ginzburg, A. C. Balazs, *Macromolecules* **33**, 8085 (2000).
37. W. C. K. Poon, *J. Phys. Cond. Matter* **14**, R859 (2002).

38. Supported by NSF DMR-0520415, NSF CTS-0400840, NSF NIRT-0210247, NSF-CTS-0417640, NSF NIRT-0506309, U.S. Department of Energy DE-FG02-90ER45418, DE-FG02-05ER46211, U.S. Department of the Army, ARO W911NF-05-1-0357, NSF DMR-0135233 (Z.G. CAREER), NSF CHEM-0456719, ARO DAAD19-01-1-0686, and the U.S. Department of Energy, Basic Energy Sciences–Materials Science, under contract W-31-109-ENG-38 to the University of Chicago. We thank P. Thiyagarajan, D. Wozniak, and developers of data reduction routines at Argonne National Laboratory in gathering and analyzing the neutron scattering data; C. Popeney and D. Camacho for their help in synthesis of the dendritic polyethylene; D. Bohnsack for its characterization; A. Pastor for help with TEM; A. Frischknecht for valuable input on this work; K. Schweizer for illuminating discussions and suggesting that we should have a negative mixing enthalpy (χ parameter) to be consistent with the observed dispersion; and E. McGarrity for help with the figures.

Supporting Online Material

www.sciencemag.org/cgi/content/full/311/5768/1740/DC1
Materials and Methods
References

4 November 2005; accepted 18 January 2006
10.1126/science.1122225

Microheterogeneity of Singlet Oxygen Distributions in Irradiated Humic Acid Solutions

Douglas E. Latch and Kristopher McNeill*

Singlet oxygen ($^1O_2$) is a highly reactive species formed through solar irradiation of organic matter in environmental waters. Implicated in a range of reactions, it has proven difficult to quantify its spatial distribution in natural waters. We assessed the microheterogeneous distribution of $^1O_2$ in irradiated solutions containing chromophoric dissolved organic matter (CDOM) by using molecular probes of varying hydrophobicity. The apparent $^1O_2$ concentrations ($[^1O_2]_{app}$), measured by recently developed hydrophobic trap-and-trigger chemiluminescent probe molecules, were orders of magnitude higher than those measured by the conventional hydrophilic probe molecule furfuryl alcohol. The differential $[^1O_2]_{app}$ values measured by these probes reflect a steep concentration gradient between the CDOM macromolecules and the aqueous phase. A detailed kinetic model based on the data predicts probabilistic $^1O_2$ distributions under different solvent conditions.

Singlet oxygen ($^1O_2$), or molecular oxygen that is in its first electronic excited state ($^1\Delta_g$), has been known to be photochemically produced in natural waters since the work of Zepp *et al.* in 1977 (*1*). It is formed through interaction of dissolved oxygen with excited

triplet states of chromophoric dissolved organic matter (^{3}CDOM) (*2*, *3*). In the environment, $^1O_2$ is responsible for oxidative transformations of certain classes of organic contaminants, particularly those containing phenolic, heterocyclic, olefinic, and sulfidic moieties (*4*), and may be involved in the weathering of dissolved organic matter itself. In addition, $^1O_2$ reacts with proteins, DNA, and other biomolecules and thus is capable of damaging cells, causing mutations, inducing cell death, and inactivating viruses (*5*).

Dissolved organic matter (DOM) in natural waters is a polydisperse mixture of macromolecules derived from biological sources. With the notable exception of the open ocean (*6*), the chromophoric subset of DOM, CDOM, is well integrated into the total DOM pool. Indeed, the ultraviolet absorbance of natural waters can be used as a proxy for DOM content in a given system (*7*). Although the structure of CDOM is not known, it is believed to be composed of amphiphilic macromolecular species that have micelle-like properties (*8*). These properties allow CDOM to enhance the solubility of hydrophobic molecules (*9*–*11*). In this way, CDOM solutions resemble systems in which a $^1O_2$ sensitizer is localized within a hydrophobic microregion of an aqueous solution or suspension, where it has been demonstrated that dramatic differences in the $^1O_2$ concentration exist between the microphase and the bulk aqueous phase (*12*–*14*). Some authors have discussed the implications of microheterogeneous $^1O_2$ distributions in biological membrane–containing systems (*12*), and others have demonstrated that this effect can be used to enhance singlet oxygenation in synthetic systems (*13*, *14*). Previous work with CDOM has provided evidence for localization of other excited states and radicals (*15*–*17*).

In aquatic systems, such elevated $^1O_2$ concentrations within CDOM could have important implications. For example, the contribution of $^1O_2$ to the photoweathering and photobleaching of CDOM will be higher than expected based on the average $^1O_2$ concentration in the bulk aqueous phase. Moreover, the fact that CDOM provides a hydrophobic microenvironment in natural waters suggests that hydrophobic pollutants that partition into CDOM may be particularly susceptible to $^1O_2$-mediated photodegradation. In this case, the hydrophobic pollutants are exposed to the relatively high $^1O_2$ concentration associated with the CDOM microregion, rather than the low concentration in the bulk aqueous phase. For these reasons, we are interested in assessing the spatial distribution of $^1O_2$ in natural waters and in testing whether CDOM macromolecules may provide regions of enhanced photoreactivity. We present here evidence for the microheterogeneous distribution of $^1O_2$ in irradiated CDOM solutions.

In this study, we used stable dioxetane precursors as probe molecules to measure intra-CDOM $^1O_2$ concentrations. We chose to use these alkene probe molecules (**1**) because of their proven sensitivity and selectivity to reaction with $^1O_2$ over other reactive oxygen species and because the hydrophobicity of the probes can be tuned by altering the alkoxy substituent (*18*, *19*). The probe molecules work by a trap-and-trigger detection method, which leads to an additional experimental advantage; elicitation of the chemiluminescent signal can be temporally delayed from the $^1O_2$ photogeneration. We thus quantify photochemically produced steady-state $^1O_2$ concentrations in the absence of the irradiation source, leading to a sensitive detection method with minimal interferences. The two probes used in this study were the methoxy (**1a**, R = Me) and tetraglycol [**1b**, R = $(CH_2CH_2O)_4H$] analogs (Fig. 1), which have log octanol-water partition coefficients (log K_{OW}) of 8.1 and 6.5, respectively, estimated using the reverse-phase high-performance liquid chromatography retention time method (*20*).

Aldrich humic acid (AHA), a natural organic matter sample isolated from coal, was employed as the source of CDOM in our experiments. Although AHA's shortcomings as a model for CDOM present in natural waters has been well documented (*21*, *22*), we chose this material because of its relatively high molecular weight; its close correspondence to soil organic matter, for which good correlations between K_{OW} and organic matter–water partition coefficients (K_{OM}) exist (*23*, *24*); its use in fluorescence quenching studies, which have demonstrated associations between hydrophobic compounds and macromolecular organic matter (*25*, *26*); and for comparison to the work of Burns *et al*., who used AHA in their study of the intra-CDOM photodegradation of mirex (*16*, *17*).

Irradiation of AHA solutions with four 175-W borosilicate-filtered Hg vapor lamps led to the production of $^1O_2$. The apparent singlet oxygen concentration ($[^1O_2]_{app}$) was determined by using the rate of dioxetane formation with probes **1a** and **1b** as well as the photodegradation rate of furfuryl alcohol (FFA), a commonly used hydrophilic $^1O_2$ probe molecule. Dramatic differences in $[^1O_2]_{app}$ were observed between the three probe systems (Fig. 2, left). Consistent with previous studies, FFA reported low $[^1O_2]_{app}$ values (10^{-15} to 10^{-13} M) that varied directly with the concentration of AHA ([AHA], quantified as the amount of dissolved organic carbon per liter, i.e., mass C/liter) (*27*). Slight deviations from linearity were seen at high [AHA], likely due to light screening by the CDOM. By contrast, probe **1a** reported high $[^1O_2]_{app}$ values of about 3×10^{-12} M that varied little with [AHA]. Probe **1b** displayed intermediate behavior, reporting $[^1O_2]_{app}$ values ranging from 10^{-13} to 10^{-12} M with a distinct dependence on [AHA].

These measurements are consistent with a hydrophobic binding model (Fig. 1). From this model and the kinetic scheme that accompanies it (Fig. 3), we predict sigmoidal dependencies of $[^1O_2]_{app}$ versus log [CDOM], with the midpoint at the K_{OM} value and the magnitude related to the ratio of the intra-CDOM and bulk aqueous phase $^1O_2$ concentrations (Eq. 1) [see (*28*) for derivation]:

$$[^1O_2]_{app} = f_{CDOM}[^1O_2]_{CDOM} + f_{aq}[^1O_2]_{aq} \quad (1)$$

where $[^1O_2]_{CDOM}$ is the average $^1O_2$ concentration in the CDOM microregion, $[^1O_2]_{aq}$ is the average aqueous phase $[^1O_2]$, f_{CDOM} is the fraction of probe molecules in the CDOM

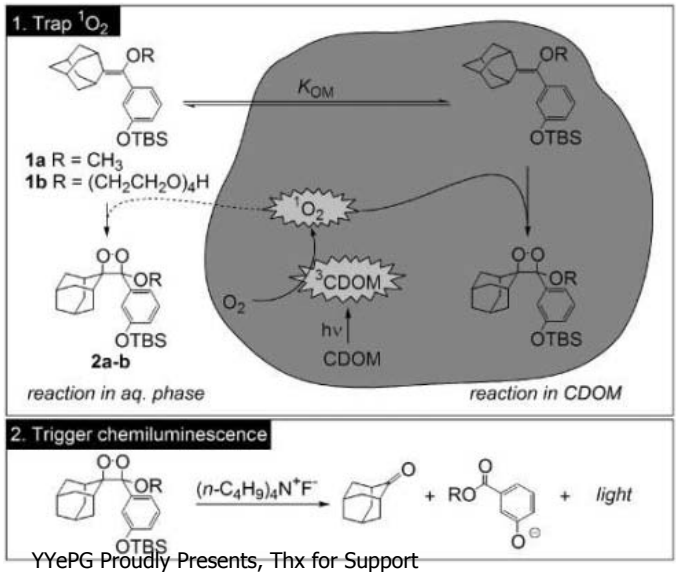

Fig. 1. Measurement of $^1O_2$ concentration using dioxetane precursors **1a** and **1b**. The probe molecules partition between CDOM and the aqueous phase, and they trap $^1O_2$ in both regions. Subsequent quantitation of the trapped $^1O_2$ is achieved by triggering chemiluminescent decomposition of the dioxetane through fluoride-induced removal of the *tert*-butyldimethylsilyl (TBS) protecting group.

Department of Chemistry, 76 Kolthoff Hall, University of Minnesota, Minneapolis, MN, 55455, USA.

*To whom correspondence should be addressed. E-mail: mcneill@chem.umn.edu

microregion, and f_{aq} is the fraction in the aqueous phase. The calculated log K_{OM} values were 6.5 for **1a** and 5.1 for **1b**, based on the empirical relations between K_{OW} and K_{OM} developed by Chiou *et al*. (*23*), and the measured values using the $[^1O_2]_{app}$ data from the AHA photolysis experiments were log K_{OM} = 7.1 for **1a** and 5.6 for **1b**. These results provide evidence for enhanced intra-CDOM $[^1O_2]$, such that at 1 mg C/liter AHA, the ratio $[^1O_2]_{CDOM}/[^1O_2]_{aq}$ was 130.

Singlet oxygen has a short lifetime, 4 μs in water (*29*), and thus has a limited average diffusion length; estimating the diffusion length by $l = (Dt)^{0.5}$, half of the $^1O_2$ produced will diffuse ~80 nm before being quenched, and <0.1% will diffuse 250 nm. Treating the humic acid molecules as spherical microregions leads to three regions of differential $^1O_2$ abundance: the interior of the sphere with the highest $[^1O_2]$, the aqueous corona surrounding the sphere that receives diffusive flux of $^1O_2$, and the bulk aqueous phase that lies outside the diffusion length, where the $[^1O_2]$ is negligible. To calculate the concentrations of $^1O_2$ in the CDOM and aqueous corona regions (i.e., those regions that contain substantial amounts of $^1O_2$), we employed the three-zone kinetic model presented in Fig. 3. Analytical solutions can be derived by applying a steady-state approximation for both $[^1O_2]_{CDOM}$ and $[^1O_2]_{corona}$ and two boundary conditions for the interfaces between zones, where $[^1O_2]_{corona}$ is the average $[^1O_2]$ in the aqueous corona. In this model, the $[^1O_2]$ at the corona/bulk aqueous phase interface is set to zero ($[^1O_2]_{bulk}$ = 0), and $[^1O_2]$ on each side of the CDOM/corona interface is determined by its partition coefficient $K_{OM}^{^1O_2}$.

For the calculations performed in this study, a lower-limit $K_{OM}^{^1O_2}$ value of 1 and an upper-limit value of 5.6 were used. The upper-limit value comes from the K_{OW} of ground-state O_2 (*30*), and K_{OM} is expected to be lower. We chose to use upper and lower limits instead of an intermediate estimate derived from known correlations between K_{OM} and K_{OW} because these relationships are not robust for molecules with relatively low K_{OW} values.

Expressions for the steady-state $[^1O_2]_{CDOM}$, $[^1O_2]_{corona}$, and $[^1O_2]_{aq}$ can be derived (*28*). For $[^1O_2]_{CDOM}$, the steady-state concentration is a balance between sources and sinks. The sources we considered were photochemical formation of $^1O_2$ (k_f) and back-diffusion of $^1O_2$ from the corona ($k_{diff,-1}$). For CDOM microspheres with radii (r_{CDOM}) <10 nm, back-diffusion of $^1O_2$ from the aqueous phase is negligible because of the steep concentration gradient at the CDOM/corona interface, and k_f is the main source term. The sinks considered were first-order quenching by the CDOM medium (k_{CDOM}), diffusion into the corona ($k_{diff,1}$), and quenching by quenchers associated with the CDOM phase ($k_q[Q]_{CDOM}$). Deactivation of $^1O_2$ by the CDOM material is a kinetically insignificant loss process compared with the diffusive loss of $^1O_2$ from the microregion, despite the high $^1O_2$ quenching rate constant associated with CDOM (*31*). Thus, $[^1O_2]_{CDOM}$ can be approximated by

$$[^1O_2]_{CDOM} \approx \frac{k_f}{k_{diff,1} + k_q[Q]_{CDOM}} \quad (2)$$

Similarly, $[^1O_2]_{aq}$ is determined by the balance of sources and sinks. Here, diffusion of $^1O_2$ from the CDOM microregion is the only source, and it is scaled by the $^1O_2$ partition coefficient and by the volume fraction that the CDOM microspheres occupy (V_{CDOM}/V_{tot}). The main loss processes are quenching by the solvent (k_{H_2O}) and by quenchers located in the aqueous phase ($k_q[Q]_{aq}$). $[^1O_2]_{aq}$ can be determined by

$$[^1O_2]_{aq} = \frac{k_{diff,1}[^1O_2]_{CDOM}\frac{1}{K_{OM}^{^1O_2}}\frac{V_{CDOM}}{V_{tot}}}{k_{H_2O} + k_q[Q]_{aq}} \quad (3)$$

Eq. 3 is in the same hyperbolic form as expressions used in conventional aqueous phase $^1O_2$ analyses (*1*, *29*).

According to Eqs. 1 to 3, specific predictions can be made about the effects of adding $^1O_2$ quenchers and changing the solvent from H_2O to D_2O on $[^1O_2]_{CDOM}$, $[^1O_2]_{aq}$, and the $[^1O_2]_{app}$ values measured by various probe molecules. In addition, because the diffusion terms in Eqs. 2 and 3 are dependent on the radius of the sensitizing species, the measured $[^1O_2]_{CDOM}/[^1O_2]_{aq}$ ratio can be used to assess the size of the CDOM macromolecules that the hydrophobic probes are sampling. From our experimental results and analytical solutions of the $[^1O_2]_{CDOM}/[^1O_2]_{aq}$ ratio arising from the three-zone model for CDOM of different radii, we calculate an AHA radius of 1.3 nm for $K_{OM}^{^1O_2}$ = 1. Using an upper-limit value of $K_{OM}^{^1O_2}$ = 5.6, we calculated a radius of 0.6 nm. With a density of 1.5 g/mL (*28*), these sizes correspond to a molecular weight range of 820 to 8300 Da. This molecular weight range agrees with the average value of 4100 Da determined through size exclusion chromatography measurements of the same material (*32*).

Hydrophobic quenchers that partition into the CDOM microphase lower $[^1O_2]_{CDOM}$ by adding an additional intra-CDOM $^1O_2$ loss process. Because these quenchers are concentrated through association to the CDOM microphase, their potency is increased. We have tested this idea by measuring $[^1O_2]_{app}$ values in irradiated AHA solutions using probe molecule **1a** in the presence of low concentrations of the hydrophobic $^1O_2$ quencher β-carotene (60 to 120 nM). Unexpectedly, significant quenching of $^1O_2$ was observed. From a Stern-Volmer analysis using the nominal concentrations of β carotene, k_q was determined to be 2.4×10^{12} M^{-1} s^{-1}, higher than the diffusion-controlled limit. This is strong qualitative evidence supporting the association of β-carotene with the CDOM microphase. For a quantitative analysis of the quenching, we employed the Poisson distribution model described by Burns *et al*. for the intra-CDOM scavenging of reactive intermediates (*16*). The adjustable parameter in this model is the ratio of bound quencher molecules to CDOM macromolecules, and we find a best-fit value of [CDOM] = 150 nM at 1.5 mg C/liter AHA, which roughly corresponds to a molecular weight of 20,000 Da (*28*).

Similarly, the three-zone model predicts that hydrophilic quenchers should have a significant impact on $[^1O_2]_{aq}$, as has been observed by others [e.g., refs. (*1*, *29*)], but little effect on $[^1O_2]_{CDOM}$. In photolysis experiments with AHA sensitizer (1.5 mg C/liter) and 1.3 mM sodium azide, a commonly used aqueous phase $^1O_2$

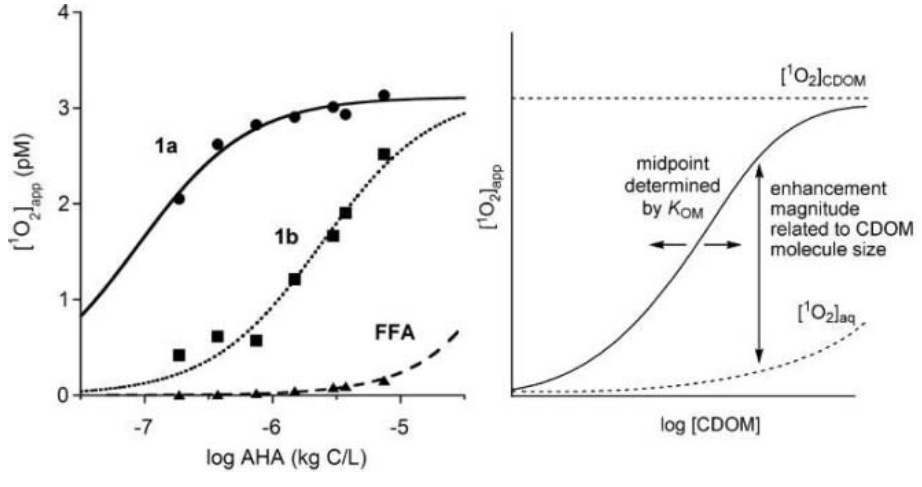

Fig. 2. (**Left**) Apparent singlet oxygen concentrations ($[^1O_2]_{app}$) measured by probes **1a** (circles), **1b** (squares), and FFA (triangles) upon photolysis of aqueous solutions of various humic acid concentrations. The data were fit to Eq. 1 with a global nonlinear least squares approach in which the calculated literature value of 0.94 was entered for K_{OM}^{FFA} in determining the fraction of FFA in the CDOM and aqueous phase (*23*). In this fit, all three probe molecules shared values of $[^1O_2]_{CDOM}$ and $[^1O_2]_{corona}$ at each [AHA]. (**Right**) Relation between probe molecule hydrophobicity, CDOM particle size, and $[^1O_2]_{app}$.

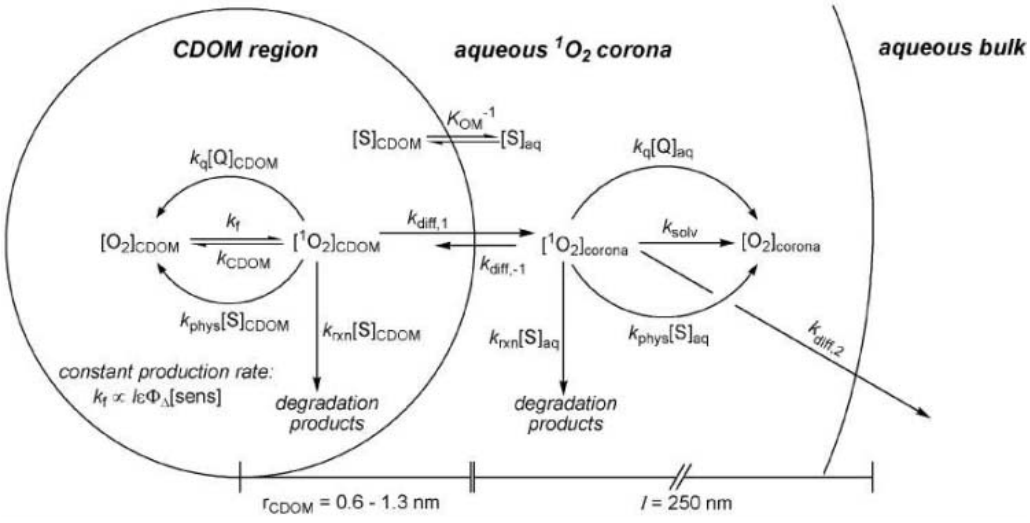

Fig. 3. Kinetic scheme describing the formation and reactivity of $^1O_2$ in the CDOM region, aqueous $^1O_2$ corona, and aqueous bulk region of a microheterogeneous mixture. O_2 is ground-state molecular oxygen, S is the substrate, Q is a physical quencher, k_f is the zero-order formation rate constant, I is light intensity, ε is the absorption coefficient of the sensitizer, Φ_Δ is the quantum yield for $^1O_2$ formation, sens is sensitizer, and k_{solv}, k_q, k_{phys}, and k_{rxn} are the rate constants for deactivation by solvent, physical quenching by Q, physical quenching by S, and chemical reaction with S, respectively. The subscripts CDOM, corona, and aq refer to CDOM, corona, and aqueous phase concentrations of various chemical species (i.e., O_2, $^1O_2$, S, and Q), respectively. The terms $k_{diff,1}$, $k_{diff,-1}$, and $k_{diff,2}$ are rate constants for diffusion of $^1O_2$ from the CDOM phase to the aqueous corona, from the corona back into the CDOM phase, and from the corona into the bulk water region, respectively. The fraction of a given chemical species in the CDOM phase is f_{CDOM}, f_{aq} is the fraction in the aqueous phase, and K_{OM} is the organic matter–water partition coefficient for a given compound.

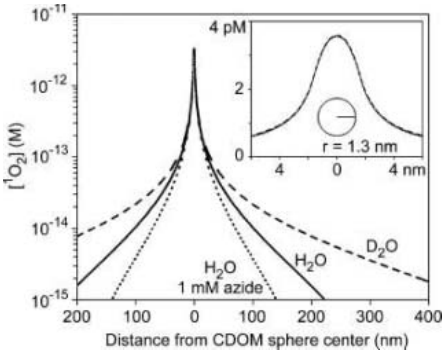

Fig. 4. Calculated $^1O_2$ distributions about a 1.3-nm-radius CDOM macromolecule in aqueous solutions. Calculations were performed for a CDOM particle in H_2O (solid line), D_2O (dashed line), and H_2O with 1 mM sodium azide (dotted line). In these calculations, $K_{OM}^{^1O_2} = 1$. The inset shows the near-CDOM gradients for the three calculations on a linear concentration scale, emphasizing that very little difference is expected between the three conditions near the CDOM molecule.

quencher (*29*, *33*), we see a significant reduction in $[^1O_2]_{aq}$, as measured by FFA (79 ± 2%), and a small reduction in $[^1O_2]_{CDOM}$, as determined with probe **1a** (6 ± 9%). The magnitude of the quenching in the aqueous phase corresponds to a k_q of 7×10^8 M^{-1} s^{-1} for azide, which is consistent with previous reports (*29*). The small 6% quenching observed for $[^1O_2]_{CDOM}$ is within experimental error of the 0% prediction of the three-zone model.

An additional test commonly used to verify $^1O_2$ processes in aqueous solutions is to measure the kinetic solvent isotope effect (KSIE) upon changing from H_2O to D_2O solvent. The solvent-dependent $^1O_2$ deactivation rate constant is lower by a factor of about 13 for D_2O than it is for H_2O (*29*, *34*), which leads to higher $[^1O_2]_{aq}$ values in the deuterated solvent. Accordingly, $[^1O_2]_{app}$ values measured by hydrophilic probes in D_2O should be higher by a factor of 13 than those measured in H_2O for a given [AHA]; the KSIE values measured by FFA over a range of [AHA] were consistent with this treatment [KSIE = 11.3 to 14.0, [AHA] = 0.7 to 7.3 mg C/liter (*35*)]. A change in the aqueous solvent is not expected to alter $[^1O_2]_{CDOM}$, however, and hydrophobic probes **1a** and **1b** reported insignificant KSIEs over the same range of [AHA] (KSIE = 0.9 to 1.2).

To visualize the spatial distribution of $^1O_2$ inside the CDOM microphase and in the aqueous phase, we performed numerical calculations similar to those outlined in the radial distribution model described by Wu and Gschwend for sorption/desorption of pollutants into spherical natural aggregates (*36*, *37*). In these calculations, we divided the CDOM and aqueous regions into a series of concentric spheres with incrementally increasing radii of 0.1 nm. The concentration of $^1O_2$ within each shell was allowed to change at each time step as a result of source and sink processes, including formation, quenching, and diffusion. Iterative calculations with 2-ps time steps were performed until a steady-state distribution was achieved (less than 100 parts per billion change in $[^1O_2]$ at the corona/bulk interface in 2 ps). With 0.1-nm-long steps, it was determined that time steps ≤2 ps were needed to prevent instability in the iterative calculations.

The probabilistic $^1O_2$ distributions determined for three such calculations, in which the medium was pure H_2O, pure D_2O, and 1 mM azide ion in H_2O, are shown in Fig. 4. The calculated radial distributions of $^1O_2$ reflect the quenching by azide and the enhanced $^1O_2$ lifetime in D_2O. The calculated distributions reveal that the radial concentration profiles inside and near the CDOM particle are virtually unaffected by change in the solvent medium. The near-CDOM profiles are controlled by mass-transfer kinetics, and the primary effect of changing the quenching efficiency of the bulk solvent is to change the size of the corona.

Because $^1O_2$ is also a good proxy for ^{3}CDOM, our results predict similar behavior for other hydrophobic compounds transformed by excited-state triplet species. In addition to $^1O_2$, other photochemically produced reactive intermediates are expected to display microheterogeneous distribution profiles. The radial distributions for these species will be controlled by their characteristic diffusion lengths.

References and Notes

1. R. G. Zepp, N. L. Wolfe, G. L. Baughman, R. C. Hollis, *Nature* **267**, 421 (1977).
2. N. V. Blough, R. G. Zepp, in *Active Oxygen in Chemistry*, C. S. Foote, J. S. Valentine, A. Greenberg, J. F. Liebman, Eds. (Chapman and Hall, New York, 1995), pp. 280–333.
3. W. J. Cooper, R. G. Zika, R. G. Petasne, A. M. Fischer, in *Aquatic Humic Substances: Influence on Fate and Treatment of Pollutants*, I. H. Suffet, P. MacCarthy, Eds. (American Chemical Society, Washington, DC, 1989), pp. 333–362.
4. R. A. Larson, E. J. Weber, *Reaction Mechanisms in Environmental Organic Chemistry* (CRC Press, Boca Raton, FL, 1994).
5. K. Briviba, L. O. Klotz, H. Sies, *Biol. Chem.* **378**, 1259 (1997).
6. D. A. Siegel, S. Maritorena, N. B. Nelson, D. A. Hansell, M. Lorenzi-Kayser, *J. Geophys. Res.* **107**, 21 (2002).
7. P. MacCarthy, J. A. Rice, in *Humic Substances in Soil, Sediment, and Water*, G. Aiken, D. M. McKnight, R. L. Wershaw, P. MacCarthy, Eds. (Wiley, New York, 1985), pp. 527–559.
8. R. L. Wershaw, *Soil Sci.* **164**, 803 (1999).
9. Y.-P. Chin, G. R. Aiken, K. M. Danielsen, *Environ. Sci. Technol.* **31**, 1630 (1997).
10. J. C. Means, R. Wijayaratne, *Science* **215**, 968 (1982).
11. G. Ogner, M. Schnitzer, *Science* **170**, 317 (1970).
12. Y. Fu, J. R. Kanofsky, *Photochem. Photobiol.* **62**, 692 (1995).
13. S. Hecht, J. M. J. Frechet, *J. Am. Chem. Soc.* **123**, 6959 (2001).
14. D. C. Neckers, J. Paczkowski, *J. Am. Chem. Soc.* **108**, 291 (1986).
15. N. V. Blough, *Environ. Sci. Technol.* **22**, 77 (1988).

16. S. E. Burns, J. P. Hassett, M. V. Rossi, *Environ. Sci. Technol.* **30**, 2934 (1996).
17. S. E. Burns, J. P. Hassett, M. V. Rossi, *Environ. Sci. Technol.* **31**, 1365 (1997).
18. L. A. MacManus-Spencer, K. McNeill, *J. Am. Chem. Soc.* **127**, 8954 (2005).
19. L. A. MacManus-Spencer, D. E. Latch, K. M. Kroncke, K. McNeill, *Anal. Chem.* **77**, 1200 (2005).
20. G. D. Veith, N. M. Austin, R. T. Morris, *Water Res.* **13**, 43 (1979).
21. R. L. Malcolm, P. MacCarthy, *Environ. Sci. Technol.* **20**, 904 (1986).
22. Preliminary experiments with Suwannee River humic acid are very similar to those presented here for AHA and support the extension of the results to CDOM in natural waters.
23. C. T. Chiou, P. E. Porter, D. W. Schmedding, *Environ. Sci. Technol.* **17**, 227 (1983).
24. S. W. Karickhoff, D. S. Brown, T. A. Scott, *Water Res.* **13**, 241 (1979).
25. D. A. Backhus, P. M. Gschwend, *Environ. Sci. Technol.* **24**, 1214 (1990).
26. T. D. Gauthier, E. C. Shane, W. F. Guerin, W. R. Seitz, C. L. Grant, *Environ. Sci. Technol.* **20**, 1162 (1986).
27. W. R. Haag, J. Hoigne, E. Gassman, A. M. Braun, *Chemosphere* **13**, 641 (1984).
28. Materials and methods are available as supporting material on *Science* Online.
29. F. Wilkinson, W. P. Helman, A. B. Ross, *J. Phys. Chem. Ref. Data* **24**, 663 (1995).
30. R. Battino, *Oxygen and Ozone*, IUPAC Solubility Data Series (Pergamon, New York, 1981).
31. D. P. Hessler, F. H. Frimmel, E. Oliveros, A. M. Braun, *J. Photochem. Photobiol. B* **36**, 55 (1996).
32. Y.-P. Chin, G. Aiken, E. O'Loughlin, *Environ. Sci. Technol.* **28**, 1853 (1994).
33. W. R. Haag, T. Mill, *Photochem. Photobiol.* **45**, 317 (1987).
34. P. B. Merkel, R. Nilsson, D. R. Kearns, *J. Am. Chem. Soc.* **94**, 1030 (1972).
35. The KSIE from the two lowest concentrations, 0.18 and 0.37 mg C/liter, were found to be 33 and 21, respectively. These unrealistically high values are attributed to experimental difficulties in obtaining accurate photolysis rates over the long photolysis times needed for low sensitizer concentrations. For this reason, they were not included in the comparison.
36. S. C. Wu, P. M. Gschwend, *Environ. Sci. Technol.* **20**, 717 (1986).
37. S. C. Wu, P. M. Gschwend, *Water Resour. Res.* **24**, 1373 (1988).
38. We thank an anonymous reviewer for bringing to our attention the utility of the Burns *et al.* model (*16*) for interpreting our experimental data. We thank P. M. Gschwend and J. D. Thoemke for helpful comments on previous drafts of the manuscript. D.E.L. thanks the University of Minnesota Graduate School for a Dissertation Fellowship. This research was funded by the University of Minnesota.

Supporting Online Material

www.sciencemag.org/cgi/content/full/1121636/DC1
Materials and Methods
Figs. S1 to S6
Tables S1 to S3
References

21 October 2005; accepted 12 January 2006
Published online 23 February 2006;
10.1126/science.1121636
Include this information when citing this paper.

Paleoclimatic Evidence for Future Ice-Sheet Instability and Rapid Sea-Level Rise

Jonathan T. Overpeck,[1]* Bette L. Otto-Bliesner,[2] Gifford H. Miller,[3] Daniel R. Muhs,[4] Richard B. Alley,[5] Jeffrey T. Kiehl[2]

Sea-level rise from melting of polar ice sheets is one of the largest potential threats of future climate change. Polar warming by the year 2100 may reach levels similar to those of 130,000 to 127,000 years ago that were associated with sea levels several meters above modern levels; both the Greenland Ice Sheet and portions of the Antarctic Ice Sheet may be vulnerable. The record of past ice-sheet melting indicates that the rate of future melting and related sea-level rise could be faster than widely thought.

Millions of people and their infrastructure are concentrated near coastlines and are thus vulnerable to sea-level rise (*1*); entire countries may be submerged by a rise of a few meters. The Intergovernmental Panel on Climate Change (IPCC) Third Assessment (TAR) (*2*) suggested a rise of 0.09 to 0.88 m by the year 2100 unless greenhouse gas (GHG) emissions are reduced substantially. The IPCC TAR also suggested that continuing GHG emissions could trigger polar ice-cap melting beyond 2100, with sea-level rise in excess of 5 m within the next millennium (*2*). More-recent modeling (*3*) indicated that the Earth will be warm enough by 2100 to melt the Greenland Ice Sheet (GIS) over the next millennium or so, and more-recent theoretical considerations (*4*) suggested that the melting could be faster and hence more challenging for society.

Ongoing Arctic warming is already melting ice, including sea-ice thinning and retreat and also enhanced melting of the GIS (*5*). These changes, coupled with recent changes in western Antarctica (*6*, *7*) and the enormous potential market and nonmarket costs of large sea-level rise, led us to reexamine the climate associated with the last major sea-level rise above modern levels that occurred in Earth history. Corals on tectonically stable coasts from the last interglaciation period (LIG) provided strong evidence that sea level was 4 to >6 m above present levels during a sea-level high stand that likely lasted from 129,000 ± 1000 years ago to at least 118,000 years ago (*8*–*13*). Our goal is to untangle the causes of this past sea-level change in order to understand how sea levels may change in the next 100 years and beyond.

Recent assessments of the LIG climate and the sea-level high stand have pointed mostly to the likelihood that melting of the GIS contributed 2 or more m of sea-level equivalent at that time (*14*, *15*). This hypothesis is supported by the substantial orbitally driven excess of Northern Hemisphere summer insolation 130,000 years ago relative to the present day, with no corresponding Antarctic excess (Fig. 1) (*16*). More-recent work (*17*) coupled new climate and ice-sheet modeling with Arctic paleoclimatic data to make a strong case that the central part of GIS was intact throughout the LIG and that the GIS and other Arctic ice fields likely contributed 2.2 to 3.4 m of sea-level rise during the LIG. The low-end (4 m) estimate of observed LIG sea-level rise can thus be explained by the high-end possible contribution from the GIS, Iceland, and other Arctic ice fields (*17*), plus additional small contributions from Northern Hemisphere mountain-glacier melt. However, the low to midrange estimates of LIG Arctic sea-level contribution imply at least some Antarctic contribution, and an important Antarctic contribution is required to explain a total observed LIG sea-level rise in the 4 to >6 m range.

Recent thinning along the margins of the East Antarctic Ice Sheet (EAIS) and, in particular, over notable portions of the West Antarctic Ice Sheet (WAIS) (*18*–*20*) suggests there may have been LIG contributions to sea level from both parts of the Antarctic Ice Sheet. There has been longstanding concern regarding the potential for rapid WAIS collapse and the ≤5-m sea-level rise that might follow warming-induced loss of buttressing ice shelves (*21*). That concern was downplayed subsequently but has reemerged because warming-induced ice-shelf reduction along the Antarctic Peninsula and in the Amundsen Sea region was followed by accelerated flow of tributary glaciers (*6*, *7*, *20*). Although state-of-the-art knowledge of ice sheet dynamics may not be sufficient to simulate cur-

[1]Institute for the Study of Planet Earth, Department of Geosciences, and Department of Atmospheric Sciences, University of Arizona, Tucson, AZ 85721, USA. [2]National Center for Atmospheric Research, Post Office Box 3000, Boulder, CO 80307, USA. [3]Institute of Arctic and Alpine Research and Department of Geological Sciences, University of Colorado, Campus Box 450, Boulder, CO 80309, USA. [4]U.S. Geological Survey, Mail Stop 980, Box 25046, Federal Center, Denver, CO 80225, USA. [5]Department of Geosciences and Penn State Ice and Climate Exploration Center, Pennsylvania State University, 0517 Deike Building, University Park, PA 16802, USA.

*To whom correspondence should be addressed. E-mail: jto@u.arizona.edu

rent or future changes in the WAIS (*6*, *20*), our inference that the Antarctic Ice Sheet likely contributed to sea-level rise during the LIG indicates that it could do the same if the Earth's climate warms sufficiently in the future.

Although the low-end (≤4 m) estimates of the observed LIG sea-level high stand may not require a substantial contribution from the Antarctic Ice Sheet, there are two lines of evidence that support a WAIS contribution (in addition to the evidence that LIG sea level may have been substantially more than 4 m above present). First, diatom and ^{10}Be data collected from sediments below the ice-stream region of the Ross Embayment indicate that the central WAIS was likely smaller at some point in the last several hundred thousand years (*22*), and it now appears that the LIG, not an earlier interglaciation [i.e., marine isotope stage 11, circa (ca.) 400,000 years ago (*23*)], is the most likely candidate for an associated sea-level rise of the needed magnitude. Second is the evidence from multiple ice cores (*24*–*26*) that some process caused substantial (2.5° to over 5°C) warming over East Antarctica beginning at the same early LIG time as the observed sea-level high stand [as suggested by the coincidence of the peak isotope-inferred LIG warming and CH_4 levels (*26*)]. This is surprising given the lack of a positive summertime south polar insolation anomaly (Fig. 1) and simulated (*27*) LIG cooling over Antarctica (Fig. 2). A possible explanation is the presence of a much-reduced WAIS that would have lowered albedo and altered atmospheric circulation over a large area of Antarctica. These changes could have driven the observed warmer temperatures over the Antarctic region in Southern Hemisphere summer.

Assuming that the GIS and WAIS both may have contributed to the LIG sea-level high stand, we used a state-of-the-art coupled atmosphere-ocean climate model to simulate the climate of 130,000 years ago and then compared this simulation with simulations of the next 140 years made with the same model to learn how much sea-level rise might be expected in the future (*27*). Results of our LIG climate simulation are in good agreement with observed Northern Hemisphere warming for the LIG (*17*) and reveal several key aspects of the LIG climate (Fig. 2). First, the simulated LIG was warmer than the present period in the Northern Hemisphere but not in the Southern, consistent with strong northern but near-zero southern summer insolation anomalies at that time (Fig. 1). This result indicates that sea-level rise at 130,000 to 128,000 years ago probably started first with the melting of the GIS and not the Antarctic Ice Sheet. Simulated summertime LIG warming of Greenland is less than 5°C everywhere and averages less than 3.5°C above modern temperatures (Fig. 2), providing our estimate of the warmth needed to cause the shrinkage of GIS that occurred during the LIG. These temperatures were associated with a simulated net annual reduction in snowfall over Greenland (Fig. 2). Simulated summer sea ice in the Arctic Ocean was greatly reduced at ca. 130,000 years ago, in accord with the paleoenvironmental record from this region [references in (*17*)]. Lastly, because of the latitudinally asymmetric insolation anomalies during the LIG, simulated annual average global temperature was not notably warmer than present, implying that sea-level rise due to ocean expansion at that time was likely minimal.

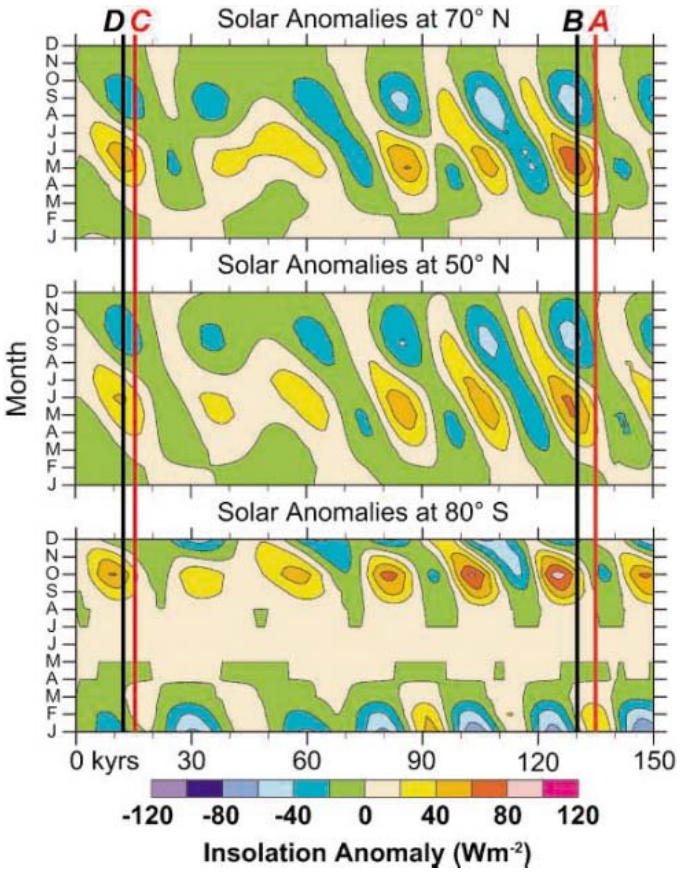

Fig. 1. Comparison of insolation anomalies (*16*) over the past 150,000 years for 70°N (**top**), 50°N (**middle**), and 80°S (**bottom**). Insolation sufficient to begin major melting leading to the last interglaciation occurred only after ca. 135,000 years ago (line labeled "A"); an inference based on the observation that major melting over the more well-constrained and recent deglaciation did not begin until the same level of insolation was reached at ca. 15,000 years ago (*30*) (line labeled "C"). A much higher rate of Northern Hemisphere summertime insolation increase existed over the penultimate deglaciation (line labeled "B," ca. 130,000 years ago) than over the most recent deglaciation (line labeled "D," ca. 12,000 years ago).

Comparison of the summer-season warmth sufficient to have melted much of the GIS 130,000 years ago with simulated future climate (Fig. 2) indicates that at (or before) 2100 A.D. (and three times the amount of preindustrial CO_2), the high northern latitudes around Greenland will be as warm as or warmer than they were 130,000 years ago and hence warm enough to melt at least the large portions of the GIS that apparently melted during the LIG (*17*). This finding assumes that GHG concentrations will rise at a rate equivalent to 1% per year through the end of this century; slowed increases would delay the ice-sheet response, and faster increases would accelerate the response. As with our paleoclimate LIG simulation, it does not appear likely that increased snowfall (Fig. 2) or ocean circulation changes (*17*) will offset GIS melting.

Recent assessment of future climate change (*2*) indicates that the amount of future warming is highly dependent on the model used, with some models less sensitive to elevated atmospheric GHG concentrations than others. The model we used has midrange sensitivity and appears reasonably accurate (*27*). Both past and future simulations are characterized by large Arctic warmings (i.e., to above freezing) that extend from the spring into the fall. The future susceptibility of the GIS to melting is also likely to be exacerbated by soot-induced snow aging (*28*), a factor that probably did not play a role 130,000 years ago. Lastly, Greenland could be much warmer by 2130 than it was during the LIG (Fig. 2), assuming a 1% per year increase in CO_2 or equivalent GHGs. Thus, by any account the GIS could be even more susceptible to melting in the near future than it was 130,000 years ago.

Recent rates of sea-level rise (2.6 ± 0.04 mm/year) (*29*) are already nearing the maximum average rate (3.5 mm/year) projected to occur over the next 1000 years by the IPCC (*2*). This anticipated rate is substantially less than the 11 mm/year average rate of sea-level rise measured for the last deglaciation between 13,800 and 7000 years ago (*30*). As mentioned earlier, however, the penultimate deglaciation, culminating with the LIG sea-level high stand 4 to >6 m above that of the present day, was driven by a substantially larger northern high

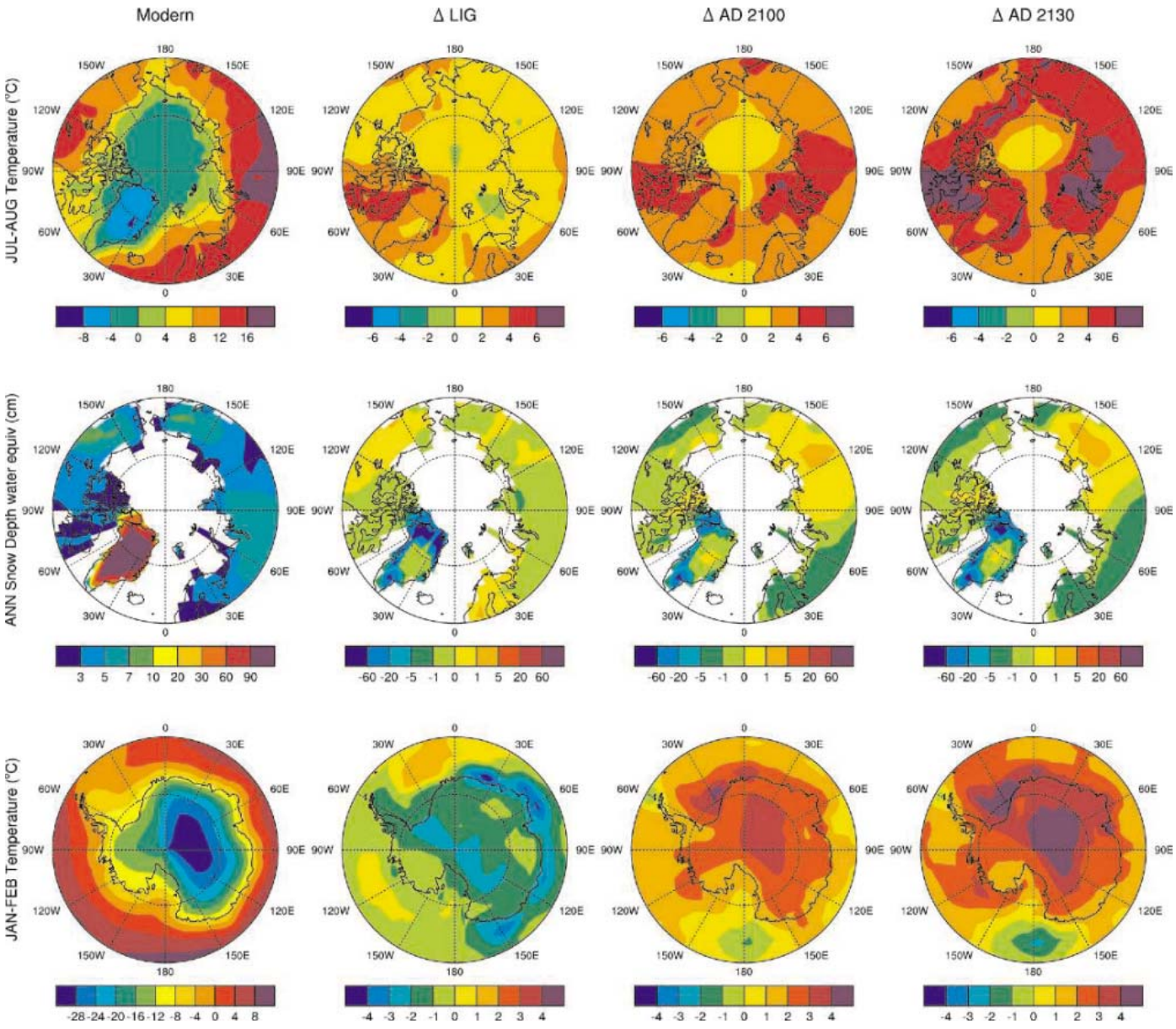

Fig. 2. Simulated climate for each of four time periods, from left to right: present day (Modern), 130,000 years ago (anomalies from present day, Δ LIG), 2100 A.D. (the time atmosphere reaches three times preindustrial CO_2 levels, climate anomalies from present day, Δ AD 2100), and 2130 A.D. (four times preindustrial CO_2 levels, climate anomalies from present day, Δ AD 2130). Shown for each time period are peak summertime (July to August and January to February means) surface air temperature and annual snow depth. Note significant warming at north polar latitudes and the lack of any summer warming over Antarctic at 130,000 years ago.

latitude summertime insolation anomaly (Fig. 1). It seems likely, therefore, that ice-sheet melting leading to the LIG sea-level rise should have been at least as fast as the sea-level rise (11 mm/year) associated with the close of the last glacial period. Although a well-constrained record of sea-level rise leading to the LIG high stand is not yet available, there is well-dated yet controversial coral evidence that sea-level rise over this interval may have occurred at rates higher than 20 mm/year, perhaps right up to the LIG sea-level high stand (*31*). This makes sense given the much higher insolation (and warming) anomaly at this time and also the very real possibility that a LIG shrinkage of the WAIS (*21*) may be required to explain the large amount of sea-level rise above that of the present day at that time. Other recent paleo–sea-level studies indicate that very rapid sea-level rise is indeed possible (*32*).

Our analysis, as well as ongoing changes in coastal Antarctica, are at least suggestive that the WAIS can indeed shrink rapidly as originally envisioned by Mercer (*21*). Given that there was no positive summer (melt-season) insolation anomaly at high southern latitudes in the several millennia before 129,000 years ago, it appears that two factors may have led to a LIG collapse of the WAIS (or perhaps portions of the EAIS). The first may have been the sea-level rise associated with pre–129,000- to 128,000 years ago GIS melting, and the second factor may have been shallow ocean warming around and under the Antarctic ice shelves that buttress portions of the Antarctic Ice Sheet. Sea-level rise seems to have had minor effects on the WAIS during the most recent deglaciation (*33*), but perhaps the greater speed of sea-level rise into the LIG compared with that from the Last Glacial Maximum (ca. 21,000 years ago) played a role by reducing the ability of isostatic rebound after grounding-line retreat to shallow sub–ice-shelf cavities and promote regrounding. As for the subsurface warming of south polar oceans, our LIG simulation showed modest (generally less than 0.5° but up to 1°C) warming in the

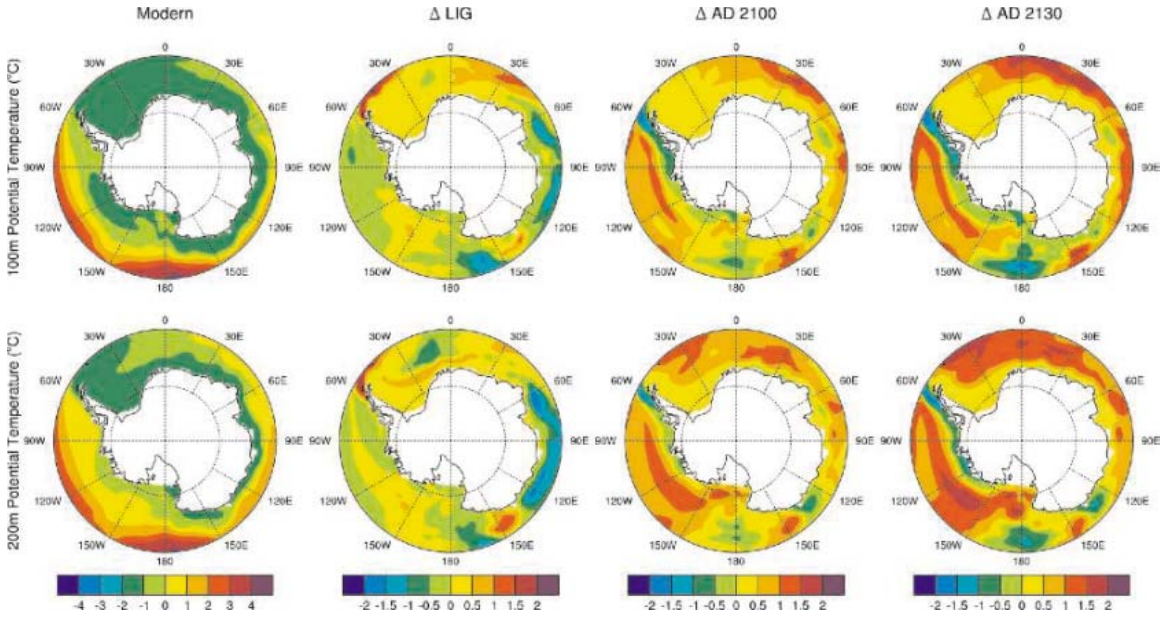

Fig. 3. Simulated shallow (100 m, **top**; 200 m, **bottom**) annual mean ocean potential temperatures for each of four time periods, from left to right: present day, 130,000 years ago (anomalies from present day), 2100 A.D. (time atmosphere reaches three times preindustrial CO_2 levels, climate anomalies from present day), and 2130 A.D. (four times preindustrial CO_2 levels, climate anomalies from present day). A ca. 2-month-long positive insolation anomaly in austral spring (Fig. 1) fails to warm surface air temperatures over Antarctica to above freezing but nonetheless acts to warm the subsurface shallow ocean, as well as ice shelves of the same depth.

upper 200 m of the ocean (Fig. 3) that would have further weakened ice shelves by thinning them from below; Shepherd *et al*. (*34*) find that such a modest warming increases sub–ice-shelf melt rates substantially, by perhaps 5 m/year up to 10 m/year. In our simulation, this small but notable warming was due to a positive springtime (October) insolation anomaly driving reduced sea ice and enhanced subsurface warming; note that this cool-season warming was not large enough to generate positive surface air temperature anomalies over the Antarctic in summer (Fig. 2). Even more dramatic ocean warming is likely in the future (Fig. 3), along with surface air temperature increases (in all seasons) and continued sea-level rise that could destabilize ice shelves that buttress the Antarctic Ice Sheet. Heat transport beneath ice shelves is highly complex, so caution is required, but the LIG may provide a conservative constraint on the future dynamics of the Antarctic Ice Sheet and particularly the WAIS. Moreover, the same parts of the Antarctic Ice Sheet may prove vulnerable even given increased precipitation [e.g., (*35*)].

The ice-sheet origin of the LIG sea-level high stand in response to relatively small warming, together with recent results showing rapid response of ice to warming [e.g., (*36*, *37*)], pose important challenges for ice-sheet modeling; whole ice sheet models do not yet incorporate important physical processes implicated in these changes (*6*, *20*). Even in the absence of more-realistic models of ice-sheet behavior, it remains that ice sheets have contributed meters above modern sea level in response to modest warming, with peak rates of sea-level rise possibly exceeding 1 m/century. Current knowledge cannot rule out a return to such conditions in response to continued GHG emissions. Moreover, a threshold triggering many meters of sea-level rise could be crossed well before the end of this century, particularly given that high levels of anthropogenic soot may hasten future ice-sheet melting (*28*), the Antarctic could warm much more than 129,000 years ago (Figs. 2 and 3), and future warming will continue for decades and persist for centuries even after the forcing is stabilized (*38*, *39*).

References and Notes

1. R. J. Nicholls, *Global Environ. Change* **14**, 69 (2004).
2. IPCC, Ed., *Climate Change 2001: The Scientific Basis. Contribution of Working Group I to the Third Assessment Report of the Intergovernmental Panel on Climate Change* (Cambridge Univ. Press, Cambridge, 2001), p. 881.
3. J. M. Gregory, P. Huybrechts, S. C. B. Raper, *Nature* **428**, 616 (2004).
4. J. E. Hansen, *Clim. Change* **68**, 269 (2005).
5. Arctic Climate Impact Assessment, *Impacts of a Warming Arctic: Arctic Climate Impact Assessment* (Cambridge Univ. Press, Cambridge, 2004), pp. 184–242.
6. M. Oppenheimer, R. B. Alley, *Clim. Change* **64**, 1 (2004).
7. A. J. Cook, A. J. Fox, D. G. Vaughan, J. G. Ferrigno, *Science* **308**, 541 (2005).
8. J. H. Chen, H. A. Curran, B. White, G. J. Wasserburg, *Geol. Soc. Am. Bull.* **103**, 82 (1991).
9. C. H. Stirling, T. M. Esat, M. T. McCulloch, K. Lambeck, *Earth Planet. Sci. Lett.* **135**, 115 (1995).
10. C. H. Stirling, T. M. Esat, K. Lambeck, M. T. McCulloch, *Earth Planet. Sci. Lett.* **160**, 745 (1998).
11. C. Israelson, B. Wohlfarth, *Quat. Res.* **51**, 306 (1999).
12. C. Fruijtier, T. Elliott, W. Schlager, *Geol. Soc. Am. Bull.* **112**, 267 (2000).
13. D. R. Muhs, K. R. Simmons, B. Steinke, *Quat. Sci. Rev.* **21**, 1355 (2002).
14. K. Cuffey, S. Marshall, *Nature* **404**, 591 (2000).
15. L. Tarasov, W. R. Peltier, *J. Geophys. Res.* **108**, 10.1029/2001JB001731 (2003).
16. A. L. Berger, *Quat. Res.* **9**, 139 (1978).
17. B. L. Otto-Bliesner *et al.*, *Science* **311**, 1751 (2006).
18. V. Masson-Delmotte *et al.*, *Nature* **436**, 681 (2005).
19. C. H. Davis, Y. H. Li, J. R. McConnell, M. M. Frey, E. Hanna, *Science* **308**, 1898 (2005); published online 19 May 2005 (10.1126/science.1110662).
20. R. B. Alley, P. U. Clark, P. Huybrechts, I. Joughin, *Science* **310**, 456 (2005).
21. J. H. Mercer, *Nature* **271**, 321 (1978).
22. R. P. Scherer *et al.*, *Science* **281**, 82 (1998).
23. A. W. Droxler, R. Z. Poore, L. H. Burckle, Eds., *AGU Monogr.* **137**, 240 (2003).
24. J. Jouzel *et al.*, *J. Geophys. Res.* **108**, 10.1029/2002JD002677 (2003).
25. O. Watanabe *et al.*, *Nature* **422**, 509 (2003).
26. L. Augustin *et al.*, *Nature* **429**, 623 (2004).
27. Materials and methods are available as supporting material on *Science* Online.
28. J. Hansen, L. Nazarenko, *Proc. Natl. Acad. Sci. U.S.A.* **101**, 423 (2004).
29. A. Cazenave, R. S. Nerem, *Rev. Geophys.* **42**, 10.1029/2003RG000139 (2004).
30. E. Bard *et al.*, *Nature* **382**, 241 (1996).
31. M. T. McCulloch, T. Esat, *Chem. Geol.* **169**, 107 (2000).
32. W. G. Thompson, S. L. Goldstein, *Science* **308**, 401 (2005).
33. H. Conway, B. L. Hall, G. H. Denton, A. M. Gades, E. D. Waddington, *Science* **286**, 280 (1999).
34. A. Shepherd, D. Wingham, E. Rignot, *Geophys. Res. Lett.* **31**, 10.1029/2004GL021106 (2004).
35. P. Huybrechts, J. Gregory, I. Janssens, M. Wild, *Global Planet. Change* **42**, 83 (2004).
36. H. J. Zwally *et al.*, *Science* **297**, 218 (2002); published online 6 June 2002 (10.1126/science.1072708).
37. T. A. Scambos, J. A. Bohlander, C. A. Shuman, P. Skvarca, *Geophys. Res. Lett.* **31**, 10.1029/2004GL020670 (2004).
38. G. A. Meehl *et al.*, *Science* **307**, 1769 (2005).
39. T. M. L. Wigley, *Science* **307**, 1766 (2005).

40. We thank T. Ager, P. Anderson, J. Brigham-Grette, J. Chappell, T. Crowley, L. Edwards, M. Edwards, J. Gregory, V. Masson-Delmotte, J. Jouzel, M. Oppenheimer, W. R. Peltier, D. Raynaud, and R. Thompson for helpful discussions; numerous reviewers for excellent suggestions; and the NSF for funding support.

Supporting Online Material

www.sciencemag.org/cgi/content/full/311/5768/1747/DC1
Materials and Methods
Fig. S1

23 May 2005; accepted 2 March 2006
10.1126/science.1115159

Simulating Arctic Climate Warmth and Icefield Retreat in the Last Interglaciation

Bette L. Otto-Bliesner,[1]* Shawn J. Marshall,[2] Jonathan T. Overpeck,[3] Gifford H. Miller,[4] Aixue Hu,[1] CAPE Last Interglacial Project members

In the future, Arctic warming and the melting of polar glaciers will be considerable, but the magnitude of both is uncertain. We used a global climate model, a dynamic ice sheet model, and paleoclimatic data to evaluate Northern Hemisphere high-latitude warming and its impact on Arctic icefields during the Last Interglaciation. Our simulated climate matches paleoclimatic observations of past warming, and the combination of physically based climate and ice-sheet modeling with ice-core constraints indicate that the Greenland Ice Sheet and other circum-Arctic ice fields likely contributed 2.2 to 3.4 meters of sea-level rise during the Last Interglaciation.

Determining the sensitivity of the Arctic climate system to anomalous forcing and understanding how well climate models can simulate the future state of the Arctic are critical priorities. Over the past 30 years, Arctic surface temperatures have increased 0.5°C per decade (*1*); September Arctic sea ice extent has decreased 7.7% per decade (*2*); and the seasonal ablation area for Greenland has increased, on average, by 16% (*3*–*5*). The global climate models being used to estimate future scenarios of Arctic warmth give polar warming of 0.7°C to 4.4°C—a large range—as well as a reduction of Arctic sea ice of up to 65% at the time of the doubling of atmospheric CO_2 (*6*). The Last Interglaciation (LIG, ~130,000 to 116,000 years ago) is the last time that the Arctic experienced summer temperatures markedly warmer than those in the 20th century and the late Holocene, and it also featured a significantly reduced Greenland Ice Sheet (GIS). Climate models need to be able to reproduce this large, warm climate change in the Arctic if they are to be trusted in their representation of Arctic processes and their predictions for the future.

Paleorecords indicate much warmer Arctic summers during the LIG. Storm beaches and ancient barrier islands with extralimital mollusks of LIG age indicate that the open water north of Alaska was more extensive and lasted seasonally longer (*7*). Boreal forest communities expanded poleward by as much as 600 to 1000 km in Russia (*8*), reaching the coast everywhere except in Alaska (*9*) and central Canada. Total gas evidence from LIG ice in the Greenland Ice Core Project (GRIP) ice core indicates that the Summit region remained ice-covered, although possibly up to ~500 m lower than the ice level at present, at some time in the LIG (*10*). In contrast, basal ice at Dye-3 (southern Greenland), in the Agassiz, Devon, and Meighen ice caps in the Canadian Arctic, and possibly in Camp Century (northwest Greenland), suggest that these drill sites were ice-free during the LIG (*10*, *11*). The increased presence of vegetation over southern Greenland is reconstructed from plant macrofossils (*12*) and fern spores (*13*). Elsewhere; pollen, insects, marine plankton, and other proxies document the magnitude of LIG summer warmth across the Arctic (*14*).

We conducted climate simulations for the LIG with a global, coupled ocean-atmosphere-land-sea–ice general circulation model [NCAR Community Climate System Model (CCSM)] (*15*). We also used ice-sheet simulations with a three-dimensional, coupled ice and heat flow model (*16*), which spans the entire western Arctic from 57°N to 85°N, including Greenland and smaller scale ice caps in Iceland and the Canadian Arctic (*14*). We chose to simulate the start of the LIG, approximately 130,000 years ago (130 ka), reflecting evidence of early LIG summer Arctic warmth (*14*) and of an LIG sea-level high stand of 4 to 6 m above present day likely by 129 ka ± 1000 years (*17*, *18*).

Our climate simulation was forced with the large insolation anomalies of the LIG at 130 ka; anomalies driven by changes in Earth's orbit, which are known to have caused warm Northern Hemisphere climate (*19*–*21*). The anomalous forcing for the start of the LIG (130 to 127 ka) was concentrated in the late spring and early summer because of the nature of Milankovitch solar anomalies. This timing is important because the GIS is extremely sensitive to warm, early-summer conditions (*22*). Positive solar anomalies at the top of the atmosphere exceeded 60 W m^{-2} at high northern latitudes in May to June for 130 ka (Fig. 1) and until 127 ka. After 127 ka, these positive solar anomalies decreased considerably, and by 125 ka, they were less than the maximum May-to-June solar anomalies of ~45 W m^{-2} during the Holocene, which were not enough to melt the GIS much beyond its modern configuration. Annual mean changes of insolation at high northern latitudes for 130 ka were much smaller, less than 6 W m^{-2}; global annual mean forcing was very small, 0.2 W m^{-2}.

A comparison between proxy-based reconstructions for the Arctic LIG and those simulated with the CCSM climate model shows good agreement (Fig. 2). Solar anomalies drive significant simulated summer (June, July, and August) warming in the Arctic (for 60°N to 90°N, an average warming of 2.4°C with significant regional variation) (Fig. 2). In agreement with paleoclimatic observations, simulated warming in excess of 4°C occurs in the northern Hudson Bay–Baffin Island–Labrador Sea region, and across to the seas adjacent to northern and eastern Greenland. Greenland warms by 3°C or greater along the edges of the ice cap and by 2.8°C in central Greenland in CCSM, somewhat less than observed. Less summer warming is indicated for northern Europe (2°C to 3°C), as well as Alaska and western Canada (0°C to 2°C), in both the proxy reconstruction and CCSM. The simulated warming over Siberia is 2°C to 4°C, somewhat less than the paleodata in parts of this region.

The insolation anomalies result in increased sea ice melting early in the summer season, with reduced sea ice extending from April into November. The minimum LIG Arctic sea-ice area simulated in August and September is 50% less than that simulated for present day, with 50% summer coverage in the Arctic Ocean only occurring poleward of 80°N (fig. S1). The reduction of summer sea ice leads to simulated warming of the Arctic Ocean north of Alaska by ~2°C. The North Atlantic warms by 1°C to 2°C, with above-freezing temperatures extending northward along circumcoastal regions, and substantial warming extending as far east as Severnaya Zemlya in CCSM. The CCSM is in accord with marine records that indicate modest warming (0°C to 4°C) at LIG (Fig. 2).

The simulated temperature response of the Arctic to altered LIG insolation is significant over the ice sheet and the surrounding waters of Greenland. Feedbacks associated with reduced sea ice and a warmer North Atlantic Ocean and Labrador Sea act to warm all of Greenland during the summer months, with the southern quarter and far northern coastal regions averaging above freezing for multiple months. Maximum daily surface temperatures during the summer are above freezing over the entire ice sheet. Annual snow depths decrease significantly along the southern, western, and northern edges of the ice sheet (*17*). These decreases are primarily due to melting with warmer surface temperatures. Modeled precipitation rates are generally not significantly different from present, except for marginally significant increases in northwest and central Greenland and southeast Iceland, associated with warmer nearby oceans.

Simulated margins of the GIS, as well as smaller Arctic icefields, respond immediately to

[1]Climate and Global Dynamics Division, National Center for Atmospheric Research (NCAR), Boulder, CO 80305, USA. [2]Department of Geography, University of Calgary, Calgary, Alberta, T2N 1N4, Canada. [3]Institute for the Study of Planet Earth, Department of Geosciences, and Department of Atmospheric Sciences, University of Arizona, Tucson, AZ 85721, USA. [4]Institute of Arctic and Alpine Research and Department of Geological Sciences, University of Colorado, Boulder, CO 80309, USA.

*To whom correspondence should be addressed. E-mail: ottobli@ucar.edu

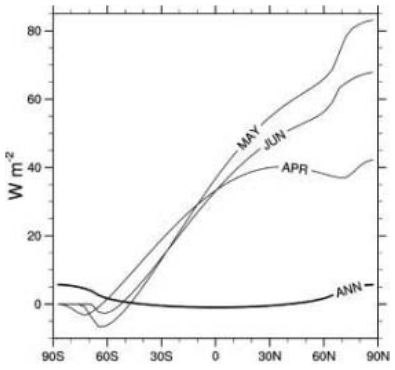

Fig. 1. Anomalies of solar radiation incoming at the top of the atmosphere at 130 ka relative to present as a function of latitude. Large positive anomalies occur over the Arctic during boreal late spring and early summer. Northern high-latitude annual mean anomalies are small and positive, whereas global annual mean anomalies are close to zero. Similar high-latitude anomalies occur for boreal late spring and early summer through 127 ka, diminishing considerably after that time. Jun, June; Apr, April; Ann, annual.

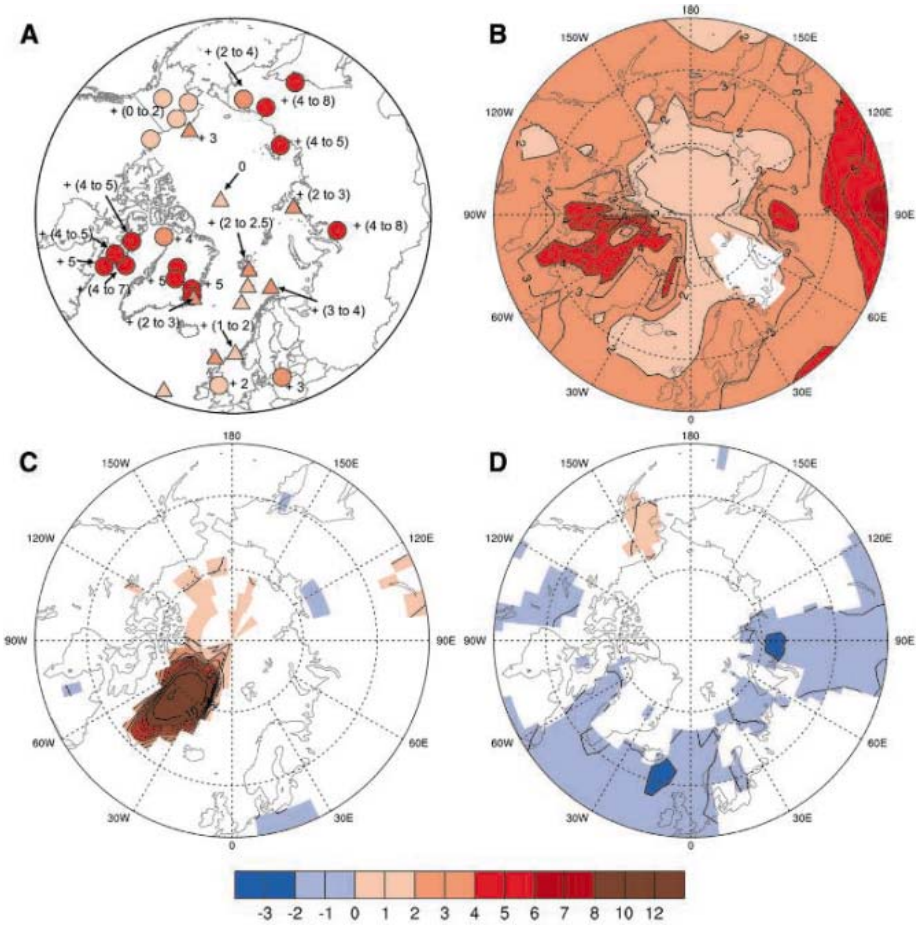

Fig. 2. Arctic summer surface-temperature anomalies. (**A**) Maximum observed LIG summer temperature anomalies relative to present derived from quantitative [terrestrial (circles) and marine (triangles)] paleotemperature proxies as part of CAPE Last Interglacial Project (*14*). (**B**) LIG summer (June, July, and August) temperature anomalies relative to present simulated by CCSM for 130 ka. (**C**) Additional LIG summer warming for our no–Greenland Ice Sheet sensitivity simulation relative to our LIG simulation with the GIS. (**D**) Summer temperature anomalies for a freshwater anomaly of 0.1 sverdrup to the North Atlantic for 100 years simulated by CCSM. For the CCSM simulations, only anomalies significantly different from natural model variability at 95% confidence interval are shown.

the warmer spring and summer temperatures. The total icefield ablation area increases from 2.64×10^5 km^2 for modern time to 5.25×10^5 km^2 in the LIG, with melt rates near the ice margins increasing by as much as 1 m/year. Greater snow accumulation compensates for elevated melt rates in southeast Iceland, central Greenland, and isolated coastal sites in Greenland, giving small, positive mass-balance perturbations for the LIG of ~0.2 m/year. Elsewhere in the western Arctic, increased melt rates and an extended ablation season lead to negative mass-balance perturbations, with initial losses of –0.3 to –0.6 m/year in most of coastal Greenland. On average over the western Arctic, the mass-balance perturbation is –0.19 m/year.

As the simulated ice caps retreat over several millennia in response to the orbitally induced warming, loss of ice mass leads to surface lowering, an amplification of the mass-balance perturbation, and accelerated retreat. The sustained negative mass-balance perturbations cause the almost-complete demise of icefields in the Queen Elizabeth Islands, consistent with the ice-core inferences discussed in Koerner (*11*, *23*). In approximately 2000 years, the GIS has retreated such that Dye-3 becomes ice-free, in agreement with LIG paleorecords (Fig. 3A) (*11*–*13*). In this configuration, Greenland and the western Arctic icefields contribute 2.2 m of sea-level rise; this is the minimum sea-level rise that the Arctic likely contributed during the LIG. After an additional millennium, the simulated LIG surface drawdown at the paleodivide is ~570 m, near the constraint provided by ice-core data (*10*). This minimal GIS configuration (Fig. 3B) yields a maximum Arctic sea-level contribution of 3.4 m.

Our simulated GIS is not in equilibrium, and continued warmth would drive a smaller and lower ice sheet and continued sea-level rise. However, the GIS configurations in Fig. 3 are consistent, in terms of height and area, with observed ice-core data, thus providing a constraint on the Canadian Arctic and Iceland icefields and of the GIS at their smallest size during the LIG (Fig. 3). Moreover, our use of observations and model together indicate that the minimal LIG GIS was a steeply sided ice sheet in central and northern Greenland (Fig. 3) and that this ice sheet, combined with the change in other Arctic ice fields, likely generated 2.2 to 3.4 m of early LIG sea-level rise (1.9 to 3.0 m from Greenland and 0.3 to 0.4 m from Arctic Canada and Iceland). Previous modeling studies of the LIG, based on independent, ice-core–derived temperature histories (*24*, *25*) from GRIP (Greenland) $\delta^{18}O$ and Vostok (Antarctica) δD data, also suggest a minimum GIS within a few millennia of the maximum LIG insolation anomaly.

Our climate model captures the terrestrial warming within the uncertainties of proxy estimates, except over Siberia. In Siberia, the model underestimates the observed warming by up to 1°C to 2°C. Previous modeling studies have shown that Arctic vegetation changes act as a positive feedback for past periods of enhanced summer solar radiation, including the Holocene (*26*, *27*) and the LIG (*28*). Our simulation lacked this positive feedback, just as this feedback is missing in most projections of future warming. However, our results indicate that CCSM does a good job of simulating much of the observed Arctic response to altered radiative forcing without this feedback, confirming that the size of the missing vegetation feedback is likely smaller than was previously estimated (*14*, *19*, *27*).

A sensitivity simulation with CCSM with all ice removed from Greenland and replaced with lower-albedo bedrock gives a measure of the large positive feedbacks associated with the large reduction of surface albedos due to ice sheet retreat and vegetation growth over Greenland (Fig. 2C). The additional warming is primarily a

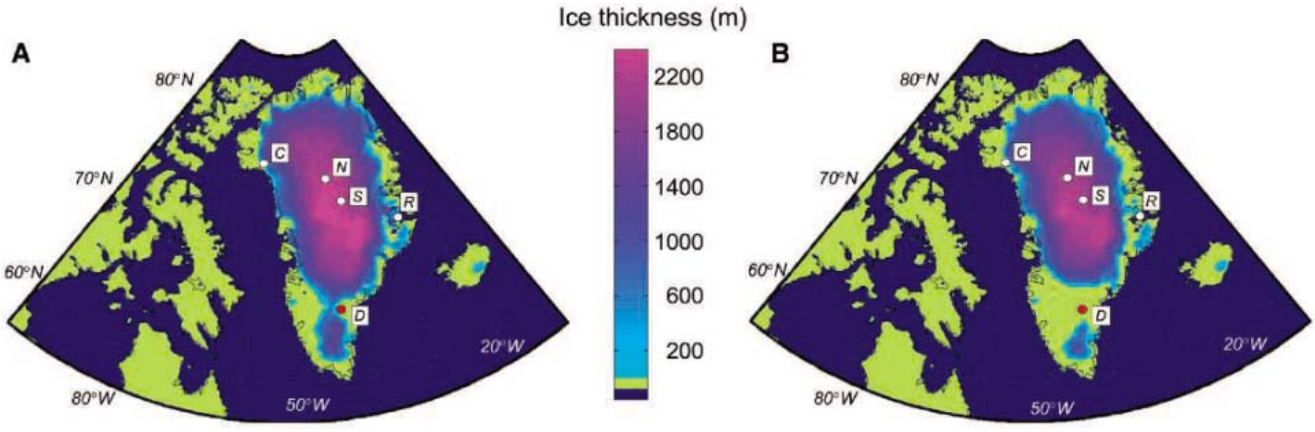

Fig. 3. Simulated ice-sheet thickness maps for LIG climate forcing. (**A**) Configuration for when the location of Dye-3 ice core becomes ice-free. This configuration gives the minimum sea-level rise (2.2 m) that the Arctic likely contributed during the LIG. (**B**) Configuration for a paleodivide elevation of 570 m lower than present. This configuration gives the maximum Arctic sea-level rise (3.4 m) that the Arctic likely contributed during the LIG. Greenland ice-core observations indicate early LIG ice (white circles) at Renland (marked R; 71.3°N, 26.7°W), North Greenland Ice Core Project (NGRIP) (marked N; 75.1°N, 42.3°W), Summit [GRIP and Greenland Ice Sheet Project 2 (GISP2)] (marked S; 72.5°N, 37.3°W), and possibly Camp Century (marked C; 77.2°N, 61.1°W), but not (red circle) at the Dye-3 ice core site (marked D; 65.2°N, 43.8°W).

local response over Greenland. Surface temperatures warm an additional 7°C at Renland and Dye-3 and more than 10°C at GRIP. This warming is clearly an overestimate compared with ice-core and other proxy estimates (Fig. 2), confirming the likelihood that the GIS retreated only to the smaller and steeper configuration that we simulated (Fig. 3).

A sea-level rise of 3.4 m over 3000 years is equivalent to freshwater forcing of the North Atlantic and Labrador Sea of 0.013 sverdrup. It is reasonable to assume, however, that the rate of meltwater discharge would not have been constant in time, and could have been greater at some times than others during the drawdown of the GIS. We thus performed a sensitivity simulation with 0.1 sverdrup of water inserted into the present-day North Atlantic over 100 years. This freshwater forcing yields a simulated 25% slowdown of the North Atlantic thermohaline circulation and annual cooling of 1.5°C south of Greenland, within the range of sensitivities of 12 climate model simulations of –3.9°C to +0.7°C (*29*). Simulated summer cooling is generally 1°C to 2°C over much of the North Atlantic and Labrador Sea (Fig. 2D). Even with this more extreme freshwater forcing than is implied by our simulated average LIG meltwater rate, summer surface temperature anomalies over Greenland remain positive, which is an indication of the implied primacy of the large orbital forcing anomalies. These results therefore indicate that the likely impact on the North Atlantic of any Greenland meltwater would not have inhibited the meltback of Greenland.

Our results confirm that the NCAR climate model (with doubled atmospheric carbon dioxide equilibrium sensitivity of 2.2°C) captures key aspects of Arctic sensitivity to anomalous LIG forcing. Simulated summer Arctic warming is up to 5°C (as compared with a simulated global cooling of 0.7°C and Northern Hemisphere warming of 1.3°C), and simulated sea-ice retreats by 50%. The climate model anomalies drive large-scale ice-sheet retreat in the Western Arctic that is consistent with available ice-core records. Within a few millennia, most of the icefields in Arctic Canada and Iceland melted away, and the GIS was reduced to a steep ice dome in central and northern Greenland. We cannot comment on exactly when this ice configuration could have occurred during the LIG; there are no paleoclimatic observational constraints on the time evolution of ice-sheet retreat, and the lack of meltwater-driven, ice-dynamical processes in current ice-sheet models (*30*) prevents an evaluation of ice-sheet model sensitivity. However, our results give a likely Arctic (including Greenland) contribution to LIG sea-level rise above modern day of no more than 3.4 m. Despite the different mechanisms of warming, these results indicate that the impact on Arctic environments over the next century can be expected to be substantial if predicted future climate change comes to pass (*17*).

References and Notes

1. J. C. Comiso, *J. Clim.* **16**, 3498 (2003).
2. J. C. Stroeve *et al.*, *Geophys. Res. Lett.* **32**, L04501 (2005).
3. W. Abdalati, K. Steffen, *J. Geophys. Res.* **106**, 33983 (2001).
4. W. Krabill *et al.*, *Science* **289**, 428 (2000).
5. W. S. B. Paterson, N. Reeh, *Nature* **414**, 60 (2001).
6. G. M. Flato *et al.*, *Clim. Dyn.* **23**, 229 (2004).
7. J. Brigham-Grette, D. M. Hopkins, *Quaternary Res.* **43**, 154 (1995).
8. A. V. Lozhkin, P. M. Anderson, *Quaternary Res.* **43**, 147 (1995).
9. M. E. Edwards, T. D. Hamilton, S. A. Elias, N. H. Bigelow, A. P. Krumhardt, *Arctic Antarctic Alpine Res.* **35**, 460 (2003).
10. D. Raynaud, J. A. Chappellaz, C. Ritz, P. Matinerie, *J. Geophys. Res.* **102**, 26607 (1997).
11. R. M. Koerner, *Science* **244**, 964 (1989).
12. O. Bennike, J. Böcher, *Boreas* **23**, 479 (1994).
13. C. Hillaire-Marcel, A. De Vernal, G. Bilodeau, A. J. Weaver, *Nature* **410**, 1073 (2001).
14. Materials and methods are available as supporting material on *Science* Online.
15. J. T. Kiehl, P. R. Gent, *J. Clim.* **17**, 3666 (2004).
16. S. J. Marshall, K. M. Cuffey, *Earth Planet. Sci. Lett.* **179**, 73 (2000).
17. J. T. Overpeck *et al.*, *Science* **311**, 1747 (2006).
18. M. T. McCulloch, T. Esat, *Chem. Geol.* **169**, 107 (2000).
19. M. Montoya, H. von Storch, T. J. Crowley, *J. Clim.* **13**, 1057 (2000).
20. J. E. Kutzbach, R. G. Gallimore, P. J. Guetter, *Quaternary Int.* **10-12**, 223 (1991).
21. T. J. Crowley, K.-Y. Kim, *Science* **265**, 1566 (1994).
22. W. Krabill *et al.*, *Geophys. Res. Lett.* **31**, L24402 (2004).
23. R. M. Koerner, D. A. Fisher, *Ann. Glaciology* **35**, 19 (2002).
24. K. M. Cuffey, S. J. Marshall, *Nature* **404**, 591 (2000).
25. L. Tarasov, W. R. Peltier, *J. Geophys. Res.* **108**, 2143 (2003).
26. J. A. Foley, J. E. Kutzbach, M. T. Coe, S. Levis, *Nature* **371**, 52 (1994).
27. M. Kerwin *et al.*, *Paleoceanography* **14**, 200 (1999).
28. S. P. Harrison, J. E. Kutzbach, I. C. Prentice, P. J. Behling, M. T. Sykes, *Quaternary Res.* **43**, 174 (1995).
29. R. J. Stouffer *et al.*, *J. Clim.*, in press.
30. R. B. Alley, P. U. Clark, P. Huybrechts, I. Joughin, *Science* **310**, 456 (2005).

31. Circum-Arctic PaleoEnvironments (CAPE) is a program within the International Geosphere-Biosphere Program (IGBP)–Past Global Changes (PAGES); the CAPE-LIG compilation was supported by the NSF–Office of Polar Programs–Arctic System Science (PARCS) and PAGES. The CAPE Last Interglacial Project Members are P. Anderson, O. Bennike, N. Bigelow, J. Brigham-Grette, M. Duvall, M. Edwards, B. Fréchette, S. Funder, S. Johnsen, J. Knies, R. Koerner, A. Lozhkin, G. MacDonald, S. Marshall, J. Matthiessen, G. Miller, M. Montoya, D. Muhs, B. Otto-Bliesner, J. Overpeck, N. Reeh, H. P. Sejrup, C. Turner, and A. Velichko. We thank E. Brady and D. Schimel for helpful discussions; R. Tomas and M. Stevens for figures; and C. Shields for design and running of the simulations. We acknowledge the efforts of a large group of scientists at the NCAR, at several Department of Energy and National Oceanic and Atmospheric Administration labs, and at universities across the United States who contributed to the development of CCSM2. Computing was done at NCAR as part of the Climate Simulation Laboratory. Funding for NCAR and this research was provided by NSF.

Supporting Online Material

www.sciencemag.org/cgi/content/full/311/5768/1751/DC1
Materials and Methods
Figs. S1 to S4
References

30 September 2005; accepted 1 March 2006
10.1126/science.1120808

Measurements of Time-Variable Gravity Show Mass Loss in Antarctica

Isabella Velicogna[1,2]* and John Wahr[1]*

Using measurements of time-variable gravity from the Gravity Recovery and Climate Experiment satellites, we determined mass variations of the Antarctic ice sheet during 2002–2005. We found that the mass of the ice sheet decreased significantly, at a rate of 152 ± 80 cubic kilometers of ice per year, which is equivalent to 0.4 ± 0.2 millimeters of global sea-level rise per year. Most of this mass loss came from the West Antarctic Ice Sheet.

The Antarctic ice sheet is Earth's largest reservoir of fresh water. Accurate estimates of its mass variability, accompanied by realistic error bars, would greatly reduce current uncertainties in projected sea-level change, with obvious societal and economic impacts. There have been substantial improvements in monitoring the ice sheet in the past few years (*1*–*3*), although recent studies have provided contrasting mass balance estimates (*1*, *3*).

Antarctic mass variability is difficult to measure because of the ice sheet's size and complexity. Previous estimates have used a variety of techniques (*1*), each with intrinsic limitations and uncertainties. A problem common to all these techniques is the difficulty of monitoring the entire ice sheet. Studies that rely on a single method can provide estimates for only a portion of the ice sheet, and even studies that synthesize results from several techniques suffer from sparse data in critical regions.

The most recent Intergovernmental Panel on Climate Change (IPCC) assessment estimated that the Antarctic contribution to sea-level rise during the past century was 0.2 ± 0.3 mm/year (*2*). The report predicted that the Antarctic ice sheet will probably gain mass during the 21st century because of increased precipitation in a warming global climate. Recent radar altimeter measurements (*3*) have shown an increase in the overall thickness of the East Antarctic Ice Sheet's (EAIS's) interior during 1992–2003. However, the IPCC prediction does not consider possible dynamic changes in coastal regions, and radar altimetry provides only sparse coverage of those areas (*2*). Detailed interferometric synthetic-aperture radar and airborne laser altimeter surveys of glaciers along the edge of the West Antarctic Ice Sheet (WAIS) show rapid increases in near-coastal discharge during the past few years (*4*). The overall contribution of the Antarctic ice sheet to global sea-level change thus depends on the balance between mass changes in the interior and those in coastal areas (*1*). The gravitational survey of Antarctica provided by the Gravity Recovery and Climate Experiment (GRACE) satellites and discussed in this paper is a comprehensive survey of the entire ice sheet and is thus able to overcome the issue of limited sampling.

GRACE (*5*) provides monthly estimates of Earth's global gravity field at scales of a few hundred kilometers and larger. Time variations in the gravity field can be used to determine changes in Earth's mass distribution. GRACE mass solutions have no vertical resolution, however, and do not reveal whether a gravity variation over Antarctica is caused by a change in snow and ice on the surface, a change in atmospheric mass above Antarctica, or post-glacial rebound (PGR: the viscoelastic response of the solid Earth to glacial unloading over the past several thousand years). Users must employ independent means to separate those contributions.

We used GRACE gravity-field solutions for 34 months between April 2002 and August 2005 to estimate the mass change of the Antarctic ice sheet. Each solution consists of spherical harmonic (Stokes) coefficients, C_{lm} and S_{lm} (*5*), up to $l,m \leq 120$. Here, l and m are the degree and order of the harmonic, and the horizontal scale is ≈20,000/l km. The GRACE C_{20} coefficients show anomalously large variability, so we replace them with values derived from satellite laser ranging (*6*). The Stokes coefficients can be used to solve for monthly variations in Earth's surface mass distribution. The GRACE fields provide high-latitude (above 60°) estimates of monthly mass changes to accuracies of 10 mm in equivalent water thickness when averaged over discs of radius 600 to 700 km and larger (*7*–*10*).

We used the Stokes coefficients to estimate monthly mass changes of the entire Antarctic ice sheet and of EAIS and WAIS separately. We defined an averaging function for each region that minimizes the combined measurement error and signal leakage (*11*). GRACE does not recover $l = 1$ coefficients, so we removed $l = 1$ terms from the averaging function.

Our averaging function for all Antarctica (Fig. 1) includes, with about equal weighting, both the ice sheet interior and the coastal margins, although there is decreased sensitivity to the far end of the Antarctic Peninsula. This uniform and complete sensitivity allows us to use GRACE to obtain a comprehensive average of all Antarctica. The averaging functions are less than 1.0 over most of their respective regions. Thus, they give results that are biased low. To recover unbiased mass estimates for each region, we scaled the estimated mass signals to restore the original amplitudes (*12*).

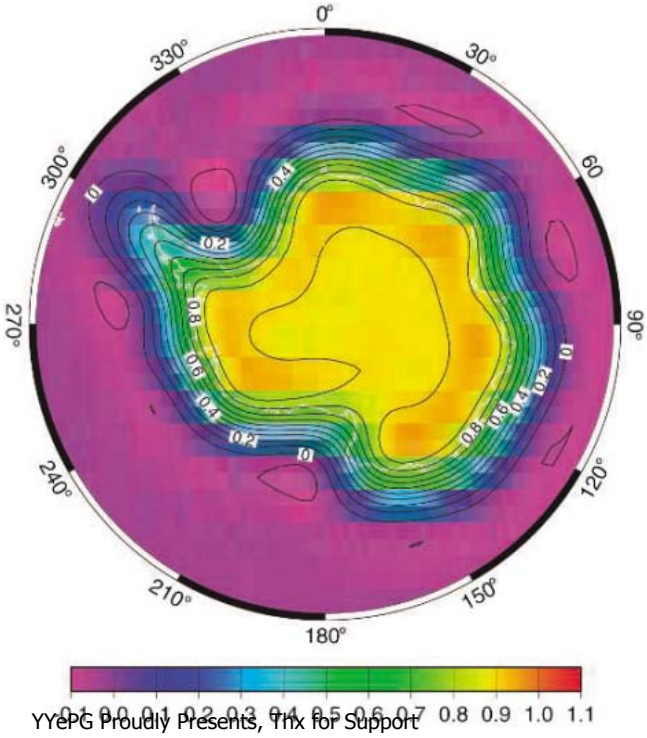

Fig. 1. The averaging function used to estimate the change in total Antarctic mass.

[1]University of Colorado, Cooperative Institute for Research in Environmental Sciences and Department of Physics, University Campus Box 390, Boulder, CO 80309–0390, USA. [2]Jet Propulsion Laboratory, California Institute of Technology, Mail Stop 300-233, Pasadena, CA 91109–8099, USA.

*To whom correspondence should be addressed. E-mail: isabella@colorado.edu (I.V.); wahr@colorado.edu (J.W.)

Before interpreting the scaled results as ice sheet change, we had to address the issues of errors in the GRACE gravity fields and the contamination from other geophysical sources of gravity-field variability. To estimate the effects of errors, we convolved our averaging functions with uncertainty estimates for the GRACE Stokes coefficients (*13*). We obtained 1σ error estimates that can be interpreted as 68.3% confidence intervals.

There are two types of geophysical contamination: one caused by signals outside Antarctica and the other from Antarctic signals unrelated to snow and ice. Leakage from outside Antarctica occurs because the averaging function extends beyond the boundaries of Antarctica. The leakage is increased because our omission of $l = 1$ terms causes the averaging function to have a small-amplitude tail that extends around the globe.

We considered two sources of external leakage: continental hydrology outside Antarctica and ocean mass variability. The hydrological contamination was estimated using monthly global water storage fields from the Global Land Data Assimilation System (*14*). The ocean contamination was estimated using a Jet Propulsion Laboratory version of the Estimating the Circulation and Climate of the Ocean general circulation model (*15*). In both cases, we added a uniform layer to the global ocean so that the total land plus ocean mass was conserved at every time step. We removed the predicted hydrology leakage from the GRACE monthly mass estimates to obtain the monthly Antarctic mass estimates shown in Fig. 2. The predicted oceanic leakage was negligible and so was not removed.

The Antarctic mass change from GRACE shows a trend superimposed on shorter period variability (Fig. 2). We simultaneously fit a trend and annually and semiannually varying terms to the GRACE-minus-leakage results. Interpreting the trend as being due entirely to a change in ice, we inferred an ice volume increase of 39 ± 14 km³/year (the trend obtained without removing the hydrology leakage is 51 ± 14 km³/year). The uncertainty reflects the errors in the GRACE gravity-field solutions and was computed using the GRACE monthly error bars (Fig. 2).

This ice mass estimate is contaminated by variations in atmospheric mass and from PGR. European Centre for Medium-Range Weather Forecasts (ECMWF) meteorological fields were used to remove atmospheric effects from the raw data before constructing gravity fields. But there are errors in those fields. We estimated the secular component of those errors by finding monthly differences between meteorological fields from ECMWF and from the National Centers for Environmental Prediction, applying the Antarctic averaging function to those differences and fitting a trend, and annually and semiannually varying terms to the results. The linear trend was small, equivalent to about 10 km³/year, and was interpreted as the uncertainty due to atmospheric errors. We took the root sum square (RSS) with the effects of GRACE gravity-field errors, to obtain a new error estimate of ±16 km³/year.

A PGR signal is indistinguishable from a linear trend in ice mass. PGR effects are large and must be independently modeled and removed. There are two important sources of error in PGR estimates: the ice history and Earth's viscosity profile. We estimated the PGR contribution and its uncertainties using two ice history models: ICE-5G (*16*) and IJ05 (*17*). IJ05 is available only for Antarctica, so we combined it with ICE-5G outside Antarctica. We convolved these ice histories with viscoelastic Green's functions for an incompressible Earth (*18*). We computed trends in the Stokes coefficients for all plausible combinations of two-layer viscosity profiles and convolved these trends with the averaging function. ICE-5G trends are consistently larger than the IJ05 trends. We estimated the range of possible PGR contributions by defining our lower bound to be the minimum IJ05 trend (over all viscosity profiles) and our upper bound to be the maximum ICE-5G trend. Our best estimate of PGR trend is the midpoint of this range. This estimate translates to an apparent ice increase of 192 ± 79 km³/year, where the uncertainty corresponds to the bounds of our PGR range.

We subtracted this PGR contribution from the GRACE-minus-leakage ice mass estimates (Fig. 2). The best-fitting linear trend, and our final estimate of the decrease in total Antarctic mass between the summers of 2002 and 2005, is 152 ± 80 km³/year. The uncertainty is the RSS of the errors in the GRACE fit and in the PGR contribution. This rate of ice loss corresponds to 0.4 ± 0.2 mm/year of global sea-level rise.

The PGR contribution (192 ± 79 km³/year) is much larger than the uncorrected GRACE trend (39 ± 14 km³/year). A significant ice mass trend does not appear until the PGR contribu-

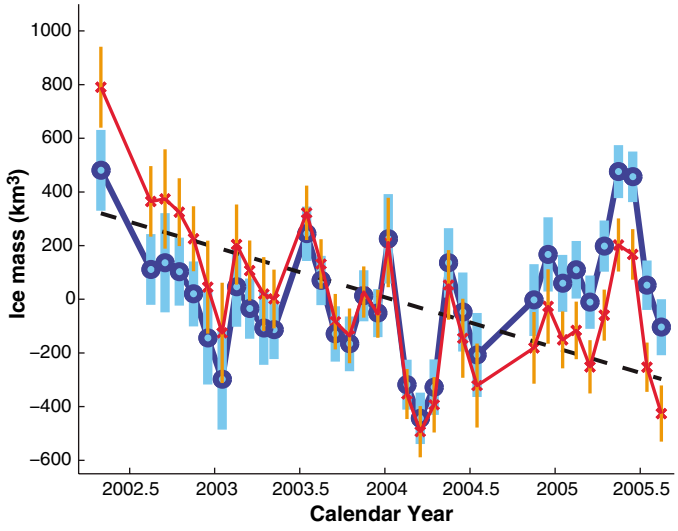

Fig. 2. GRACE monthly mass solutions for the Antarctic ice sheet for April 2002 to August 2005. Blue circles show results after removing the hydrology leakage. Red crosses show results after also removing the PGR signal. The latter represent our best estimates of the mass variability. The error bars include only the contributions from uncertainties in the GRACE gravity fields and represent 68.3% confidence intervals (*13*). Also shown is the linear trend that best fits the red crosses.

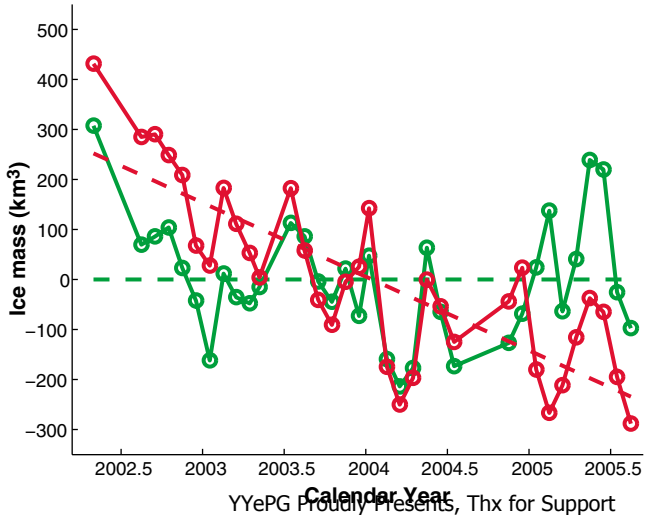

Fig. 3. Monthly ice mass changes and their best-fitting linear trends for WAIS (red) and EAIS (green) for April 2002 to August 2005. The GRACE data have been corrected for hydrology leakage and for PGR.

tion is removed. The implication is that when averaged over all Antarctica, the gravity signals from PGR and from ice variability are closely coincident (with opposing signs), and it underscores the importance of obtaining a meaningful PGR uncertainty. Our uncertainty accommodates all plausible PGR contributions, and removing even the smallest such contribution still implies a loss of ice mass.

We also determined results for WAIS and EAIS separately (Fig. 3). We estimated the errors, the leakage, and the PGR contamination of each signal, as described above for the entire ice sheet. Both these ice sheets appear to have lost mass at higher rates during 2002–2004 than during 2004–2005; this is even more evident in the total Antarctic results (Fig. 2).

By fitting a trend and annual and semiannual terms to the WAIS and EAIS results, we find that most of the Antarctic mass loss comes from WAIS. After correcting for the hydrology leakage and the PGR signal, we obtain a WAIS mass loss of 148 ± 21 km^3/year. The EAIS mass loss is 0 ± 56 km^3/year. Because of its relatively large uncertainty, we are not able to determine whether EAIS is in balance or not. The final error bars for WAIS and EAIS, like those for all Antarctica, are dominated by the PGR uncertainty. The predicted PGR gravity signals at individual points in WAIS are actually somewhat larger than the PGR signals at EAIS points. The overall EAIS mass error is larger than that for WAIS simply because EAIS covers an area almost three times larger, so the EAIS averaging function is sensitive to the PGR signal integrated over a much larger area.

For these individual ice sheets, but unlike for all Antarctica, the PGR and ice mass signals do not cancel one another. For EAIS, the uncorrected GRACE trend is about equal to the PGR signal, and so we find no significant trend after removing PGR. For WAIS, the uncorrected GRACE trend and the PGR signal have about the same magnitudes but opposite signs, so the WAIS trend becomes even larger after PGR is removed.

The GRACE result for total Antarctic ice mass change includes complete contributions from such regions as the East Antarctic coastline and the circular cap south of 82°S, which have not been completely surveyed with other techniques. The comprehensive nature of this result arises because a gravity signal at the altitude of GRACE is sensitive to mass variations averaged over a broad region of the underlying surface, not just at the point directly beneath the satellite. The main disadvantage of GRACE is that it is more sensitive than other techniques to PGR; in fact, our error estimates are dominated by PGR uncertainties. As more GRACE data become available, it will become feasible to search for long-term changes in the rate of mass loss. A change in the rate would not be contaminated by PGR errors, because the PGR rates will remain constant over the satellite's lifetime.

References and Notes

1. E. Rignot, R. Thomas, *Science* **297**, 1502 (2002).
2. J. A. Church *et al.*, in *Climate Change 2001: The Scientific Basis*, Third Assessment Report of the IPCC (Cambridge Univ. Press, Cambridge, 2001), pp. 639–694.
3. C. Davis, Y. Li, J. McConnell, M. Frey, E. Hanna, *Science* **308**, 5730 (2005).
4. R. Thomas *et al.*, *Science* **306**, 255 (2004).
5. GRACE, launched in March 2002 and administered by NASA and the Deutsches Zentrum für Luft-und Raumfahrt, is mapping Earth's gravity field every 30 days during its 10- to 11-year lifetime. GRACE consists of two identical satellites in identical orbits, separated by ~220 km. The satellites use microwaves to monitor their separation distance. Onboard accelerometers and Global Positioning System receivers detect nongravitational accelerations and geocentric orbital motion.
6. M. Cheng, B. Tapley, *J. Geophys. Res.* **109**, B09402 (2004).
7. J. Wahr, S. Swenson, V. Zlotnicki, I. Velicogna, *Geophys. Res. Lett.* **31**, L11501 (2004).
8. B. Tapley, S. Bettadpur, M. Watkins, C. Reigber, *Geophys. Res. Lett.* **31**, L09607 (2004).
9. I. Velicogna, J. Wahr, *Geophys. Res. Lett.* **32**, L18505 (2005).
10. M. Tamisiea, E. Leuliette, J. Davis, J. Mitrovica, *Geophys. Res. Lett.* **32**, L20501 (2005).
11. S. Swenson, J. Wahr, P. C. D. Milly, *Water Resour. Res.* **39**, 1223 (2003).
12. To determine the scaling factor for the entire ice sheet, we applied our averaging function to the gravitational signature of a uniform 1-cm water mass change spread evenly over the ice sheet. We obtained an estimate of 0.62 cm. We thus multiplied each GRACE estimate by 1/0.62. Determining scaling factors for WAIS and EAIS is more complicated because the EAIS averaging function extends slightly over WAIS and vice versa. We applied each averaging function to a uniform mass change over each region individually and used the four resulting values to determine the linear combination of WAIS and EAIS results that correctly recovers the mass in each region.
13. J. Wahr, S. Swenson, I. Velicogna, *Geophys. Res. Lett.*, in press.
14. M. Rodell *et al.*, *Bull. Am. Meteorol. Soc.* **85**, 381 (2004).
15. T. Lee, I. Fukumori, D. Menemenlis, Z. Xing, L. Fu, *J. Phys. Oceanogr.* **32**, 1404 (2002).
16. W. R. Peltier, *Annu. Rev. Earth Planet. Sci.* **32**, 111 (2004).
17. E. Ivins, T. S. James, *Antarct. Sci.* **17**, 541 (2005).
18. I. Velicogna, J. Wahr, *J. Geophys. Res.* **107**, 2376 (2002).

19. We thank S. Bettadpur, J. Cheng, J. Reis, E. Rignot, and M. Watkins for data and advice. This work was supported by NASA's Cryospheric and Solid Earth Programs and by the NSF Office of Polar Programs. This research was partially carried out at the Jet Propulsion Laboratory.

13 December 2005; accepted 21 February 2006
Published online 2 March 2006;
10.1126/science.1123785
Include this information when citing this paper.

Seasonality and Increasing Frequency of Greenland Glacial Earthquakes

Göran Ekström,[1]* Meredith Nettles,[2] Victor C. Tsai[1]

Some glaciers and ice streams periodically lurch forward with sufficient force to generate emissions of elastic waves that are recorded on seismometers worldwide. Such glacial earthquakes on Greenland show a strong seasonality as well as a doubling of their rate of occurrence over the past 5 years. These temporal patterns suggest a link to the hydrological cycle and are indicative of a dynamic glacial response to changing climate conditions.

Continuous monitoring of seismic waves recorded at globally distributed stations (*1*) has led to the detection and identification of a new class of earthquakes associated with glaciers (*2*, *3*). These "glacial earthquakes" are characterized by emissions of globally observable low-frequency waves that are incompatible with standard earthquake models for tectonic stress release but can be successfully modeled as large and sudden glacial-sliding motions (*4*). Seismic waves are generated in the solid earth by the forces exerted by the sliding ice mass as it accelerates down slope and subsequently decelerates. The observed duration of sliding is typically 30 to 60 s. All detected events of this type are associated with mountain glaciers in Alaska or with glaciers and ice streams along the edges of the Antarctic and Greenland ice sheets. The Greenland events are most numerous, and we present new data indicating a strong seasonality and an increasing frequency of occurrence for these events since at least 2002.

For the period January 1993 to October 2005, we have found 182 earthquakes on Greenland by analysis of continuous records from globally distributed seismic stations (*5*). None of these earthquakes are reported in standard seismicity catalogs. We have modeled seismograms for 136 of the best-recorded events to confirm their glacial-sliding source mechanism and obtain improved locations (Fig. 1) (*6*, *7*). This analysis yields an estimate of the twice–time-integrated active force couple at the earthquake source, a quantity that can be interpreted as the product of sliding mass and sliding distance (*2*, *8*). All events have long-period seismic magnitudes in the range 4.6 to 5.1, corresponding to a product

[1]Department of Earth and Planetary Sciences, Harvard University, 20 Oxford Street, Cambridge, MA 02138, USA. [2]Lamont-Doherty Earth Observatory of Columbia University, Palisades, NY 10964, USA.

*To whom correspondence should be addressed. E-mail: ekstrom@seismology.harvard.edu

of sliding mass and sliding distance of 0.1 to 2.0 × 10^{14} kg m. The locations resulting from our seismogram modeling have an uncertainty of approximately 20 km. All 136 earthquakes analyzed can be spatially associated with major outlet glaciers of the Greenland Ice Sheet (Fig. 1).

We investigate the seasonality of the glacial earthquakes by counting the number of events occurring in each month over the 12-year period 1993 to 2004. Greenland earthquakes occur in each month of the year but are more frequent during the late summer months (Fig. 2A). Seasonal variations in background seismic noise, with higher noise levels during winter months, may influence the detection of seismic events. A control group consisting of standard (non-glacial) earthquakes located north of 45°N, detected by the same method and in the same magnitude range as the glacial earthquakes (4.6 to 5.1), displays no seasonality, indicating that variations in the detection threshold are not the cause of the observed behavior (*9*, *10*). Summer surface melting followed by transport of meltwater to the glacier base and the consequent lowering of the effective friction at the base provide a plausible explanation for the seasonal signal (*11*, *12*). However, the occurrence of events during the coldest months of the year suggests that the influx of water accelerates the events rather than controls them.

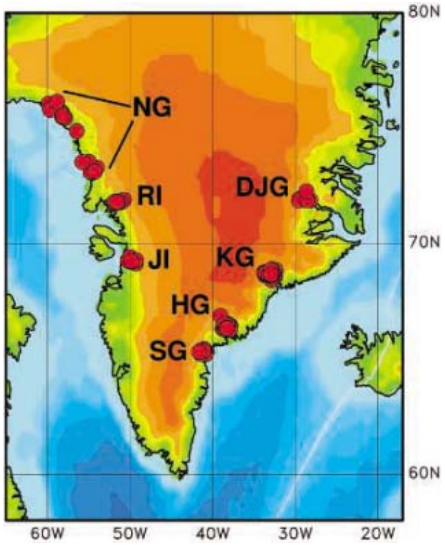

Fig. 1. Topographic map of southern Greenland and vicinity. The locations of 136 glacial earthquakes defining seven groups are indicated with red circles: DJG, Daugaard Jensen Glacier (5 events); KG, Kangerdlugssuaq Glacier (61); HG, Helheim Glacier (26); SG, southeast Greenland glaciers (6); JI, Jakobshavn Isbrae (11); RI, Rinks Isbrae (10); NG, northwest Greenland glaciers (17). Owing to the tight clustering of the earthquakes, many of the individual symbols on the map overlap.

Summer melting of the Greenland Ice Sheet has become more widespread during the past decade (*13*), and many outlet glaciers have thinned, retreated, and accelerated during the same time period (*14*–*19*). We investigate temporal changes in the frequency of Greenland glacial earthquakes by counting events for each year since 1993 (Fig. 2B). Detections for 2005 are for January to October and are based on the subset of seismic data available in near-real time. A clear increase in the number of events is seen starting in 2002. To date in 2005, twice as many events have been detected as in any year before 2002. The control group of detected events was used to determine whether an improvement in the detection capability of the seismic network could explain the observed increase (*9*). No clear trend is seen in the number of control events detected, indicating that the observed increase in the number of glacial earthquakes is real.

Recent evidence suggests that ice sheets and their outlet glaciers can respond very quickly to changes in climate, primarily through dynamic mechanisms affecting glacier flow (*12*, *15*). The seasonal signal and temporal increase apparent in our results are consistent with a dynamic response to climate warming driven by an increase in surface melting and the supply of meltwater to the glacier base. The number of events detected at each outlet glacier using the global seismic network is relatively small, and it is therefore difficult to draw robust conclusions about behavior at any single glacier. However, both the seasonal and temporal patterns reported here are observed for independent subsets of the data corresponding to east and west Greenland. The increase in number of glacial earthquakes over time thus appears to be a response to large-scale processes affecting the entire ice sheet. We note also that a part of the increase in the number of glacial earthquakes in west Greenland is due to the occurrence of more than two dozen of these earthquakes in 2000 to 2005 at the northwest Greenland glaciers, where only one event (in 1995) had previously been observed.

Understanding the mechanisms of the dynamic response of ice sheets to climate change is important in part because ice-sheet behavior itself affects global climate, through, for example, the modulation of freshwater input to the oceans (*20*). Glacial earthquakes represent one mechanism for the dynamic thinning of outlet glaciers, providing for the transport of a large mass of ice a distance of several meters (e.g., 10 km^3 by 10 m) over a duration of 30 to 60 s. Although the mechanics of sudden sliding motions at the glacier base are not known, the seasonal and temporal patterns reported here suggest that the glacial earthquakes may serve as a marker of ice-sheet response to external forcing. Continuous monitoring of ice velocity at outlet glaciers, along with regional seismic monitoring, would provide important insight into the nature of the dynamic response of ice sheets to changes in climate.

References and Notes

1. R. Butler *et al.*, *EOS* **85**, 225 (2004).
2. G. Ekström, M. Nettles, G. A. Abers, *Science* **302**, 622 (2003).
3. G. Ekström, *Bull. Seismol. Soc. Am.*, in press.
4. Seismograms from the glacial earthquakes are predicted poorly by standard faulting models in which the earthquake source is represented by a moment tensor or a double-couple force system. The seismic data are explained well by a single-force system like that used to describe landslide sources (*2*, *8*).
5. Initial detections and locations of the glacial earthquakes are obtained by array analysis of continuous seismic data (*1*), using a set of globally distributed test locations that allows for earthquake epicenters to be determined on a 0.5°

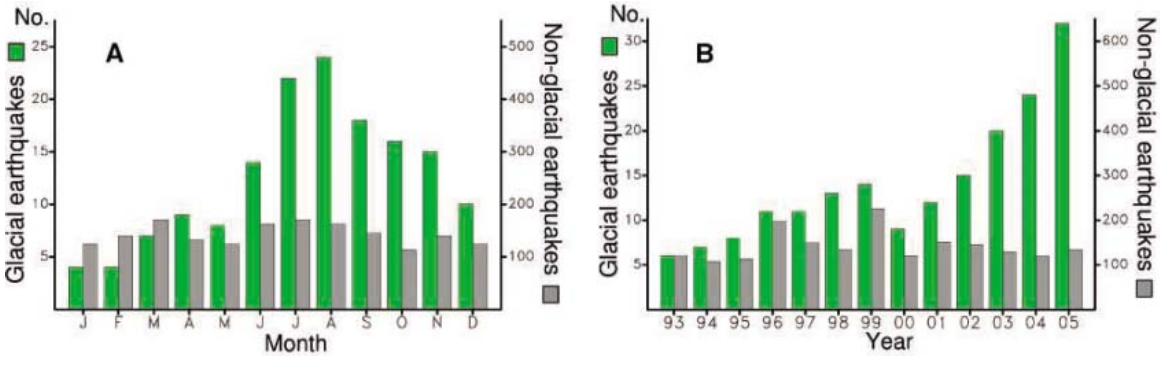

Fig. 2. (**A**) Histogram showing seasonality of glacial earthquakes on Greenland. Green bars show the number of detected Greenland glacial earthquakes in each month during the period 1993 to 2004. Gray bars show the number of earthquakes of similar magnitude detected elsewhere north of 45°N during the same period. (**B**) Histogram showing the increasing number of Greenland glacial earthquakes (green bars) since at least 2002. No general increase in the detection of earthquakes north of 45°N (gray bars) is observed during this time period.

by 0.5° grid. The quality of each detection and location is assessed based on the correlation between the observed signal envelope and that predicted for the selected location (*2*, *3*). Only events with high-quality detections are discussed in this report.
6. V. C. Tsai, G. Ekström, *EOS* **86**, Abstract C43A-02 (2005).
7. The earthquakes were analyzed by centroid-single-force (CSF) inversion (*2*, *8*) to obtain estimates of the best fitting source parameters, including the centroid location, time, size, and direction of sliding for each event.
8. H. Kawakatsu, *J. Geophys. Res.* **94**, 12,363 (1989).
9. The control group consists of all detected events north of 45°N that are not identified as glacial earthquakes on Greenland. Of this group of 1832 events, 98% are also found in standard earthquake catalogs. The remaining 35 events occur in seismically active areas and are also likely to be standard earthquakes. The observed rate of regular tectonic earthquakes at high northern latitudes, a proxy for detection-threshold stability, shows neither seasonality nor a temporal trend.
10. Although the glacial earthquakes discussed here have defining characteristics (including size, geometry, and duration) that distinguish them from other types of seismic events associated with glaciers, seasonality has been observed in calving-related glacial microearthquake activity in previous studies, for example, at Columbia Glacier, Alaska (*21*).
11. M. Meier *et al.*, *J. Geophys. Res.* **99**, 15,219 (1994).
12. H. J. Zwally *et al.*, *Science* **297**, 218 (2002).
13. K. Steffen, S. V. Nghiem, R. Huff, G. Neumann, *Geophys. Res. Lett.* **31**, L20402, 10.1029/2004GL020444 (2004).
14. I. Joughin, W. Abdalati, M. Fahnestock, *Nature* **432**, 608 (2004).
15. W. Krabill *et al.*, *Geophys. Res. Lett.* **31**, L24402, 10.1029/2004GL021533 (2004).
16. A. Luckman, T. Murray, *Geophys. Res. Lett.* **32**, L08501, 10.1029/2005GL023813 (2005).
17. I. M. Howat, I. Joughin, S. Tulaczyk, S. Gogineni, *Geophys. Res. Lett.* **32**, L22502, 10.1029/2005GL024737 (2005).
18. G. S. Hamilton, L. A. Stearns, *EOS* **86**, Abstract C23A-1159 (2005).
19. E. Rignot, *EOS* **86**, Abstract C41A-02 (2005).
20. P. U. Clark, R. B. Alley, D. Pollard, *Science* **286**, 1104 (1999).
21. A. Qamar, *J. Geophys. Res.* **93**, 6615 (1988).
22. Supported by National Science Foundation grants EAR-0207608 and OPP-0352276 and a National Science Foundation Graduate Fellowship (V.C.T.). The seismic data were collected and distributed by the Incorporated Research Institutions for Seismology and the U.S. Geological Survey.

1 November 2005; accepted 9 January 2006
10.1126/science.1122112

The Preparation and Structures of Hydrogen Ordered Phases of Ice

Christoph G. Salzmann,[1,2]* Paolo G. Radaelli,[3,4] Andreas Hallbrucker,[1] Erwin Mayer,[1] John L. Finney[4]

Two hydrogen ordered phases of ice were prepared by cooling the hydrogen disordered ices V and XII under pressure. Previous attempts to unlock the geometrical frustration in hydrogen-bonded structures have focused on doping with potassium hydroxide and have had success in partially increasing the hydrogen ordering in hexagonal ice I (ice I*h*). By doping ices V and XII with hydrochloric acid, we have prepared ice XIII and ice XIV, and we analyzed their structures by powder neutron diffraction. The use of hydrogen chloride to release geometrical frustration opens up the possibility of completing the phase diagram of ice.

Water molecules in all of the 12 known crystalline phases (Fig. 1) are tetrahedrally hydrogen bonded to four neighbors. A consequence of this connectivity is that individual water molecules may adopt, in principle, six different orientations. In ice structures, the Bernal Fowler rules (*1*, *2*) require that one hydrogen atom participates in each hydrogen bond. Therefore, the orientation of a given molecule is restricted by its local environment and cannot rotate to another hydrogen-bonded orientation without its neighbors also reorienting. In spite of these restrictions, a very large number of nearly degenerate molecular configurations, which are all related to each other by cooperative reorientation, exist near the true ground state. This is a consequence of the inherent geometrical frustration of the ice lattice, a particularly interesting aspect of these hydrogen-bonded systems that is relevant for other geometrically frustrated systems such as protein folding and neural networks (*3*, *4*). Furthermore, there are important parallels with frustrated magnetic systems (*5*), which themselves have been called "spin ices."

At high temperatures, water ices can explore their configurational manifold thanks to the presence of mobile point defects, which locally lift the constraints of the geometrical frustration (*6*–*8*). The two types of thermally induced point defects uniquely found in ices are rotational defects, in which either two (D defect) or no hydrogen atoms (L defect) are found between neighboring oxygen atoms, and ionic defects (H_3O^+ and OH^-) (*6*). These defects can migrate along chains of molecules through the crystal structure leaving reoriented molecules behind them, thus providing the mechanism for collective reorientation in ice. The molecular orientations found in the high-temperature, liquidus phases of ice (I*h*, III, IV, V, VI, VII, and XII) are more or less random, so that the space-time averaged structure of those phases is hydrogen disordered (*6*, *7*, *9*, *10*). As the temperature is lowered, the tendency to occupy the energetically most favored orientations increases. However, for most phases, this ordering process is hampered by the decreasing number density and mobility of the point defects. Except for disordered ices III and VII, intrinsic point defects are not sufficient to facilitate phase transitions from the hydrogen disordered phases, including ice V (*7*, *9*, *11*–*13*) or ice XII (*10*, *14*, *15*), to their energetic (hydrogen ordered) ground-state phases. Instead, ergodicity is lost before the long-range ordering transition, and the hydrogen disordered structures are frozen-in. For this reason, the hydrogen ordered ground states of ices V and XII remain undiscovered so far.

Point defects can also be introduced by doping ices with impurities. However, the effectiveness of each particular dopant to pre-

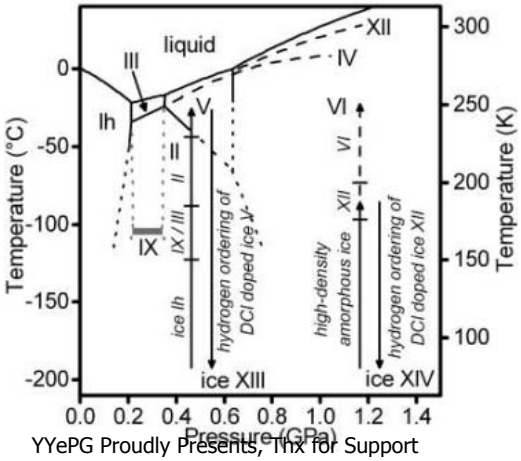

Fig. 1. The phase diagram of ice, including liquidus lines of metastable ices IV and XII (long dashed lines) and extrapolated equilibria lines at low temperatures (short dashed lines). The pathways of preparation of DCl-doped ices V and XII are indicated by arrows. Ice V was produced by isobarically heating ice I*h* to 250 K at 0.5 GPa. Pure ice XII was crystallized from high-density amorphous ice by isobaric heating at 1.2 GPa at 11 K min^{-1} to 190 K, which is 10 K below the temperature where transition to more stable ice VI would occur. Both ice V and ice XII can be handled at ambient pressure up to temperatures of ~150 K, where conversion to cubic ice I*c* occurs (*19*, *20*).

[1]Institute of General, Inorganic, and Theoretical Chemistry, University of Innsbruck, Innrain 52a, 6020 Innsbruck, Austria. [2]Inorganic Chemistry Laboratory, University of Oxford, South Parks Road, Oxford OX1 3QR, UK. [3]ISIS Facility, Rutherford Appleton Laboratory, Council for the Central Laboratory of the Research Councils (CCLRC), Chilton, Didcot OX11 0QX, UK. [4]Department of Physics and Astronomy, University College London, Gower Street, London WC1E 6BT, UK.

*To whom correspondence should be addressed. E-mail: christoph.salzmann@chemistry.oxford.ac.uk

serve ergodicity is poorly understood, because it depends on the number density of the created defects (hence on the solubility of a dopant in ice), on the mobility of the defects, and on defect-defect interactions (*6*).

Ordering of ice I*h* to ice XI has been partially achieved through KOH (potassium hydroxide) doping (*16*). This is thought to create extrinsic L and OH^- defects (*6*), and was also studied calorimetrically (*17*) and spectroscopically (*18*) for ice V. Handa and co-workers (*17*) observed that an endothermic peak on heating ice V could be intensified by KOH doping. This transition was discussed, therefore, in terms of a hydrogen order-disorder transition. However, hydrogen ordering could not be confirmed by Raman spectroscopy (*18*). Similar endothermic events were also found for undoped ice XII (*19*, *20*). Doping experiments for ice XII have not been reported so far.

Reasoning that the L and OH^- defects expected from KOH doping are unable to promote hydrogen ordering in ice V, we explored the effect of HCl (hydrochloric acid) doping, which is thought to produce L and H_3O^+ defects (*6*). Doped ice V samples were prepared by freezing 0.01 mol L^{-1} solutions of HCl or KOH in H_2O, or DCl or KOD in D_2O, in a piston-cylinder apparatus precooled to 77 K and then by heating the frozen ice isobarically at 0.5 GPa to 250 K (Fig. 1). For Raman spectroscopy, 5 weight percent D_2O was added to the initial H_2O solution. Thereafter, the samples were cooled from 250 K at 0.8 K min^{-1} to 77 K, decompressed, and recovered under liquid nitrogen. The transition to ice II on cooling was not observed at 0.5 GPa, which is in agreement with (*7*).

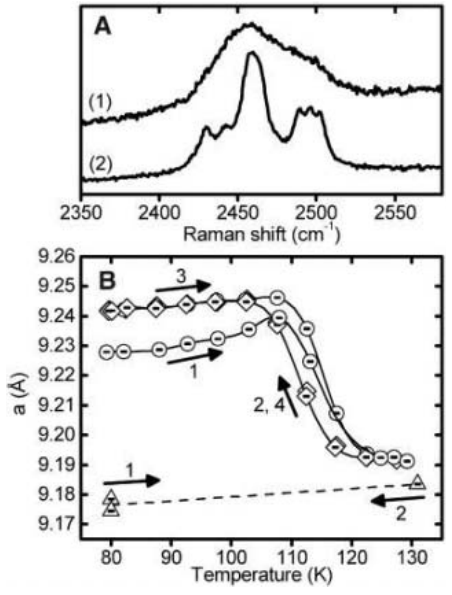

Fig. 2. (**A**) Raman spectra of the decoupled O-D stretching transitions of KOH- (1) and HCl- (2) doped ice V samples recorded at 80 K in vacuum. (**B**) Change of lattice constant *a* from powder neutron diffraction during heating and cooling of a KOD-doped ice V sample (triangles) measured on the D2B instrument at ILL, and heating (circles) and cooling (diamonds) of a DCl-doped ice V sample measured on the General Materials Diffractometer (GEM) at ISIS. The sequence of heating and cooling (~0.2 K min^{-1}) is indicated by numbered arrows. Solid lines are guides to the eye.

The samples were characterized first by Raman spectroscopy. Figure 2A shows the spectral region of the decoupled O-D stretching transitions, which result from HDO molecules in a dilute solution in an H_2O crystal. The observed spectra give information on different molecular environments in an H_2O crystal (*21*). For example, the full width at half height of the band for a decoupled O-D stretching transition in hydrogen ordered H_2O ice II is only ~5 cm^{-1}, but it is ~30 cm^{-1} in hydrogen disordered ice I (*22*). Spectra 1 and 2 (Fig. 2A) show the decoupled O-D stretching transitions of KOH- and HCl-doped ice V samples, respectively. The former shows the typical broad features of disordered ice V (*12*, *18*). However, substantial sharpening of the features can be seen in spectrum 2, and at least six distinct peaks become observable, indicating considerable hydrogen ordering in the HCl-doped phase.

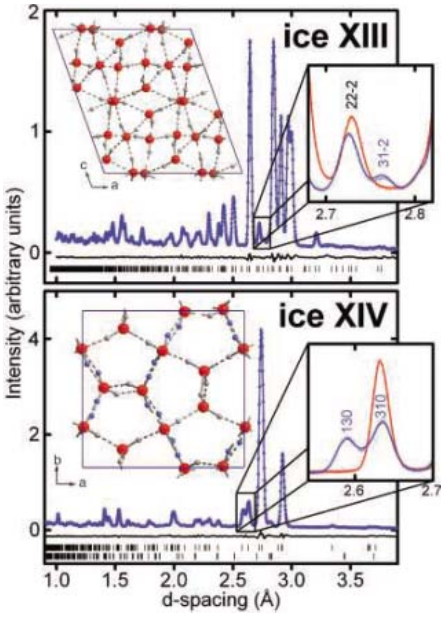

Fig. 3. Observed, calculated, and difference profiles for the observed phases of ice at 80 K and ambient pressure. The structures were refined using the GSAS program (*24*). Linear constraints and chemical composition restraints were applied to maintain stoichiometry of the water molecules. Data were recorded on the GEM diffractometer at ISIS. Data for hydrogen ordered ice V (ice XIII) are shown in the upper plot (least squares refinement R_{wp} = 0.0297, R_p = 0.0347), and data for hydrogen ordered ice XII (ice XIV) are shown in the lower plot (R_{wp} = 0.0366, R_p = 0.0374). Tick marks indicate the positions of the Bragg peaks. For ice XIV, the lower tick marks represent a small ice IV impurity. Both plots show magnifications of regions where new reflections (ice XIII) or peak splitting (ice XIV) were observed for the ordered phases (blue). The diffractograms of the corresponding disordered phases, which were obtained on heating to 130 K (ice V) or 118 K (ice XII), are shown in red. Unit cell projections of the refined structures are shown in both plots. Oxygen and deuterium atoms are drawn in red and gray, respectively. Deuterium positions in ice XIV still containing some disorder are depicted in blue. Covalent and hydrogen bonds are indicated by solid and dashed lines, respectively.

Doped D_2O ice V samples were subsequently analyzed by powder neutron diffraction. Figure 2B shows the changes of the lattice constant *a* as a function of temperature at ambient pressure. This quantity was found to be a very sensitive indicator of changes in hydrogen order. Upon heating the DCl-doped sample, a stepwise contraction of the lattice parameter *a* was observed between ~110 and ~120 K. The reversibility of this transition was observed by cooling back to 80 K at ~0.2 K min^{-1} and by an additional heating/cooling cycle. Slow cooling at ambient pressure seemed to enhance the ordering process, as demonstrated by a further increase of the lattice parameter *a* observed on cooling (Fig. 2B).

Space group symmetry reduction and thus formation of a different phase upon cooling is indicated by the appearance of the (31-2) (Fig. 3, inset) and (110) reflections in the neutron powder pattern. The highest symmetry space group that meets the observed reflection conditions is monoclinic $P2_1/a$, which is a subgroup of the ice V space group ($A2/a$). [$P2_1/a$ was previously proposed by Kamb and La Placa for ordered ice V in an abstract (*23*), but their data were never published.] The structural parameters of ordered ice V were refined by using the General Structure Analysis System (GSAS) program (*24*), by using the values for disordered ice V as a starting point. The refinement of the ordered structure after slow cooling at ambient pressure (Fig. 2B) revealed the formation of highly ordered molecules as the refined occupation probabilities of the deuterium positions converged within the errors to either 0 or 1 (Table 1). The unit cell of this hydrogen ordered phase is shown as an inset in Fig. 3. It comprises 28 molecules with 7 crystallographically distinct oxygen atoms (Table 1). This makes the $P2_1/a$ structure even more complicated than ice V and thus the most complicated structure among the known crystalline phases of ice.

In contrast with the DCl-doped sample, neither cooling under pressure from 250 to 80 K nor cooling at ambient pressure from 130 to 80 K at 0.2 K min^{-1} of the KOD-doped ice V sample led to new reflections. Furthermore, heating and cooling at ambient pressure induced no substantial changes in the lattice constant (Fig. 2B), and all collected data could be refined using the disordered structural model of ice V. However, we could reproduce the endothermic features observed by Handa and co-workers for KOH-

Table 1. Fractional coordinates and isotropic atomic-displacement parameters (U_{iso}) for ice XIII (80 K and ambient pressure). Numbers in parentheses are statistical errors of the last significant digit. Deuterium positions with refined fractional occupancies <0.1 are omitted from the table. The spacegroup is $P2_1/a$ and the unit cell parameters are as follows: a = 9.2417(1) Å, b = 7.4724(1) Å, c = 10.2970(1) Å, β = 109.6873(9)°. Data were collected after cooling the sample at ~0.2 K min^{-1} from 130 to 80 K at ambient pressure. All atoms lie on general positions (multiplicity = 4).

	x	*y*	*z*	U_{iso}*100	Occupancies
O1	0.2541(6)	0.5629(5)	0.2517(5)	0.41(3)	1.0000
O2	0.4771(6)	0.7992(5)	0.4089(5)	0.41(3)	1.0000
O3	0.0503(6)	0.8082(6)	0.0941(5)	0.41(3)	1.0000
O4	0.2613(5)	0.4045(6)	0.4992(5)	0.41(3)	1.0000
O5	0.2113(4)	0.4029(5)	0.0034(5)	0.41(3)	1.0000
O6	0.4147(5)	0.1103(7)	0.2336(4)	0.41(3)	1.0000
O7	0.1245(5)	0.1142(6)	0.2643(4)	0.41(3)	1.0000
D8	0.3444(4)	0.6427(5)	0.3008(3)	1.01(3)	0.991(6)
D10	0.2458(5)	0.4942(5)	0.3299(5)	1.01(3)	0.943(5)
D13	0.1074(4)	0.7187(5)	0.1563(4)	1.01(3)	0.952(6)
D16	0.4820(4)	0.9075(5)	0.3558(4)	1.01(3)	0.968(6)
D18	0.5763(5)	0.7499(5)	0.4437(4)	1.01(3)	0.974(7)
D19	0.9486(5)	0.7508(5)	0.0478(4)	1.01(3)	1.037(5)
D21	0.2372(3)	0.4543(5)	0.0989(4)	1.01(3)	1.015(6)
D24	0.3043(4)	0.4904(6)	0.5777(4)	1.01(3)	0.896(5)
D26	0.1708(4)	0.3555(6)	0.5137(4)	1.01(3)	1.015(5)
D27	0.3072(4)	0.3737(6)	0.9904(3)	1.01(3)	1.014(5)
D29	0.0781(4)	0.0194(6)	0.1989(4)	1.01(3)	0.938(5)
D30	0.3250(5)	0.1374(5)	0.2554(5)	1.01(3)	0.916(6)
D32	0.3823(5)	0.0496(6)	0.1467(5)	1.01(3)	0.920(6)
D35	0.0509(4)	0.2082(6)	0.2548(5)	1.01(3)	0.911(7)

Table 2. Fractional coordinates and isotropic atomic-displacement parameters (U_{iso}) for ice XIV (80 K and ambient pressure). Numbers in parentheses are statistical errors of the last significant digit. Deuterium positions with refined fractional occupancies <0.1 are omitted from the table. The spacegroup is $P2_12_12_1$ and the unit cell parameters are as follows: a = 8.3499(2) Å, b = 8.1391(2) Å, c = 4.0825(1) Å. Data were collected after cooling the sample at ~0.8 K min^{-1} from 180 to 80 K at 1.2 GPa. Fractional occupancies of ordered deuterium positions were fixed during the refinement. All atoms lie on general positions (multiplicity = 4).

	x	*y*	*z*	U_{iso}*100	Occupancies
O1	0.0059(3)	0.2568(5)	0.1304(7)	1.53(2)	1.0000
O2	0.6308(3)	–0.0078(3)	0.2485(7)	1.53(2)	1.0000
O3	0.2525(4)	0.8858(3)	0.0063(6)	1.53(2)	1.0000
D4	0.0557(7)	0.3284(7)	0.9845(1)	2.03(1)	0.407(3)
D5	0.5275(5)	0.8410(4)	0.4684(1)	2.03(1)	0.620(4)
D6	0.0920(2)	0.2056(3)	0.2671(6)	2.03(1)	1.0000
D9	0.7895(3)	0.9679(3)	0.8954(7)	2.03(1)	1.0000
D11	0.7340(3)	0.4630(3)	0.3225(6)	2.03(1)	1.0000
D12	0.4111(4)	0.5790(5)	0.3625(1)	2.03(1)	0.593(3)
D13	0.9018(8)	0.1018(7)	0.8552(2)	2.03(1)	0.380(4)
D15	0.8472(3)	0.3248(3)	0.4010(6)	2.03(1)	1.0000

doped ice V samples (*17*). According to diffraction and spectroscopic data given here and in (*18*), we conclude that that these calorimetric features are not caused by a phase transition from ordered ice V. KOH doping was thus confirmed to be ineffective in promoting hydrogen ordering in ice V.

DCl-doped D_2O ice XII samples were prepared by following a procedure described in (*25*). First, high-density amorphous ice (HDA) was prepared by compression of ice I*h* doped with 0.01 mol L^{-1} DCl at 77 K (*26*). HDA was then heated isobarically starting from 77 K at 1.2 GPa at ~11 K min^{-1} to crystallize pure ice XII (Fig. 1) (*25*). After cooling from 180 to 77 K at 0.8 K min^{-1}, the sample was decompressed, recovered in liquid nitrogen, and characterized at 80 K by powder neutron diffraction.

Again, hydrogen ordering was indicated by changes in the lattice constants: A transition from tetragonal ice XII ($a = b$) to an orthorhombic phase ($a \neq b$) could be observed and is visualized most clearly by the splitting of the tetragonal (310) reflection to (130) and (310) orthorhombic reflections (Fig. 3, inset). The highest symmetry orthorhombic space group that meets the observed reflection conditions is $P2_12_12_1$, which is a subgroup of the ice XII spacegroup ($I\bar{4}2d$). The unit cell of ordered ice XII, which contains 12 water molecules with three crystallographically distinct oxygen atoms (Table 2), is shown in Fig. 3. Hydrogen positions still containing some residual disorder are drawn in blue. The structural refinement shows the possible existence of a strain effect in the sample, which may prevent the sample from becoming completely ordered in a similar manner to the transition of ice I*h* to ice XI (*27*).

The generally accepted view for the naming of phases of ice is that Roman numeral labels should only be given for experimentally established crystalline phases, with crystallographic or at least spectroscopic evidence (*6*, *10*). Consequently, we label the reported ordered phases ice XIII for ordered ice V and ice XIV for ordered ice XII, in chronological accordance with their dates of discovery.

Hydrogen ordered ices XIII and XIV represent the lowest energy structures at low temperatures for their given oxygen positions. We believe that strain prevents ice XIV from becoming completely ordered, and therefore the fully ordered structure would be described by rounding the less ordered occupancies to 1 or 0, respectively (Table 2). The fully ordered configuration found for ice XIII is one out of 70 possibilities allowed by symmetry of the space group and stoichiometry of the H_2O molecule. It would be a challenging test of the ability of modern day computational methods to reproduce our experimentally found lowest energy state. This would provide a critical test for current water potentials widely used in computational chemistry and structural biology.

References and Notes

1. J. D. Bernal, R. H. Fowler, *J. Chem. Phys.* **1**, 515 (1933).
2. L. Pauling, *J. Am. Chem. Soc.* **57**, 2680 (1935).
3. J. N. Onuchic, Z. Luthey-Schulten, P. G. Wolynes, *Annu. Rev. Phys. Chem.* **48**, 545 (1997).
4. J. J. Hopfield, *Proc. Natl. Acad. Sci. U.S.A.* **81**, 3088 (1984).
5. J. Snyder, J. S. Slusky, R. J. Cava, P. Schiffer, *Nature* **413**, 48 (2001).
6. V. F. Petrenko, R. W. Whitworth, *Physics of Ice* (Oxford Univ. Press, Oxford, 1999).
7. C. Lobban, J. L. Finney, W. F. Kuhs, *J. Chem. Phys.* **112**, 7169 (2000).
8. G. P. Johari, *J. Chem. Phys.* **112**, 10957 (2000).
9. B. Kamb, A. Prakash, C. Knobler, *Acta Crystallogr.* **22**, 706 (1967).
10. C. Lobban, J. L. Finney, W. F. Kuhs, *Nature* **391**, 268 (1998).
11. W. C. Hamilton, B. Kamb, S. J. La Placa, A. Prakash, in *Physics of Ice*, N. Riehl, B. Bullemer, H. Engelhardt, Eds. (Plenum, New York, 1969), pp. 44–58.
12. B. Minceva-Sukarova, G. E. Slark, W. F. Sherman, *J. Mol. Struct.* **143**, 87 (1986).
13. G. P. Johari, E. Whalley, *J. Chem. Phys.* **115**, 3274 (2001).
14. M. M. Koza, H. Schober, T. Hansen, A. Tölle, F. Fujara, *Phys. Rev. Lett.* **84**, 4112 (2000).
15. C. Salzmann, I. Kohl, T. Loerting, E. Mayer, A. Hallbrucker, *J. Phys. Chem. B* **106**, 1 (2002).
16. Y. Tajima, T. Matsuo, H. Suga, *Nature* **299**, 810 (1982).
17. Y. P. Handa, D. D. Klug, E. Whalley, *J. Phys. Colloq.* **48**, 435 (1987).
18. B. Minceva-Sukarova, G. Slark, W. F. Sherman, *J. Mol. Struct.* **175**, 289 (1988).

19. C. G. Salzmann, I. Kohl, T. Loerting, E. Mayer, A. Hallbrucker, *Phys. Chem. Chem. Phys.* **5**, 3507 (2003).
20. C. G. Salzmann, E. Mayer, A. Hallbrucker, *Phys. Chem. Chem. Phys.* **6**, 1269 (2004).
21. C. Haas, D. F. Hornig, *J. Chem. Phys.* **32**, 1763 (1960).
22. J. E. Bertie, E. Whalley, *J. Chem. Phys.* **40**, 1637 (1964).
23. B. Kamb, S. J. La Placa, *Trans. Am. Geophys. Union* **56**, 1202 (1974).
24. A. C. Larsen, R. B. Von Dreele, General Structure Analysis System (GSAS), Los Alamos National Laboratory Report LAUR 86-748 (2000).
25. C. G. Salzmann, E. Mayer, A. Hallbrucker, *Phys. Chem. Chem. Phys.* **6**, 5156 (2004).
26. O. Mishima, L. D. Calvert, E. Whalley, *Nature* **310**, 393 (1984).
27. C. M. B. Line, R. W. Whitworth, *J. Chem. Phys.* **104**, 10008 (1996).

28. We thank CCLRC and the Institut Laue-Langevin (ILL) for access to the ISIS and ILL neutron facilities, respectively. We also thank E. Suard for helping with the experiment at the ILL; K. Wurst, C. S. Tautermann, and M. Mayr for discussions; and the University of Innsbruck for financial support (C.G.S.).

15 December 2005; accepted 22 February 2006
10.1126/science.1123896

Structure of Tracheal Cytotoxin in Complex with a Heterodimeric Pattern-Recognition Receptor

Chung-I Chang,[1,2] Yogarany Chelliah,[1,2] Dominika Borek,[2] Dominique Mengin-Lecreulx,[3] Johann Deisenhofer[1,2]*

Tracheal cytotoxin (TCT), a naturally occurring fragment of Gram-negative peptidoglycan, is a potent elicitor of innate immune responses in *Drosophila.* It induces the heterodimerization of its recognition receptors, the peptidoglycan recognition proteins (PGRPs) LCa and LCx, which activates the immune deficiency pathway. The crystal structure at 2.1 angstrom resolution of TCT in complex with the ectodomains of PGRP-LCa and PGRP-LCx shows that TCT is bound to and presented by the LCx ectodomain for recognition by the LCa ectodomain; the latter lacks a canonical peptidoglycan-docking groove conserved in other PGRPs. The interface, revealed in atomic detail, between TCT and the receptor complex highlights the importance of the anhydro-containing disaccharide in bridging the two ectodomains together and the critical role of diaminopimelic acid as the specificity determinant for PGRP interaction.

The innate immune system in multicellular animals has developed to discriminate infectious nonself from noninfectious self. Central to this first line of host defense against microbial infections are pattern-recognition receptors (PRRs), which recognize unique structures of conserved components found in pathogens but not in the host (*1*). In *Drosophila*, several PRRs responsible for detecting bacterial infections belong to the family of peptidoglycan recognition proteins (PGRPs), which contain a conserved PGRP domain structurally similar to the bacteriophage T7 lysozyme (*2*). Peptidoglycan (PG) is one of the pathogen-associated components found only in bacteria but not in eukaryotes and is exploited by the innate immune system as the signature of microbial nonself. Polymeric PG is composed of repeating units of muropeptide composed of disaccharide *N*-acetyl glucosaminyl (GlcNAc)-*N*-acetylmuramic acid (MurNAc) linked to a stem peptide of D- and L- (or *meso*-) amino acids, where the third amino acid is mostly lysine in Gram-positive bacteria and diaminopimelic acid (DAP) in Gram-negative bacteria.

DAP-type PG induces innate immune responses in *Drosophila* by activating the immune deficiency pathway (*3*–*5*). A naturally occurring fragment of DAP-type PG, known as tracheal cytotoxin (TCT; GlcNAc-1,6-anhydro-MurNAc-L-Ala-γ-D-Glu-*meso*-DAP-D-Ala), strongly activates the immune deficiency pathway, and its recognition requires PGRP-LCa and -LCx (*3*, *5*), which are generated by alternative splicing from the *PGRP-LC* gene (*6*). PGRP-LCa and -LCx contain identical cytoplasmic and transmembrane domains but distinct PGRP-like ectodomains (*6*). TCT is found in cells of most Gram-negative bacteria because this cell-wall fragment (muropeptide) is constantly released from PG during the remodeling of the polymer that occurs during cell growth and division and is then recycled and its sugar and peptide components reincorporated back into PG (*7*). TCT, which is released from growing cells of *Bordetella*, is a virulence factor responsible for epithelial cytopathology associated with pertussis infection (*8*). TCT binds directly to the ectodomain of PGRP-LCx but not to PGRP-LCa; however, TCT induces heterodimerization of the LCa and LCx ectodomains (*9*, *10*). TCT requires its unique GlcNAc-MurNAc(anhydro) moiety for optimal immunestimulatory activity (*3*, *5*). Recently, the structure of the LCa ectodomain was shown to explain its lack of TCT-binding ability by revealing an obstructed PG-docking groove, which has led to a model of TCT recognition by the PGRP-LCa/LCx complex (*9*). In this model, the LCx ectodomain first engages a typical muropeptide-docking interaction, as observed in the structure of PGRP-IαC in complex with a synthetic PG subunit analog (*11*). Next, PGRP-LCa recognizes the exposed structural features of TCT while the latter is bound to the LCx ectodomain. This model explains how TCT brings PGRP-LCa and -LCx receptors in close vicinity, allowing their cytoplasmic domains to dimerize for receptor activation (*12*). The confirmation of this model, however, requires structural determination of TCT bound to the PGRP-LCa and -LCx complex.

We expressed the LCa and LCx ectodomains in Hi-5 cells and purified the two fragments as described (*13*). TCT was purified from *Escherichia coli* as described previously (*5*). The three components were mixed at a molar ratio of 1:1:6 (LCa:LCx:TCT) before crystallization screening. Crystals with the symmetry of space group $P2_12_12_1$ (a = 41.123 Å, b = 79.695 Å, c = 114.389 Å) were grown from a mother liquor containing 20% polyethylene glycol 1500, 5% ethylene glycol, and 100 mM phosphate–citrate at pH 4.2. The structure of LCa-TCT-LCx complex was determined by molecular replacement with coordinates of the LCa ectodomain and PGRP-SA as search models (*9*, *14*). The final model contains all 64 nonhydrogen atoms of TCT, residues Asp^{354} to the C-terminal residue Ser^{520} of PGRP-LCa and residues Met^{334} to Glu^{499} of PGRP-LCx, with 198 solvent molecules; as well as N-linked glycans to the LCa residues Asn^{389} and Asn^{515} (see table S1 for crystallographic data and refinement statistics).

Both PGRP-LCx and PGRP-LCa are type II membrane proteins with N-terminal cytoplasmic and C-terminal ectodomains. Both the LCx and LCa ectodomains contain a central five-stranded β sheet flanked by five major helices (Fig. 1, A and B). However, unlike PGRP-LC, whose surface groove is obstructed by two LCa-specific helical insertions and cannot bind TCT (*9*), the LCx ectodomain possesses a typical PG-docking groove found in other PGRPs (*11*, *14*–*17*). In the complex, TCT binds into the docking groove on LCx and makes intimate contacts with the groove-lining residues (Fig. 1C), so that one side of TCT is buried within the docking groove. The TCT-loaded LCx ectodomain buries a total surface of 1326 Å^2, consistent with their nanomolar affinity (*18*). The GlcNAc-MurNAc(anhydro) moiety of bound TCT, the B1-H2 loop and the H2 helix of the docking groove, as well as the H3-B4 loop of LCx together form the rec-

[1]Howard Hughes Medical Institute and [2]Department of Biochemistry, University of Texas Southwestern Medical Center at Dallas, 6001 Forest Park Road, Dallas, TX 75390–9050, USA. [3]Institut de Biochimie et Biophysique Moléculaire et Cellulaire, Centre National de la Recherche Scientifique, Université de Paris-Sud, 91405 Orsay, France.

*To whom correspondence should be addressed. E-mail: johann.deisenhofer@utsouthwestern.edu

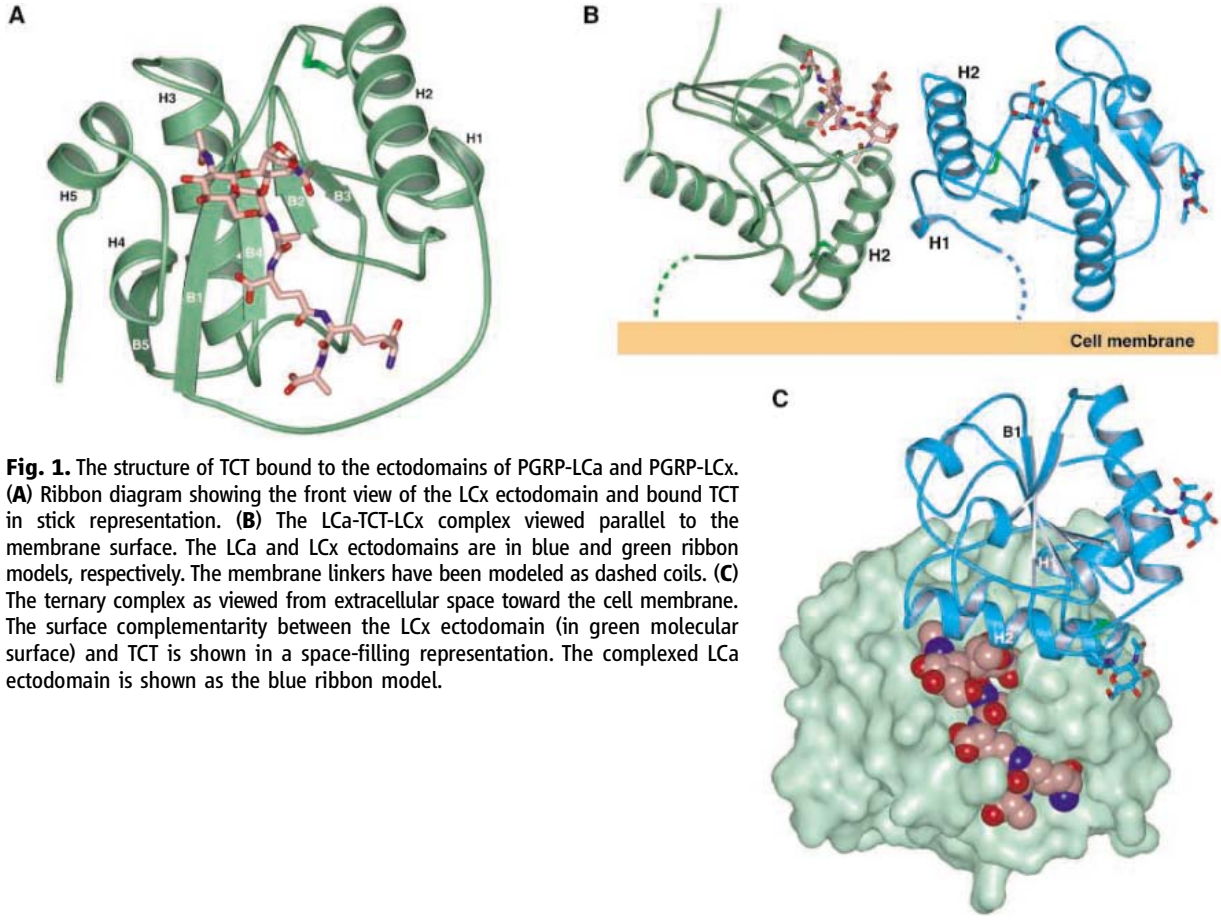

Fig. 1. The structure of TCT bound to the ectodomains of PGRP-LCa and PGRP-LCx. (**A**) Ribbon diagram showing the front view of the LCx ectodomain and bound TCT in stick representation. (**B**) The LCa-TCT-LCx complex viewed parallel to the membrane surface. The LCa and LCx ectodomains are in blue and green ribbon models, respectively. The membrane linkers have been modeled as dashed coils. (**C**) The ternary complex as viewed from extracellular space toward the cell membrane. The surface complementarity between the LCx ectodomain (in green molecular surface) and TCT is shown in a space-filling representation. The complexed LCa ectodomain is shown as the blue ribbon model.

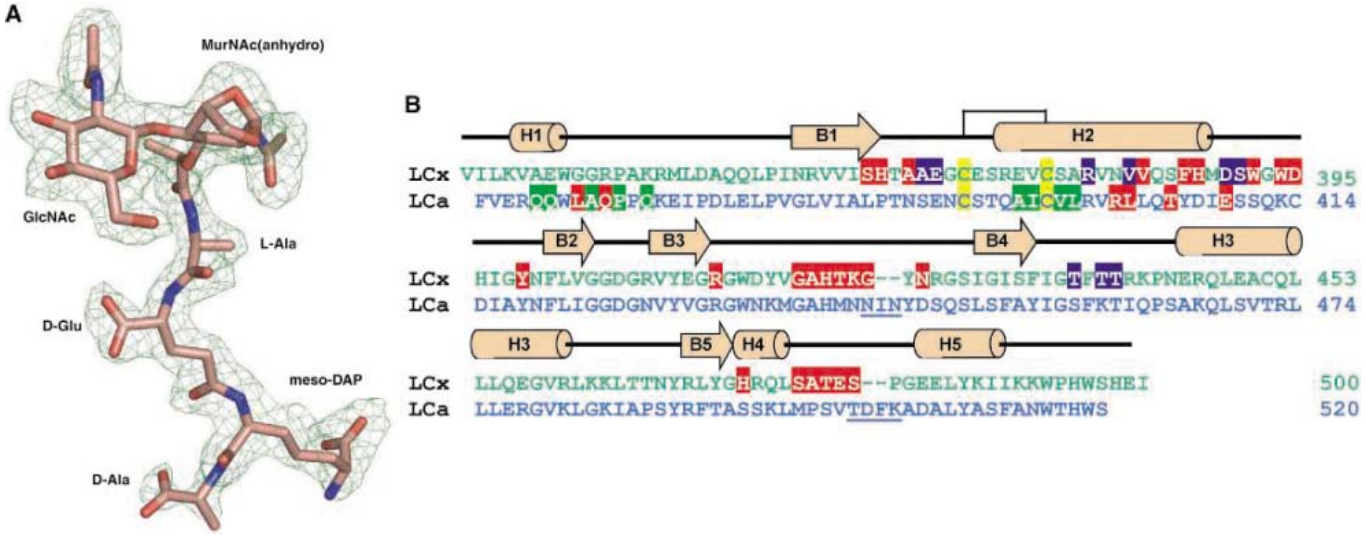

Fig. 2. TCT in the crystal and its recognition residues in the LCa and LCx ectodomains. (**A**) $F_o - F_c$ difference-Fourier omit map of TCT at 2.1 Å resolution displayed in green mesh at 2.0σ level. (**B**) Aligned sequences of the LCx (green) and LCa (blue) ectodomains highlight the TCT-interacting residues in red. The LCx residues contacting the LCa ectodomain are shaded in blue; the LCa residues that interact with the LCx ectodomain are shaded in green. LCa-specific insertion residues are underlined. Secondary-structure elements in the LCx ectodomain are indicated above the alignment. The disulfide-linked Cys residues are boxed in yellow. Abbreviations for the amino acid residues are as follows: A, Ala; C, Cys; D, Asp; E, Glu; F, Phe; G, Gly; H, His; I, Ile; K, Lys; L, Leu; M, Met; N, Asn; P, Pro; Q, Gln; R, Arg; S, Ser; T, Thr; V, Val; W, Trp; and Y, Tyr.

ognition surface of 685 Å^2 for PGRP-LCa and interact with LCa residues from the H1 helix, the H1-B1 loop, and the H2 helix (Fig. 1, B and C). The groove region and the N-linked glycans of the LCa ectodomain are not involved in interaction with TCT and PGRP-LCx. No conformational change is induced in the LCa ectodomain upon binding; the root mean square deviation (RMSD) of the Cα positions of the complexed and uncomplexed structures after superposition is 0.42 Å. Also, no major conformational change is expected in the LCx

ectodomain upon TCT binding; the overall structure of TCT-docked LCx is comparable to that of PGRP-SA, with an RMSD of 0.84 Å.

The entire TCT is well ordered in the complex crystal (Fig. 2A). The PG-docking groove of LCx exhibits a high degree of shape complementarity to TCT and accommodates the ligand in its low-energy extended conformation. TCT makes van der Waals contacts throughout its elongated stem peptide chain with the docking-groove residues. The TCT-contacting residues of LCx are concentrated in the two sequence regions where insertions occur in LCa (Fig. 2B) (*9*). The TCT-LCx interaction is further stabilized by 25 strategic hydrogen bonds (Fig. 3 and table S2). In the structure, the pyranose ring of MurNAc, adopting an envelope conformation due to an anhydro bond (Fig. 2A), is cradled by the LCx groove base formed by Thr^{366}/x and Ala^{367}/x. The carbonyl group of 2-acetamide and the equatorial 3-OH of GlcNAc, in the chair form, contact the imidazole ring of His^{365}/x and the backbone amide of Glu^{480}/x, respectively (Fig. 3). GlcNAc appears to dock loosely to the LCx groove with its pyranose ring partially protruding into the solvent space. However, the GlcNAc ring is tethered to the lactyl group of MurNAc and the carbonyl group of D-Glu in TCT, as well as to Ser^{477}/x, Ala^{478}/x, and Thr^{479}/x, through an extensive network of hydrogen bonds involving three water molecules (Fig. 3).

All PGs from bacteria contain the same carbohydrate backbone; however, dependent upon bacterial species, the stem peptides that linked to MurNAc vary in the composition and modification of the amino acid in the third position. In most Gram-positive bacteria, the third amino acid is Lys; in most Gram-negative bacteria, the third residue is *meso*-DAP. It was suggested that the third amino acid of the PG stem peptide is the specificity determinant for recognition by PGRPs (*4*). *meso*-DAP differs from Lys only by the presence of a carboxyl group on the Cε with D-chirality. In the structure, the carboxyl group of *meso*-DAP is the only residue recognized by an electrostatic interaction; it forms a bidentate salt bridge with the guanidinium group of Arg^{413}/x and hydrogen bonds to the main-chain amide of Asp^{395}/x (Fig. 3); these two residues and Trp^{394}/x form a binding pocket for the DAP group. Furthermore, because the groove that accommodates DAP is guarded by three solvent-exposed basic residues Arg^{349}/x, Lys^{423}/x, and Arg^{427}/x (not shown), a lysine in a monomeric PG ligand would strongly destabilize docking interaction. However, it should be noted that the ε-amino group of Lys in polymeric PG will not retain a basic charge if a cross bridge linking this amino group to the carboxyl group of D-Ala of another stem peptide via the pentaglycine linker is present. Mellroth and colleagues have observed binding of PGRP-LCx toward both polymeric Lys- and DAP-type PGs in vitro (*10*). The residue corresponding to Arg^{413}/x in PGRP-SA is a threonine. The absence of positively charged residues in PGRP-SA in this region is consistent with its preferred binding to Lys-type PG.

It has been shown that the disaccharide moiety and the 1,6-anhydro bond of MurNAc are required for the stimulatory activity (*3*, *5*). In the complex structure, the GlcNAc and MurNAc(anhydro) of TCT bridge together the LCa and LCx ectodomains (Fig. 4A). The formation of 1,6-anhydro bond in MurNAc creates a unique diozolane ring that makes van der Waals contacts with side chains of Leu^{362}/a, Arg^{401}/a, and Thr^{405}/a from LCa, where the folded Arg^{401} side chain is stabilized by hydrogen bonding to Gln^{364}/a and to ring O5 of MurNAc(anhydro) (Fig. 4A). In addition, the 3-OH of GlcNAc pyranose and 2-acetamide NH make hydrogen bonds to the side chain of Glu^{409}/a, and to Gln^{364}/a and Thr^{405}/a via a water molecule. Several residues from the LCx ectodomain also form part of the LCa interaction surface (Figs. 2B and 4A). Notably, side chains of Phe^{387}/x and Trp^{392}/x from H2 helix make hydrophobic contacts with three leucine residues from LCa (Leu^{362}/a, Leu^{398}/a,

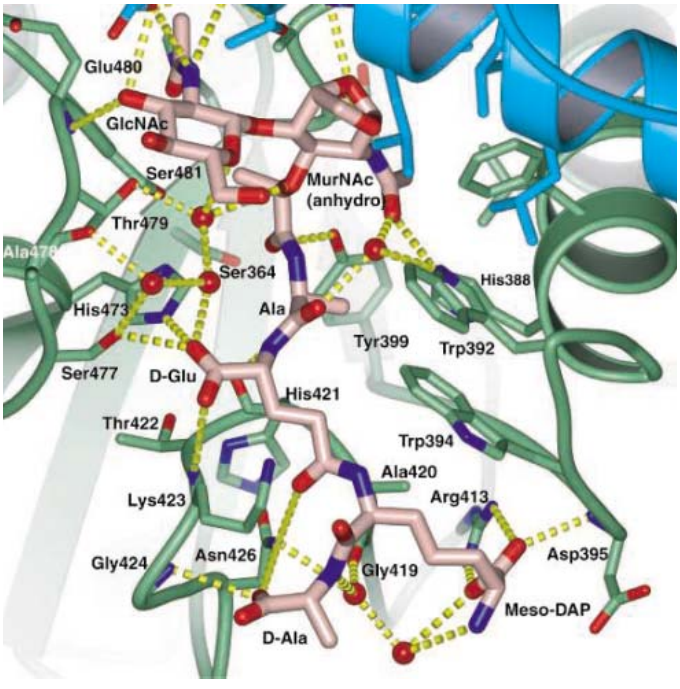

Fig. 3. Interaction of TCT with the PG-docking groove in the LCx ectodomain. TCT is shown as pink sticks, and the LCx ectodomain is in ribbon representation with side chains of the TCT-interacting residues shown as green sticks. Hydrogen-bonding interactions are shown in yellow and listed in table S2. Water molecules are shown as red spheres.

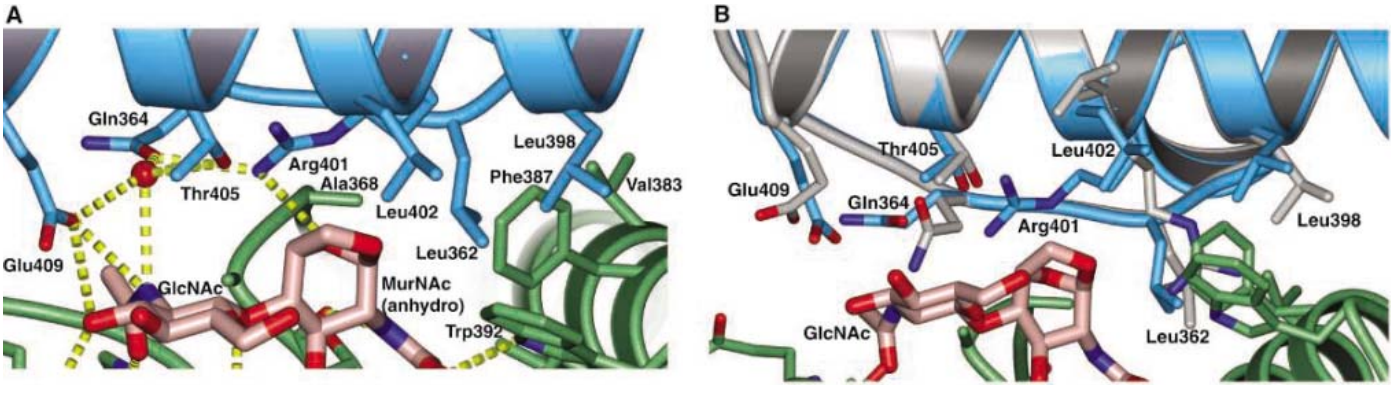

Fig. 4. The LCa ectodomain interface for GlcNAc-MurNAc(anhydro) moiety of TCT and the LCx ectodomain. (**A**) Interaction of the disaccharide moiety presented by the LCx ectodomain (green) with the LCa ectodomain (blue). (**B**) Superposition of the interface residues in the complexed (blue) and uncomplexed (gray; PDB code 1Z6I) LCa ectodomains showing induced-fit conformational change of the side chains shown as sticks.

and Leu^{402}/a). Moreover, the side chain of Leu^{362}/a is buried within the hydrophobic cleft formed by MurNAc(anhydro) from TCT, and Ala^{368}/x, Val^{383}/x, and Phe^{387}/x (Fig. 4A). Most of the interface residues in LCa show an induced-fit conformational change (Fig. 4B). Likewise, the orientations of many side chains of the LCx interface residues may also be induced as a result of TCT docking. The indole ring of Trp^{392}/x is stacked against the indole ring of Trp^{394}/x, which in turn stacks against the elongated side chain of DAP (Fig. 3); the aromatic ring of Phe^{387}/x is in intimate van der Waals contact with MurNAc. Without bound TCT, both Phe^{387}/x and Trp^{392}/x would not have their side chains oriented properly for LCa interaction. This notion is favored by previous observation that a lactyl-tetrapeptide still retains some stimulatory activity despite the lack of a disaccharide moiety (*3*, *5*); presumably, the stem peptide alone can bind to the LCx docking groove and induce properly oriented Trp^{392}/x through stacking interactions to allow heterodimerization.

In conclusion, the structure of the LCa-TCT-LCx complex has revealed the molecular interaction between a naturally occurring PG subunit and its PRR complex. The complex structure shows that TCT binds to the docking groove of LCx primarily through its elongated stem peptide and that the bound TCT conformation, which allows its disaccharide GlcNAc-MurNAc(anhydro) to be presented for LCa interaction, is further stabilized by extensive hydrogen bonding. DAP, the specificity determinant of TCT, engages a key electrostatic interaction with Arg^{413}/x. Stacking interactions with the DAP side chain and the MurNAc ring induce proper orientations of side chains of Phe^{387}/x and Trp^{392}/x, which contribute part of the TCT-LCx interface for LCa binding by induced fit. The present complex structure represents the receptor activation step where a monomeric PG ligand brings PGRP-LCa and -LCx receptors together to allow cytoplasmic domains to interact for activation of the immune deficiency pathway. By contrast, activation of this pathway by polymeric PG only requires PGRP-LCx, which can be brought to close proximity by binding to adjacent muropeptide subunits (*9*, *10*). Protein-protein interaction induced by monomeric ligand as visualized by the present work is likely to serve as the general mechanism for pattern recognition for other PGRPs, such as PGRP-SA, that play a double role as both a PG sensor and a signaling molecule.

Note added in proof: During the revision of this paper, the structure of TCT bound to PGRP-LE was reported (*19*).

References and Notes

1. R. Medzhitov, C. A. Janeway Jr., *Cell* **91**, 295 (1997).
2. J. A. Hoffmann, *Nature* **426**, 33 (2003).
3. T. Kaneko *et al.*, *Immunity* **20**, 637 (2004).
4. F. Leulier *et al.*, *Nat. Immunol.* **4**, 478 (2003).
5. C. R. Stenbak *et al.*, *J. Immunol.* **173**, 7339 (2004).
6. T. Werner *et al.*, *Proc. Natl. Acad. Sci. U.S.A.* **97**, 13772 (2000).
7. D. Mengin-Lecreulx, B. Lemaitre, *J. Endotoxin Res.* **11**, 105 (2005).
8. W. E. Goldman, D. G. Klapper, J. B. Baseman, *Infect. Immun.* **36**, 782 (1982).
9. C. I. Chang *et al.*, *Proc. Natl. Acad. Sci. U.S.A.* **102**, 10279 (2005).
10. P. Mellroth *et al.*, *Proc. Natl. Acad. Sci. U.S.A.* **102**, 6455 (2005).
11. R. Guan *et al.*, *Proc. Natl. Acad. Sci. U.S.A.* **101**, 17168 (2004).
12. K. M. Choe, H. Lee, K. V. Anderson, *Proc. Natl. Acad. Sci. U.S.A.* **102**, 1122 (2005).
13. Materials and methods are available as supporting material on *Science* Online.
14. C. I. Chang *et al.*, *PLoS Biol.* **2**, E277 (2004).
15. R. Guan, Q. Wang, E. J. Sundberg, R. A. Mariuzza, *J. Mol. Biol.* **347**, 683 (2005).
16. J. B. Reiser, L. Teyton, I. A. Wilson, *J. Mol. Biol.* **340**, 909 (2004).
17. M. S. Kim, M. Byun, B. H. Oh, *Nat. Immunol.* **4**, 787 (2003).
18. C. Liu, E. Gelius, G. Liu, H. Steiner, R. Dziarski, *J. Biol. Chem.* **275**, 24490 (2000).
19. J. H. Lim *et al.*, *J. Biol. Chem.* 10.1074/jbc.M513030200 (20 January 2006).

20. We thank K. Ihara and S. Wakatsuki for sharing their beamtime for screening crystals at the Photon Factory, Japan, and for helpful advice and technical assistance. This work was supported by the Howard Hughes Medical Institute (to J.D.) and the Centre National de la Recherche Scientifique (to D.M.-L.). Coordinates and structural factors have been submitted to the Protein Data Bank (PDB) with accession number 2F2L.

Supporting Online Material

www.sciencemag.org/cgi/content/full/311/5768/1761/DC1
Materials and Methods
Tables S1 and S2
References

28 November 2005; accepted 21 February 2006
10.1126/science.1123056

The Effect of Oxygen on Biochemical Networks and the Evolution of Complex Life

Jason Raymond[1] and Daniel Segrè[1,2]

The evolution of oxygenic photosynthesis and ensuing oxygenation of Earth's atmosphere represent a major transition in the history of life. Although many organisms retreated to anoxic environments, others evolved to use oxygen as a high–potential redox couple while concomitantly mitigating its toxicity. To understand the changes in biochemistry and enzymology that accompanied adaptation to O_2, we integrated network analysis with information on enzyme evolution to infer how oxygen availability changed the architecture of metabolic networks. Our analysis revealed the existence of four discrete groups of networks of increasing complexity, with transitions between groups being contingent on the presence of key metabolites, including molecular oxygen, which was required for transition into the largest networks.

Because the myriad biochemical mechanisms that modern organisms possess for detoxifying reactive oxygen derivatives had yet to evolve (*1*), the introduction of O_2 into an anaerobic biosphere around 2.2 billion years ago must have represented a cataclysm in the history of life (*2*). Strong selection pressure on ancient microbes, such as the ancestors of modern cyanobacteria that were first responsible for producing O_2 via oxygenic photosynthesis, precipitated the development of novel enzymes and new pathways. These included adaptations that mediated the biotoxicity of O_2 derivatives, including superoxide and hydroxyl radicals, and countered the inherent O_2/redox sensitivity of many proteins, such as iron-sulfur cluster–containing electron shuttles (*3*). Recent evidence suggests that as molecular oxygen became integral to biochemical pathways, many enzymatic reactions central to anoxic metabolism were effectively replaced in aerobic organisms (*4*). The availability of molecular oxygen also made possible a highly exergonic respiratory chain based on O_2 as a terminal electron acceptor, an event that is widely held to have been closely coincident with, if not requisite for, the development of complex eukaryotic life (*5*, *6*) and for adaptation to electron acceptor–limited terrestrial environments. The evolution of cyanobacteria and the ensuing oxidation of Earth's atmosphere left distinct, though not entirely congruent, signatures in the geological record (*7*–*9*) and provide an opportunity to understand the evolution of biochemical pathways by integrating geological clues with metabolic network modeling and phylogenetic analysis. By comparing metabolic networks attainable under oxic and anoxic conditions, we have attempted to elucidate the global metabolic reorganization resulting from this major environmental shift.

Our primary goal was to determine what effect the presence or absence of common biomolecules such as O_2 has on the complexity—the overall structure, including size and connectivity—of

[1]Microbial Systems Division, Biosciences Directorate, Lawrence Livermore National Laboratory, Livermore, CA 94550, USA. [2]Bioinformatics Program, Department of Biology and Department of Biomedical Engineering, Boston University, Boston, MA 02215, USA.

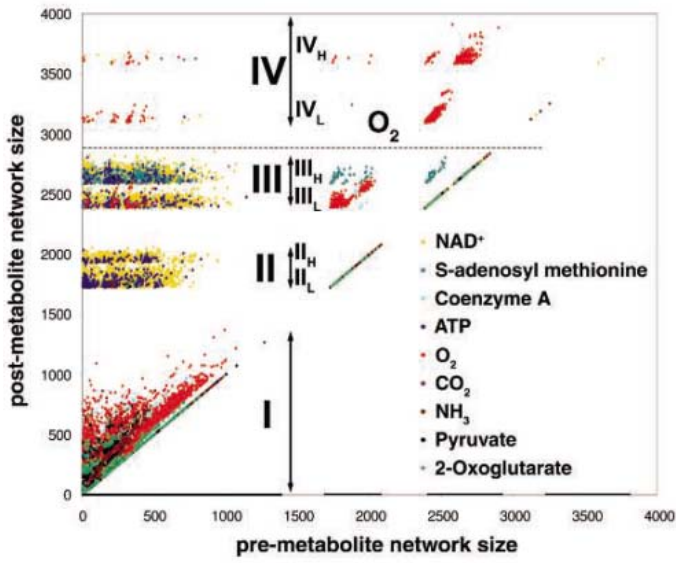

Fig. 1. The effect of various metabolites (legend at right) on the total number of reactions in ecosystem-level metabolic networks, as computed with the network expansion algorithm. Each point represents two consecutively generated networks: The first network, whose size is the abscissa value, is generated from a randomly chosen set of seed metabolites, and the second network, whose size is the ordinate value, is generated from that same seed set amended with the addition of one of the nine metabolites shown in the legend. Points are colored based on the amended metabolite, shown in the legend. All networks occupy four broadly similar groups (bold lines and roman numerals) and subgroups (H, higher; L, lower) that result from often very different but chemically interconvertible seed sets. Only networks that include O_2 as a metabolite are able to transition into group IV (dashed line), with other transitions being determined by the availability of key metabolites.

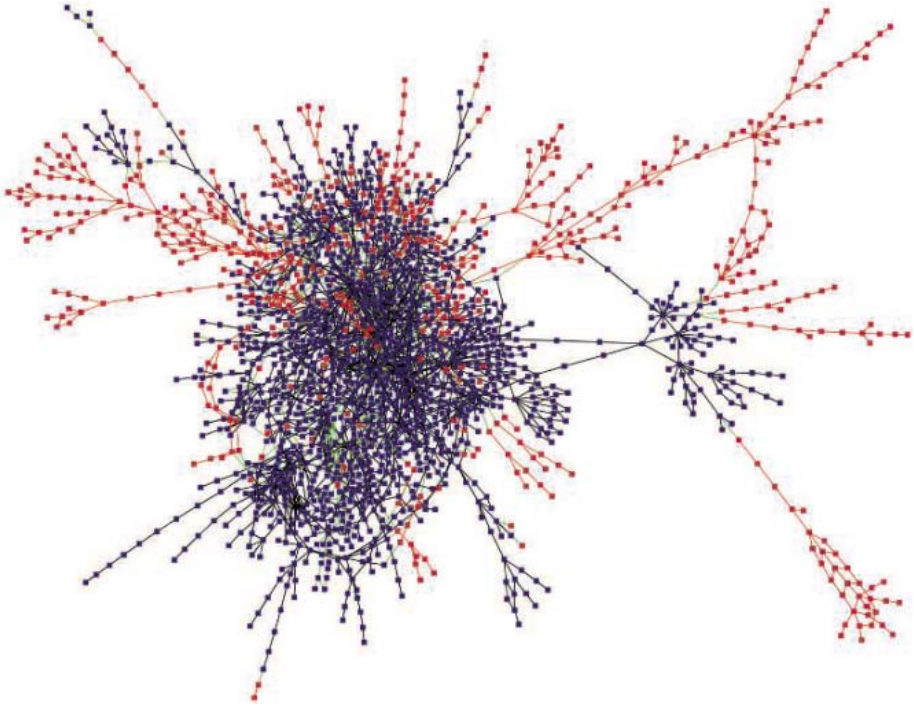

Fig. 2. The effect of oxygen on KEGG's metabolic "backbone" (pictured as a pruned version of the full network, with 1861 metabolites and 2652 possible reactions; see SOM for detailed description). Blue nodes and edges represent metabolites and reactions, respectively, that are present in anoxic metabolic networks. Red nodes and edges are oxic network metabolites and reactions whose presence is contingent on oxygen availability either directly or secondarily. Green edges correspond to reactions that are found only in the oxic network but use at least one anoxic metabolite, representing replacement or rewiring of anoxic pathways to take advantage of oxygen, as in thiamin and B_{12} biosynthesis.

metabolic networks. This process was carried out following a heuristic recently developed in detail by Ebenhöh *et al.* (*10*) and referred to as metabolic network expansion, whereby a set of pre-specified "seed" compounds are allowed to react according to enzymatic reaction rules, for example as enumerated by the KEGG (Kyoto Encyclopedia of Genes and Genomes) database (*11*). As implemented here, a reaction can occur only if all of its reactants are present in the seed set. Once all possible reactions have been carried out, the products of those reactions then join the seed compounds, potentially allowing new reactions to occur. This process is iterated until convergence: when no new products are generated and no new reactions are possible (*12*) (fig. S1). The network converged upon is thereby a product of the initial seed metabolites and the KEGG reactions that are allowed [all KEGG reactions were allowed here, although additional constraints can be added in the form of selection rules (*10*); for example, based on the phylogenetically inferred antiquity of enzymes].

Because the KEGG database is a collection of data from across known genomes, these metabolic networks correspond not to the reactions tenable within any one organism but to the metabolic potential of the collective (and currently characterized) biosphere that can be thought of as a meta-metabolome. The initial pool of seed metabolites was determined by two procedures: random sampling of metabolites by Monte Carlo (MC) simulations and deterministic selection from putatively prebiotic compounds [see the supporting online material (SOM) for detailed information]. The current KEGG database (*11*, *13*) encompasses 6836 reactions extending across 70 genomes and involving 5057 distinct compounds. O_2 is among the most-utilized compounds, superseding biomolecules such as adenosine triphosphate (ATP) and nicotinamide adenine dinucleotide (NAD^+) in rank (table S1). O_2 is further distinguished by the steep thermodynamic gradient favoring its reduction, resulting in oxygen being produced only by a single biological reaction: oxygenic photosynthesis. Although O_2 does occur as a by-product of some biological reactions, such as that of the enzyme catalase, those reactions depend ultimately on the presence of oxygen, so that they do not result in net O_2 generation. In contrast, based on current information about reaction reversibility, most compounds are produced in roughly the same number of reactions that they are consumed in ($r^2 = 0.926$, $P < 0.01$).

MC sampling of highly variable seed conditions and simulation of $\sim 10^5$ networks show that all resultant metabolic networks converge to just four discrete groups of increasing size and connectivity (Fig. 1). These four groups act as basins of attraction in network space, converged on from often completely different and limitless ($\sim 10^{16536}$ distinct seed sets) initial conditions, but sharing within each group >95% identical reactions and metabolites. Further, the networks in smaller groups are largely nested within those in larger groups; for example, most reactions and metabolites in group II networks are a subset of those in group III and IV networks. This coalescence of growing networks into distinct groups is consistent with models of hierarchical modularity in metabolic networks (*14*, *15*), a consequence of the asymmetric distribution of biomolecule con-

nectivity (some biomolecules are used in a disproportionately large number of reactions), the intrinsic reversibility and cyclic nature of many biochemical pathways, and gene duplication as a primary mechanism for expanding complexity (*16*) (see SOM for further discussion).

Networks simulated in the presence of molecular oxygen were able to transition into a group (Fig. 1, group IV) unreachable under any anoxic conditions explored by MC simulation. Networks in group IV had as many as 10^3 reactions more than those of the largest networks achieved in the absence of O_2. On average, 52% of these additional reactions do not explicitly use O_2, indicating the presence of pathways whose function is contingent on but does not require molecular oxygen. Among these O_2-dependent pathways are several steps associated with aerobic cobalamin synthesis, confirming that this approach successfully discovers pathway-level contingencies not detectable by previous analysis that focused on O_2-dependent enzymes as proxies for O_2-dependent pathways (*4*). Figure S2, A to F, indicates that the effect of oxygen on biochemical network expansion is robust to reaction database modifications, such as the characterization and addition of new reactions to KEGG (*17*).

Transitions between smaller groups, as well as the subsplitting of groups II to IV into "high" (H) and "low" (L) clusters (Fig. 1), are determined by the availability of biomolecules involved in the assimilation and cycling of key elements and whose essentiality may have manifested early in the evolution of metabolism (*17*, *18*). For example, sulfur-compound availability governs the splitting in each of the three larger groups (II to IV). Elemental sulfur is required in the synthesis of a broad range of compounds, such as the amino acids methionine and cysteine and, by way of cysteine, coenzyme A (CoA). In turn, CoA is essential to organisms across all three domains of life, most notably in central carbon cycling and in biosynthesis and metabolism involving a diverse range of lipids. Including sulfur in seed networks, by way of a highly utilized "hub" compound such as sulfide or cysteine, allows group II and group III_L networks to transition into group III_H, as well as the group $IV_L \rightarrow IV_H$ transition in oxic networks. Other highly connected compounds, particularly those central to cycling fundamental elements such as carbon, nitrogen, and phosphorus, appear to be responsible for the discrete clusters of network sizes, as shown for example in Fig. 1 and as recently elucidated by Ebenhöh *et al*. (*19*).

Genomic information provides insight into how biomolecule availability and use shape enzyme content in diverse organisms. To this end, two representative networks were seeded with or without O_2 (oxic and anoxic networks, respectively), along with a putatively prebiotic set of metabolites, including NH_3, H_2S, CO_2, and the cofactors pyridoxal phosphate, ATP/ADP, tetrahydrofuran (THF), and NAD^+/H. The expanded anoxic network (Fig. 2, blue links) encompassed 2162 distinct reactions involving 1672 metabolites, analogous to a group III network. The detection of homologs in complete genomes allowed recovery of the distribution of enzymes catalyzing these 1672 reactions in 44 prokaryotic and eukaryotic genomes. Clustering organisms by shared patterns of enzyme distribution (Fig. 3A) reveals an overall pattern consistent with ribosomal RNA (rRNA)– and genome-based phylogenies.

The oxic network resulted in a very different topology and enzyme distribution (Figs. 2 and 3B), spanning 3283 total reactions with 2317 metabolites, which is consistent with a group IV network. A common core of reactions was shared with the anoxic set, and this core was subtracted out to reveal novel and augmented pathways, which occur largely at the periphery of the network (Fig. 2, red, and table S2). A total of 747 reactions and 645 metabolites comprised pathways specific to the oxic network, whereas 273 metabolites were present in both networks but had an augmented set of reactions with O_2 available (Fig. 2, green). These 273 augmented reactions are an extension of those highlighted by (*8*) as plausible convergent enzyme replacements: enzymes in anaerobic organisms whose role has been supplanted or replaced by O_2-dependent enzymes in aerobes. Of the 747 oxic network reactions, only 359 explicitly used molecular oxygen, confirming that metabolic expansion is not simply a result of the invention of O_2-dependent enzymes but involves the development of novel pathways, such as those shown in table S2 and the multistep pathways in red in Fig. 2. Although the total number of reactions and metabolites increased by 1.5-fold in the oxic network, the density of the network increased only slightly, exemplified by a decrease in path length between any two metabolites from 4.55 to 4.22 in the anoxic and oxic networks, respectively. This suggests that although some pathway "rewiring" indeed occurred after O_2 became available, the most prolific change was in the evolution of new reactions and pathways, making available an entirely new set of metabolites. "Clickable" representations of Fig. 2 and oxic/anoxic reaction databases are available online at http://prelude.bu.edu/O2/.

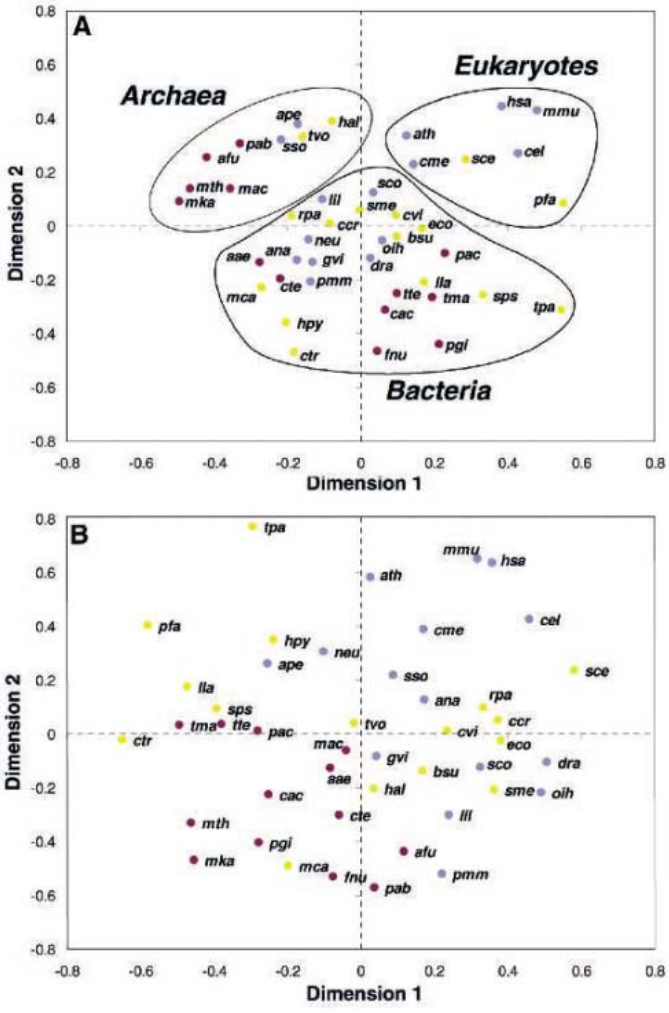

Fig. 3. (**A**) Similarity in anoxic network enzyme distribution in 44 different genomes, fit to two dimensions (see SOM) and broadly consistent with rRNA- and genome-based phylogenies. Blue points are obligate aerobes, yellow points are facultative aerobes that also have anaerobic modes of growth, and maroon points are strict anaerobes. Organism abbreviations are given in Fig. 4. (**B**) Similarity in oxic network enzyme distribution in 44 different genomes, largely inconsistent with organismal phylogeny but, as illustrated, following a trend consistent with an aerobic versus anaerobic growth mode (see also Fig. 4). Axes are in arbitrary units, with closely spaced points representing genomes with greater similarities in enzyme content.

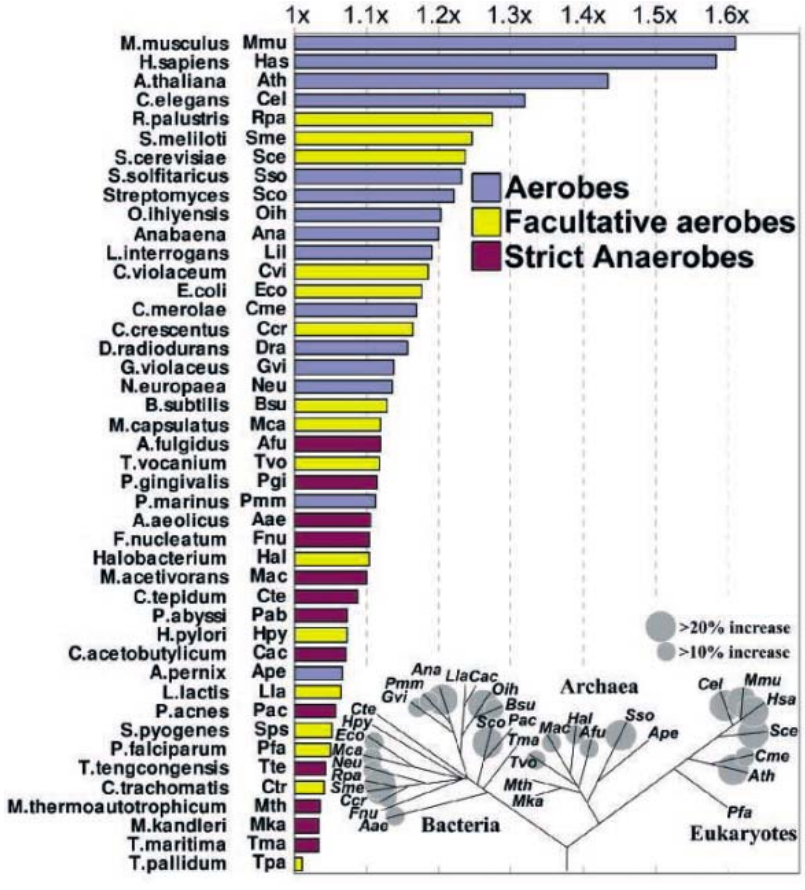

Fig. 4. Increase in total number of reactions catalyzed by individual genomes after the inclusion of O_2 in a network originally seeded with N_2, H_2S, CO_2, and the cofactors pyridoxal phosphate, ATP/ADP, THF, and NAD^+/H. Horizontal bars represent the percent increase in oxic versus anoxic network size on a genome-by-genome basis, colored according to the growth mode of the organism (colors are consistent with those in Fig. 3). The inset superimposes this data on a species tree for these organisms, showing that adaptation to O_2 has occurred throughout the tree of life. Also shown are the three-letter KEGG binomen abbreviations used in the inset and in Fig. 3. Enzymes specific to the oxic network expansion observed in strict anaerobes are detailed in SOM and table S3.

By performing a multidimensional scaling analysis of enzyme distribution across different organisms (see fig. S4 for the procedure), we found that the distributions of enzymes catalyzing oxic networks were similar only for closely related organisms, which is inconsistent with the tree of life (Fig. 4, inset) and with the distribution of anoxic enzymes (Fig. 3B). Despite limited data from strict anaerobes, the underlying trend for most organisms is consistent with their preferred aerobic versus anaerobic lifestyle as opposed to taxonomic relationships (Figs. 3B and 4). For example, whereas the three-domain structure of the tree of life is clearly evident in Fig. 3A, aerobes such as the archaeon *Solfolobus solfitaricus* and the cyanobacterium *Anabaena* instead cluster with other aerobes, independent of taxonomic domain, in Fig. 3B. Oxic network expansion was most prolific in eukaryotes and aerobic prokaryotes (Fig. 4). Eukaryote-specific reactions make up roughly half of the oxic network—versus 21% of the anoxic network—and among these expanded pathways are examples important and in some cases specific to plants and metazoans, such as steroid and alkaloid biosynthesis (table S2).

The fact that enzyme distribution in aerobic pathways was largely incongruent with organismal speciation suggests that adaptation to molecular oxygen occurred after the major prokaryotic divergences on the tree of life. This is supported by data from geological and molecular evolutionary analyses, showing that all three domains of life, and many phyla within these domains, had appeared by the time that oxygen became widely available (*20*–*22*). The relatively late onset of atmospheric oxidation argues against the invention of O_2-dependent enzymes or pathways in the last common ancestor of modern organisms, suggesting that adaptation to molecular oxygen took place independently in organisms from diverse lineages exposed to O_2. Our data support the idea that O_2 availability is coupled to an increase in network complexity beyond that reachable by any anoxic network, and they highlight enzymes and pathways that might have been important in the adaptation to an oxic atmosphere and the subsequent development of multicellular life. Whether this enabled the concurrent increase in biological complexity evident in the geological record, or simply was a result of subsequent adaptation and evolution among new classes of aerobes, is of considerable interest but remains to be determined.

References and Notes

1. J. L. Kirschvink *et al.*, *Proc. Natl. Acad. Sci. U.S.A.* **97**, 1400 (2000).
2. A. H. Knoll, *Geobiology* **1**, 3 (2003).
3. D. C. Rees, J. B. Howard, *Science* **300**, 929 (2003).
4. J. Raymond, R. E. Blankenship, *Geobiology* **2**, 199 (2004).
5. G. C. Dismukes *et al.*, *Proc. Natl. Acad. Sci. U.S.A.* **98**, 2170 (2001).
6. D. J. Des Marais, *Science* **289**, 1703 (2000).
7. R. Rye, H. D. Holland, *Am. J. Sci.* **298**, 621 (1998).
8. R. E. Summons, L. L. Jahnke, J. M. Hope, G. A. Logan, *Nature* **400**, 554 (1999).
9. J. Farquhar, H. Bao, M. Thiemens, *Science* **289**, 756 (2000).
10. O. Ebenhoh, T. Hendorf, R. Heinrich, *Genome Informatics* **15**, 35 (2004).
11. M. Kanehisa, S. Goto, *Nucleic Acids Res.* **28**, 27 (2000).
12. Briefly, the heuristic can be expressed as (i) specify or randomly choose seed metabolites, (ii) allow metabolites to react according to KEGG reactions, and (iii) incorporate newly synthesized metabolites into seed set. Steps ii and iii are then iterated until convergence, when no further new reactions are possible.
13. During manuscript review and revision, an updated KEGG database (release 37, available 4 January 2006) became available. Results from this latest release are consistent with our findings and are presented along with the SOM.
14. D. Segre, A. Deluna, G. M. Church, R. Kishony, *Nat. Genet.* **37**, 77 (2005).
15. E. Ravasz, A. L. Somera, D. A. Mongru, Z. N. Oltvai, A. L. Barabasi, *Science* **297**, 1551 (2002).
16. R. Pastor-Satorras, E. Smith, R. V. Sole, *J. Theor. Biol.* **222**, 199 (2003).
17. T. Handorf, O. Ebenhoh, R. Heinrich, *J. Mol. Evol.* **61**, 498 (2005).
18. H. Morowitz, *Complexity* **4**, 39 (1999).
19. O. Ebenhoh, T. Handorf, R. Heinrich, *Genome Inform. Ser. Workshop Genome Inform.* **16**, 203 (2005).
20. J. Xiong, W. M. Fischer, K. Inoue, M. Nakahara, C. E. Bauer, *Science* **289**, 1724 (2000).
21. J. J. Brocks, G. A. Logan, R. Buick, R. E. Summons, *Science* **285**, 1033 (1999).
22. J. M. Hayes, *Global Methanotrophy at the Archean-Proterozoic Transition, Early Life on Earth, Nobel Symposium No. 84*, S. Bengtson, Ed. (Columbia Univ. Press, New York, 1994).

23. We thank R. Blankenship and E. Branscomb for critical review and fruitful discussions. J.R. acknowledges support through the E. O. Lawrence Fellowship at Lawrence Livermore National Laboratory (LLNL). D.S. is supported at LLNL as a Faculty Scholar. This work was performed under the auspices of the U.S. Department of Energy at LLNL, contract no. W-7405-ENG-48.

Supporting Online Material

www.sciencemag.org/cgi/content/full/311/5768/1764/DC1
SOM Text
Figs. S1 to S4
Tables S1 to S3
References

4 August 2005; accepted 1 February 2006
10.1126/science.1118439

Genomic Islands and the Ecology and Evolution of *Prochlorococcus*

Maureen L. Coleman,[1] Matthew B. Sullivan,[1] Adam C. Martiny,[1] Claudia Steglich,[1]* Kerrie Barry,[2] Edward F. DeLong,[1] Sallie W. Chisholm[1]†

Prochlorococcus ecotypes are a useful system for exploring the origin and function of diversity among closely related microbes. The genetic variability between phenotypically distinct strains that differ by less that 1% in 16*S* ribosomal RNA sequences occurs mostly in genomic islands. Island genes appear to have been acquired in part by phage-mediated lateral gene transfer, and some are differentially expressed under light and nutrient stress. Furthermore, genome fragments directly recovered from ocean ecosystems indicate that these islands are variable among co-occurring *Prochlorococcus* cells. Genomic islands in this free-living photoautotroph share features with pathogenicity islands of parasitic bacteria, suggesting a general mechanism for niche differentiation in microbial species.

Closely related bacterial isolates often contain remarkable genomic diversity (*1*, *2*). Although its functional consequences have been described in a few model heterotrophic microbes (*3*), little is known about genomic microdiversity in the microbial phototrophs that dominate aquatic ecosystems. The marine cyanobacterium *Prochlorococcus* offers a useful system for studying this issue, because they are globally abundant, have very simple growth requirements, have a very compact genome [1.7 to 2.4 megabases (Mb)], and live in a well-mixed habitat. Although the latter appears to offer few opportunities for niche differentiation, *Prochlorococcus* populations consist of multiple coexisting ecotypes (*4*), whose relative abundances vary markedly along gradients of light, temperature, and nutrients (*5*–*9*). Even two high-light adapted (HL) ecotypes, whose type strains (MED4 and MIT9312) differ by only 0.8% in 16*S* ribosomal RNA (rRNA) sequence, have substantially different distributions in the wild (*5*–*9*).

Although whole-genome comparisons between the most distantly related *Prochlorococcus* isolates (97.9% 16*S* rRNA identity) have revealed the gross signatures of this niche differentiation (*10*), important insights into the evolution of diversity in this group likely lie in comparisons between very closely related strains, and between coexisting genomes from wild populations. Thus, we compared the complete genomes of the type strains, MED4 and MIT9312, that represent the two HL clades, and we analyzed genome fragments from wild cells belonging to these clades from the Atlantic and Pacific oceans.

The 1574 shared genes of MED4 and MIT9312 have conserved order and orientation, except for a large inversion around the replication terminus (Fig. 1). The average G + C content is similar in both genomes (31%), and the median sequence identity of the shared genes is 78%, surprisingly low for strains so similar at the rRNA locus (*11*). For most genes, synonymous sites are saturated and protein sequence identity is low (median 80%); this is likely a function of high mutation rates, given that HL *Prochlorococcus* lack several important DNA-repair enzymes (*10*, *12*).

The strain-specific genes between MED4 and MIT9312 (236 in MIT9312 and 139 in MED4) occur primarily (80 and 74%, respectively) in five major islands (Fig. 1). Thus, these genomes have a mosaic structure similar to that of *Escherichia coli* genomes (*1*), though on a smaller scale. The islands are located in the same position in both genomes, implying that they are hotspots for recombination, and the length of island genes is similar to the whole-genome average, suggesting that they are not degraded. We hypothesize that these islands arose via lateral gene transfer and continually undergo rearrangement, on the basis of a number of characteristics. First, three islands are associated with tRNA genes (fig. S1), which are common integration sites for mobile elements (*13*). Second, the 3′ end of tRNA-proline, which flanks ISL3 in both genomes, is repeated 13 times in MIT9312-ISL3 (Fig. 2A) and three times in MED4-ISL3 (fig. S2), suggesting repeated remodeling of this island. Third, some of the genes found in a particular island in MED4 are found in a different island in MIT9312 (Fig. 1), a rearrangement that may have been mediated by a 48–base pair sequence element we call PRE1 (*Prochlorococcus* repeat element 1; fig. S3); portions of PRE1 are repeated, almost exclusively in islands, 13 times in MED4 (fig. S2), and 9 times in MIT9312 (Fig. 2A). Finally, up to 80% of the genes in any given MIT9312 island are most similar to the genes of noncyanobacterial organisms including phage, Eukarya, and Archaea, consistent with the recent observation that horizontally acquired genomic islands reflect a gene pool that differs from that of the core genome (*14*).

It is likely that phage, which often carry host genes (*15*, *16*), mediate some of the island-associated lateral gene transfer, and the *hli* gene family in particular appears to have undergone repeated phage-host gene exchange (*16*). Of the 24 *hli* genes in MIT9312, 18 are found in the five major islands or their flanking regions. All 18 belong to the multicopy and sporadically distributed group that includes phage copies (Fig. 2A) and is well differentiated from widespread single-copy *hli* genes found in cyanobacteria (*16*). Other phagelike genes in islands include an integrase, DNA methylases, a second *phoH*, a MarR-family transcriptional regulator, a putative hemagglutinin neuraminidase, and an endonuclease (*15*), further supporting a link between phage and island dynamics.

Many island genes in the two strains appear to encode functions related to physiological stress and nutrient uptake and thus may be important in the high-light, low-nutrient surface waters dominated by HL *Prochlorococcus*. ISL2 and ISL5 in MIT9312, for example, encode 12 of the 24 *hli* genes, known to be important under a variety of stress conditions (*17*); they also encode two outer-membrane transport

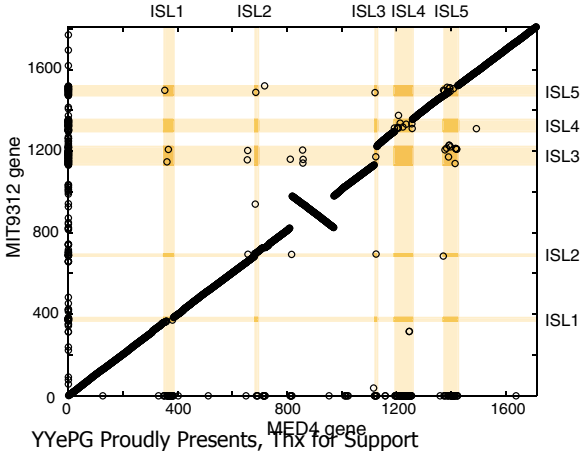

Fig. 1. Whole-genome alignment showing the positions of orthologous genes in MED4 and MIT9312. Strain-specific genes appear on the axes. The locations of five major islands defined by whole-genome alignment (*25*) are shaded.

[1]Massachusetts Institute of Technology, Department of Civil and Environmental Engineering, 15 Vassar Street, Cambridge, MA 02139, USA. [2]U.S. Department of Energy Joint Genome Institute, Production Genomics Facility, Walnut Creek, CA 94598, USA.

*Present address: University Freiburg, Department of Biology II/Experimental Bioinformatics, Schänzlestrasse 1, D-79104 Freiburg, Germany.

†To whom correspondence should be addressed. E-mail: chisholm@mit.edu

proteins; and a cyanophage-like homolog of *phoH* thought to be involved in the phosphate stress response (*15*). ISL3 in this strain contains a paralog of *psbF*, which encodes part of cytochrome b559, thought to protect against photoinhibition (*18*). Islands also contain genes involved in nutrient assimilation, including a cyanate transporter and lyase in MED4 and two transporters, for manganese/iron and amino acids, in MIT9312 (fig. S1).

In addition to genes involved in potentially growth-limiting processes, islands also contain genes that could play a role in selective mortality. ISL4 in both MED4 and MIT9312 encodes proteins involved in cell surface modification, including biosynthesis of lipopolysaccharide, a common phage receptor (*19*) (fig. S1). Phages are important agents of mortality in the oceans (*20*), and thus cell surface properties are likely under strong selection.

Clearly, for island genes to influence a cell's fitness, they must be expressed. When MED4 cells are starved for phosphorus, nine ISL5 genes are differentially expressed, nearly all of unknown function (table S1). When cells are shifted to high light, 38 island genes are differentially expressed, including seven *hli* genes (table S1) that in *Synechocystis* encode proteins that accumulate when cells absorb excess excitation energy (e.g., under high light, nutrient limitation, and low temperatures) (*17*). Thus, 26% of all MED4 island genes are differentially expressed under P starvation or high-light stress; only one of these is differentially expressed under both conditions (conserved hypothetical gene PMM1416), suggesting that island genes contribute to specific stress responses.

The genome variation within the eMIT9312 clade [sensu (*7*)] was examined in wild populations of *Prochlorococcus* by aligning short genome fragments from the Sargasso Sea (*21*), where this clade dominates (*7*), against the MIT9312 genome (Fig. 2B). Nearly constant coverage was observed, confirming a stable core genome, except for notable gaps at ISL1, ISL3, and ISL4. This finding indicates that very few wild sequences match genes in these islands, and it supports the hypothesis that these regions are hypervariable in HL *Prochlorococcus* genomes. In contrast, genes belonging to ISL2 and ISL5 are relatively well represented in the Sargasso Sea data set (Fig. 2B, fig. S2). In MED4 and MIT9312, these islands contain about half of the *hli* genes, lack the tRNA genes implicated in integration of mobile elements, and contain a smaller fraction of noncyanobacterial genes than do the other islands. This finding suggests that the genes in these islands have become fixed in this wild population.

Examination of 36 large genome fragments (1.1 Mb total sequence; median size 34 kb) (table S2) from the Hawaii Ocean Time-Series Station (*22*) further confirms that a stable core genome surrounds islands of variability, because most fragments showed remarkable conservation of gene content and order with respect to the MED4 and MIT9312 genomes. Thirty-four of the 36 fragments were more similar to MIT9312 than to MED4; two contained rRNA operons, confirming their phylogenetic affiliation with the eMIT9312 clade (fig. S4). The eMIT9312 fragments have about 90% identity with the MIT9312 genome and about 80% with MED4 (Table 1). Collectively, these results suggest that the wild eMIT9312 population is a coherent group identifiable by sequence similarity in the absence of an rRNA operon (*11*). eMIT9312 genome fragments from this wild population are more similar to each other than to the genome of the type strain MIT9312 (isolated from the Atlantic Ocean), but still share only 93% average sequence identity (Table 1), indicating high coexisting diversity in core genes.

Five eMIT9312 genome fragments from the Hawaii sample border the major islands defined above. About 60% of the genes in these islands have no ortholog in either MED4 or MIT9312, and two fragments border ISL1, yet their gene content is largely different from each other and from the MIT9312 and MED4 genomes (fig. S5). Indeed, a third of the island genes in these two fragments are novel, i.e., have no detectable homologs, implying that cells have access to a large novel gene pool in the oceans (*14*). Like the islands in the MED4 and MIT9312 genomes, these two fragments contain signatures of mobility, including duplicated tRNA genes, copies of the repeat PRE1, and an integrase gene. This reveals that islands are dynamic even within a single ecotype clade as we have defined it.

One observation that stimulated this work is the dramatic difference in distribution and abundance of the two HL *Prochlorococcus* ecotype clusters (*5*–*9*), as defined by their rRNA internal transcribed spacer (ITS) sequence similarity. Although strains belonging to these two clusters have different island gene content, so do cells from field populations that belong to a single cluster. Therefore, other genomic features are likely to be important in explaining niche differentiation between eMED4 and eMIT9312 cells in the wild. Differential temperature adaptation, for example, which is thought to be an important determinant of ecotype distribu-

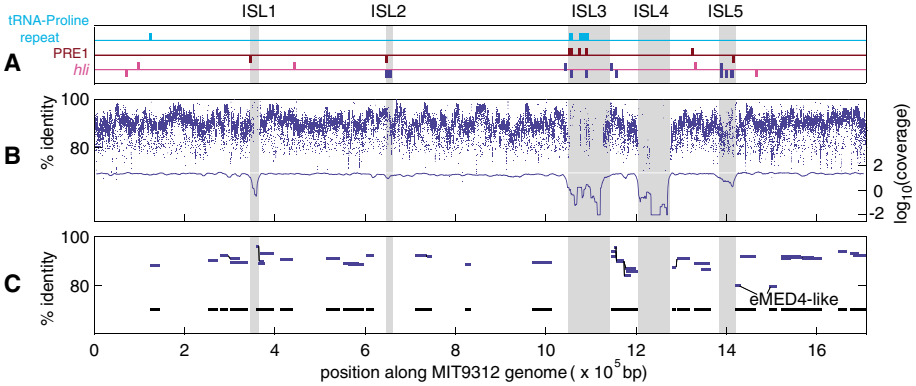

Fig. 2. Features of genomic islands (shaded) in the *Prochlorococcus* strain MIT9312 genome compared with wild sequences from the Atlantic and Pacific Oceans. (**A**) Locations of repetitive elements and *hli* genes in MIT9312, shown above or below the horizontal line for the forward or reverse strand, respectively. *hli* genes shown in pink belong to the single-copy conserved group and those shown in blue belong to the multicopy phage-encoded group (*16*). (**B**) Percent identity of Sargasso Sea shotgun database sequences (*21*) aligned to MIT9312 (top, left axis) and average coverage in the database of a given position in the MIT9312 genome (bottom, right axis). Log_{10}(coverage) is set to −2 when coverage equals 0. (**C**) Genomic locations and percent identity of wild genome fragments (eMIT9312-like unless noted) aligned to MIT9312. Where the alignment is interrupted, a black line connects aligned segments of a single fragment. Fragments are projected down to 70% horizontal to visualize total coverage.

Table 1. Median pairwise percent identities, for all orthologous gene pairs and for large aligned regions >4 kb (*25*). Numbers in parentheses indicate the number of orthologous gene pairs from which the median was calculated.

	MED4-MIT9312	MED4-eMIT9312 fragments	MIT9312-eMIT9312 fragments	Overlapping fragments
Orthologs (nucleotides)	78.4 (1574)	79.5 (1063)	90.6 (1092)	93.2 (434)
Orthologs (amino acids)	80.0 (1574)	82.4 (1063)	92.9 (1092)	95.2 (434)
Large aligned regions	79.0	79.9	90.7	92.6

tions (*5*), can be achieved through sequence (*23*) or regulatory (*24*) changes in the core genome. Nonetheless, given their prevalence, mobility, and expression under relevant conditions, islands likely play a role in adaptation, but on shorter time scales, or more local spatial scales, in the context of large populations that harbor substantial genomic variability.

Thus, although streamlined for life in the oligotrophic oceans, the genomes of HL *Prochlorococcus* are not static. Cell-to-cell genome variability is concentrated in islands containing genes that are differentially expressed under stresses typical of oceanic environments. Just as pathogenicity islands alter the host specificity and virulence of pathogenic bacteria (*3*), genomic islands in *Prochlorococcus* may contribute to niche differentiation in the surface oceans. Although other factors, such as small insertions and deletions, substitutions in homologous proteins, and differential regulation are important contributors to diversity, the prevalence of genomic islands and their features argue that these also play an influential role. We postulate that lateral gene transfer in genomic islands is an important mechanism for local specialization in the oceans. If true, genomic islands of natural taxa should contain genes that are ecologically important in a given environment, regardless of the core genome phylogeny. Testing this hypothesis will not only advance our understanding of microbial diversity in the ocean, but also contribute to a unified understanding of genomic evolutionary mechanisms and their impact on microbial ecology.

References and Notes

1. R. A. Welch *et al.*, *Proc. Natl. Acad. Sci. U.S.A.* **99**, 17020 (2002).
2. J. R. Thompson *et al.*, *Science* **307**, 1311 (2005).
3. J. Hacker, J. B. Kaper, *Annu. Rev. Microbiol.* **54**, 641 (2000).
4. L. R. Moore, G. Rocap, S. W. Chisholm, *Nature* **393**, 464 (1998).
5. Z. I. Johnson *et al.*, *Science* **311**, 1737 (2006).
6. E. R. Zinser *et al.*, *Appl. Environ. Microbiol.* **72**, 723 (2006).
7. N. Ahlgren, G. Rocap, S. W. Chisholm, *Environ. Microbiol.* **8**, 441 (2006).
8. N. J. West, D. J. Scanlan, *Appl. Environ. Microbiol.* **65**, 2585 (1999).
9. N. J. West *et al.*, *Microbiology* **147**, 1731 (2001).
10. G. Rocap *et al.*, *Nature* **424**, 1042 (2003).
11. K. T. Konstantinidis, J. M. Tiedje, *Proc. Natl. Acad. Sci. U.S.A.* **102**, 2567 (2005).
12. A. Dufresne, L. Garczarek, F. Partensky, *Genome Biol.* **6**, R14 (2005).
13. W. D. Reiter, P. Palm, S. Yeats, *Nucleic Acids Res.* **17**, 1907 (1989).
14. W. W. Hsiao *et al.*, *PLoS Genet.* **1**, e62 (2005).
15. M. B. Sullivan, M. L. Coleman, P. Weigele, F. Rohwer, S. W. Chisholm, *PLoS Biol.* **3**, e144 (2005).
16. D. Lindell *et al.*, *Proc. Natl. Acad. Sci. U.S.A.* **101**, 11013 (2004).
17. Q. He, N. Dolganov, O. Bjorkman, A. R. Grossman, *J. Biol. Chem.* **276**, 306 (2001).
18. D. H. Stewart, G. W. Brudvig, *Biochim. Biophys. Acta* **1367**, 63 (1998).
19. A. Wright, M. McConnell, S. Kanegasaki, in *Virus Receptors*, L. L. Randall, L. Philipson, Eds. (Chapman and Hall, New York, 1980), pp. 27–57.
20. J. A. Fuhrman, *Nature* **399**, 541 (1999).
21. J. C. Venter *et al.*, *Science* **304**, 66 (2004).
22. E. F. DeLong *et al.*, *Science* **311**, 496 (2006).
23. G. N. Somero, *Annu. Rev. Physiol.* **57**, 43 (1995).
24. M. M. Riehle, A. F. Bennett, R. E. Lenski, A. D. Long, *Physiol. Genomics* **14**, 47 (2003).
25. Materials and methods are available as supporting material on *Science* Online.

26. We thank T. Rector, N. Hausman, and R. Steen for Affymetrix microarray processing; M. Polz for helpful discussions; and D. Lindell and A. Tolonen for comments on the manuscript. This work was supported by grants from NSF Biological Oceanography (S.W.C.) and Microbial Observatory (E.F.D.) Programs, the U.S. Department of Energy (DOE) GTL Program (to S.W.C. and G. Church), and the Gordon and Betty Moore Foundation (S.W.C. and E.F.D.). Sequencing support came from the DOE Microbial Genomics Program (E.F.D.) and DOE GTL and Community Sequencing Program (S.W.C.), conducted at the DOE Joint Genome Institute. Sequences are available in GenBank: BX548174 (MED4 genome), CP000111 (MIT9312 genome), and DQ366711 to DQ366746 (environmental genome fragments).

Supporting Online Material

www.sciencemag.org/cgi/content/full/311/5768/1768/DC1
Materials and Methods
Figs. S1 to S5
Tables S1 to S3
References

31 October 2005; accepted 17 February 2006
10.1126/science.1122050

Toll-Like Receptor Triggering of a Vitamin D–Mediated Human Antimicrobial Response

Philip T. Liu,[1,2]* Steffen Stenger,[4]* Huiying Li,[3] Linda Wenzel,[4] Belinda H. Tan,[1,2] Stephan R. Krutzik,[2] Maria Teresa Ochoa,[2] Jürgen Schauber,[5] Kent Wu,[1] Christoph Meinken,[4] Diane L. Kamen,[6] Manfred Wagner,[7] Robert Bals,[8] Andreas Steinmeyer,[9] Ulrich Zügel,[10] Richard L. Gallo,[5] David Eisenberg,[3] Martin Hewison,[11] Bruce W. Hollis,[12] John S. Adams,[11] Barry R. Bloom,[13] Robert L. Modlin[1,2]†

In innate immune responses, activation of Toll-like receptors (TLRs) triggers direct antimicrobial activity against intracellular bacteria, which in murine, but not human, monocytes and macrophages is mediated principally by nitric oxide. We report here that TLR activation of human macrophages up-regulated expression of the vitamin D receptor and the vitamin D-1–hydroxylase genes, leading to induction of the antimicrobial peptide cathelicidin and killing of intracellular *Mycobacterium tuberculosis*. We also observed that sera from African-American individuals, known to have increased susceptibility to tuberculosis, had low 25-hydroxyvitamin D and were inefficient in supporting cathelicidin messenger RNA induction. These data support a link between TLRs and vitamin D–mediated innate immunity and suggest that differences in ability of human populations to produce vitamin D may contribute to susceptibility to microbial infection.

The innate immune system provides a rapid host mechanism for defense against microbial pathogens. In *Drosophila*, innate immunity is mediated in part by the Toll family of pattern-recognition receptors, whose activation induces expression of a series of antimicrobial peptides (*1*). The mammalian TLR homologs, including the TLR2 and TLR1 heterodimer (*2*), similarly recognize a variety of microbial-derived ligands, including bacterial lipopeptides. Activation of TLRs results in a direct antimicrobial response in monocytes and macrophages in vitro. In mice, this activity is mediated principally through generation of nitric oxide (*3*, *4*). However, we found that TLR2/1-induced antimicrobial activity in human macrophages is not affected by inhibitors of nitric oxide or reactive oxygen intermediates (*5*), and the mechanism of human microbicidal activity remains unresolved.

In studies of resistance to *M. tuberculosis*, we observed that activation of TLR2/1 reduced the viability of intracellular *M. tuberculosis* in human monocytes and macrophages but not in monocyte-derived dendritic cells (DCs) [Fig. 1A and (*5*, *6*)]. Consequently, we used DNA microarrays to examine gene expression profiles of monocytes and DCs stimulated with a synthetic 19-kD *M. tuberculosis*–derived lipopeptide (TLR2/1L) or treated with medium (*6*). A two-way ANOVA was applied to the array data to identify genes differentially expressed in the two cell types after TLR2/1L treatment (*6*). Genes up-regulated in monocytes, but not in DCs, with significant P values [$P < 0.05$; the false discovery rate (FDR), which is the expected proportion of false rejections among all rejections, was 0.09] were cross-referenced against a list of genes associated with known antimicrobial function, yielding two candidates: vitamin D receptor (VDR) and S100A12, a calcium-binding proinflammatory molecule (*7*) (Fig. 1B). Although TLR2/1 stimulation of DCs up-regulated specific genes characteristic of activation (Fig. 1B), the selective up-regulation of the VDR gene in monocytes prompted us to examine further selected VDR-related genes. From these analyses,

Cyp27B1, the enzyme that catalyzes the conversion of inactive provitamin D_3 hormone [25-hydroxyvitamin D_3; $25(OH)D_3$] into the active form [1,25-dihydroxyvitamin D_3; $1,25(OH)_2D_3$], was observed to be significantly up-regulated at 12 and 24 hours (Fig. 1C). However, there was no evidence for mRNA up-regulation of other VDR downstream target genes, including cathelicidin antimicrobial peptide (CAMP) (a cathelicidin precursor), β-defensin 4 (DEFB4), and the $1,25(OH)_2D_3$-regulated VDR-specific Cyp24 hydroxylase gene (Fig. 1C) (*8*). Quantitative polymerase chain reaction (qPCR) confirmed the microarray data, demonstrating up-regulation of mRNAs for both VDR and Cyp27B1 in monocytes and macrophages, but not DCs (Fig. 1D) (*6*). However, again no observable up-regulation of cathelicidin, DEFB4, and Cyp24 mRNAs was seen in TLR2/1L-treated monocytes (Fig. 1E). Together, these data suggest that TLR induces up-regulation of the VDR and Cyp27B1 gene expression in monocytes and macrophages, but raise the question of its functional significance.

To determine the functional status of the VDR, $1,25(OH)_2D_3$ was added to primary human monocytes, and downstream target gene induction was assessed. Treatment led to the dose-dependent up-regulation of both cathelicidin and Cyp24 mRNA by qPCR, although the expression of DEFB4 remained unchanged (Fig. 2A). The induction of cathelicidin was also evident by intracellular flow cytometry and was found to be processed to its active peptide form (LL-37) by surface-enhanced laser desorption ionization–time of flight (SELDI-TOF) mass spectrometry (Fig. 2, B and C) (*6*). In monocytes infected with *Mycobacterium bovis* Bacille Calmette-Guérin–expressing green fluorescent protein (BCG-GFP), cathelicidin was observed to colocalize with the bacteria-containing vacuoles with $1,25(OH)_2D_3$ treatment, but not in untreated samples (Fig. 2D) (*6*). A direct antimicrobial effect of the cathelicidin peptide on *M. tuberculosis* could be demonstrated by both [^{3}H]uracil uptake and colony-forming unit (CFU) assay (Fig. 2E) (*6*). Addition of $1,25(OH)_2D_3$ to primary human macrophages infected with virulent *M. tuberculosis* reduced the number of viable bacilli (Fig. 2F), consistent with earlier studies performed with monocytic cell lines (*9*, *10*). Taken together, these data indicate that the VDR is functional in primary human monocytes and that its activation triggers induction of at least one known antimicrobial peptide, cathelicidin, capable of mediating antimicrobial activity.

Because the VDR is functional when exogenous $1,25(OH)_2D_3$ is added, we hypothesized that the TLR2/1 induction of Cyp27B1 and the conversion of $25(OH)D_3$ to $1,25(OH)_2D_3$ could represent key aspects of the TLR pathway. Monocytes were activated by TLR2/1L in medium containing fetal calf serum (FCS), in the presence and absence of $25(OH)D_3$. Although addition of either $25(OH)D_3$ or TLR2/1L alone had no effect, their simultaneous addition up-regulated cathelicidin and Cyp24 mRNA (Fig. 3A). In the viability assays, where exogenous $25(OH)D_3$ was not required for killing, the experiments were performed in human serum to facilitate uptake of bacteria. Only in the presence of human serum did the TLR2/1 stimulation up-regulate cathelicidin and Cyp24 mRNA without addition of exogenous $25(OH)D_3$ (Fig. 3B). We attribute this to the finding that the $25(OH)D_3$ levels in human serum were five times those in FCS (Fig. 3C), which suggests that culture of human cells in human serum may be critical for study of innate immune responses in humans (*6*).

Specific inhibition of Cyp27B1 blocked TLR2/1L activation of cathelicidin mRNA by 80% (Fig. 4A). Addition of a VDR antagonist inhibited induction of cathelicidin mRNA by greater than 80% (Fig. 4B), and the antimicrobial activity was reduced about 70% (Fig. 4C). Taken together, these data demonstrate that activation of TLRs on human monocytes triggers a microbicidal pathway that is dependent

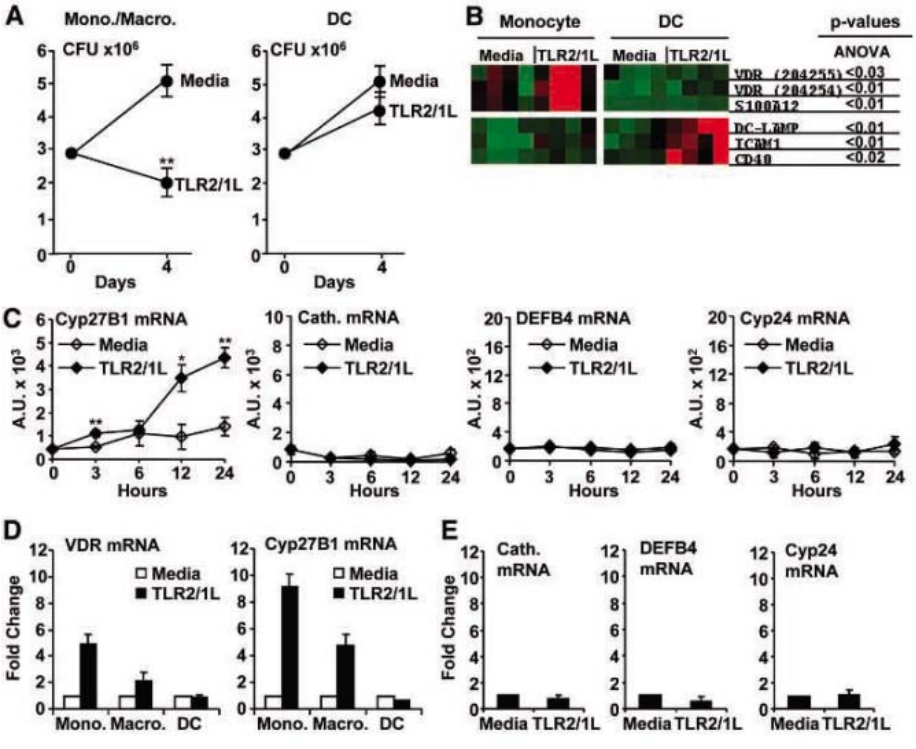

Fig. 1. Comparison of gene expression profiles in human primary monocytes and macrophages and DCs. (**A**) Antimicrobial activity of monocytes, macrophages, and DCs against intracellular *M. tuberculosis*. Infected cells were stimulated with a TLR2/1 ligand, and viable *M. tuberculosis* was assessed by CFU assay. Data shown are representative of 12 individual donors for both cell types. (**B**) Gene expression profile in TLR2/1-activated monocytes and DCs. Cells were obtained from four donors, stimulated with TLR2/1L for 12 hours, and their gene expression was profiled by gene microarrays. A two-way ANOVA was applied, and genes induced in monocytes and significantly different ($P < 0.05$) from DCs were cross-referenced against genes with known antimicrobial functions. The profile of genes known to be characteristic of DC function, DC-LAMP maturation marker, the intercellular cell adhesion molecule ICAM1, and CD40 were examined. (**C**) Time course of Cyp27B1, cathelicidin, DEFB4, and Cyp24 mRNA expression in TLR2/1L-activated monocytes. Cells from four donors were stimulated with either medium (◊) or TLR2/1L (♦) for 0, 3, 6, 12, or 24 hours, and the gene expression was profiled by using microarrays. Regulation of VDR and Cyp27B1 mRNA (**D**) and cathelicidin, DEFB4, and Cyp24 mRNA (**E**) in monocytes, macrophages, and DCs. Cells were treated with TLR2/1L at 24 hours, and gene expression was assessed by qPCR (mean fold change ± SEM, $n = 4$). $^*P \leq 0.05$, $^{**}P \leq 0.01$.

[1]Department of Microbiology, Immunology, and Molecular Genetics; [2]Division of Dermatology, Department of Medicine, David Geffen School of Medicine; [3]Department of Chemistry and Biological Chemistry, Howard Hughes Medical Institute; and Department of Energy Institute of Genomics and Proteomics, University of California at Los Angeles, Los Angeles, CA 90095, USA. [4]Institut für Klinische Mikrobiologie, Immunologie, und Hygiene, Universität Erlangen, D-91054 Erlangen, Germany. [5]Division of Dermatology, University of California at San Diego, and Veterans Affairs San Diego Healthcare Center, San Diego, CA 92161, USA. [6]Department of Medicine, Medical University of South Carolina (MUSC), Charleston, SC 29425, USA. [7]Klinikum Nürnberg, Medizinische Klinik 3, D-90340 Nürnberg, Germany. [8]Pneumologie, Universität Marburg, D-35043 Marburg, Germany. [9]Medicinal Chemistry, [10]Corporate Research Business Area (CRBA) Dermatology, Schering AG, D-13342 Berlin, Germany. [11]Department of Medicine, Division of Endocrinology, Cedars-Sinai Medical Center, Los Angeles, CA 90048, USA. [12]Departments of Pediatrics, Biochemistry, and Molecular Biology, MUSC, Charleston, SC 29425, USA. [13]Harvard School of Public Health, Boston, MA 02115, USA.

*These authors contributed equally to this work.
†To whom correspondence should be addressed. E-mail: rmodlin@mednet.ucla.edu

on both the endogenous production and action of $1,25(OH)_2D_3$ through the VDR.

These findings prompted us to address a problem that has long challenged the field, namely, differences in susceptibility of different ethnic populations to the disease. Because of skin melanin content and subsequent diminished ultraviolet (UV) light–dependent cutaneous vitamin D_3 synthetic capacity, African Americans have significantly decreased serum $25(OH)D_3$ levels (*11*) and are known to have increased susceptibility to *M. tuberculosis* infection (*12*), as well as more rapid and more severe course of disease (*13*). We observed that serum levels of $25(OH)D_3$ in African Americans were significantly lower than in a Caucasian cohort (Fig. 4D). Strikingly, when these serum samples were used to support TLR2/1 activation, the induction of cathelicidin mRNA was significantly lower in the presence of serum from African American than the Caucasian individuals [Fig. 4E and (*14*) (correlation coefficient $25(OH)D_3$ versus cathelicidin mRNA = 0.63; $P < 0.001$)]. Finally, supplementation of the African American serum with

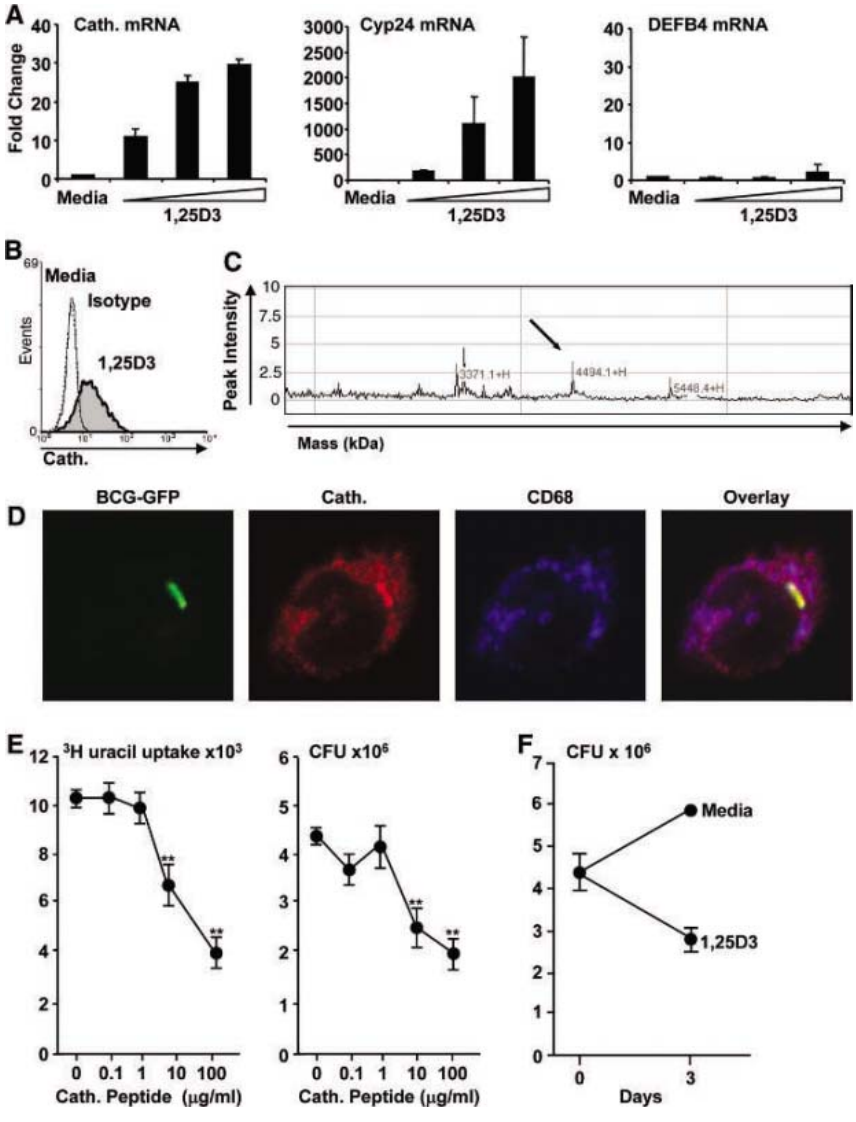

Fig. 2. Monocyte response to $1,25(OH)_2D_3$ (1,25D3). (**A**) Regulation of VDR downstream genes cathelicidin, Cyp24, and DEFB4 mRNA on stimulation with $1,25(OH)_2D_3$ (mean fold change ± SEM, $n = 4$). (**B**) Detection of cathelicidin in monocytes by intracellular flow cytometry. Monocytes were stimulated with either control (solid line) or $1,25(OH)_2D_3$ (gray shaded area). Isotype control is represented by the dashed line. Data shown are representative of four separate experiments. (**C**) Detection of cathelicidin-derived peptides in monocytes by SELDI-TOF. In three separate experiments, SELDI-TOF analysis of monocyte cell pellets detected a peak around 4.5 kD consistently, as indicated by the arrow, corresponding to the cathelicidin peptide (LL-37). (**D**) Colocalization of mycobacteria and cathelicidin. Monocytes were infected with BCG-GFP (green) then stimulated with $1,25(OH)_2D_3$ and labeled using a monoclonal antibody specific for cathelicidin (red). CD68 is used as a marker for monocytes (blue). Data shown are representative of three separate experiments. (**E**) *M. tuberculosis* viability following incubation with recombinant cathelicidin peptide. Experiments were performed at various concentrations of cathelicidin peptide incubated with bacteria for 3 days. The bacterial viability was measured by both [^{3}H]uracil uptake [mean counts per minute ± SEM, $n = 3$] and CFU assay (mean CFU ± SEM, $n = 3$). (**F**) Antimicrobial activity of alveolar macrophages following $1,25(OH)_2D_3$ stimulation. Cells were infected with *M. tuberculosis* and stimulated with $1,25(OH)_2D_3$. The number of viable *M. tuberculosis* bacteria was assessed by CFU assay. Data shown are representative of four experiments. $^{**}P \leq 0.01$.

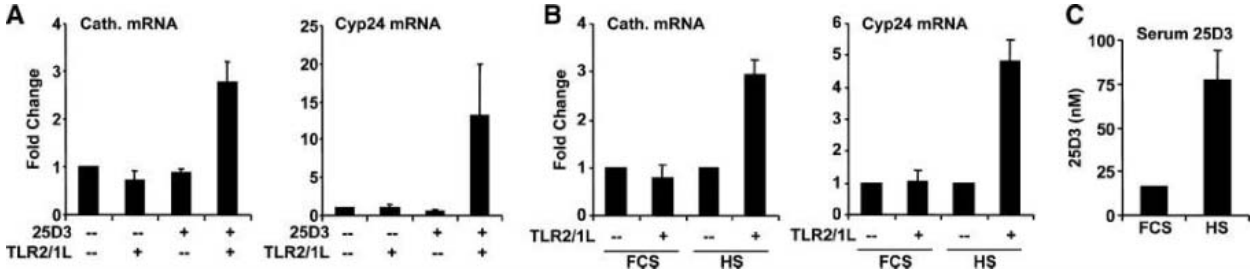

Fig. 3. Effect of human serum (HS) on vitamin D receptor activation. (**A**) Effects of $25(OH)D_3$ (25D3) supplementation to TLR2/1-stimulated monocytes cultured in FCS (mean fold change ± SEM, $n = 3$). (**B**) Effect of FCS and human serum on TLR-induced VDR downstream genes. The ability of monocytes cultured in either FCS or human serum to up-regulate cathelicidin and Cyp24 mRNA upon TLR2/1L stimulation measured by qPCR (mean fold change ± SEM, $n = 4$). (**C**) $25(OH)D_3$ levels in FCS and human serum as measured by radioimmunoassay. FCS data represent the same lot used throughout this study, and human serum is the mean concentration (nM) ± SEM of four individual donors.

25(OH)D_3 to a physiologic range restored TLR induction of cathelicidin mRNA (Fig. 4F).

Although the antimicrobial effects of vitamin D have been previously documented and reduced vitamin D status is known to be associated with susceptibility to *M. tuberculosis* infection, our work describes a potential mechanism by which this might influence the innate immune response. By demonstrating that TLR stimulation of human macrophages induces (i) the enzyme that catalyzes conversion of 25(OH)D_3 to active 1,25$(OH)_2D_3$; (ii) the expression of the vitamin D receptor (VDR); and, (iii) relevant downstream targets of VDR (including cathelicidin), the present results provide an explanation for the action of vitamin D as a key link between TLR activation and antibacterial responses in innate immunity. We do not imply that this is the only antimicrobial mechanism available to human macrophages. This innate immune pathway is likely complemented by T cell–dependent adaptive immune mechanisms, which include macrophage activation by cytokines and release of granulysin (*15*).

We believe these findings may explain a number of puzzling problems: the increased 1,25$(OH)_2D_3$ levels at the site of disease in a localized form of tuberculosis (*16*), TLR-induced induction of antimicrobial peptides in epithelial cells (*17*), and the evolution of divergent antimicrobial pathways in mice (nocturnal animals that use nitric oxide) versus humans (daytime creatures that synthesize vitamin D_3 in the skin on exposure to UV light). These findings also provide new insight into the history of tuberculosis treatment, including the importance of sunlight in the sanatorium movement created by Brehmer and Trudeau, and the award of the 1903 Nobel Prize for Medicine to Niels Ryberg Finsen for demonstrating that UV light was beneficial to patients with lupus vulgaris, tuberculosis of the skin, consistent with the importance of vitamin D in all forms of tuberculosis. The harmful effects of sunlight are well documented, but there is also epidemiologic evidence that vitamin D sufficiency has a positive association with lower incidences of colorectal and prostate cancers (*18*). The findings reported here are consistent with the possibility that variation in the ability to synthesize vitamin D, including polymorphisms in the VDR (*19*), may be a contributing factor to increased tuberculosis susceptibility. Consequently, consideration might be given to clinical trials of inexpensive vitamin D supplementation at appropriate doses to enhance innate immunity to microbial infections and possibly neoplastic disease in African or Asian populations.

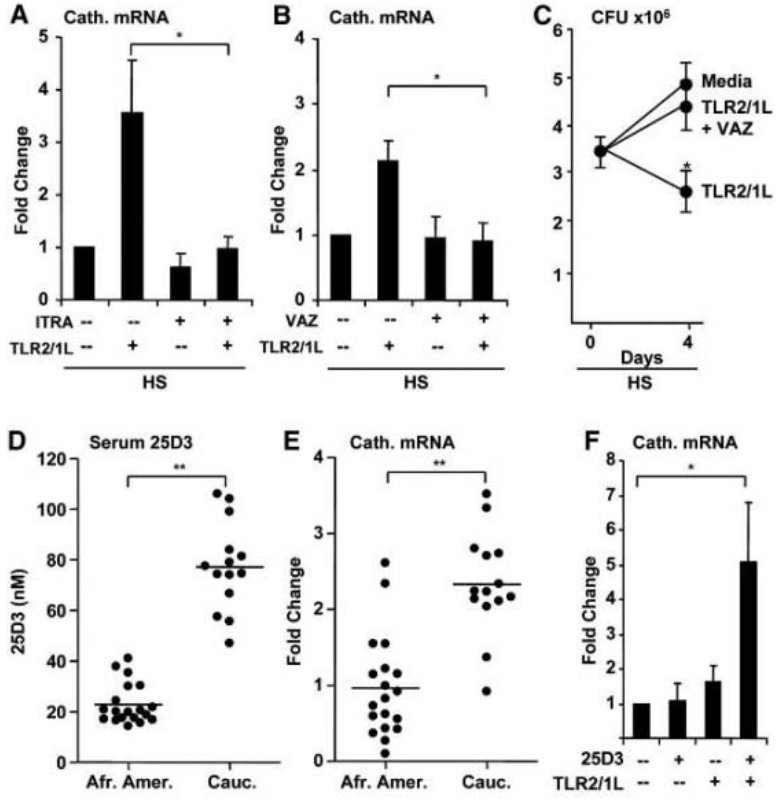

Fig. 4. Role of the vitamin D pathway in induction of cathelicidin mRNA and antimicrobial activity. Role of VDR (**A**) and Cyp27B1 (**B**) in induction of cathelicidin mRNA. Monocytes were cultured in human serum and pretreated with the Cyp27B1 antagonist itraconazole (ITRA) (A) or the VDR antagonist VAZ (VDR-antagonist ZK159222) (B), then induced with TLR2/1L; the cathelicidin mRNA levels were determined by qPCR (mean fold change ± SEM, $n = 4$). (**C**) The role of the VDR in TLR2/1L-induced antimicrobial activity. Alveolar macrophages were infected with *M. tuberculosis* and stimulated with medium, TLR2/1L, or TLR2/1L with VAZ. Viable bacteria were quantified by CFU assay after 4 days of growth. Data shown are representative of eight experiments. (**D**) Serum concentration (nM) of 25(OH)D_3 in African American and Caucasian donors as measured by radioimmunoassay. The mean of the values is represented by the line. (**E**) Effect of serum from African Americans or Caucasians on TLR2/1L-induced cathelicidin mRNA levels. Monocytes were cultured in either African American or Caucasian serum, activated with TLR2/1L, then cathelicidin mRNA levels were determined by qPCR. Points are fold change of each individual donor tested, with the mean value indicated by the line. (**F**) Effect of supplementation of African American sera with 25(OH)D_3 on TLR2/1L-induced cathelicidin mRNA levels. Monocytes were cultured in African American sera without supplementation or with exogenous 25(OH)D_3 at physiologic concentrations ranging from 1 to 100 nM to optimize the signal-to-noise ratio due to monocyte variability, then stimulated with the TLR2/1L. Cathelicidin levels were determined by qPCR and averaged (mean fold change ± SEM, $n = 3$). $^*P \leq 0.05$, $^{**}P \leq 0.01$.

References and Notes

1. S. Tauszig, E. Jouanguy, J. A. Hoffmann, J. L. Imler, *Proc. Natl. Acad. Sci. U.S.A.* **97**, 10520 (2000).
2. R. L. Modlin, G. Cheng, *Nat. Med.* **10**, 1173 (2004).
3. J. Chan, Y. Xing, R. S. Magliozzo, B. R. Bloom, *J. Exp. Med.* **175**, 1111 (1992).
4. J. D. MacMicking *et al.*, *Cell* **81**, 641 (1995).
5. S. Thoma-Uszynski *et al.*, *Science* **291**, 1544 (2001).
6. Materials and methods are available as supporting material on *Science* Online.
7. J. Roth, T. Vogl, C. Sorg, C. Sunderkotter, *Trends Immunol.* **24**, 155 (2003).
8. T. T. Wang *et al.*, *J. Immunol.* **173**, 2909 (2004).
9. K. A. Rockett *et al.*, *Infect. Immun.* **66**, 5314 (1998).
10. L. M. Sly, M. Lopez, W. M. Nauseef, N. E. Reiner, *J. Biol. Chem.* **276**, 35482 (2001).
11. L. Y. Matsuoka, J. Wortsman, J. G. Haddad, P. Kolm, B. W. Hollis, *Arch. Dermatol.* **127**, 536 (1991).
12. W. W. Stead, J. W. Senner, W. T. Reddick, J. P. Lofgren, *N. Engl. J. Med.* **322**, 422 (1990).
13. A. R. Rich, *The Pathogenesis of Tuberculosis* (Charles C Thomas, Springfield, IL, 1944).
14. All volunteers in the study were categorized by self-identification or visual determination as African Americans or Caucasians (non-Hispanic, White). There were 19 African Americans and 14 Caucasians studied in Fig. 4, D and E. Although the studies were performed using samples from African Americans, we believe that the implications are likely to be relevant for all individuals of African descent and possibly of Asian decent. Future studies will be directed towards comparing responses according to measured skin pigmentation.
15. S. Stenger *et al.*, *Science* **282**, 121 (1998).
16. P. F. Barnes, R. L. Modlin, D. D. Bikle, J. S. Adams, *J. Clin. Invest.* **83**, 1527 (1989).
17. C. J. Hertz *et al.*, *J. Immunol.* **171**, 6820 (2003).
18. E. Giovannucci, *Cancer Causes Control* **16**, 83 (2005).
19. L. Bornman *et al.*, *J. Infect. Dis.* **190**, 1631 (2004).

20. We would like to thank G. Cheng at UCLA for his helpful discussion and O. Sorensen for the cathelicidin antibody. This work was supported by NIH grants AI47868, AI22553, HD043921, AR50626, AI48176, AI052453, AR45676, and RR00425; and also by the Deutsche Forschungsgemeinschaft (SFB 643 and GRK 592); Deutsche Akademie der Naturforscher Leopoldina; and U.S. Department of Veterans Affairs Merit Award.

Supporting Online Material

www.sciencemag.org/cgi/content/full/1123933/DC1
Materials and Methods
References

16 December 2005; accepted 8 February 2006
Published online 23 February 2006;
10.1126/science.1123933
Include this information when citing this paper.

Reversal of Diabetes in Non-Obese Diabetic Mice Without Spleen Cell–Derived β Cell Regeneration

Anita S. Chong,[1]* Jikun Shen,[1] Jing Tao,[1] Dengping Yin,[1,3] Andrey Kuznetsov,[2] Manami Hara,[2] Louis H. Philipson[2]

Autoimmune destruction of β cells is the predominant cause of type 1 diabetes mellitus (T1DM) in humans and is modeled in non-obese diabetic (NOD) mice. Many therapeutic interventions prevent the development of T1DM in NOD mice, but few can induce its reversal once established. Intervention with Freund's complete adjuvant, semi-allogeneic splenocytes, and temporary islet transplantation has been reported to cure NOD mice of established T1DM. Using the same approach, we report here that this treatment cured 32% of NOD mice of established diabetes (>340 milligrams per deciliter blood glucose), although β cells in these mice were not derived from donor splenocytes.

Current therapy for T1DM, based on the replacement of insulin or on islet transplantation and immune suppression, has substantial limitations (*1*). An alternative approach to curing T1DM is through the simultaneous reversal of preexisting autoreactivity and restoration of endogenous β cell function. Recent studies by Kodama *et al*. (*2*) suggested that treatment with Freund's complete adjuvant (FCA), semi-allogeneic spleen cells, and temporary islet transplantation leads to the control of autoimmunity and alloreactivity and to a marked restoration in β cell mass through the in vivo differentiation of stem cells from the spleen. We attempted to independently replicate these findings using spleen cells from a transgenic mouse strain in which the mouse insulin promoter drives the expression of green fluorescent protein (MIP-GFP); thus, GFP is expressed only in their β cells and not in their spleen cells (*3*).

Severely diabetic NOD mice (blood glucose levels of >300 mg/dl for 2 consecutive days; table S1) were injected with FCA and live semi-allogeneic spleen cells (CByB6F1) from MIP-GFP mice. To initially control blood glucose levels, 400 to 500 islets from NOD-*scid* mice were implanted under a single kidney capsule of NOD recipients. Of the 22 diabetic NOD mice that were transplanted and treated with FCA and spleen cells, 14 (63.6%) redeveloped diabetes (blood glucose >200 mg/dl) within 40 days, and one within 80 days, of initiation of treatment (Fig. 1A and table S1). To confirm that the redevelopment of diabetes was due to a recurrence of autoimmunity, a second syngeneic islet transplant (200 islets per mouse) was performed in six mice (with >200 mg/dl blood glucose levels for 2 to 30 days). Four of the six mice became diabetic again within 1 week of retransplantation, consistent with recurrent autoimmunity. Two of the six remained normoglycemic, one for >52 days and the other for >100 days, suggesting that the initial recurrence of diabetes was due not to the inability of the treatment to control autoimmunity but to insufficient β cell mass. Thus, treatment with FCA and spleen cells reversed autoimmunity in 41% (9 out of 22) of the diabetic NOD mice. Seven of the nine mice remained normoglycemic for ≥90 days; the remaining two mice with normal glycemia were observed for only 52 and 53 days. Six of the seven mice were successfully nephrectomized, after which all remained normoglycemic for >29 days (Fig. 1B and table S1), indicating that normoglycemia could be maintained by endogenous β cells. All four of the successfully treated (Rx-NOD) mice that were subject to intraperitoneal glucose tolerance testing displayed almost normal responses (fig. S1).

Histological examination of the entire pancreas indicated that five of the six Rx-NOD mice had very few hyperplastic islets (Fig. 1, D to F) and that one had few small islets that stained very weakly or did not stain for insulin, similar to the observations by Suri *et al*. (*4*). The mean number of hyperplastic islets (±SEM) in the pancreas of the five Rx-NOD mice examined was 12.2 ± 2.2. This number is con-

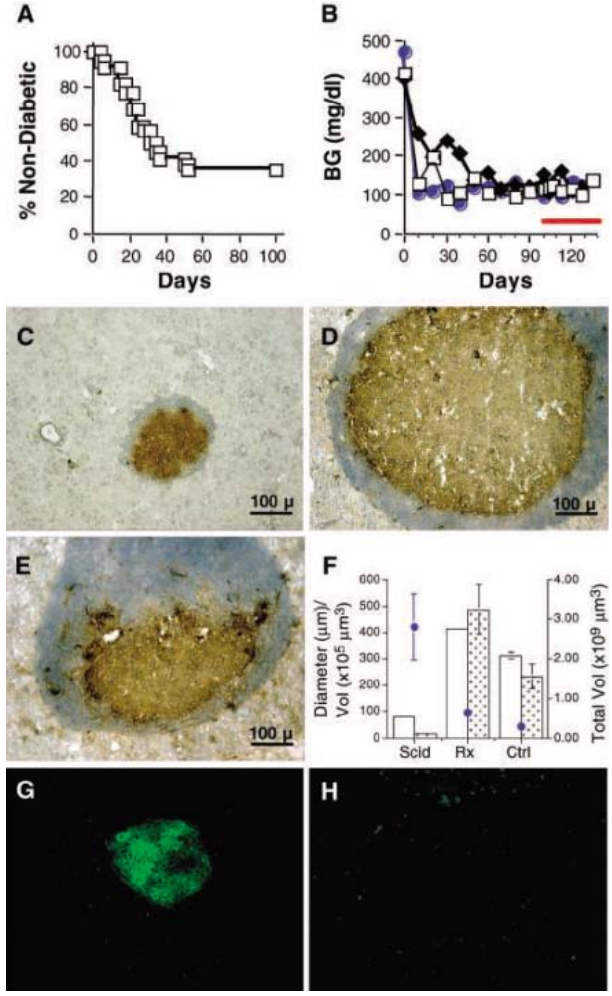

Fig. 1. Reversal of established diabetes in NOD mice. (**A**) Kaplan-Meier plot of the percentage of nondiabetic mice after the first islet transplantation (n = 22). (**B**) The blood glucose (BG) levels of three NOD mice successfully treated with FCA, biweekly infusions for 6 weeks of semi-allogeneic spleen cells, and a subrenal transplant of syngeneic islets. The bar indicates the period of normoglycemia after the subrenal islet grafts were removed. (**C** to **E**) Immunohistochemistry of β cells. Pancreatic sections from age-matched NOD-*scid* (C), successfully treated NOD mice (D), and age-matched (≥45 weeks old) NOD mice that did not spontaneously develop diabetes (E). (**F**) The maximal diameter (empty bars) and average volume (shaded bars; Vol = $^4/_3\pi r^3$, where r is the radius) of the islets ± SEM were calculated for all the islets observed in successfully treated (Rx) and control (Ctrl) NOD mice, and all insulin-positive islets (>80 per section) from two randomly selected sections per NOD-*scid* (Scid) mouse (n = 3 per group). The total volume ± SEM (filled circles) of β cells was estimated by multiplying the average volume by the total number of islets (NOD-*scid* mice were assumed to have 2000 islets). (**G** to **H**) Visualization of β cells from control MIP-GFP (G) or successfully treated NOD mice (H). Occasional green fluorescence observed in the pancreas of successfully treated NOD mice was due to autofluorescence and was not associated with β cells.

[1]Section of Transplantation, Department of Surgery, [2]Section of Endocrinology, Department of Medicine, The University of Chicago, Chicago, IL 60637, USA. [3]Department of Surgery, University of Illinois at Chicago, Chicago, IL 60612, USA.

*To whom correspondence should be addressed. E-mail: achong@uchicago.edu

siderably lower than that observed in age- and sex-matched NOD-*scid* mice or young prediabetic NOD mice [which are estimated to have ≥2000 islets per NOD mouse (*5*)]. The average diameter of the islets from Rx-NOD mice was 5.2 ± 0.1 times as large as that of age-matched NOD-*scid* mice (Fig. 1, C, D, and F; $P < 0.05$). This increase in islet size was due not to hypertrophy of individual β cells but to increased numbers of β cells and not of glucagon-expressing α cells (fig. S2). We estimated that the total β cell volume in the Rx-NOD mice was 22.5 ± 4.1% of that of age-matched NOD-*scid* mice. Similarly low numbers (12.2 ± 1.7) of significantly enlarged islets ($P < 0.05$) were observed in age-matched NOD mice that failed to develop spontaneous diabetes (Fig. 1, D to F).

To determine whether the β cells in the Rx-NOD were of host origin or derived from donor spleen cells, we examined all the Rx-NOD islets for expression of GFP. No β cells expressing GFP were detected in any of the islets examined (Fig. 1, G and H) or in the organs outside of the pancreas. Thus, our data do not support a conclusion of β cell regeneration from spleen-derived stem cells. All the hyperplastic islets from the five cured Rx-NOD mice were associated with circumferentially distributed lymphocytes (peri-insulitis) of donor origin (fig. S3) and devoid of invasive insulitis. The majority of these peri-islet lymphocytes were $CD4^+CD25^+$ cells, with a small portion expressing the transcriptional factor $FoxP3^+$ (fig. S3) (*6*). These observations suggest that regulatory T cells may function to control autoimmunity locally where β cells are situated. The islets that stained very weakly or did not stain for insulin in the one Rx-NOD mouse without hyperplasia did not have a notable peri-islet lymphocytic infiltrate.

The finding that autoimmune diabetes in NOD mice can be reversed by a complex protocol combining islet transplantation, FCA treatment, and transfer of semi-allogeneic splenocytes suggests a potential for novel β cell replacement therapies for human T1DM (*2*, *7*). We confirmed these observations and demonstrated restoration of diabetic NOD mice to normoglycemia with this therapeutic protocol. We did not observe β cell reconstitution from the infused spleen cells, and these studies were not designed to determine whether the observed host-derived β cells were the result of replication of preexisting β cells or differentiation from stem-cell precursors. Our studies indicate that normoglycemia in Rx-NOD mice can be maintained by a very low number of hyperplastic islets or, in one case, by weakly insulin-positive or insulin-negative islets surviving the autoimmunity. The consistent association between islet hyperplasia and peri-insulitis (*8*, *9*) suggests a hypothesis that autoreactivity, when restrained by regulatory T cells, may facilitate the development of islet hyperplasia. The limited β cell mass required to maintain normoglycemia in this model contrasts with the large numbers of transplanted islets required to maintain normal glycemia (*1*, *10*). Our studies confirm that autoimmune diabetes can be reversed and that sufficient endogenous β cell mass can be restored to cure diabetic NOD mice with the treatment protocol developed by Faustman and colleagues (*2*, *7*). Translating these findings into therapies useful for curing T1DM in humans remains a challenge.

References and Notes

1. K. I. Rother, D. M. Harlan, *J. Clin. Invest.* **114**, 877 (2004).
2. S. Kodama, W. Kuhtreiber, S. Fujimura, E. A. Dale, D. L. Faustman, *Science* **302**, 1223 (2003).
3. M. Hara *et al.*, *Am. J. Physiol. Endocrinol. Metab.* **284**, E177 (2003).
4. A. Suri *et al.*, *Science* **311**, 1778 (2006).
5. T. Bock, B. Pakkenberg, K. Buschard, *Diabetes* **54**, 133 (2005).
6. J. D. Fontenot *et al.*, *Immunity* **22**, 329 (2005).
7. S. Ryu, S. Kodama, K. Ryu, D. A. Schoenfeld, D. L. Faustman, *J. Clin. Invest.* **108**, 63 (2001).
8. A. Jansen *et al.*, *J. Autoimmun.* **9**, 341 (1996).
9. J. G. M. Rosmalen *et al.*, *Lab. Invest.* **80**, 769 (2000).
10. R. D. Molano *et al.*, *Transplantation* **75**, 1812 (2003).

11. We thank I. Boussy and A. Chervonsky for helpful comments. We acknowledge grant support from the Juvenile Diabetes Research Foundation, Chester Foundation, and NIH (DK073529, DK20595, DK4894, and DK063493).

Supporting Online Material

www.sciencemag.org/cgi/content/full/311/5768/1774/DC1
Materials and Methods
Figs. S1 to S3
Table S1
References

6 December 2005; accepted 10 February 2006
10.1126/science.1123510

Islet Recovery and Reversal of Murine Type 1 Diabetes in the Absence of Any Infused Spleen Cell Contribution

Junko Nishio, Jason L. Gaglia, Stuart E. Turvey,* Christopher Campbell, Christophe Benoist,† Diane Mathis†

A cure for type 1 diabetes will probably require the provision or elicitation of new pancreatic islet β cells as well as the reestablishment of immunological tolerance. A 2003 study reported achievement of both advances in the NOD mouse model by coupling injection of Freund's complete adjuvant with infusion of allogeneic spleen cells. It was concluded that the adjuvant eliminated anti-islet autoimmunity and the donor splenocytes differentiated into insulin-producing (presumably β) cells, culminating in islet regeneration. Here, we provide data indicating that the recovered islets were all of host origin, reflecting that the diabetic NOD mice actually retain substantial β cell mass, which can be rejuvenated/regenerated to reverse disease upon adjuvant-dependent dampening of autoimmunity.

Type 1 diabetes, an autoimmune disease that targets pancreatic islet β cells, is an important and increasing health problem. It is generally believed that effective therapy for autoimmune diabetes will require two scientific advances: (i) restoration of insulin production by providing or eliciting new β cells, and (ii) repair of the breakdown in immunological tolerance that precipitated the disease in the first place.

Recently, successful achievement of both of these advances was reported, culminating in disease abrogation in a fraction of severely diabetic NOD mice (*1*), a widely used murine model of the human type 1 disorder. The protocol incorporated injection of a single dose of Freund's complete adjuvant (FCA) into severely diabetic mice, coupled with repeated infusion of allogeneic splenocytes, resulting in restoration of normoglycemia and permanent disease extinction. The conclusion of this study was that the FCA had eliminated anti-islet autoimmunity and that the donor splenocytes had differentiated into insulin-producing (presumably β) cells, ultimately leading to islet regeneration.

Although FCA has been used for a number of years in a variety of experimental protocols to modulate diabetes in NOD mice (*2*, *3*), the concept of donor splenocytes giving rise to islets in a host pancreas was a novel and exciting one, prompting the suggestion that the function of the spleen should be radically reappraised to include a role as a reservoir of multilineage stem cells (*4*). We set out to further dissect the underlying mechanisms of diabetes reversal by this treatment regime.

As a first step, we attempted to replicate the original findings, following closely the protocol published by Kodama *et al.* (*1*) and incorpo-

Section on Immunology and Immunogenetics, Joslin Diabetes Center, and Department of Medicine, Brigham and Women's Hospital, Harvard Medical School, and Harvard Stem Cell Institute, 1 Joslin Place, Boston, MA 02215, USA.

*Present address: Division of Infectious and Immunological Diseases, Children's Hospital, Vancouver, British Columbia V6H 3V4, Canada.

†To whom correspondence should be addressed. E-mail: cbdm@joslin.harvard.edu

Table 1. Response profiles of treated mice. The treatment protocol is described in (*5*). BG, blood glucose.

	Mouse ID	Age at onset (weeks)	Maximum BG before transplantation	Days with BG >400 mg/dl	Number of transplanted islets	BG on first day after transplantation (mg/dl)	Number of days with BG <250 mg/dl after transplantation*	Overall course
Successful transplantation for 120 days → nondiabetic after nephrectomy	132	23	476	3	650	129	151	Nephrectomy on day 120, still nondiabetic at day 151
	138	30	499	3	800	147	186	Nephrectomy on day 120, still nondiabetic at day 186
	154	26	401	3	800	120	180	Nephrectomy on day 120, still nondiabetic at day 180
	155	35	406	7	800	74	151	Nephrectomy on day 124, still nondiabetic at day 151
	89	19	459	7	800	135	144	Nephrectomy on day 124, still nondiabetic at day 144
Successful transplantation for 120 days → diabetic after nephrectomy	78	37	403	3	650	51	122	Nephrectomy on day 120, diabetic 3 days later
	114	39	458	7	800	105	120	Nephrectomy on day 120, diabetic 1 day later
	11	29	597	7	800	83	123	Nephrectomy on day 123, diabetic 1 day later
	76	27	458	3	800	50	123	Nephrectomy on day 124, diabetic 1 day later
Recurrent diabetes before day 120	15	29	586	3	800	68	60	Spontaneously diabetic
	174	20	>600	3	800	139	46	Spontaneously diabetic
	74	24	584	3	800	101	46	Spontaneously diabetic
	78	18	547	3	800	136	25	Spontaneously diabetic
	84	24	591	14	650	134	24	Spontaneously diabetic
	128	27	505	3	800	125	22	Spontaneously diabetic
	120	44	>600	7	650	93	11	Spontaneously diabetic
	10	25	532	3	800	104	11	Spontaneously diabetic
	81	18	450	3	800	97	11	Spontaneously diabetic
	159	26	502	3	800	97	5	Spontaneously diabetic
	141	21	513	1	650	86	4	Spontaneously diabetic
	72	17	514	3	800	64	4	Spontaneously diabetic
	89	25	>600	8	650	134	2 to 7	Spontaneously diabetic
	86	26	>600	12	650	125	2 to 7	Spontaneously diabetic
	98	26	>600	1	650	90	2 to 7	Spontaneously diabetic
	136	19	541	7	650	83	2 to 3	Spontaneously diabetic
	170	16	581	7	800	172	2 to 3	Spontaneously diabetic
	36	30	543	3	800	84	2 to 3	Spontaneously diabetic
	81	40	>600	7	650	81	2	Spontaneously diabetic
	23	25	432	7	800	113	2	Spontaneously diabetic
	47	24	412	3	800	86	2	Spontaneously diabetic

*A few mice showed transient blood glucose values >250 mg/dl during the follow-up period, but these normalized in the following days, and these excursions were not considered in the evaluation of posttransplant success or failure.

rating additional details from more extensive protocols provided by the authors (*5*). Severely diabetic NOD mice (blood glucose >400 mg/dl) were transplanted under the kidney capsule with syngeneic islets in order to maintain insulin levels; engraftment was deemed a failure when hyperglycemia reappeared before 2 days. Thirty successfully transplanted mice were injected with FCA and infused with live allogeneic [C57BL/6 × Balb/c (referred to as CB6 F1)] splenocytes (Table 1). The majority (21 of 30) developed diabetes before the end of the 120-day observation period (2 to 60 days after islet transfer). We do not know why the 70% reversion rate observed here was higher than the 8% reported by Kodama *et al*. (*1*). After removal of the transplanted islets from the nine mice that had completed the 120-day observation period, four animals became diabetic shortly thereafter, indicating that the insulin that permitted their survival prenephrectomy was produced mainly by the grafted islet cells. The other five animals remained normoglycemic to termination, indicating that they carried insulin-producing cells outside the islet graft, which the immune system no longer destroyed. This 56% of long-term survivors that were insulin–self-sufficient was similar to the 67% reported by Kodama *et al*. (*1*).

Histology of the pancreas revealed islets of various sizes (fig. S1A), including a hyperplastic subset found in both the "cured" and "revertant" long-term survivors, although more frequent in the former (e.g., fig. S1B). All mice had insulitis (fig. S1, A to D) as well as some islets free of

D

Mouse ID	DNA sample ID	Dissected area	Nucleotide at SNP		
			rs4223216 (Chr 2)	rs4230624 (Chr 15)	rs4151928 (Chr 16)
#132	#132_1	normal size islet without insulitis	x	A	x
#138	#138_2	hyperplastic islet with peri-insulitis	x	x	x
	#138_3	hyperplastic islet with peri-insulitis	G	A	C
	#138_4	hyperplastic islet with peri-insulitis	G	A	C
	#138_5	exocrine tissue	G	A	C
#154	#154_1	hyperplastic islet with peri-insulitis	n.d.	n.d.	C
	#154_2	normal size islet without insulitis	G	A	C
	#154_3	normal size islet without insulitis	G	A	C
	#154_4	normal size islet without insulitis	G	A	C
	#154_5	exocrine tissue	G	A	C
control	NOD	islet	G	A	C
	F1	islet	A	C	G

Fig. 1. Laser-capture microdissection and genotyping of islets from "reverted" mice. (**A**) Anti-insulin staining of an islet from mouse 154. (**B**) An adjacent section before (left) and after (right) microdissection. (**C**) Typical genotyping by fluorogenic polymerase chain reaction for SNP rs4151928, detecting the alleles present in NOD or CB6 F1 mice as FAM or VIC fluorescence, respectively. Controls shown are DNA from microdissected islets of a nondiabetic NOD mouse and from an F_1 mouse. Solid triangles denote several samples microdissected from islets of mouse 154. (**D**) Summary of SNP genotyping of microdissected islets from mice 132, 138, and 154 (all from the first group in Table 1). Nucleotides detected for three different SNP positions (rs4223216, rs4230624, and rs4151928) in microdissected islets are shown, with the corresponding nucleotides for control NOD and F_1 DNA (x, unsuccessful amplification; n.d., not done).

infiltrate (fig. S1, A and E). Many islets exhibited an innocuous-looking infiltrate like that described in a number of contexts wherein insulitis does not progress to overt diabetes (*6*). Indeed, there was a striking similarity to the islets of recent-onset diabetic NOD mice treated with anti-CD3 monoclonal antibody (mAb) (fig. S1F). Insulitis was also observed in the syngeneic islet graft (fig. S1G).

We next evaluated the possibility that pancreatic islets were regenerated through differentiation of donor splenocytes. Because the fluorescence in situ hybridization (FISH) assays used in the previous study (*1*) can be challenging and their results can be equivocal, we established a more robust test based on single-nucleotide polymorphism (SNP) analysis of DNA derived from islet tissue isolated from histological sections by laser-capture microdissection (LCM). Islet tissue and any associated inflammation could be definitively identified by staining sections with hematoxylin and/or anti-insulin mAb (Fig. 1A) and could be cleanly excised (Fig. 1B). The SNP analysis assessed three polymorphic loci on three separate chromosomes (Fig. 1C) and clearly distinguished cells of NOD and CB6 F1 origin. In all "cured" animals tested, all tissue was derived from NOD host or graft cells; none came from CB6 F1 donor splenocytes (Fig. 1D).

This result is actually the expected one, given that the NOD host should make a strong alloresponse to the splenocytes' large major histocompatibility complex (MHC) divergence (K^b, D^b, L^d, A^d, E^d, and A^b in the CB6 F1s). We found no evidence of chimerism in the spleen or lymph nodes subsequent to the splenocyte infusions (fig. S2). Instead, strong alloreactivity was evident from the development of antibodies to the allogeneic splenocytes at titers up to 1/5000 (*7*).

The fleeting presence of the splenocytes raised the possibility that the protocol's beneficial effects might derive primarily from the FCA injection. This adjuvant is known to have immunomodulatory effects in the NOD context (*2*, *3*), but a FCA-alone control was not included in the report by Kodama *et al.* (*1*). Therefore, under otherwise the same protocol, we treated 13 severely diabetic NOD mice with FCA and a syngeneic islet transplant but not with allogeneic splenocytes. Four of these animals maintained normal glucose levels during the 120-day observation period, and three of these remained normoglycemic after removal of the transplanted islets (table S1).

A likely source of the insulin that permitted certain long-term survivors to remain nondiabetic is residual islets that expanded through either differentiation or replication once autoimmunity had been muted. Such a scenario is consistent with recent reports that substantial β cell mass can be detected in diabetic NOD mice (*8*). To test this notion, we performed a morphometric analysis of pancreatic β cell mass both in the prediabetic state (n = 3) and in the first weeks after the development of severe hyperglycemia (n = 23). Residual β cell mass was detected in essentially all of the diabetic mice (fig. S3), although it was variable in quantity and was always diminished relative to that of prediabetic comparators. There was no correlation between the blood glucose value and residual β cell mass (*9*). These results indicate that host β cells can contribute to islet regeneration promoting disease reversal in severely diabetic NOD mice.

Our experiments, like those of Kodama *et al.* (*1*), yielded a fraction of previously diabetic NOD mice that survived for a long term after syngeneic islet transplantation, a proportion of which remained normoglycemic even after the removal of the grafted islets. On the other hand, we found no evidence that the source of insulin underlying the reversal of diabetes was islet cells derived from donor splenocytes. Rather, we found that the diabetic hosts had substantial residual β cell mass and that the recovered/expanded islets were all of NOD origin rather than splenocyte CB6 F1 origin. Our conclusions match very well those of two accompanying reports (*10*, *11*). Given recent reports of active β cell replication in both nondiabetic (*12*) and diabetic (*8*) states, the most likely explanation for islet recovery in this context is that the dampening of autoimmunity permitted β cell replication to outdo β cell death. However, other explanations remain possible: differentiation of new host β cells or seeding and expansion of islet graft–derived cells (also of NOD genotype).

Should the autonomous efficacy of FCA demonstrated in our study prompt a reconsideration of the use of the analogous reagent Bacille Calmette-Guérin (BCG), in isolation, to treat diabetic humans? Although a preliminary study with 17 newly diagnosed individuals appeared to show some therapeutic efficacy (*13*), three more extensive, double-blind trials failed to demonstrate a positive effect (*14*). Likely explanations for the divergent outcomes are simply that FCA and BCG are different reagents, or that the footpad injection of FCA

used for mice and the subcutaneous injection of BCG applied to humans are radically different interventions, the former provoking a massive systemic inflammatory response (*15*) difficult to contemplate for human patients.

References and Notes

1. S. Kodama, W. Kühtreiber, S. Fujimura, E. A. Dale, D. L. Faustman, *Science* **302**, 1223 (2003).
2. M. W. Sadelain, H. Y. Qin, J. Lauzon, B. Singh, *Diabetes* **39**, 583 (1990).
3. T. Wang, B. Singh, G. L. Warnock, R. V. Rajotte, *Diabetes* **41**, 114 (1992).
4. S. Kodama, M. Davis, D. L. Faustman, *Trends Mol. Med.* **11**, 271 (2005).
5. See supporting material on *Science* Online.
6. L. Chatenoud, E. Thervet, J. Primo, J. F. Bach, *Proc. Natl. Acad. Sci. U.S.A.* **91**, 123 (1994).
7. J. Nishio *et al.*, unpublished data.
8. S. Sreenan *et al.*, *Diabetes* **48**, 989 (1999).
9. J. Nishio *et al.*, data not shown.
10. A. Suri *et al.*, *Science* **311**, 1778 (2006).
11. A. S. Chong *et al.*, *Science* **311**, 1774 (2006).
12. Y. Dor, J. Brown, O. I. Martinez, D. A. Melton, *Nature* **429**, 41 (2004).
13. N. Shehadeh *et al.*, *Lancet* **343**, 706 (1994).
14. B. Singh, J. F. Elliot, *Diabetes Metab. Rev.* **13**, 320 (1997).
15. A. Bekierkunst, I. S. Levij, E. Yarkoni, E. Vilkas, E. Lederer, *Infect. Immun.* **4**, 245 (1971).

16. We thank S. Bonner-Weir, A. McGettrick, J. Lock, L. Marselli, C. Cahill, and R. Kulkarni for materials and advice; D. Faustman and D. Melton for protocols; N. Asinovski, V. Bruklich, K. Hattori, and A. Pinkhasov for assistance; and V. Tchipashvili, G. Chandra, V. Kostaras, and the Islet Core. Supported by grants from the Juvenile Diabetes Research Foundation and by Joslin's Diabetes and Endocrinology Research Center core facilities (funded by the National Institute of Diabetes and Digestive and Kidney Diseases), by fellowships from the Japan Health Science Foundation, Mochida Memorial Foundation, and American Diabetes Association (J.N.), and by NIH grant T32 CA09382 (J.L.G.).

Supporting Online Material

www.sciencemag.org/cgi/content/full/311/5768/1775/DC1
Materials and Methods
Figs. S1 to S3
Table S1

19 December 2005; accepted 10 February 2006
10.1126/science.1124004

Immunological Reversal of Autoimmune Diabetes Without Hematopoietic Replacement of β Cells

Anish Suri,* Boris Calderon, Thomas J. Esparza, Katherine Frederick, Patrice Bittner, Emil R. Unanue*

Type 1 diabetes mellitus results from the autoimmune destruction of the β cells of the pancreatic islets of Langerhans and is recapitulated in the nonobese diabetic strain of mice. In an attempt to rescue islet loss, diabetic mice were made normoglycemic by islet transplantation and immunization with Freund's complete adjuvant along with multiple injections of allogeneic male splenocytes. This treatment allowed for survival of transplanted islets and recovery of endogenous β cell function in a proportion of mice, but with no evidence for allogeneic splenocyte–derived differentiation of new islet β cells. Control of the autoimmune disease at a crucial time in diabetogenesis can result in recovery of β cell function.

It is now generally accepted that two issues must be addressed for the successful treatment of type 1 diabetes mellitus (T1DM), an autoimmune disease in which T cells kill the β cells responsible for insulin production (*1*). The persistent autoreactivity to β cell antigens that characterize the disease needs to be controlled and the β cell mass, which is extensively reduced at the time of onset of clinical disease, must be restored. A treatment protocol was recently developed in nonobese diabetic (NOD) mice, an extensively used model of T1DM, that resulted in cessation of autoimmunity and reversal of diabetes through the generation of new β cells from splenic cells (*2*, *3*). Because of the importance of these conclusions in offering novel clinical strategies for disease intervention, we repeated the same experimental protocol as a prelude to further analysis of the process.

The major protocol from the paper of Kodama *et al*. involved three experimental manipulations in female diabetic NOD mice made between 7 and 20 days after the development of hyperglycemia (*2*, *3*). First, a single subcutaneous injection of Freund's complete adjuvant (FCA) was administered, which is known to stop the autoimmune process in diabetic NOD mice (*4*–*6*). Second, the mice were given a series of intravenous injections of spleen cells derived from major histocompatibility complex (MHC)–mismatched donor F1 (CByB6F1) male mice. Finally, to control the hyperglycemia, syngeneic islets were transplanted under the capsule of one kidney. The mice were followed for a period of at least 120 days after transplant, at which time nephrectomy was performed to remove the islet grafts. Most mice remained normoglycemic, which indicates that β cell function in the pancreas was restored during the time of immunological control (*2*). Moreover, the islets were reported to be derived from the injected spleen cells because they contained the male Y-chromosome marker of the injected male cells (*2*).

In our experiments, female NOD mice were maintained on insulin for 7 to 20 days before the three treatments after the first indications of hyperglycemia, to ensure that the islet β cell mass was depleted (*7*). Mice that remained persistently normoglycemic (22 out of 53) were followed for at least 120 days after treatments. (The 31 transplanted mice that developed periods of hyperglycemia before the 120-day observation period were eliminated.) A nephrectomy, which also removed the transplanted islets placed under the capsule, was performed between days 120 and 146 after transplantation. Examples of experimental mice that reverted back to diabetes, or that maintained normoglycemia after nephrectomy, are shown in Fig. 1. The large majority of the mice (82%) subsequently reverted to the diabetic state (Table 1), which suggests that endogenous β cell function had not been restored in these individuals, and histological analysis confirmed the presence of very few small islets made up entirely of glucagon-positive cells (*8*). Thus, no insulin-positive cells were detected either in the few remaining small islets or in the ducts of revertant mice (*8*). In other experiments, the same manipulations were performed with FCA injections and islet transplants (*5*) but without the inocula of allogeneic cells. In this case, 20 of 29 mice became normoglycemic, some for as long as >100 days (*8*), an indication that the

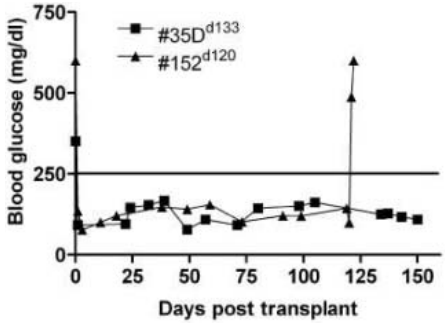

Fig. 1. Serum glucose levels of two representative mice treated according to the major protocol of Kodama *et al*. (*2*, *7*). Transplanted mice were followed for at least 120 days, after which the islet transplant under the kidney capsule was removed by nephrectomy. The day of nephrectomy for each animal is indicated in superscript. Of the two mice, one became diabetic immediately after nephrectomy, whereas the other remained normoglycemic.

Department of Pathology and Immunology, Washington University School of Medicine, St. Louis, MO 63110, USA.

*To whom correspondence should be addressed. E-mail: anish@pathology.wustl.edu (A.S.); unanue@pathbox.wustl.edu (E.R.U.)

FCA injection was sufficient for control of the autoimmune process in these mice.

In the four remaining mice of the original experiment (Table 1) that maintained normoglycemia after nephrectomy, few islets were found, all of which contained about 75% or more glucagon- and somatostatin-positive cells (*8*). However, some islets also contained insulin-positive cells and were also positive for the β cell–specific transcription factor PDX-1 (fig. S1, A and B) (*7*, *9*). A few cells were negative for insulin but positive for PDX-1, which suggests that such β cells had undergone extensive insulin degranulation (fig. S1B) (*7*). Fluorescence in situ hybridization (FISH) analysis failed to detect the presence of Y chromosome–positive cells in any of the islets examined (Fig. 2A and fig. S2) (*7*).

No evidence of chimerism of the F1 male cells in the NOD female mice was detected with flow cytometry analysis (Table 1 and fig. S3A) (*7*). Moreover, the spleen cells exhibited a mixed lymphocyte reaction when tested with irradiated F1 cells (Table 1 and fig. S3B) (*7*), and the sera contained alloantibodies against the F1 cells (Table 1 and fig. S3C) (*7*). Taken together, these demonstrate a clear host immune response against the injected allogeneic male F1 cells. In addition, the spleen cells from the treated mice transferred diabetes when injected into NOD.scid recipients (Table 1 and fig. S3D) (*7*), which demonstrates that diabetogenic T cells had persisted, most likely in a quiescent state, in mice treated with FCA and F1 cells (*5*, *10*).

In the second of their protocols, Kodama *et al*. treated prediabetic NOD female mice with FCA and green fluorescent protein (GFP)–expressing male (CByB6F1) spleen cells (*2*). These mice failed to develop diabetes and expressed GFP in their islets. Repeating this second protocol, 12-week-old prediabetic NOD

Table 1. Compiled results of 22 diabetic female NOD mice after nephrectomy. Mice marked with an asterisk (*) were transplanted with 300 islets; all others received a transplant of 600 to 650 islets. The kidney containing the islet graft was removed between days 120 and 146 after transplant, after which most mice reverted to a diabetic state ("yes" in third column) and few remained normoglycemic ("no" in third column). Many transplanted mice were analyzed for the presence of chimerism (i.e., presence of CByB6F1 cells in spleen and peripheral blood); the presence of alloantibodies (Allo-Abs) to CByB6F1 cells in serum; the ability to mount a mixed lymphocyte reaction (MLR) against CByB6F1 cells; and the ability of their spleen cells to transfer diabetes into NOD.scid recipient mice. n.d., not determined.

Mouse	Nephrectomy (day)	Diabetic	Chimerism	Allo-Abs	MLR	Transfer of diabetes into NOD.scid recipients
2*	126	yes	no	+++	+++	5/5 (100%)
35D*	133	no	no	+++	+++	5/5 (100%)
38*	133	yes	no	+++	+++	3/3 (100%)
61*	136	yes	no	+++	+++	5/5 (100%)
66	122	yes	no	+++	n.d.	3/3 (100%)
79	146	yes	no	+++	+++	4/5 (80%)
122	130	yes	no	+++	–	n.d.
124	130	yes	no	+++	+++	4/5 (80%)
136D	124	no	no	+++	+++	1/3 (33%)
137	124	yes	no	+++	+++	3/5 (60%)
138	123	no	no	+++	n.d.	n.d.
140	138	no	no	+++	n.d.	n.d.
147	124	yes	no	+++	n.d.	n.d.
152	120	yes	no	+++	n.d.	n.d.
157	139	yes	n.d.	n.d.	n.d.	n.d.
158	134	yes	n.d.	n.d.	n.d.	n.d.
164	134	yes	n.d.	n.d.	n.d.	n.d.
159	132	yes	n.d.	n.d.	n.d.	n.d.
160	132	yes	n.d.	n.d.	n.d.	n.d.
166	128	yes	n.d.	n.d.	n.d.	n.d.
174	121	yes	n.d.	n.d.	n.d.	n.d.
175	125	yes	n.d.	n.d.	n.d.	n.d.

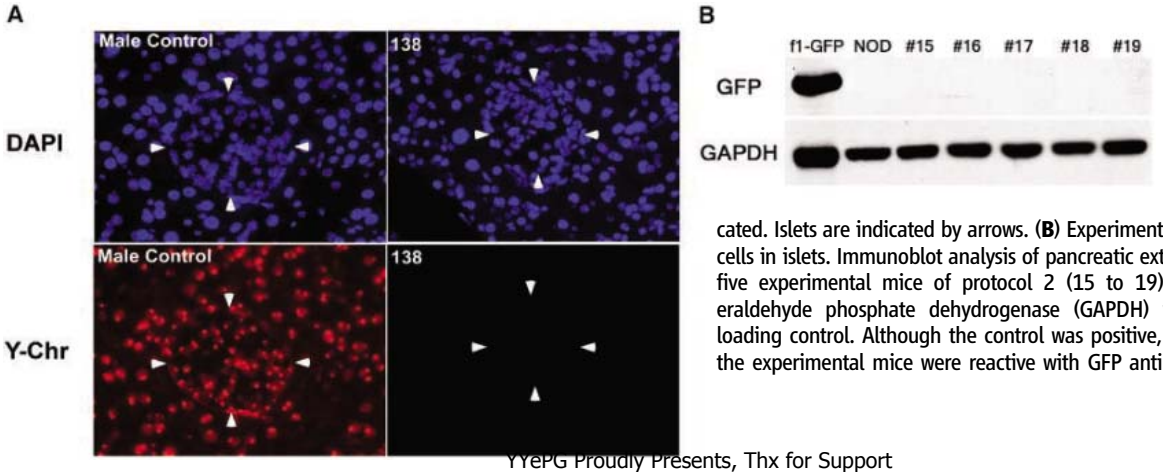

Fig. 2. (**A**) FISH analysis of islets from mouse 138 to detect the presence of Y chromosome (*18*). Nuclei are stained with 4′,6′-diamidino-2-phenylindole (DAPI). Positive control is indicated. Islets are indicated by arrows. (**B**) Experiment searching for GFP-positive cells in islets. Immunoblot analysis of pancreatic extracts from F1-GFP, NOD or five experimental mice of protocol 2 (15 to 19) searching for GFP. Glyceraldehyde phosphate dehydrogenase (GAPDH) was used as an internal loading control. Although the control was positive, none of the extracts from the experimental mice were reactive with GFP antibodies.

female mice received a single injection of FCA, along with four injections of GFP-expressing CByB6F1spleen cells (5×10^5 per injection, administered over 2 weeks). Included was a control group of 12-week-old prediabetic NOD female mice that received a single injection of FCA alone. In both cases, all mice were protected from diabetes (fig. S4) (*7*). Moreover, intact islets, some with evidence of insulitis, were present in both groups of protected mice. However, we failed to detect GFP^+ cells by immunohistochemistry or Western blot analyses (Fig. 2B). In addition, spleen cells from GFP-treated mice retained the capacity to transfer diabetes into third-party NOD.scid recipients (fig. S5) (*7*).

In our experiments, no evidence of replacement of islets by the allogeneic spleen cells was observed. Moreover, immunological reaction to the injected cells was seen, as would be anticipated. Finally, the presence of diabetogenic T cells, albeit in a quiescent state, indicated that the abnormal autoimmune process persisted in these treated mice. It is likely that the normoglycemia observed in the four mice from the original protocol resulted from a few β cells that had survived the initial T cell attack and subsequently expanded to maintain blood glucose levels. Potentially, these could derive from precursor cells found in ducts or from surviving pre-existing β cells, which is consistent with a similar conclusion found in two recent studies (*11*, *12*). We also examined the pancreas of 14 diabetic mice maintained on insulin for 2 to 3 weeks, that is, under the same initial situation as the mice in the original protocol. We observed in this experiment a large variation in the number of surviving islets and β cells, with 3 of the 14 mice examined containing about 6% of the normal content of β cells and the rest having less (fig. S6A) (*7*). Most of the islets were abundant in glucagon-positive cells, although some cells were PDX-1 positive but negative for insulin (fig. S6B) (*7*). Thus, even in the presence of marked hyperglycemia, an indication of advanced diabetes, some β cells can survive for at least a period of time. It is possible that, as their insulin content decreases, the surviving β cells become less susceptible to attack by the insulin-specific T cells that dominate the immunological reaction (*13*–*15*). It is noteworthy that at the time of the first reading of hyperglycemia, the number of β cells was decreased by 71% in five mice examined. Between the time of the first evidence of hyperglycemia and the time the protocol was started [that is, 7 to 20 days (*2*, *3*)], there was a precipitous drop in islet β cell numbers. Along these lines, other studies demonstrated the successful reversion of disease with antibodies to CD3 or CD4 molecules, but only in newly diabetic NOD mice (*16*, *17*). In sum, the present findings in the 20% of mice displaying restored islet function when there is immunological regulation indicate that some β cells survived immunologic attack. Finding means of preserving these cells and stimulating their expansion could represent an exciting new approach to the prevention and treatment of T1DM.

References and Notes

1. R. Tisch, H. McDevitt, *Cell* **85**, 291 (1996).
2. S. Kodama, W. Kuhtreiber, S. Fujimura, E. A. Dale, D. L. Faustman, *Science* **302**, 1223 (2003).
3. S. Ryu, S. Kodama, K. Ryu, D. A. Schoenfeld, D. L. Faustman, *J. Clin. Invest.* **108**, 63 (2001).
4. M. W. Sadelain, H. Y. Qin, J. Lauzon, B. Singh, *Diabetes* **39**, 583 (1990).
5. D. Ulaeto, P. E. Lacy, D. M. Kipnis, O. Kanagawa, E. R. Unanue, *Proc. Natl. Acad. Sci. U.S.A.* **89**, 3927 (1992).
6. M. F. McInerney, S. B. Pek, D. W. Thomas, *Diabetes* **40**, 715 (1991).
7. Materials and methods are available as supporting material on *Science* Online.
8. A. Suri *et al.*, unpublished data.
9. L. C. Murtaugh, D. A. Melton, *Annu. Rev. Cell Dev. Biol.* **19**, 71 (2003).
10. A. Suri *et al.*, *Eur. J. Immunol.* **34**, 447 (2004).
11. J. Nishio, J. L. Gaglia, S. E. Turvey, C. Campbell, C. Benoist, D. Mathis, *Science* **311**, 1775 (2006).
12. A. S. Chong *et al.*, *Science* **311**, 1774 (2006).
13. D. R. Wegmann *et al.*, *J. Autoimmun.* **6**, 517 (1993).
14. D. R. Wegmann, M. Norbury-Glaser, D. Daniel, *Eur. J. Immunol.* **24**, 1853 (1994).
15. D. R. Wegmann, R. G. Gill, M. Norbury-Glaser, N. Schloot, D. Daniel, *J. Autoimmun.* **7**, 833 (1994).
16. L. Makhlouf *et al.*, *Transplantation* **77**, 990 (2004).
17. L. Chatenoud, E. Thervet, J. Primo, J. F. Bach, *Proc. Natl. Acad. Sci. U.S.A.* **91**, 123 (1994).
18. K. L. Johnson, D. K. Zhen, D. W. Bianchi, *Biotechniques* **29**, 1220 (2000).

19. This work was supported by a grant from the Juvenile Diabetes Research Foundation. We thank M. Levisetti and K. Polonsky for valuable suggestions and critical reading of the manuscript.

Supporting Online Material

www.sciencemag.org/cgi/content/full/311/5768/1778/DC1
Materials and Methods
Figs. S1 to S6
References

6 December 2005; accepted 10 February 2006
10.1126/science.1123500

Synergistic Antitumor Effects of Immune Cell-Viral Biotherapy

Steve H. Thorne,[1] Robert S. Negrin,[2] Christopher H. Contag[1]*

Targeted biological therapies hold tremendous potential for treatment of cancer, yet their use has been limited by constraints on delivery and effective tumor targeting. We combined an immune effector cell population [cytokine-induced killer (CIK) cells] with an oncolytic viral therapy to achieve directed delivery to, and regression of, tumors in both immunodeficient and immunocompetent mouse models. Preinfection of CIK cells with modified vaccinia virus resulted in a prolonged eclipse phase with the virus remaining hidden until interaction with the tumor. Whole-body imaging revealed that the cells retained their ability to traffic to and to infiltrate the tumor effectively before releasing the virus. These results illustrate the potential of combining biotherapeutics for synergistic effects that more effectively treat cancer.

A variety of immune cell–based cancer therapies have been proposed, many of which rely on the identification of tumor-associated antigens that are often weakly expressed on only a subset of tumor cells. Cytokine-induced killer (CIK) cells are a population of cells derived from human peripheral blood or mouse splenocytes after ex vivo expansion with interferon-γ, CD3-specific antibody, and interleukin-2 (*1*, *2*). They bear phenotypic markers of natural killer (NK) and T cells, express the receptor natural killer group 2D (NKG2D), and are not major histocompatibility complex (MHC)–restricted. Instead, they mediate killing of tumor cells through recognition of a class of stress-associated ligands expressed on the tumor cell surface (NKG2D ligands) (*3*). CIK cells, therefore, do not rely on one antigen. They have been shown to target a variety of tumors and can exert their cytotoxic effects following systemic delivery (*4*). Previous imaging studies in mice showed that, by 72 hours after intravenous delivery, CIK cells were localized primarily at the tumor site (*4*).

We reasoned that we could further functionalize the CIK cells by combining them with the enhanced tumor-killing capabilities of oncolytic viruses. Oncolytic viruses are replication-selective, or tropism-modified, viruses that complete a successful infection cycle only within transformed cells (*5*). The early success and lessons learned from first-generation adenovirus-based vectors, notably ONYX-015 (*6*), have led to the development of alternative oncolytic vectors based on other well-studied viruses, including

[1]Departments of Pediatrics, Radiology, Microbiology, and Immunology and [2]Department of Medicine and Division of Bone Marrow Transplantation, Stanford University School of Medicine, Stanford, CA 94305, USA.

*To whom correspondence should be addressed. E-mail: ccontag@cmgm.stanford.edu

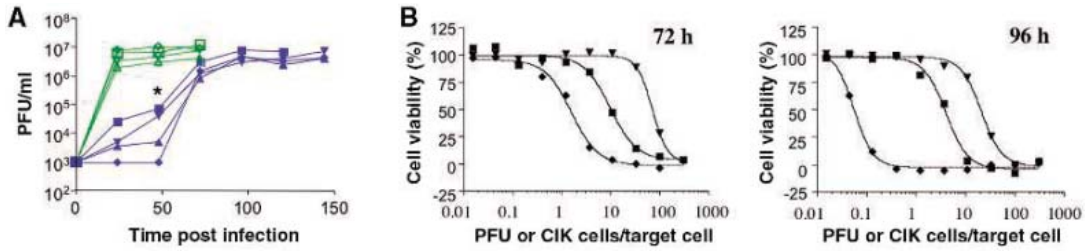

Fig. 1. Vaccinia virus displays unusual replication kinetics and increased cytopathic effect in human CIK cells. (**A**) Viral replication was followed for different vaccinia strains [WR (parental strain) (■); WR TK⁻ (▲); WR VGF⁻ (▼); vvDD (♦)] in human CIK cells (blue lines) and OCI-ly8 cells (human lymphoma, green lines) after infection at a multiplicity of infection (MOI) of 1.0 plaque-forming units (PFUs) per cell (* burst WR relative to vvDD in CIK; $P = 0.034$, t test). (**B**) Cytopathic effect on UCI-101 human ovarian cancer cell monolayers was measured in a cell viability assay at 72 and 96 hours after addition of different doses of human CIK cells (▼), vvDD (■), or preinfected CIK cells (♦). The replication of vaccinia in CIK is delayed, and preinfected CIK cells are more tumoricidal than either agent alone.

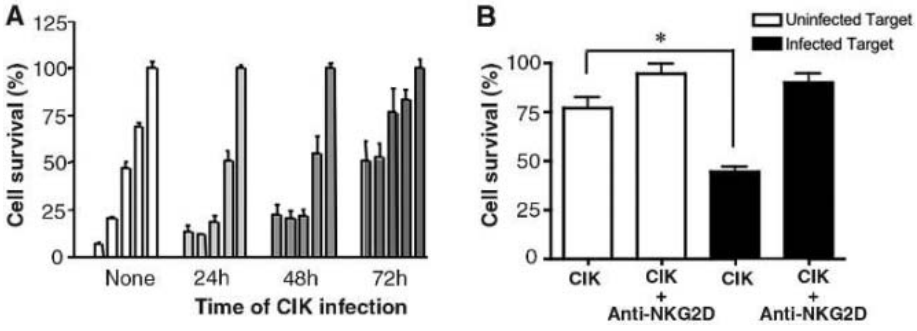

Fig. 2. In vitro interactions between human CIK cells, vvDD, and tumor cells. (**A**) Effects of preinfection on the cytolytic ability of CIK cells. UCI-101 target human ovarian tumor cells expressing luciferase were mixed with different numbers of CIK effector cells (ratios of 100:1, 50:1, 20:1, 10:1, and target only; left to right). CIK effector cells were uninfected (none) or preinfected with vvDD for 24, 48, or 72 hours. Luciferase output was measured as an indication of target cell survival after 4 hours. (**B**) Infected tumor cells display increased susceptibility to CIK cell killing. SKOV-3 target human ovarian tumor cells expressing luciferase, alone or preinfected with vvDD for 24 hours, were mixed with CIK cells at effector:target ratios of 20:1. In some experiments, CIK cells were premixed with NKG2D-blocking antibody. Luciferase signal was measured after 8 hours (*$P = 0.0076$, t test; error bars, SEM). Infected targets are killed more effectively by CIK cells; this success appears to be mediated by NKG2D on CIK cells and recognition of its ligands on the tumor target.

strains of poxviruses, such as vaccinia virus (*7*). Vaccinia, unlike most viruses proposed for use in virotherapy, has the advantage of systemic delivery potential and has a long history of use in humans, both during the smallpox eradication campaign and also as a tumor vaccine and oncolytic agent (*8*). However, because the virus infects many different cell types, only a small fraction of the inoculum of any strain used for virotherapy may reach the tumor, and this is likely to be further reduced in previously vaccinated individuals. Therefore, development of an effective means of delivering oncolytic viruses to tumor targets is needed. Here, using syngeneic and xenograft mouse models, we investigate the efficacy of a clinically relevant dual biotherapy that combines immune cell–mediated systemic delivery with the oncolytic ability of viruses.

We first determined the replication kinetics in human CIK cells of selected vaccinia virus strains and their parental strain (Western Reserve, WR). In contrast to the rapid and lytic replication seen in other cell lines such as the human lymphoma OCI-ly8 (Fig. 1A), all vaccinia strains displayed a two-step growth curve in CIK cells, with an initial extended eclipse period of slow replication followed by a rapid burst of replication 48 to 72 hours after infection. Poxviruses have been proposed to spread systemically after initial infection both as free virus and within infected hematopoietic cell populations (secondary viremia) (*9*), and these unusual replication kinetics may be characteristic of such spread. Deletion of the viral thymidine kinase (TK) gene restricts viral replication to cells in the G_2 and S phases of the cell cycle, during which the cells have elevated, compensatory levels of TK (*10*, *11*), and to cancer cells, where TK activity is constitutively high (*12*). TK-deleted vaccinia replicated both in the CIK cultures, where cell division was stimulated, and in tumor cells (Fig. 1A). The vaccinia viral growth factor (VGF) gene product promotes host cell growth after secretion from infected cells, by interacting with cellular growth factor receptors (*13*). VGF deletions restrict viral replication to cells with mutations in the Ras/mitogen-activated protein kinase/extracellular signal–regulated kinase (Ras/MAPK/ERK) pathway (*14*), offering additional tumor selectivity, while having a minimal effect on viral replication in CIK cells, which do not express growth factor receptors (Fig. 1A). A high degree of tumor selectivity, in culture and in vivo, has been demonstrated for a double-deleted vaccinia virus (vvDD) containing deletions in both TK and VGF (*15*). CIK cultures infected with vvDD produced almost no virus during the first 48 hours (Fig. 1A and fig. S1). Infection of human or mouse CIK cells with vvDD did not affect the expression of CIK phenotypic markers [CD3 and CD16/CD56 (human) or DX5 (mouse)] or NKG2D levels (fig. S2). In addition, infected CIK cells did not appear to present vaccinia antigens on their surface and were unaffected in their ability to produce interferon-γ (fig. S2). These data support the potential of CIK cells as carrier vehicles to deliver oncolytic vvDD to tumors.

We next investigated the interactions between CIK and tumor cells when either was infected with virus. vvDD-infected human CIK cells were highly effective for destroying human ovarian tumor cell monolayers in vitro (Fig. 1B), with a burst of cell killing between 72 and 96 hours after treatment. This correlated with the dispersal of virus from CIK cells onto the tumor cells instead of the slower cell-to-cell spread and plaque formation seen with virus alone (fig. S1B). When infected, CIK cells also retained their ability to kill the tumor targets (Fig. 2A).

CIK cells recognize NKG2D ligands on target cells (*3*), which are usually up-regulated under conditions of cellular stress, such as those encountered in the tumor microenvironment or after viral infection (*16*). Two of the best characterized NKG2D ligands in humans are MHC class I polypeptide-related sequences A and B (MICA and MICB) (*17*, *18*). We found that the surface expression levels of these proteins in the tumor cells directly correlated with their sensitivity to CIK cell–mediated killing (fig. S3). Furthermore, infection of the SKOV-3 cell line with vvDD virus resulted in an increase in the percentage of cells expressing MICA or MICB and increased the sensitivity of this

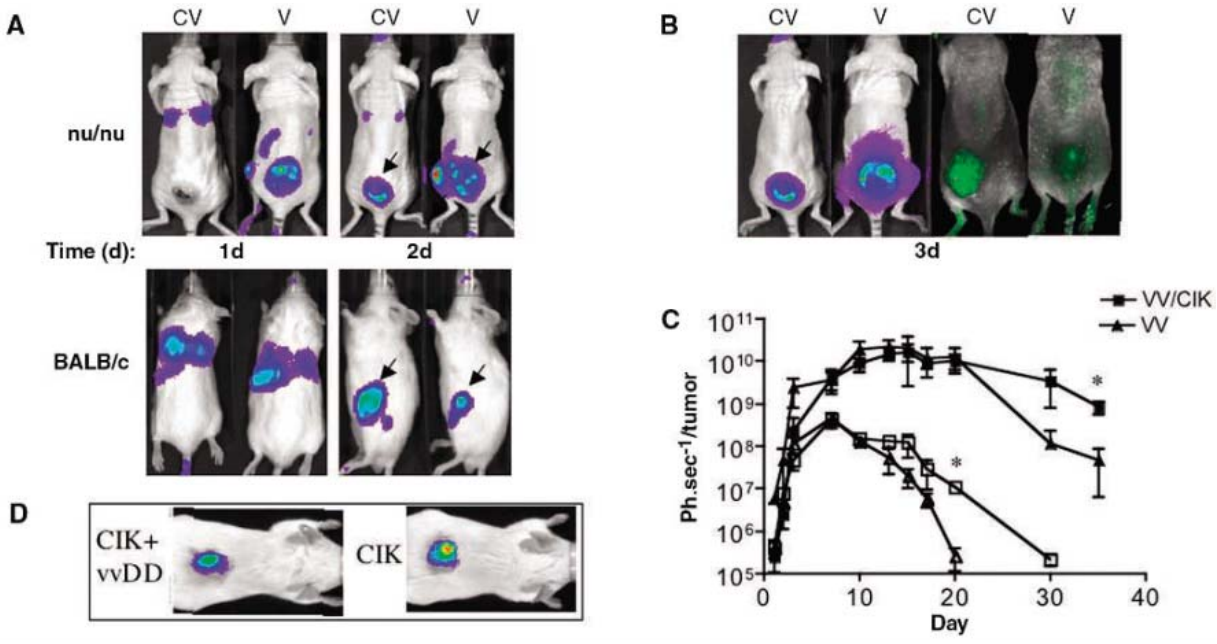

Fig. 3. Efficient trafficking of infected CIK cells to tumors improves delivery of oncolytic viruses. (**A**) Mice on the right received vvDD virus encoding luciferase alone (1×10^7 PFU; denoted V) or on the right in preinfected CIK cells (1×10^7 cells preinfected with virus at a multiplicity of infection of 1.0, 2 hours before delivery; denoted CV) via tail vein injection on day 0. Mice were imaged at the times indicated (in days post therapy) using an IVIS200 system (Xenogen Corp., Alameda, CA). nu/nu mice bearing UCI-101 xenograft human ovarian tumors (top) received human CIK cells; BALB/c immunocompetent mice bearing 4T1 murine mammary tumors (bottom) received murine CIK cells (arrows point to tumors). (**B**) At day 3 after treatment, bioluminescent and fluorescent signals were imaged. Mice were treated as before, but some received vvDD encoding green fluorescent protein (right panels), and all were imaged using a spectral unmixing camera (Maestro, CRI Ltd., Woburn, MA) to detect fluorescent signals and to demonstrate uniform distribution in tumors after viral delivery in CIK cells and nonuniform distribution in tumors where virus was given alone. (**C**) Quantification of bioluminescence output per tumor is plotted over time as an indication of viral gene expression for mice treated with vvDD or CIK cells preinfected with vvDD. Values are averages for three animals per group, error bars are SEM; $P = 0.0079$ for nu/nu mice (closed symbols) (day 35) and $P = 0.0089$ for BALB/c mice (open symbols) (day 20) (*t* test). (**D**) BALB/c mice bearing 4T1 murine mammary tumors were treated with murine CIK cells labeled with Cy5.5 dye, alone or after vvDD preinfection. Fluorescence imaging 72 hours after tail delivery was performed using an IVIS200 system. CIK-mediated delivery was more uniform than virus only, and preinfection did not prevent CIK trafficking to tumors.

otherwise resistant tumor cell to CIK-mediated killing ($P = 0.0076$), an effect that was reversed by addition of NKG2D-blocking antibody (Fig. 2B).

To investigate the in vivo trafficking of preinfected CIK cells to tumors and the subsequent biodistribution of virus, we used noninvasive optical imaging. Human CIK cells were used in immunodeficient mice with xenografts of human ovarian tumors, and murine CIK cells were used in immunocompetent mice with murine breast cancers. Although vaccinia replicates to significantly lower levels in mouse cells, the immunocompetent models allow the study of trafficking in the presence of an intact immune system. Luciferase-labeled vvDD and bioluminescence imaging revealed the distribution and duration of viral gene expression (Fig. 3). At 24 hours after injection, we observed the same pattern of viral gene expression within the lung, liver, and spleen, regardless of viral delivery method. However, the ratios were different. Virus delivered alone produced signal predominantly in the spleen, whereas virus within CIK cells produced signal predominantly in the lungs. Although the systemic delivery potential of vaccinia to tumors has been described previously (*15*, *19*), we observed a delay in detectable tumor signal following intravenous delivery of virus alone in immunocompetent mice compared with immunodeficient animals. By comparison, the use of preinfected CIK cells to deliver virus to the tumor resulted in the same patterns of viral biodistribution regardless of immune status or species of CIK origin (Fig. 3, A and B), with very little virus detected in any organ other than the tumor by 48 hours after treatment. The two delivery methods produced equivalent levels of viral gene expression from the tumor by 3 days after treatment (Fig. 3, B and C). Signals in the immunocompetent mice were weaker and began to decline earlier because of poor replication in murine cell lines and clearance by the immune response. Signal from CIK cell–delivered virus was sustained within the tumor for longer periods of time compared with signals for virus alone (Fig. 3C).

Labeling of CIK cells, by conjugation to a fluorescent dye (Cy5.5) or with luciferase, before intravenous delivery enabled visualization of cells at the tumor site (Fig. 3D and fig. S4). Preinfection with vvDD did not affect the trafficking of CIK cells to syngeneic or xenograft tumor models, confirming that the CIK cells carry the virus to the tumor. When mice bearing CIK-resistant SKOV-3 tumors were treated, accumulation of CIK cells was not observed in the tumor unless they were infected with vvDD virus (fig. S4), and this accumulation was found to colocalize to regions of the tumor where MICA or MICB had been up-regulated by vvDD infection (fig. S5). Also, it was found that, whereas vvDD delivered alone initially infected only tumor cells surrounding the vasculature, vvDD-infected CIK cells were capable of carrying the virus into the tumor mass and away from the vasculature (fig. S6). This produced more uniform distribution of viral infection within the tumor, which would likely contribute to sustained viral gene expression and increased tumor destruction in vivo.

To investigate the in vivo efficacy of the combination therapy, we first treated immunodeficient mice bearing xenografts of human ovarian tumor cell lines (Fig. 4A). Mice bearing established peritoneal tumors were treated with a single tail vein injection of each therapy. CIK cells alone were able to extend the median survival of mice bearing UCI-101 tumors by 8 days but had no effect on mice bearing the CIK-resistant SKOV-3 tumors. vvDD virus alone

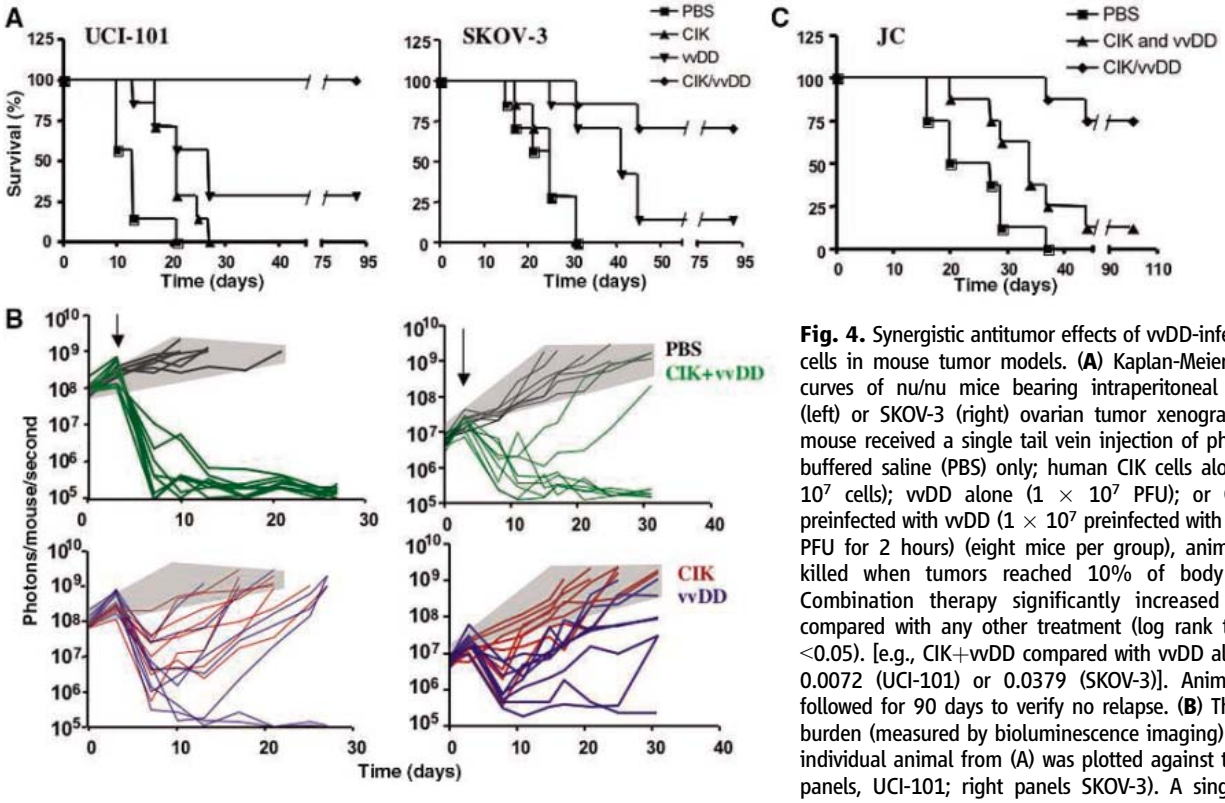

Fig. 4. Synergistic antitumor effects of vvDD-infected CIK cells in mouse tumor models. (**A**) Kaplan-Meier survival curves of nu/nu mice bearing intraperitoneal UCI-101 (left) or SKOV-3 (right) ovarian tumor xenografts. Each mouse received a single tail vein injection of phosphate-buffered saline (PBS) only; human CIK cells alone (1×10^7 cells); vvDD alone (1×10^7 PFU); or CIK cells preinfected with vvDD (1×10^7 preinfected with 1×10^7 PFU for 2 hours) (eight mice per group), animals were killed when tumors reached 10% of body weight. Combination therapy significantly increased survival compared with any other treatment (log rank test; $P = <0.05$). [e.g., CIK+vvDD compared with vvDD alone; $P = 0.0072$ (UCI-101) or 0.0379 (SKOV-3)]. Animals were followed for 90 days to verify no relapse. (**B**) The tumor burden (measured by bioluminescence imaging) for each individual animal from (A) was plotted against time (left panels, UCI-101; right panels SKOV-3). A single intravenous treatment was delivered on day 3 (arrows). Gray shaded area indicates range of tumor burden for the PBS-treated group. (**C**) Survival curves of immunocompetent BALB/c mice bearing murine breast cancer JC tumors (implanted into the fat pad, treated when 50 to 100 mm^3) after a single intravenous treatment with PBS alone; both murine CIK cells and vvDD were delivered separately; versus CIK cells preinfected with vvDD. The last-mentioned therapy significantly increased survival compared with the two therapies delivered separately ($P = 0.0046$) and control animals ($P < 0.0001$) (log rank test).

also increased median survival in both mouse models (by 15 to 16 days), with some animals (<30%) showing complete responses (Fig. 4A). In contrast, the combination therapy produced significantly increased survival compared with either therapy alone ($P < 0.01$). Mice bearing UCI-101 tumors showed a 100% complete response rate. The combination therapy also displayed a 62% increase in complete responses against SKOV-3 tumors compared with just the vvDD vector ($P = 0.0379$), despite the fact that the CIK cells alone had no effect against these tumors. Plots of the tumor burden in individual animals (Fig. 4B) indicated that single vvDD or human CIK cell therapy against sensitive tumors produced an initial response but that the tumors subsequently relapsed. Mice with complete responses were followed for up to 90 days with no evidence of tumor relapse or any toxicities attributable to the therapy. As the immune response is a major limitation to the delivery of viruses to tumors, the same experiment was repeated in immunocompetent mice bearing murine breast cancers. Mice bearing breast adenocarcinoma JC tumors implanted into the mammary fat pad (tumors 50 to 100 mm^3) were either treated with a single tail vein injection of preinfected CIK cells or with both CIK cells and vvDD delivered separately but on the same day (Fig. 4C). One mouse (of eight) treated with the individual therapies showed a complete response, whereas mice treated with preinfected CIK cells showed a much higher incidence of complete response (six out of eight), which demonstrated that preinfection is essential for the synergistic effects of the combined therapy. Similar results were seen in immunocompetent mice bearing the highly aggressive 4T1 mammary tumor cell lines (fig. S7). Although less than half the U.S. population has been vaccinated against smallpox, and most vaccinations took place over 30 years ago, there is evidence that immunity is long-lasting (*20*), and this may limit the effectiveness of this therapy. However, immunity is measured against naked virus, and so it is possible that infected CIK cells, which do not appear to present viral antigens (fig. S2B), may evade an immune response.

In conclusion, the benefits of exploiting naturally occurring biological phenomena in the treatment of disease are well known. Here we exploit the ability of certain viruses to conceal themselves within hematopoietic cells in order to take advantage of natural tumor trafficking of some immune cells to deliver a virus efficiently to the tumor. Cole *et al.* (*21*) recently reported that T cells targeted to an artificial antigen could deliver a nonreplicating, retroviral gene therapy vector to a tumor transformed to express the target antigen, which demonstrated the use of immune cells to deliver agents to tumor targets. However, because the therapeutic use of cells with a specific T cell receptor has been limited by a lack of suitable tumor antigens and the ability of many tumors to inhibit T cell activity (*22*) and because retroviral gene therapy vectors have been withdrawn from clinical trials after insertional mutagenesis led to serious adverse events (*23*), the clinical utility of this approach is unclear. Each of the therapies in the current report has shown some success in the clinic (*24*, *25*), and their demonstrated synergy now offers the potential of a targeted, biological therapy with systemic delivery, minimal toxicities and significant antitumor effects that could translate directly to the treatment of patients.

References and Notes

1. P. H. Lu, R. S. Negrin, *J. Immunol.* **153**, 1687 (1994).
2. J. Baker, M. R. Verneris, M. Ito, J. A. Shizuru, R. S. Negrin, *Blood* **97**, 2923 (2001).
3. M. R. Verneris, M. Karami, J. Baker, A. Jayaswal, R. S. Negrin, *Blood* **103**, 3065 (2004).
4. M. Edinger *et al.*, *Blood* **101**, 640 (2003).
5. D. Kirn, R. L. Martuza, J. Zwiebel, *Nat. Med.* **7**, 781 (2001).
6. C. Heise *et al.*, *Nat. Med.* **3**, 639 (1997).
7. S. H. Thorne, T. Hermiston, D. Kirn, *Semin. Oncol.* **32**, 537 (2005).
8. S. H. Thorne, D. H. Kirn, *Expert Opin. Biol. Ther.* **4**, 1307 (2004).

9. R. M. Buller, G. J. Palumbo, *Microbiol. Rev.* **55**, 80 (1991).
10. R. M. Buller, G. L. Smith, K. Cremer, A. L. Notkins, B. Moss, *Nature* **317**, 813 (1985).
11. M. Puhlmann *et al.*, *Cancer Gene Ther.* **7**, 66 (2000).
12. M. Hengstschlager *et al.*, *J. Biol. Chem.* **269**, 13836 (1994).
13. R. M. Buller, S. Chakrabarti, B. Moss, T. Fredrickson, *Virology* **164**, 182 (1988).
14. A. A. Andrade *et al.*, *Biochem. J.* **381**, 437 (2004).
15. J. A. McCart *et al.*, *Cancer Res.* **61**, 8751 (2001).
16. J. A. Hamerman, K. Ogasawara, L. L. Lanier, *Curr. Opin. Immunol.* **17**, 29 (2005).
17. S. Bauer *et al.*, *Science* **285**, 727 (1999).
18. V. Groh *et al.*, *Nat. Immunol.* **2**, 255 (2001).
19. Y. A. Yu *et al.*, *Nat. Biotechnol.* **22**, 313 (2004).
20. E. Hammarlund *et al.*, *Nat. Med.* **9**, 1131 (2003).
21. C. Cole *et al.*, *Nat. Med.* **11**, 1073 (2005).
22. G. P. Dunn, A. T. Bruce, H. Ikeda, L. J. Old, R. D. Schreiber, *Nat. Immunol.* **3**, 991 (2002).
23. S. Hacein-Bey-Abina *et al.*, *Science* **302**, 415 (2003).
24. T. Leemhuis, S. Wells, C. Scheffold, M. Edinger, R. S. Negrin, *Biol. Blood Marrow Transplant.* **11**, 181 (2005).
25. M. J. Mastrangelo *et al.*, *Cancer Gene Ther.* **6**, 409 (1999).
26. We thank W. Liang, L. Howe, and T. Doyle for their help with cell and animal imaging; J. Chan for cell lines; D. Bartlett for virus strains, Y.-A. Cao for retroviral vectors, and R. Critchley-Thorne and S. Schultz for help with the immunofluorescence microscopy studies. Supported by grants; NIH Small Animal Imaging Resource Program (SAIRP; R24 CA 92862), the Stanford Program Project Grant for Bone Marrow grafting for leukemia and lymphoma (P01 CA49605), the Molecular and Cellular Imaging Centers (ICMIC; P50 CA114747), and the John A. and Cynthia Fry Gunn Research Fund. All animal studies were performed according to Stanford University's Institutional Animal Care and Use Committee (IACUC)–approved protocols.

Supporting Online Material

www.sciencemag.org/cgi/content/full/311/5768/1780/DC1
Materials and Methods
Figs. S1 to S7
Reference

17 October 2005; accepted 2 March 2006
10.1126/science.1121411

Conical Tube Centrifuge Adapter

A new adapter spins 50-ml conical tubes in the Allegra X-15R and X-12 series benchtop centrifuges. The new adapter accommodates 28 tubes per run in a BioCertified, self-balancing rotor and is suitable for cell harvesting and blood separation applications. The adapter runs at up to 5,250 × g in the Aries 4 × 750 mL self-balancing rotor, which detects and automatically corrects for imbalance, continuing the run without shutdown.

Beckman Coulter For information 800-742-2345 www.beckmancoulter.com

Small Nucleic Acid PAGE

ElectroSNAP is a proprietary acrylamide buffer blend that is a convenient solution to everyday polyacrylamide gel electrophoresis (PAGE) of small-size DNA and RNA (> 20 bp). ElectroSNAP is mainly used in the preparation of polyacrylamide gels that can be used in routine analysis of polymerase chain reaction (PCR) products, for monitoring nuclease and ligase reactions, and for the chemical modification of oligonucleotides, analysis, and small-scale purification of nucleotide from mixtures of oligonucleotides. ElectroSNAP is formulated to resolve even smaller oligonucleotides and nucleic acid fragments using lower concentrations of polyacrylamide gels that tris-borate-EDTA (TBE), a commonly used buffer for nucleic acid analysis.

Amresco For information 800-448-4442 www.amresco-inc.com

Yeast Transformation Kit

A rapid, single-step yeast transformation kit takes less than 10 min to prepare competent yeast cells. The cells can be used immediately or frozen for up to one year. The kit is suitable for both circular and linear plasmid transformations and has a high transformation efficiency, producing about 10^6 transformations per microgram of circular DNA. The kit covers a broad spectrum of yeasts.

Genotech For information 314-991-6034 www.genotech.com

Genome Amplification

The GenomePlex Whole Genome Amplification (WGA) family of products has two new additions: the GenomePlex Complete WGA Kit and the GenomePlex WGA Reamplification Kit. The kits are designed to meet researchers' needs for increased amplification accuracy and preserving precious source material. The GenomePlex Complete WGA Kit contains an optimized enzyme that provides increased accuracy in amplification by producing no amplicon in the negative control reactions. Assays using the kit provide results showing complete representation of the entire genome with no detectable allele bias. The Reamplification Kit allows subsequent reamplifications of the initial whole genome amplification product. The successive reamplification process provides microgram quantities of DNA with little genetic bias when compared with the original genome.

Sigma-Aldrich For information 800-521-8956 www.sigma-aldrich.com

MicroRNA Detection

The miRCURY Arrays are for sensitive profiling of microRNAs in human, mouse, and rat. The miRCURY Array product allows for microRNA expression profiling in samples down to 1 μg of labeled total RNA. The miRCURY product series also includes the miRCURY Array Labeling Kit for direct labeling of microRNAs from total RNA. The kit provides microRNA labeling on as little as 1 μg of total RNA in 1.5 hours. The labeling kit includes one or two colors for comparative experiments and provides uniform, sequence-independent labeling.

Exiqon For information 45 45 65 04 20 www.exiqon.com

Confocal Imager

The ImageXpressUltra is a high-speed, laser-scanning, confocal imager. The benchtop system features up to four configurable solid-state lasers. Its throughput and resolution are comparable to larger, more expensive confocal commercial systems. It is available with a robotic plate handling option for high-throughput image-based screening. The ImageXpressUltra system complements the ImageXpressMicro wide-field charge-coupled device imager, both of which are controlled by the new MetaXpress Acquisition software and integrated into the modular image analysis and cellular informatics software, AcuityXpress.

Molecular Devices For information 408-548-6344 www.moleculardevices.com

shRNA Libraries

The Mission TRC shRNA (small hairpin RNA) library line has been expanded to include purified plasmid DNA in addition to the previously released frozen bacterial glycerol stock format. This new format of the lentiviral-based shRNA clones, which target human and mouse genomes for RNA interference-mediated gene silencing, will save researchers time and expense in purifying transfection-quality plasmid DNA.

Sigma-Aldrich For information 314-286-7626 www.sigma-aldrich.com

Newly offered instrumentation, apparatus, and laboratory materials of interest to researchers in all disciplines in academic, industrial, and government organizations are featured in this space. Emphasis is given to purpose, chief characteristics, and availability of products and materials. Endorsement by *Science* or AAAS of any products or materials mentioned is not implied. Additional information may be obtained from the manufacturer or supplier by visiting www.science.labvelocity.com on the Web, where you can request that the information be sent to you by e-mail, fax, mail, or telephone.

TaKaRa

CELL BIOLOGY

Accurately Measure Your Toxicity Level

LDH Cytotoxicity Detection Kit

The LDH Cytotoxicity Detection Kit is a simple, sensitive, non-radioactive assay which measures cell viability. It is based upon the measurement of lactate dehydrogenase (LDH) released by damaged cells into the cell culture supernatant. With this kit, LDH present in the culture supernatant participates in a coupled reaction converting yellow tetrazolium salt (INT) into red formazan product. The amount of enzyme activity, measured as absorbance using a microplate reader at 490/492 nm, correlates to the number of damaged cells in the culture.

- **Measures LDH Enzymatic Activity:** from damaged cells.
- **Accurate Correlation:** between the number of damaged cells and kit results.
- **Detects Low Cell Numbers:** (i.e. 0.2-2 x 10^4 cells/wells).

Premix WST-1 Cell Proliferation Assay System

The Premix WST-1 Cell Proliferation Assay System allows fast and easy colorimetric measurement of cell proliferation and viability of cells cultured in 96-well plates. This system provides a non-radioactive and spectrophotometric method of determining cell proliferation and viability without harvesting or washing steps, and can be performed in a single multi-well plate.

- **Convenient:** no washing steps or harvesting.
- **Accurate:** conversion of tetrazolium salt strongly correlates with metabolic activity.
- **Sensitive:** low cell numbers can be used.
- **Fast:** multiple plate reads over several time points.

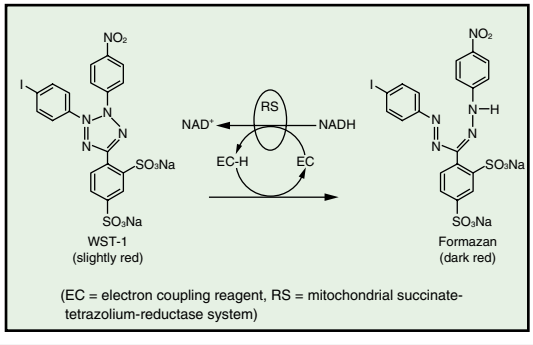

The Premix WST-1 Cell Proliferation Kit uses a colorimetric change from WST1 to Formazan to detect cell proliferation and viability.

EC = electron coupling reagent RS = mitochondrial succinate-tetrazolium-reductase system

TAKARA BIO INC.
The Biotechnology Company™

Otsu, Shiga, Japan
Phone: +81 77-543-7247
Fax: +81 77-543-9254

USA: Takara Mirus Bio Inc. Phone: 888-251-6618 • www.takaramirusbio.com
Europe: Takara Bio Europe S.A.S. Phone: +33 1 3904 6880 • www.takarabioeurope.com
Korea: Takara Korea Biomedical Inc. Phone: +82 31 739 3300 • www.takara-bio.kr.com

For more information and a list of Takara distributors worldwide, please visit our website today!

www.takara-bio.com

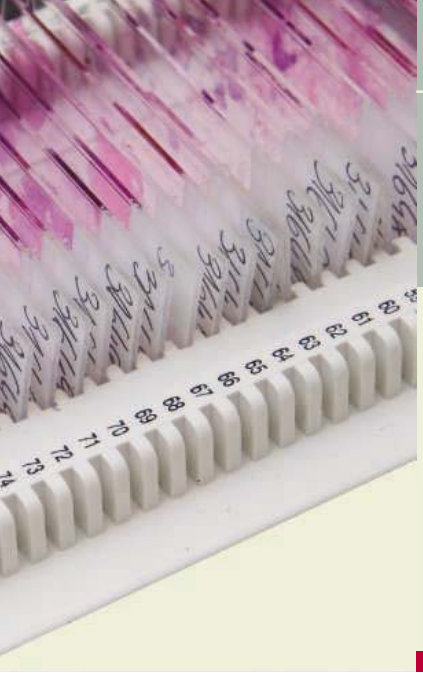

Life Science Technologies

Cell Signaling in Cancer Research

SEEKING NEW BATTLE PLANS

To fight cancerous cells, scientists continually seek new strategies. Some of the latest treatments target specific cancerous cells for destruction, thereby leaving healthy cells less affected. In other cases, new therapies starve cancerous cells. Many of these approaches depend on understanding how signals control and—hopefully—can be commandeered to contain the division of cancerous cells. **by Mike May and Gary Heebner**

Cancer continues to cause a major public health crisis. According to the **World Health Organization**'s statistics: more than 11 million new cases of cancer are diagnosed every year, and it accounts for seven million deaths annually, which makes up 12.5 percent of all deaths worldwide. By 2020, the WHO estimates that 16 million new cases of cancer will appear annually. In spite of the increase in cancer incidence, the National Cancer Institute's late-2005 biannual update indicates decreases in deaths from some forms of cancer: breast, colorectal, lung, and prostate.

In industrialized countries, the increasing age of the population accounts for much of the growth in cancer diagnoses. In addition, Robert A. Weinberg, the Daniel K. Ludwig and American Cancer Society Professor for Cancer Research at the **Massachusetts Institute of Technology**, says, "The number of cases is also an artifact—the more you look, the more you find." The good news is that "the age-adjusted death rate from cancer [i.e., per 100,000 population] is declining with the exception of tobacco-related cancers," says Weinberg.

Whatever causes the number of people diagnosed with cancer to grow, the cancer therapeutic market grows with it. According to **IMS Health**, drug sales for cancer treatments are expected to more than double in the next five years. That could make oncology therapeutics the fastest-growing drug sector, according to **RBC Capital Markets**.

The key, though, to fighting cancer through better therapeutics depends on a better understanding of the basic biology of this disease. "The major challenge in cancer research is pinpointing causes of cancer on a molecular level," says Bernhard Zimmermann, head of product management of the advanced imaging microscopy division at **Carl Zeiss**. "One needs a good understanding of signaling pathways, because that is the ultimate basis to designing more specific drugs or vaccines."

Inclusion of companies in this article does not indicate endorsement by either AAAS or *Science*, nor is it meant to imply that their products or services are superior to those of other companies.

Causes of Cancer

A variety of causes generate cancer, according to Weinberg. Cancer incidence can be affected by lifestyle choices, such as using tobacco products, and obesity, which comes from too many calories and too little exercise. There can also be heritable—or genetic—causes of cancer. "To a very small, extent," says, Weinberg, "cancer can come from environmental pollution, but that is very minimal."

No matter what causes cancer, though, it involves cell signaling at some level. Alan Barge, vice president of clinical oncology at **AstraZeneca**, says, "All cancer cells derive an advantage because they either dysregulate, upregulate, or disinhibit pathways that give these cells a proliferate advantage." He adds, "Signaling is mechanistically involved in any growth advantage."

Fighting this disease depends on many factors. "The fundamental challenge continues to be the translation of the numerous discoveries of the last two decades about malfunctioning signals into effective anticancer drugs," says Weinberg. Knowing where to go next, however, can prove difficult. Still, Weinberg believes that drugs that target specific proteins and antibodies that neutralize angiogenic factors are some of the most promising potential therapies ahead.

Selecting Cells

To study cancer, investigators need the right materials—to either watch the normal progression of a tumor or to expose it to potential therapeutics and examine the effects on its growth. This type of work often involves cell culture and specific cancer cell lines. For culture media, researchers can turn to many companies, including **Cambrex**, **HyClone**, **Mediatech**, and **Sigma-Aldrich**. For cell lines, scientists can find many types from **ArtisOptimus**, **ATCC**, Cambrex, and **Clontech** (a division of Takara Bio). **continued ›**

IN THIS ISSUE:

Life Science Technologies: CELL SIGNALING IN CANCER RESEARCH

D.G. Ferneyhough, marketing segment manager of the cell biology business unit at Cambrex, says, "Some cancers are very heterogeneous. The bottom line is that researchers want a model system that represents the disease."

Cambrex not only offers a wide range of cell culture media and reagents but also markets its Clonetics Skin Cell Systems and Models. "A cell system means a primary cell and a media culture system that is designed to make that cell act, in many ways, like it does in vivo," says Ferneyhough. "Our cell systems provide cells that perform to a certain set of specifications—month after month, year after year." Building consistency into a cell system depends on many variables. Mark Powers, senior research and development project group leader at Cambrex, says, "For cells in culture, the environment—chemical and physical—is extremely important. Cancer cells behave differently in different environments, even based on nearby cytokines and oxygen levels. So we try to recreate that in vitro."

For the Clonetics Skin Cell Systems, Cambrex offers various cell types: keratinocytes, dermal fibroblasts, and melanocytes. Powers says, "These are the basic components of skin that researchers can probe individually." Ferneyhough adds, "Some researchers use our cells to make more complex skin models. Potentially, those could be used to understand issues like UV [ultraviolet damage], or looking for molecules that would protect against UV damage."

Observing Carcinomas

To fight cancer, investigators probe continually deeper into the mechanics of this disease. That often involves microscopy. As Zimmermann explains, "Microscopy has a long history in accompanying surgery. A surgeon takes a biopsy, and then a pathologist examines the sample microscopically for disease." Such examinations play a fundamental role in treating cancer. Likewise, microscopy impacts basic cancer research. Several manufacturers—including Carl Zeiss, **Leica**, **Nikon**, and **Olympus**—have been designing and producing light microscopes for both research and clinical use for many years.

The keys to understanding cancer probably lie in microscopic, and submicroscopic, details. Zimmermann says, "When we talk about cancer or signaling pathways on cellular or organismal levels, it's critical to understand the underlying protein networks in cells, tissues, or organs." This, however, poses a tricky challenge. "These networks are very complex," says Zimmermann, "They are dynamic in space and in time. To understand the cause of a specific cancer, you need to know where and when things are happening and that is what microscopy provides." He adds that confocal microscopy delivers particularly good spatial resolution and that modern fluorescence labeling techniques add specificity, "letting you take virtually any protein and label it."

One of the newest confocal products from Zeiss is the LSM 5 LIVE. Zimmermann says, "The LSM 5 LIVE gives the three-dimensional resolution of a confocal microscope, dramatically improves sensitivity, and adds high speed image acquisition." He adds, "Some processes are so fast that you need millisecond time resolution or better, and the LSM 5 LIVE gives that." In addition, the LSM 5 LIVE DuoScan includes a second scanner, and this microscope provides sample manipulations. Zimmermann says, "Researchers can perform highly localized photomanipulation with this microscope. For example, you could use a laser to release biologically active substances in a sample and monitor the resulting reaction with extremely high spatiotemporal resolution."

In thinking of these microscopes related to cancer research, Zimmermann says, "I would argue that confocal microscopy is a basic tool in cancer research, a household technology." Just before being interviewed, Zimmermann searched Google Scholar for publications mentioning the LSM 510—another Zeiss confocal microscope—and cancer or carcinoma, and he got almost 3,000 hits, many of them from just the past few years.

Following Phosphorylation

To really follow cancer-related networks of interactions, investigators need ways to mark specific molecules. In some cases, scientists even need to mark molecules in ways that reveal the entity's state, such as being phosphorylated. Such studies depend on a wide range of antibody reagents that come from a variety of companies, including **Alexis Corporation**, **BD Biosciences**, **Biomol**, **Cell Signaling Technology**, **Chemicon**, **EMD Biosciences**, Sigma-Aldrich, and **Upstate**. continued ›

Summarizing the Signals

The **Signal Transduction Knowledge Environment** (STKE) website brings together a wide range of information. Bryan Ray, senior editor at *Science*, says, "In some ways, it is like an electronic review journal, but it is more than that. It features original reviews, perspectives, and protocols." This site also provides subscribers with alerts, saved searches, and other features. For example, Ray says, "In 'This Week in Signal Transduction,' the editors scan the journals published that week and present short summaries of the highlights." This site also provides useful sections that are free, including Teaching Resources and Connections Maps, which is a database that gives graphical displays of signaling pathways and links those to information about various components. These maps will continue to grow. As Ray says, "Signaling research is hot and shows no signs of cooling off."

HTTP://STKE.SCIENCEMAG.ORG/

Receive a free TaqMan® Low Density Array Upgrade and 20 Free TaqMan® Array cards*
Visit 7900HT.com to learn more.

Proven Performance in Labs Everywhere. Customized for Yours.

Applied Biosystems 7900HT Fast Real-Time PCR System Meets Your Changing Needs.

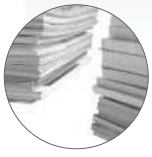

The gold standard in real-time PCR
Used by researchers all over the world and referenced in hundreds of journals, the Applied Biosystems 7900HT Fast Real-Time PCR System is the recognized gold standard in real-time PCR.

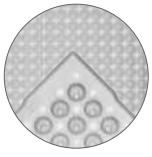

Interchangeable blocks
Configurable and highly flexible, the 7900HT Fast System offers user-interchangeable thermal cycling blocks, cycling times as low as 35 minutes and automated plate loading/unloading for higher throughput.

The world's largest collection of assays
Choose from over 2 million TaqMan® Gene Expression, Genotyping and miRNA Assays.

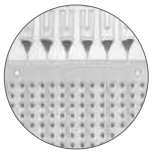

Easy, pre-loaded assays in a micro fluidic card format
For the ultimate in ease-of-use, order your assays pre-loaded in the 384-well TaqMan® Low Density Array.

To see how the 7900HT Fast System meets your changing research needs, visit www.7900HT.com

Applied Biosystems

25 YEARS
ADVANCING SCIENCE

* Receive a Low Density Array Upgrade and 20 Free TaqMan® Low Density Array cards with the purchase of an Applied Biosystems 7900HT Fast Real-Time PCR System. This offer cannot be combined with other promotions or discounts. Offer valid until March 31, 2006. Void where prohibited. This offer is for US customers only — International customers please inquire with your local sales office. Other restrictions may apply. All prices exclude any applicable delivery and/or local tax. Please contact your local Sales Representative for other details of this offer. http://www.7900HT.com

Life Science Technologies: CELL SIGNALING IN CANCER RESEARCH

In cancer, most of the mutations or defects impact the way that cells communicate with other cells. Roberto Polakiewicz, chief scientific officer at Cell Signaling Technology, says, "To study cell signaling, researchers need a variety of tools, depending on just what a study is doing. For example, genomics tools let you look directly at mutations or chromosomal abnormalities. This has been done forever." He adds, "Most people working in this field also need antibodies, and we pioneered the use of activation-site-specific antibodies, ones that recognize posttranslational modifications, like phosphorylation."

Cell Signaling Technology's antibodies reveal the activity of a molecule. Polakiewicz says, "Localizing enzyme activity tells you that something is happening in the molecule and tells you something about its function at that time." He adds, "Activation-specific antibodies speed up cancer research significantly." These antibodies can be applied to immunohistochemistry, for instance, to analyze a tumor biopsy, or flow cytometry to analyze leukemic cells. That could reveal that a pathway is "on" in an aberrant way and could be targeted by a drug. These antibodies could also be used in diagnostics, according to Polakiewicz.

Phosphorylation sites related to cancer can also be mapped through techniques on the verge of high throughput. Polakiewicz says, "In this way, tons of information and data can be applied to cell lines and tumors." He also mentions that Cell Signaling Technology always looks for new tools and biomarkers or kinases that get activated in cancerous cell lines or tumors.

Tony Ward, director of global and strategic marketing at BD Biosciences, agrees that scientists studying cancer need a collection of tools: the right cells, culture environments that make a cell behave as it would in vivo, and ways to make sure that the cells are performing as expected. He also points out that scientists need ways to look inside cells, such as using antibodies to search for specific proteins or watching the process of phosphorylation.

Ward says, "The biggest thing we have brought to the market in the past year and a half is our PhosFlow, which reveals the phosphorylation status of specific epitopes in an individual cell, whether from a cell line or from whole blood." He adds, "This lets scientists look at an activation pathway of a protein and measure the ratio of phosphorylation. In other words, you can ask: How turned on is a pathway?" For example, a scientist could apply a potential anticancer compound to a sample and see how it changes protein pathways thought to be related to the progression of that cancer.

Methlyation of so-called CpG islands—areas of increased density of guanine-phosphate diester-cytosine dinulceotides—also plays a role in cancer, because these islands are frequent sites of mutation. Scientists can study methylation of these islands with Qiagen's EpiTect Bisulfite Kit.

A Total Attack

Some companies focus primarily on products related to cancer research. For example, Jay George, chief scientific officer at **Trevigen**, says, "We are a cancer company." He adds, "We have antibodies, proteins, and tools to quantitatively measure angiogenesis. We also sell products to study and quantify DNA damage and repair, which are both intimately involved with cancer."

One of the latest products from Trevigen is a basement membrane extract. This is a specialized polymer of extracellular matrix, essentially proteins, that provides a support for cells to adhere to and then differentiate. The main components of the extract include laminin I, collagen IV, and entactin. This product has been used in assays for tumor-cell invasion, angiogenesis, and three-dimensional cell culture. These proteins can also be used to coat plastic ware to make it more amenable as a surface for cell growth. This is an important area because, as George says, "Growing cells on plastic is a very, very artificial system."

Moreover, Trevigen developed the Directed In Vivo Angiogenesis Assay, called DIVAA, in which scientists can study, for example, the development and support of blood vessel creation by tumors. This assay uses an angioreactor—licensed from the U.S. National Institutes of Health—that is a small silicone tube with basement membrane extract and growth factors in it. George says, "You can put this angioreactor in a mouse and then test a potential antiangiogenesis compound. Then, you can remove the reactor from the mouse and quantify the amount of blood vessel invasion."

Starving Tumors

As tumors grow, they require increasing vascularization to provide nutrients and eliminate cellular waste. The circulatory system within a tumor is produced and developed by the active recruitment of blood vessels from nearby normal tissue, which can be measured—as just mentioned—with an angioreactor. If compounds can be developed that inhibit this process and are specific to tumor cells, these agents can be used to shrink or eliminate the tumor without damaging normal tissue. AstraZeneca—among other companies—investigates the potential of agents that prevent the formation of new blood vessels and also attack established tumor blood vessels.

Barge of AstraZeneca explains: "Tumors could not grow beyond about one cubic millimeter in volume without parasitiz- continued ›

Look for these upcoming Life Science Technology articles

Proteomics	14 April
Biochips and Lab-on-a-Chip Devices	5 May
Pharmacogenomics	28 July
Mass Spectrometry	1 September
Functional Genomics	29 September
Aging and Neuroscience	6 October
Nanobiotechnology	3 November

Or, access recent articles at http://www.sciencemag.org/products/articles.dtl

Combinatorial and Computational Chemistry	17 March
Laboratory Automation	13 January

Explore the Store... and More!
Visit appliedbiosystems.com for web specials.

New! TaqMan® Low Density Array

Gene Signature Panels

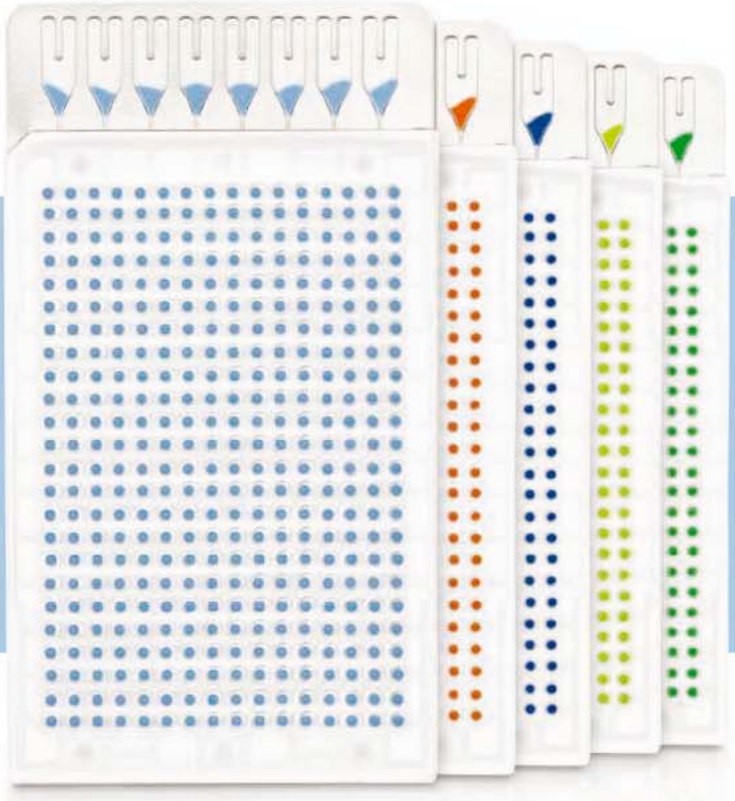

Human GPCR Panel
Drug discovery and pharmacogenomics research

Human Kinase Panel
Signal transduction and cellular pathways

Mouse Immune Panel
Cytokines, chemokines, interleukins and other antigen receptions

Human Immune Panel
Cytokines, chemokines, interleukins and other antigen receptions

Human Endogenous Controls Panel
A simple tool to select optimal controls for your studies

Real TaqMan® Assay performance in a real easy format

Get real-time PCR TaqMan® Assay performance in a convenient and affordable microfluidic card. With TaqMan® Low Density Array Gene Signature Panels, expert-selected assays are pre-loaded in a 384-well fixed panel, making them the easiest solution for screening hundreds of samples against these important gene sets. Designed for the 7900HT Fast Real-Time PCR System, you'll get highly reproducible results without liquid handling robotics or elaborate pipetting. And they're delivered in just a few days. Or, create your own signature by customizing a panel from over 40,000 TaqMan® Gene Expression Assays. Learn how you can get real-time PCR performance real easily at www.allgenes.com

Applied Biosystems

25 YEARS ADVANCING SCIENCE

YYePG Proudly Presents, Thx for Support

ing the host and acquiring their own blood supply. If you can inhibit neovascularization of tumors you could get an antitumor effect because neovascularization is a pathological process that does not occur in healthy tissue."

Consequently, many scientists explore ways to stop vascularization of tumors. "We want to understand the molecular biology of neovascularization," says Barge, "and find processes that might be specific to angiogenesis. This will enable the design of drugs that inhibit the growth of new blood vessels, without affecting the normal ones." The development of that parasitized blood supply depends on growth factors, such as vascular endothelial growth factor (VEGF). That makes VEGF a prime target.

Barge says, "We have a large number of agents in our pipeline." For example, scientists at AstraZeneca focus on growth factors and receptors for signal transduction as possible drug targets. Barge says that his company has two antiangiogenesis inhibitors in development—two of which are in Phase III trials. AstraZeneca also has two compounds in clinical trials that target the control of the cell cycle in cancer, and two more cell-cycle compounds that will go into the clinic later this year. Barge and his colleagues also study compounds that could inhibit cancerous invasion or repair DNA damage associated with cancer.

Challenges Ahead

To better understand cancer, George of Trevigen says, "Cancer is a protein disease—mutations of proteins that make them function improperly." But this complex collection of diseases generates an equally complex mountain of data. Trevigen notes that any meeting of the American Association of Cancer Research involves "miles and miles of posters," and it's just too much to consolidate. "For all I know," says George, "cancer has been cured every year, but there is no way to get all of that data in a searchable, minable form. No one person can comprehend even 0.1 percent of the content at one of these meetings." So improved informatics will always be desired.

No matter what researchers discover in terms of therapy, though, Weinberg of the Massachusetts Institute of Technology says, "Ultimately, the largest reduction in cancer mortality will come from changes in lifestyle." The most serious cancer-causing lifestyle remains the use of tobacco, says Weinberg. In addition, eating too much poses a cancer threat. Weinberg says, "An increased body-mass index correlates with increased risk of many types of cancer." So winning the cancer battle lies in the hands of both scientists and citizens.

Mike May (mikemay@mindspring.com) is a publishing consultant for science and technology based in Minnesota. Gary Heebner (gheebner@cell-associates.com) is a marketing consultant with Cell Associates in St. Louis, Missouri, U.S.A.

ScienceCareers.org

Classified Advertising

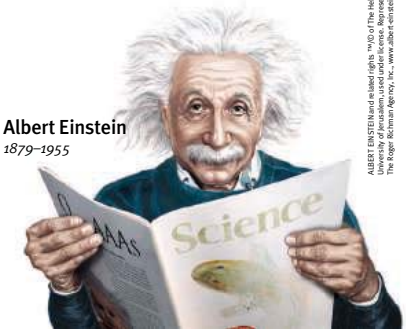

Albert Einstein
1879–1955

For full advertising details, go to **www.sciencecareers.org** and click on **How to Advertise,** or call one of our representatives.

United States & Canada

E-mail: advertise@sciencecareers.org
Fax: 202-289-6742

JILL DOWNING
(CT, DE, DC, FL, GA, MD, ME, MA, NH, NJ, NY, NC, PA, RI, SC, VT, VA)
Phone: 631-580-2445

KRISTINE VON ZEDLITZ
(AK, AZ, CA, CO, HI, ID, IA, KS, MT, NE, NV, NM, ND, OR, SD, TX, UT, WA, WY)
Phone: 415-956-2531

KATHLEEN CLARK
Employment: AR, IL, LA, MN, MO, OK, WI, Canada; Graduate Programs; Meetings & Announcements (U.S., Canada, Caribbean, Central and South America)
Phone: 510-271-8349

EMNET TESFAYE
(Display Ads: AL, IN, KY, MI, MS, OH, TN, WV; Line Ads)
Phone: 202-326-6740

GABRIELLE BOGUSLAWSKI
(U.S. Recruitment Advertising Sales Director)
Phone: 718-491-1607

Europe & International

E-mail: ads@science-int.co.uk
Fax: +44 (0) 1223-326-532

TRACY HOLMES
Phone: +44 (0) 1223-326-525

HELEN MORONEY
Phone: +44 (0) 1223-326-528

CHRISTINA HARRISON
Phone: +44 (0) 1223-326-510

SVITLANA BARNES
Phone: +44 (0) 1223-326-527

JASON HANNAFORD
Phone: +81 (0) 52-789-1860

To subscribe to *Science*:
In U.S./Canada call 202-326-6417 or 1-800-731-4939
In the rest of the world call +44 (0) 1223-326-515

Science makes every effort to screen its ads for offensive and/or discriminatory language in accordance with U.S. and non-U.S. law. Since we are an international journal, you may see ads from non-U.S. countries that request applications from specific demographic groups. Since U.S. law does not apply to other countries we try to accommodate recruiting practices of other countries. However, we encourage our readers to alert us to any ads that they feel are discriminatory or offensive.

ScienceCareers.org
We know science AAAS

6 April 2006 – San Francisco, CA

UCSF Mission Bay Community Center
Fisher Banquet Hall – 1675 Owen Street
1:00 - 4:30 pm

Science Careers has teamed up with UCSF to deliver an exciting career fair on the new UCSF Mission Bay campus.

Scientists: Meet with HR representatives of biotech, pharmaceutical, and research organizations who will be exhibiting. Visit ScienceCareers.org and click on Career Fairs on the left side for complete details.

Exhibitors: This fair typically attracts over 800 attendees. To be among the recruiters call Daryl Anderson at 202-326-6543 or visit ScienceCareers.org and click on Exhibit at a Career Fair.

We hope to see you there.

ScienceCareers.org
We know science AAAS

YYePG Proudly Presents, Thx for Support

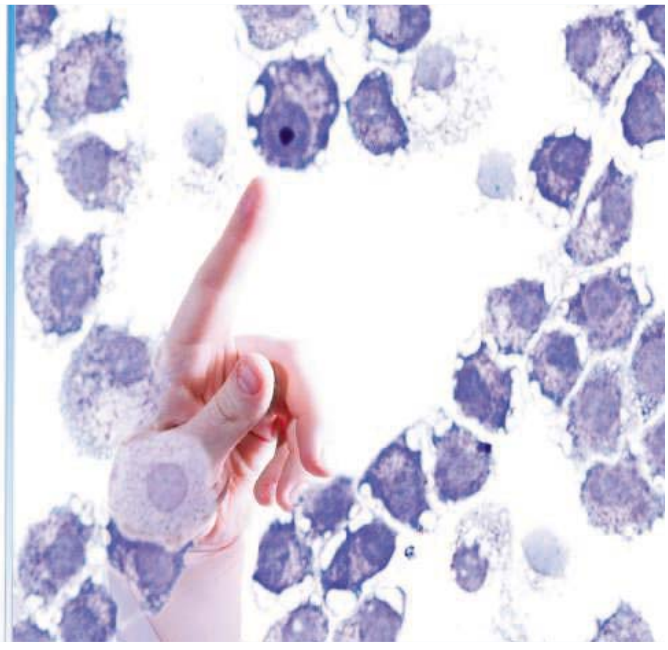

Careers in Cancer Research

Seeking Out the Source

Many cancer researchers focus on biomarkers that could provide diagnostics for the early detection of cancer. In addition, stem-like cells associated with cancer could unveil how this disease grows and spreads. These research areas provide exciting opportunities for new scientists and are certain to be active areas of investigation for decades to come, with funding available from public and private sources. BY MIKE MAY

Argonne National Laboratory
http://www.anl.gov

Harvard Medical School
http://hms.harvard.edu

The University of Texas M.D. Anderson Cancer Center
http://www.mdanderson.org/

University of Michigan
http://www.umich.edu

In early February 2006, data indicated that annual cancer deaths in the United States dropped for the first time in more than 70 years. According to the National Center for Health Statistics, cancer claimed 556,902 lives in 2003, 369 fewer than in 2002. That drop—a small one—serves mostly as a milestone. It probably arose from several changes: a reduced use of tobacco products and improved detection and treatment of cancer. Still, the battle continues. Despite the overall drop in deaths, more women actually died from cancer in 2003 than in 2002. So research on cancer will remain important, probably for decades to come.

Cancer research attracts a large number of scientists from a variety of disciplines: chemistry, drug development, epidemiology, molecular biology, and many others. Likewise, scientists from academics, government, and industry study cancer. As a result, this field produces many exciting advances. Some of the most recent include the discovery of stem-like cells related to cancer, target-specific drug therapy (Herceptin and Gleevec, for example), and the possibility of a universal molecular basis for this suite of diseases.

The experts interviewed here predict even more exciting advances ahead. Likewise, theses scientists see cancer research as a productive and sustainable career choice.

ARUL M. CHINNAIYAN

Spread Out Your Skills

When asked about the skills needed to study cancer, Diane J. Rodi, biochemistry group leader in the biosciences division at Argonne National Laboratory, says, "This is a hard question to answer, because so many different fields of science are needed to contribute to the development of a new therapy or the understanding of a disease." She adds, "Biology is more than just molecular or cellular biology today. It is increasingly computational and interdisciplinary in nature." As a result, she believes that the capability of working within a large, multidisciplinary team has become the best skill to develop. In addition, she says that a young scientist needs "the ability to grasp the significance of work far outside your field." So instead of merely specializing in one area, a future cancer researcher should develop skills and knowledge from several disciplines.

Other scientists agree. Joseph H. McCarty, assistant professor in the Department of Cancer Biology at The University of Texas M.D. Anderson Cancer Center, says, "The most important skill is to be multidisciplinary." He adds, "You need to understand diverse fields and be able to integrate them into a common connection."

That interdisciplinary flavor of cancer research also produces large amounts of data. Daniel Rhodes—a graduate student in the lab of Arul M. Chinnaiyan, who is S. P. Hicks Professor of CONTINUED »

The Institute of Cancer Research

Research Team Leaders

The Institute of Cancer Research, a College of the University of London, is a world-class cancer research organisation with UK HEFCE Research Assessment Exercise ratings of international excellence across all of its research programmes. In partnership with The Royal Marsden NHS Foundation Trust, we form the largest comprehensive cancer centre in Europe, dedicated to research that extends from epidemiology, genetics and molecular biology, through drug discovery and development, to cancer diagnosis and patient treatment. See www.icr.ac.uk.

The Institute is currently in the process of a major recruitment drive for faculty to lead research teams in the following areas:

Haemato-Oncology

Ref: CBL 90

We seek to appoint a Team Leader within the Section of Haemato-Oncology to lead a well-defined and ambitious research programme which integrates with the other activities of the Section and with The Institute in general. We are focused on the understanding of the molecular genetics of leukaemias and lymphoproliferative disorders aiming to translate this information into aetiological insights or new therapeutic opportunities, the latter by linking with the Cancer Research UK Centre for Cancer Therapeutics at The Institute. While particularly interested in a scientist with a track record in these areas, we will consider any high quality researcher in normal or malignant haemopoiesis whose interests can translate effectively into this environment.

Informal enquiries can be made to the Section Chairman, Professor Mel Greaves (email: mel.greaves@icr.ac.uk).

Molecular Carcinogenesis Prostate Cancer

Ref: HAD 64

The underlying theme of work within the Section of Molecular Carcinogenesis is the application of the latest molecular technology to clinical problems in projects that will ultimately lead to patient benefit. The Section currently provides a focus for activities within the National Cancer Research Institute's South of England Prostate Cancer Collaborative. The applicant would be expected to lead a research programme aimed at understanding the molecular basis of development of hormone refractory prostate cancer. The post would have close translational ties to the Trust and to the Cancer Research UK Centre for Cancer Therapeutics.

Informal enquiries, should be addressed to the Section Chairman, Professor Colin Cooper Tel +44 (0) 20 8722 4690.

Radioisotope Imaging Methodology

Ref: CLIN18

This team will develop numerical and computational techniques for modelling and understanding tracer dynamics, for reconstructing images from projections, for quantitating pre-clinical and clinical imaging devices, for image registration for multimodality imaging, for 4D quantitation and for extracting physiological parameters and the production of functional images. The post will link the Pre-clinical Team to clinical applications within the Trust and Institute. Imaging modalities of particular interest will be SPECT and PET. The postholder will have experience in hospital medical imaging with radiotracers and appropriate mathematical and computational skills.

Informal enquiries should be addressed to the Section Chairman Professor Steve Webb on +44 (0) 20 8661 3350.

Paediatric Oncology - Drug Development

Ref: CLIN 47

This vacancy is a new position as part of a major initiative of The Institute and the Trust - the Paediatric and Adolescent Oncology Targeted Drug Development Programme. The post will have close ties to the Royal Marsden NHS Foundation Trust Drug Development Unit and to the Cancer Research UK Centre for Cancer Therapeutics. The position will be responsible for the early clinical evaluation of new anti-cancer agents in children and young people and will take a major role in the pre-clinical evaluation of these agents.

For an informal discussion and/or to arrange a visit please contact the Section Chairman of Paediatric Oncology Professor Andy Pearson on +44 (0) 20 8661 3453.

Epidemiology

Ref: CLIN 38

The post will be within the Section of Epidemiology, which has close ties with the Section of Cancer Genetics and other laboratory scientists in The Institute, and will give an opportunity to instigate a research programme on cancer epidemiology and its interaction with genetics. Applicants from a statistical, medical, genetic or biological background would be welcome.

Informal enquires are welcomed, and should be addressed to the Section Chairman Professor Anthony Swerdlow on +44 (0) 20 8722 4192.

Appointments will be six-year tenure track, equivalent to assistant professor at US institutions, or for suitably qualified candidates at a more senior level up to full Professor. Additional staff posts, PhD studentships and start-up grants will be provided for suitable candidates. If applicable, an honorary clinical contract will be sought for clinically qualified appointees.

To apply, please send two copies of a research plan (up to 4 pages), CV and the names and contact details of three referees, to the Human Resources Office, The Institute of Cancer Research, 123 Old Brompton Road, London SW7 3RP, England, quoting the appropriate reference.

All posts are based at The Institute's Sutton campus. The job specifications are available at www.icr.ac.uk Alternatively call our 24 hour recruitment line on +44 (0) 20 7153 5475.

working in partnership with CANCER RESEARCH UK

breakthrough breast cancer

THE ROYAL MARSDEN

The Gerstner Sloan-Kettering Graduate School of Biomedical Sciences offers the next generation of basic scientists a program to study the biological sciences through the lens of cancer — while giving students the tools they will need to put them in the vanguard of research that can be applied in any area of human disease.

PhD Program in Cancer Biology

An Internationally Recognized Research Faculty in:

- Cancer genetics
- Genomic integrity
- Cell signaling and regulation
- Structural biology
- Immunology
- Chemical biology
- Developmental biology
- Computational biology
- Experimental therapeutics
- Experimental pathology
- Imaging and radiation sciences
- Oncology
- Genomics
- Animal models of disease

An Innovative, Integrated Curriculum Provides a Fundamental Understanding of:

- The nature of genes and gene expression
- Cellular organization
- Tissue and organ formation
- Cell-cell interactions
- Cellular response to the environment
- Enzyme activity

Student Support and Services:

Students receive a fellowship package that includes a stipend, tuition, textbook allowance, and health insurance. Students also have access to affordable housing within easy reach of the school.

Please visit our Web site to learn how to apply, for application deadlines, and for more information about our PhD program.

www.sloankettering.edu

gradstudies@sloankettering.edu | 646.888.6639

Gerstner Sloan-Kettering
Graduate School of Biomedical Sciences

New York City

Cancer Research UK Career Development Fellowships and Senior Cancer Research Fellowships

Cancer Research UK supports a broad portfolio of research drawn from a wide variety of scientific disciplines. We are committed to developing the next generation of leaders in cancer research through a programme of research fellowships. We are therefore pleased to invite preliminary applications for our Career Development Fellowships and Senior Cancer Research Fellowships. We would welcome applications from non-clinical researchers in any discipline and in any research field with relevance, or potential relevance, to cancer. Up to eight fellowships are available, to start no earlier than 1 April 2007.

Career Development Fellowships

The fellowships will provide:

- 6 years' support
- Salaries for the fellow, a postdoctoral researcher and a technician
- Consumables costs
- Equipment.

You should:

- Be an outstanding postdoctoral scientist who wishes to achieve independence in your research for the first time
- Have shown promise in your early work in a cancer-relevant field
- Have completed between 3 and 6 years of postdoctoral work.

You should not have had a previous opportunity to develop a research group. However, you must be able to demonstrate the potential to lead a research team and direct a small programme of work. You will usually be expected to have the status of a Junior Group Leader or equivalent.

Senior Cancer Research Fellowships

The fellowships will provide:

- 6 years' support
- Salaries for the fellow, up to two post-doctoral researchers, a technician and a student
- Consumables costs
- Equipment.

You should:

- Be an outstanding scientist who wishes to develop your independence
- Have shown exceptional ability in your previous work in a cancer-relevant field
- Have completed between 6 and 10 years of postdoctoral work
- Have a commitment from your host institution for your long-term support.

If you have previously held or currently hold a tenured position, or if you have already had a chance to establish an independent group through another fellowship, you would still be welcome to apply for this award. However, you should not have been running a group for more than 6 years at the time of application.

Please see our website (http://science.cancerresearchuk.org/gapp/grantapplications/tcdb/?version=1) for further information.

The deadline for preliminary applications is Friday 2 June 2006.

The fellowships cannot be held in the Cancer Research UK core-funded Institutes in London, Glasgow, Cambridge and Manchester. Most other UK institutions are suitable, but you should contact Cancer Research UK to check the eligibility of your chosen location before you apply.

For an application pack, please email fellowships@cancer.org.uk stating the fellowship in which you are interested in the subject of the email. If you would like to discuss your eligibility for any of these fellowships, or have any other questions, please contact Dr Simon Vincent simon.vincent@cancer.org.uk 020 7061 6082.

CANCER RESEARCH UK

YYePG Proudly Presents, Thx for Support

Others
call it research.

We call it changing the medical textbooks.




For 30 years, Genentech has been at the forefront of the biotechnology industry, using human genetic information to discover, develop, commercialize and manufacture biotherapeutics that address significant unmet medical needs. Today, Genentech manufactures and commercializes multiple biotechnology products that have helped patients suffering from serious diseases and conditions, including breast cancer, colorectal cancer, non-Hodgkin's lymphoma, lung cancer, rheumatoid arthritis, cystic fibrosis and allergic asthma. The company is the leading provider of anti-tumor therapeutics in the United States.

Genentech's research organization features world-renowned scientists who are some of the most prolific in their fields and in the industry. Our more than 650 scientists have consistently published important papers in prestigious journals and have secured more than 5,500 patents worldwide (with an equal number pending). Genentech's research organization combines the best of the academic and corporate worlds, allowing researchers not only to pursue important scientific questions but also to watch an idea move from the laboratory into development and out into the clinic. We are proud of our long history of groundbreaking science leading to first-in-class therapies, and we hope you'll consider joining us as we continue the tradition.

Our continued growth has created opportunities in Research in our South San Francisco headquarters. Please take this opportunity to learn about Genentech, where the creativity and openness of an academic environment meet the rigorous dedication of industry-leading professionals focused on improving and extending people's lives.

Seeking Cancer Research Professionals

Postdoctoral Fellows, Research Associates and Scientists in the following areas:

- Angiogenesis
- Antibody Engineering
- Assay Technology
- Bioinformatics
- Biomedical Imaging
- Cell Biology
- Immunology
- Medicinal Chemistry
- Molecular Biology
- Molecular Diagnostics
- Molecular Oncology
- Pathology
- Protein Chemistry
- Protein Engineering
- Translational Oncology
- Tumor Biology

Genentech was named #1 on FORTUNE's "100 Best Companies to Work For" list.

To learn more about these opportunities, please visit **www.gene.com/careers**. Please use "Ad - Science Mag" when a "source" is requested. Genentech is an equal opportunity employer.

Genentech
IN BUSINESS FOR LIFE
www.gene.com

Careers in Cancer Research


CHARLES DIMITROFF

Pathology and director of research informatics at the University of Michigan—says, "One common theme in many discoveries in the past few years has been high throughput approaches and looking at many genes in a single assay." Consequently, it's no surprise that Chinnaiyan encourages students to gain capabilities in bioinformatic analysis. He says, "We are nearing the age of looking at cancer with more of a systems perspective and studying all of the molecular constituents of a process."

Another of Chinnaiyan's graduate students, Scott Tomlins, also sees a growing need for skills in data analysis. He says, "Some fields are almost flooded with data. You need to think creatively about how to analyze data."

If you cannot do the analysis yourself, you must at least be able to talk with scientists who can. Tomlins says, "It's important to be able to speak in both biological and bioinformatic languages."


DANIEL RHODES

Competitive But Widespread

The predictions for future funding vary. Charles Dimitroff, assistant professor in the Department of Dermatology at Harvard Medical School, says, "As the projected U.S. National Institutes of Health budget increases are not anticipated to keep pace with inflation, significant cuts in the number of funded grants and in the funding amounts will result." But he adds, "There are many other venues for obtaining cancer research funding, but reduced NIH funding will cause a surge in grant applications to these other organizations and make it more difficult to obtain funding from these sources."

He also believes that faculty positions will become even more competitive. Nonetheless, he adds, "I'm not suggesting that aspiring cancer research scientists pick a new sport, but they should be well prepared before entertaining the thought of research independence and autonomy in academia." Instead of bypassing academics, Dimitroff suggests a strategy: "I propose seeking employment in both academic departments and clinical departments in hospitals that do not normally sustain a large percentage of cancer researchers. Departments of oncology, tumor biology, tumor immunology, or cancer therapeutics, for example, are typically dominated by cancer researchers and obtaining a position in one of these departments would be extremely competitive."

McCarty completed what he calls a fairly exhaustive job search just a year ago, and he found considerable recruiting in two areas: basic cancer research and molecular neuroscience. "Compared to many other fields," says McCarty, "cancer research is still fairly robust. Although the job market is competitive, there are lots of opportunities, especially if you can span neuroscience and cancer." He adds that there is lots of funding—both public and private—in the general area of brain cancer. He says, "There's really good funding for medulloblastoma, neuroblastoma, glioblastoma, and related areas."


DIANE J. RODI

A Translational Turn

Several of the experts interviewed here point to a growing emphasis on translational research. "It is easiest to get funding for work that is translational or nearly translational," says Chinnaiyan. For example, his own lab's work—published in the October 8, 2005, issue of —on recurrent gene fusion in prostate cancer provides an example. In addition, he points to biomarkers as good examples of potentially translational work that can be funded comparatively easily. Dimitroff agrees: "I think that research efforts attempting to elucidate a biomarker of early malignancy will always be fundable entities. Likewise, development of novel techniques or approaches that help discover these tumor-specific markers will be fundable programs. In general, cancer research funding is always available for projects that are innovative, of high risk, and interdisciplinary in nature."

When trying to predict fundable research in the future, Rodi says, "I'm not sure my crystal ball is clear enough to answer this question." Then she adds, "My bias is toward multidisciplinary approaches, especially those that can harness the power of tumor typing by gene expression pattern. In addition, new imaging platforms—made possible by advances in a range of nanotechnologies—have huge promise as methods for monitoring both disease progression and the impact of therapy." For instance, Rodi and her colleagues are working on techniques that could monitor vasculature in a tumor in vivo.


SCOTT TOMLINS

Stay Open Minded

Although many scientists might aim at academics, industry also offers many opportunities. McCarty mentions knowing several people who moved to biotechnology or pharmaceutical companies to do cancer research. "They are very happy with their decisions," he says, "and they feel challenged with their work."

Dimitroff sees lots of opportunities outside of academics in Boston. He says, "I'm obviously biased in my belief that Boston is one of the premier locales for finding a position in cancer research. Boston has become a global center for major biotechnology and small startup companies." Chinnaiyan also sees colleagues going to industry. He says, "This is happening more and more, although it is often better to do this later in your career. More seasoned academics in cancer research often get recruited by large pharma and biotech companies."

In the end, what scientists work on probably matters more than whether they work in academics, government, or industry. As Rodi says, "I'd look for a position where I can collaborate with energetic scientists who have new ideas and a vision of the future." That energy and vision can help any scientist build a career in cancer research.

Mike May (mikemay@mindspring.com) is a publishing consultant for science and technology based in Minnesota.

Molecular Imaging: Training for Oncology

Memorial Sloan-Kettering Cancer Center is one of only a few institutions awarded a molecular imaging training grant (R25T) from the NCI. The goal of the Molecular Imaging: Training for Oncology program is to train a new generation of MD, PhD or MD/PhD researchers, who are facile with both the biology and technology of advanced molecular imaging methods for application to basic, translational and clinical cancer research. The specialized curriculum emphasizes the development of molecular imaging for oncology and includes didactic training focusing on relevant molecular biology and research methodology coursework, instruction in advanced imaging methods, an individualized research program focusing on basic, translational, or clinical interdisciplinary research and experience in advanced methods of nuclear, radiographic, optical and magnetic resonance imaging/spectroscopy.

Physicians who have completed sub-specialty in a relevant imaging or clinical discipline and post-doctoral Ph.D.s with specialized skills in cellular and/or molecular biology or a related discipline are encouraged to apply. Interested applicants must either be U.S. Citizens or have U.S. Permanent Residency. Trainees are expected to have proficiency in physics, chemistry and/or computer science and a strong interest in molecular targeting probes as vehicles to advance the understanding of cancer through medical imaging.

Please send cover letter, CV and a 2-page statement of research interest to: **Dr. Hedvig Hricak, Chairman, Department of Radiology, Memorial Sloan-Kettering Cancer Center, 1275 York Avenue, New York, NY 10021** or e-mail: **guidoj@mskcc.org**.

Memorial Sloan-Kettering Cancer Center is an Equal Opportunity Employer with a strong commitment to enhancing the diversity of its faculty and staff. Women and applicants from diverse racial, ethnic and cultural backgrounds are encouraged to apply.

Faculty Position

Neuro-Oncology

The University of Texas M. D. Anderson Cancer Center is seeking a highly qualified basic scientist for a tenure-track appointment as Assistant Professor or Associate Professor in the Department of Neuro-Oncology, with appropriate joint appointment in a basic science department and the Graduate School of Biomedical Sciences. Generous start-up funds and excellent laboratory space are available. Candidates must have a Ph.D. and/or an M.D. and postdoctoral research experience. Candidates interested in the areas of mouse disease models, glial cell differentiation and development, genetic control of cell differentiation and transformation, stem cell biology and signal transduction will be preferred; however, suitable candidates with experience in all other neuro-oncology research will also be considered. Current research in the department includes signal transduction, angiogenesis, developmental/stem cell biology, transcription biology, and targeted therapeutics.

Applicants should send their curriculum vitae along with contact information for references, a brief research statement covering their past accomplishments, their current and planned research goals, and their plans to emerge as a leader in the chosen area, to:

Rakesh Kumar, Ph.D., Chair of Search Committee
Department of Molecular and Cellular Oncology, Unit 108
UT M. D. Anderson Cancer Center
1515 Holcombe Blvd.
Houston, TX 77030-4009

THE UNIVERSITY OF TEXAS
MD ANDERSON
CANCER CENTER
Making Cancer History®

M. D. Anderson Cancer Center is an equal opportunity employer and does not discriminate on the basis of race, color, national origin, gender, sexual orientation, age, religion, disability or veteran status except where such distinction is required by law. All positions at The University of Texas M. D. Anderson Cancer Center are security sensitive and subject to examination of criminal history record information. Smoke-free and drug-free environment.

FACULTY POSITION
ENDOCRINOLOGY

The Endocrine Service at Memorial Sloan-Kettering Cancer Center (MSKCC) seeks a full-time Clinical Endocrinologist/Educator at the Assistant or Associate Professor level. Applicants should be board certified in Internal Medicine and board-eligible in Endocrinology and Metabolism. The candidate should be eligible for a license to practice in the State of New York, and must have completed training in clinical endocrinology with a special emphasis on endocrine oncology and thyroid cancer. Candidates should have demonstrated evidence of scholarly interest in either basic or clinical research. It is envisioned that this position will involve 80% patient care and 20% teaching/research time. The faculty member will have a significant mentorship role in a multicenter endocrinology fellowship program, and will be expected to teach residents and medical students. A faculty appointment at the Weill Medical College of Cornell University will be available for qualified candidates.

A competitive salary and excellent benefits package are included. Interested candidates should send a curriculum vitae, a statement of academic interests, and the names of three references to: **R. Michael Tuttle, MD, Acting Chief, Endocrine Service, Memorial Sloan-Kettering Cancer Center, 1275 York Avenue, Box 296, New York, NY 10021.**

Memorial Sloan-Kettering Cancer Center is an equal opportunity employer with a strong commitment to enhancing the diversity of its faculty and staff. Women and applicants from diverse racial, ethnic and cultural backgrounds are encouraged to apply.

Memorial Sloan-Kettering Cancer Center
The Best Cancer Care. Anywhere.
www.mskcc.org

Program Leader in Cell Signaling and Translational Cancer Studies

The Vermont Cancer Center, an NCI-designated Comprehensive Cancer Center at the University of Vermont, is seeking a mid-level or senior scientist to provide strategic leadership and direction for the Cell Signaling Research Program, comprising 20+ interdisciplinary faculty members, with a focus on understanding the molecular mechanisms of signal transduction and growth regulation, especially as pertains to cancer.

The ideal candidate will have an MD, PhD or MD/PhD, with an established NCI-funded program in translational cancer research focused on cell signaling. Candidates should have a demonstrated track record of competitive, extramural support and scientific productivity. Depending on background, appointment will be in an appropriate academic department with a generous start-up package and space commensurate with senior-level recruitment.

The VCC (**www.vermontcancer.org**) was established in 1974, and supports research cores in biostatistics, cell imaging, clinical research management, flow cytometry, transgenic mice, genomics, bioinformatics, and structural biology. The University of Vermont is located on the shores of Lake Champlain in Burlington, a vibrant community frequently cited as one of the most livable cities in the U.S.

Vermont Cancer Center
at the University of Vermont

A Comprehensive Cancer Center Designated by the National Cancer Institute

Apply online at **www.uvmjobs.com** or send CV and letter of interest to **cellsignal@med.uvm.edu** or by mail to: Dr. Christopher Francklyn, B-401 Given Building, University of Vermont, Burlington, VT 05405.

The University of Vermont is an Equal Opportunity/Affirmative Action Employer. Women and those from diverse racial, ethnic and cultural backgrounds are encouraged to apply.

AWARDS

CAREERS IN CANCER RESEARCH

POSTDOCTORAL FELLOWSHIP
Department *of* Immunology

BCM Baylor College of Medicine

Applications are now being accepted from recent graduates for postdoctoral fellowship positions in the Department of Immunology at Baylor College of Medicine, through the NIH Training Grant, "Molecular and Cellular Mechanisms of Host Defense." Located in Houston TX, Baylor College of Medicine is a leader in biomedical research. More than eighteen distinguished mentors are available. The program provides mentorship in individual career development, curriculum in grant writing and presentation skills, as well as research opportunities in critical areas of immunology:

Lymphocyte signaling	Apoptosis
Lymphocyte development	Stem cells
Autoimmunity	Inflammation
Cytokines	HIV pathogenesis
Adhesion molecules	Dendritic and Treg cells
Gene therapy	Cancer research

Applicants must be recent graduates, as well as United States citizens or permanent residents. To apply, send a statement of research interest, C.V., and the names and email addresses of three references to:

Tse-Hua Tan, Ph.D., Program Director
Baylor College of Medicine
c/o Ms. Robin Cuthbert, at rmcuthbe@bcm.edu

www.bcm.edu/immuno
BCM is an equal EEOC/AA/EA employer

S&W SCOTT & WHITE

College of Medicine
The Texas A&M University System Health Science Center

Pediatric Hematology-Oncologist

The Section of Pediatric Hematology/Oncology at **Scott and White Clinic** and the **Texas A&M University System Health Science Center College of Medicine** (TAMUS HSC-COM) are seeking a clinician scientist with current research grants for a faculty position in a rapidly growing program. The candidate should be BE/BC in pediatric oncology and committed to an academic career. The successful candidates will join and enhance ongoing efforts in basic and translational research, with an institutional commitment to building a world-class experimental therapeutics program. An outstanding start-up package includes high quality laboratory space, excellent benefits and competitive salaries commensurate with academic qualifications. The position guarantees 75% protected time for research activities.

Scott & White Clinic is a 500+ physician directed multi-specialty group practice that is the leading provider of cancer care in Central Texas. Scott and White Clinic and the 486 bed tertiary Scott & White Memorial Hospital is the main clinical teaching facility for TAMUS HSC-COM. Outstanding clinical practice and laboratory facilities on campus that perform state of the art molecular and cellular biology research, flow cytometry, genomics and biostatistics are in place to support the research effort.

Please contact: **Don Wilson, M.D. Professor and Chairman, Department of Pediatrics, Scott & White, 2401 S. 31st, Temple, TX 76508. (800)725-3627 dwilson@swmail.sw.org Fax (254) 724-4974.**

For more information about Scott & White, please visit www.sw.org For Texas A&M www.tamhsc.edu. Scott & White is an equal opportunity employer.

CAREERS IN CANCER RESEARCH

Scholars in Oncologic Molecular Imaging

Postdoctoral Training in Molecular Imaging of Cancer
University of California Los Angeles, USA

The UCLA Scholars in Oncologic Molecular Imaging (SOMI) Program will uniquely train biological researchers & physicians to integrate molecular imaging into cancer research. This rapidly growing area combines the disciplines of cell/molecular biology, chemistry, biomedical physics, biomathematics, pharmacology, imaging sciences, and clinical medicine to advance cancer research, diagnosis and management. SOMI fellows will conduct innovative research in cancer imaging under the supervision of two faculty mentors from complementary fields, in a comprehensive, integrated, flexible program (up to 3 years). Funds for salary, supplies and travel are provided and can be supplemented by supervising mentors.

- **Next application deadline: June 1st for start date in September, 2006.**
- Applicants must have Ph.D. or M.D. and must be US citizens or permanent residents.
- Further information about this program found at: ww.crump.ucla.edu/public/somi
- Inquiries to SOMI Application Coordinator by telephone: 310-825-4903 or email: ecorrin@mednet.ucla.edu

---

University of Missouri Health Care

Research Faculty Position

The University of Missouri School of Medicine Department of Surgery is seeking outstanding candidates for two research faculty positions. Rank and appointment status are contingent upon qualifications.

The candidate should have experience in a field of research in which surgeons interface. This includes, but is not limited to, cancer, heart disease, inflammation, wound healing, trauma, and vascular biology. Candidate must demonstrate evidence of current or future potential for federal funding, show interests in teaching medical students and surgical residents, and have the desire to interact with surgical researchers in developing a vigorous, extramurally funded research program.

Applicants should send curriculum vitae to: **Steve Eubanks, M.D., Chairman, Department of Surgery, University of Missouri-Columbia, Health Sciences Center, One Hospital Drive, Columbia, Missouri 65212.**

E-mail: grotewielln@health.missouri.edu

MU

Equal Opportunity/ Affirmative Action/ ADA Employer

Visit the Department of Surgery's Web site at http://www.surgery.missouri.edu/. Go to "Practice Opportunities".

POSITIONS OPEN

Postdoctoral Positions in Biology of Learning & Memory

Initial Research Project, Okinawa Institute of Science and Technology (IRP-OIST)

A newly founded lab in Okinawa, a southern most island in Japan, is seeking several postdoctoral researchers in the field of learning & memory. The project aims for the elucidation of molecular and genetic basis for mammalian neuronal plasticities using multiple disciplinary approach including gene targeting, molecular biology, and behavioral psychology. Communication skill in English is essential. Priority will be given to researchers with at least a couple of experiences in the field related to neuroscience such as behavioral psychology, physiology, veterinary, molecular biology, cell biology, genetics, biochemistry, pharmacology, and anatomy. Starting annual salary of 4.8-5.5million yen depending on experience. The review of applications will begin immediately and the search will continue until positions are filled. Applicant should have the ability to work independently and supervise his/her technician. More information on IRP-OIST at http://www.irp.oist.jp. Interested applicants should send a CV, past and future research interests, and the names of three references to:

Dr. Shogo Endo, IRP OIST, 12-22 Suzaki, Uruma, Okinawa 904-2234, Japan
Or, email to: LMrecruit@irp.oist.jp

IRP-OIST is supported by Okinawa Institute of Science and Technology Promotion Corporation (OIST PC). OIST PC is EOE and encourages application from women and minorities.

A*STAR Research Fellowships

A prestigious award to recognise young scientific talent

Agency for Science, Technology and Research
SINGAPORE

Singapore's Agency for Science, Technology & Research (A*STAR, http://www.a-star.edu.sg) invites applications to the A*STAR Research Fellowships

The **A*STAR Research Fellowships** aim to nurture and groom the next generation of global leaders in science by supporting innovative and independent research. Applicants should have obtained their PhD or MD preferably within 24 months (not more than 48 months) of the application date, and demonstrated creativity in research.

Tenable at the highly regarded Institute of Molecular and Cell Biology (IMCB, www.imcb.a-star.edu.sg), **A*STAR Research Fellows** will receive attractive remuneration, support for set-up costs, research funding, research staff and access to state-of-the-art scientific equipment and facilities, including the Biopolis Shared Facilities and the Biological Resource Centre. Each laboratory may be funded up to US$500K p.a.

The fellowship will be for a 3+2-year duration, with a review at the end of the 3rd year and a possible "fast-track" promotion. **A*STAR Research Fellows** may select one or more mentors from A*STAR's research institutes but will conduct and publish their work independently.

The **A*STAR Research Fellowship Selection Panel** is composed of:-

Dr Tadataka Yamada, Chairman, R&D, GlaxoSmithKline

Dr Sir David Lane, Executive Director, Institute of Molecular & Cell Biology

Dr Alex Matter, Director, Novartis Institute for Tropical Diseases

Dr Edward Holmes, Vice Chancellor for Health Sciences, University of California, San Diego

Dr Axel Ullrich, Programme Director, Singapore OncoGenome Laboratory, Centre for Molecular Medicine, A*STAR and Director, Dept of Molecular Biology, Max Planck Institute of Biochemistry

Ten shortlisted candidates will be invited to Singapore for interviews, which will include a review based on a scientific presentation at an open symposium. These are expected to be held in August 2006. Applications will close on **31 May 2006**.

Applicants are requested to submit their CVs and a 5-page research proposal (1 hard copy & 1 soft copy) to :

A*STAR Research Fellowships
Agency for Science, Technology & Research,
20 Biopolis Way, #08-01,
Singapore 138668, Singapore
Email: A-STAR_ADMIN_BMRC@a-star.edu.sg

National Institutes of Health
Office of the Director

Chief NIH Ethics Officer

The Office of the Director, National Institutes of Health (NIH) in Bethesda, Maryland, is seeking a Chief NIH Ethics Officer (CNEO), who will also serve as Director for the NIH Ethics Office. If you are an exceptional candidate with a M.D. and/or Ph.D. and have the vision and skills to oversee and provide strategic direction to NIH activities relating to ethics policy, oversight, and operations for scientific administration, we encourage your application.

To achieve its mission of advancing biomedical and behavioral research to improve the health of the public, the NIH must have the trust of the public that the decisions and activities of the agency and its employees are unbiased. The creation of the new position of CNEO is part of a comprehensive effort to strengthen the program of ethics oversight for NIH employees. As CNEO, you will be responsible for the executive leadership, strategic direction, and oversight of the scientific, clinical, and administrative activities of NIH staff as they relate to ethics policies. This includes: assuring compliance with Federal, departmental, and agency ethics laws, regulations, and policies that apply to the official-duty activities, outside activities, and financial holdings of NIH's 18,000+ employees; overseeing a rigorous program of quality control and risk management including assessing the effectiveness activities of conflict of interest operations the NIH Ethics Office and the application of delegated authority; conducting a comprehensive ethics training program; and developing/maintaining an effective enterprise information technology system. Additional functions include serving as the NIH spokesperson and principal advisor to the Director and Deputy Director, NIH on relevant NIH ethics policy and programs. In addition, you will serve as the NIH Agency Research Integrity Liaison Officer (ARILO) and will be responsible for all matters related to NIH's intramural and extramural research integrity programs to include oversight and coordination of NIH activities related to research misconduct and the promotion of research integrity of NIH intramural and extramural research programs. Understanding the value of scientific expertise for leadership of ethics at NIH, you will have the flexibility to devote up to 25% of your time to conduct or oversee research in an NIH intramural research laboratory or in an appropriate NIH extramural scientific programmatic role.

Salary is commensurate with experience; a full package of benefits is available, including retirement, health, life, long term care insurance, Thrift Savings Plan participation, etc.

Applications for this position will be reviewed by a Search Committee chaired by Dr. Duane Alexander, Director, National Institute of Child Health and Human Development. Applicants may send a Curriculum Vitae to **Teresa Leary, 31 Center Drive - MSC 2207, Room 4B-41, Bethesda, MD 20892-2207 or visit http://www.jobs.nih.gov and apply to Announcement OD-06-109779 (for Ph.Ds) or OD-06-109626 (for M.Ds)**. If you need additional information, please contact **Ms. Teresa Leary at learyte@od.nih.gov or (301) 496-1443**. Applications must be received by close of business **May 19, 2006**.

Mouse Cancer Genetics Program
Program Director/Laboratory Chief

The National Cancer Institute (NCI), National Institutes of Health (NIH), Department of Health and Human Services (DHHS), is seeking applicants for a Program Director/Laboratory Chief of the Mouse Cancer Genetics Program (MCGP) within the Center for Cancer Research (CCR). The CCR is an NCI intramural research center located on the Bethesda and Frederick, Maryland campuses. The Mouse Cancer Genetics Program, located on the Frederick campus, currently consists of seven investigators who utilize mouse genetics to understand the biological basis of disease and mouse models to develop innovative approaches to cancer intervention (**http://ccr.cancer.gov/labs/lab.asp?labid=61**).

The Mouse Cancer Genetics Program encompasses strengths in mouse genetic engineering and bioinformatics. The program has ready access to extensive state-of- the-art mouse facilities to core facilities in pathology, histology, genotyping and microarray, and to the Developmental Therapeutics Program (DTP) of NCI, as well as the molecular imaging and nanobiology initiatives currently under development. The CCR is searching for a Program Director who can take advantage of these resources to direct the use of mouse genetics and models, to dissect complex genetic disease traits, uncover mechanisms of cancer development, and develop preventive and therapeutic interventions.

The successful candidate will have a Ph.D. and/or M.D. and a well-established research program in mouse genetics or mouse cancer biology. We are looking for an individual with strong leadership skills, experience in mentoring junior investigators, and administrative/budgetary expertise. All applicants should submit a letter indicating the position they are applying for; a statement of research interests; current curriculum vitae and complete bibliography; and the names and addresses of six references (include email addresses) by **May 15, 2006**.

Applications should be sent to: **Beverly Mock, Ph.D., MGCP Search Committee Chair, c/o Patty Farrell, Bldg. 37, Rm. 3146, 37 Convent Drive, MSC 4258, Bethesda, Maryland 20892-4258**

Or, email your applications or intent to apply to: **farrellp@mail.nih.gov (Patty Farrell, 301-496-1734, FAX: 301-402-1031)**

WWW.NIH.GOV

Department of Health and Human Services
National Institutes of Health
Office of the Director

Deputy Director of NIH for Portfolio Analysis and Strategic Initiatives
and
Director, Office of Portfolio Analysis and Strategic Initiatives

The Office of the Director, National Institutes of Health (NIH) in Bethesda, Maryland, is seeking a Director for the new Office of Portfolio Analysis and Strategic Initiatives (OPASI). If you are an exceptional candidate with an M.D. and/or Ph.D. and the vision and ability to integrate science across multiple disciplines, we encourage your application.

As the OPASI Director, you will serve as a Deputy Director of the NIH and directly report to the NIH Director. As a prominent senior leader reporting directly to the Director of NIH, you will be responsible for executive leadership and coordination of the overall NIH research portfolio analysis and strategic initiatives that fall within the OPASI's scope. The OPASI's primary objective is to develop: a transparent process of planning and priority-setting characterized by a defined scope of review with broad input from the scientific community and the public; valid and reliable information resources and tools, including uniform disease coding and accurate, current and comprehensive information on burden of disease; an institutionalized process of regularly scheduled evaluations based on current best practices; the ability to weigh scientific opportunity against public health urgency; a method of assessing outcomes to enhance accountability; and a system for identifying areas of scientific and health improvement opportunities and supporting regular trans-NIH scientific planning and initiatives. You will serve as the principal advisor to the NIH Director on issues involving OPASI's planning, analysis, and policy formulation and implementation activities, including efforts to strengthen trans-NIH strategic planning and funding, and improve data quality and develop analytical techniques for assessing the NIH research portfolio.

This position requires that the OPASI Director exercise leadership, initiative, and creativity in establishing and maintaining relationships with key Federal and non-Federal officials, nationally and internationally recognized scientific leaders and officials of academic, research, and other institutes and organizations, and professional and advocacy groups.

Salary is commensurate with experience; a full package of benefits (including retirement, health, life, long term care insurance, Thrift Savings Plan participation, etc.) is available.

Applications for this position will be reviewed by a Search Committee chaired by Dr. Jeremy Berg, National Institute of General Medical Sciences and Dr. Elizabeth Nabel, Director, National Heart, Lung and Blood Institute.

Interested applicants should send a Curriculum Vitae to **Ms. Teresa Leary, 31 Center Drive – MSC 2207, Room 4B-41, Bethesda, MD 20892-2207 OR visit: http://www.jobs.nih.gov and apply to Announcement OD-06-109905 (for Ph.Ds) or OD-06-109915 (for M.Ds).** If you need additional information, please contact **Ms. Teresa Leary at learyte@od.nih.gov or by calling 301-496-1443.**

Applications must be received by close of business May 19, 2006

DEPARTMENT OF HEALTH AND HUMAN SERVICES
FOOD AND DRUG ADMINISTRATION
CENTER FOR BIOLOGICS EVALUATION AND RESEARCH

INTERDISCIPLINARY SCIENTISTS-FULL TIME

The FDA's Center for Biologics Evaluation and Research, Office of Cellular, Tissue, and Gene Therapies is recruiting scientists to serve as Interdisciplinary Scientists in the dynamic, highly challenging, and innovative atmosphere of biological product review in the Gene Therapies Branch of the Division of Cellular and Gene Therapies (DCGT). The DCGT is strongly committed to bringing FDA and other scientists, patient advocates, and the public together in new partnerships to develop new therapies for the 21st Century, while protecting human subjects and ensuring product safety. The incumbent will serve as the scientific and technical authority on a multidisciplinary scientific/medical team that reviews, evaluates and decides on the approvability of scientific research, human testing and manufacture of human biological products. The incumbent will be responsible for reviewing meeting materials, Investigational New Drug Applications (IND), and Biological License Applications (BLA) for scientific content and compose official reviews and responses. Reviews will be based on data submitted by manufactures and sponsors of new biological products to be used for clinical investigations. Incumbent will also be responsible for relating responses and any concerns regarding IND review to sponsors or investigators of the clinical trial. Some products and issues that will be addressed by incumbents include novel gene therapy products for the treatment of cancer, hemophilia, cardiovascular disease, Alzheimer's disease and many genetic defects and rare diseases as well as new emerging therapies related to the use of stem cell research, stem cell transplantation, xenotransplantation, somatic cell therapies and/or tumor vaccines for cancer therapy.

QUALIFICATIONS: Applicants should have a doctoral degree or equivalent experience in one or more of the following disciplines: Virology, molecular biology, microbiology, cell biology or immunology. A minimum of three year's post-doctoral experience is preferred. Candidates for Civil Service or U.S. Commissioned Corps must be U.S. Citizen.

SALARY RANGE: Civil Service salary range for GS-13 is $74,782 to $97,213.

HOW TO APPLY: Submit resume or curriculum vitae with cover letter by email to: **stephanie.simek@fda.hhs.gov** or mail to: **1401 Rockville Pike, HFM-720, Rockville, MD 20852, ATTN: Stephanie Simek, Deputy Director, DCGT/OCTGT/CBER.**

FDA is an Equal Opportunity Employer and has a smoke free environment. To qualify for employment all applicants must meet all Civil Service or Commissioned Corps requirements.

Endocrinologist

Stony Brook University's Division of Endocrinology and Metabolism, Department of Medicine is seeking an individual at the Assistant, Associate, or Full Professor level to become a member of the Division. The Division has an accredited fellowship program and has six full-time faculty members with a major interest in insulin resistance and diabetes. Stony Brook University Hospital has an NIH-sponsored General Clinical Research Center that is directed by a member of the Endocrinology Division.

Required: M.D. or equivalent. Applicants must be board-certified in Internal Medicine and board-certified or eligible in Endocrinology. Candidates should have an extensive background in performing investigator-initiated clinical research or clinical trials in an area related to diabetes mellitus, insulin resistance, metabolism, or obesity. The position will also involve patient care and teaching of fellows, residents, and medical students.

Salary is commensurate with experience and faculty rank.

Please send letter of interest and CV to:
Harold E. Carlson, M.D., Chief
Division of Endocrinology and Metabolism
HSC T15-060, Stony Brook University
Stony Brook, NY 11794-8154

Equal Opportunity/Affirmative Action Employer. Visit *www.stonybrook.edu/cjo* for employment information.

STONY BROOK

POSTDOCTORAL RESEARCH ASSOCIATE

Howard Hughes Medical Institute
& Department of Biochemistry
Duke University Medical Center

A Postdoctoral position is available immediately to study the mechanism of E. coli DNA mismatch repair. We are looking for a highly motivated individual with a Ph.D. or M.D. and experience in mechanistic enzymology. Experience in pre-steady-state kinetic methods and DNA manipulations is desirable. Salary will be commensurate with experience.

Interested individuals should forward a curriculum vitae and names of three references to: **Paul Modrich, HHMI & Dept. of Biochemistry, Box 3711, Duke University Medical Center, Durham, NC 27710. e-mail: Modrich@biochem.duke.edu**

The Howard Hughes Medical Institute and Duke University are equal opportunity employers.

HHMI
HOWARD HUGHES MEDICAL INSTITUTE

Technical University of Denmark

The Hans Christian Oersted Postdoc Programme

DTU

DTU invites highly talented young researchers who have already obtained outstanding results during their PhD study and have demonstrated excellence and potential in their field of study to apply for one of the stipends under the H.C. Oersted Postdoc Programme. The programme is named after the founder of the university, H. C. Oersted, who discovered Electromagnetism.

The full text of the announcement can be seen on DTU's homepage at www.dtu.dk/job. Applications must be based on the details of the full text announcement.

Further information can be obtained from the Dean of Research Kristian Stubkjær (e-mail: forskningsdekan@adm.dtu.dk).

Application deadline: 28 June 2006 at 12.00 (noon).

Opening new frontiers in Biology

Bioinformatics Institute
A*STAR

BIOINFORMATICS INSTITUTE

The Bioinformatics Institute (BII) is a member of the Agency for Science, Technology and Research (A*STAR). We are set up as part of the national initiative to foster and advance biomedical research and human capital development for a vibrant knowledge-based Singapore. The BII is located at the **Biopolis**, Singapore's premier hub for Biomedical Sciences. **http://www.one-north.com**.

We would like to invite applications for Research Scientists and Post Doctoral Research Fellows. Candidates for **Research Scientist** positions should have a PhD in the relevant field, excellent communication skills, collaborative attitude to working in a multidisciplinary environment and a good publication record. Candidates for **Post Doctoral Research Fellow** positions should have a PhD in the relevant field and a good publication record. Appointments will be based on domain expertise, experience, track record and project focus. We currently have positions in the following areas :-

Cancer Biology Group

The Cancer Biology Group is focused on modelling the control and regulation of signaling in cancer with an initial focus on tumor suppression by the p53 pathway. We are addressing key biologically motivated questions on how the p53 pathway protects us from cancer. This work involves an experimental/ modelling collaboration with Prof. Sir David Lane and others. Concurrently, we are creating a comprehensive knowledgebase to integrate and analyze published data about p53 including DNA and protein sequences, gene expression, mutations and associated human diseases etc. that will aid us in our research.

Clinical Biomarkers Discovery Group

The Clinical Biomarkers Discovery Group is involved in a national and international collaboration (we are members of the International Biomarker Discovery Consortium led by the Fred Hutchinson Cancer Research Center). The goal is to discover biomarkers which will be validated by our clinical collaborators that are invaluable for their potential discriminatory power in molecular classification of disease (diagnosis), in predicting clinical outcome (prognosis) and response to drugs (therapy). This national effort, with an initial focus on gastric cancer, is headed by Prof. Sir David Lane (Institute of Molecular and Cell Biology) and includes scientists from the Genome Institute of Singapore, Singapore Oncology Research Institute and the Clinical School at National University Hospital.

Cell Interaction Group

The Cell Interaction Group is engaged in building a one-stop knowledgebase/computational platform for immune cell interaction, particularly focusing on the interactions of innate immune cells with cytokines/chemokines, under normal and selected pathological conditions. Computational modelling of immunology processes, dynamic pathway maps, intelligent literature mining and close interaction with immunology labs are some of the areas to be incorporated into this effort. For Research Scientist positions, you will explore immunology and biocomputing within the framework of the above project, in a mentored, semi-independent, and team-intensive environment.

Chemoinformatics Group

The Chemoinformatics Group is involved in research related to drug design/discovery. Current research is focused on three proteins and their associated partners: p53, kinases and defensins. We are looking for candidates with a few years experience in state of the art molecular simulation techniques and applications to biological systems to work on a range of collaborative projects as part of a young and dynamic team of scientists. Experience with docking, drug design and classical and quantum mechanics/density functional methods would be an advantage. Several projects are being carried out in close association with experimental groups at sister research institutes in the Biopolis, notably the p53 project with Prof. Sir David Lane (Institute of Molecular and Cell Biology) and a tyrosine kinase project with Prof Axel Ullrich (Center for Molecular Medicine).

All applications are required to submit their detailed resume with one-two page statement of research accomplishment and research goals (if applicable) via email to **recruit@bii.a-star.edu.sg** or send your detailed resume to the following address. For more information on the Bioinformatics Institute, please refer to **www.bii.a-star.edu.sg**

HR MANAGER • BIOINFORMATICS INSTITUTE • 30 Biopolis Street • #07-01 Matrix • Singapore 138671

UTD

Erik Jonsson School of Engineering and Computer Science

Department Head/ Distinguished Chaired Professorship

The Erik Jonsson School of Engineering and Computer Science is recruiting a **Department Head** with a Distinguished Chaired Professorship for a new Department of Bioengineering. In addition to being a senior faculty member with an outstanding record of research, teaching and external funding, the successful individual will have the vision, leadership skills and desire to found an outstanding Bioengineering Department. The Jonsson School has significant funds (well into 8-figures) to recruit additional outstanding faculty members with very attractive compensation and start-up packages. The new department will be housed in a new $100 million building which will open in early 2007. The successful candidate will benefit from the close working relationship between The University of Texas at Dallas and the U.T. Southwestern Medical Center, and if appropriate, the position will have a joint appointment with UTSW. Candidates must have a terminal degree in a relevant discipline, and must demonstrate evidence of the ability to conduct a nationally recognized research program.

Applicants should mail their curriculum vitae, a research and teaching plan, and the names and addresses of at least five academic or professional references as soon as possible to: **Academic Search #778, The University of Texas at Dallas, P. O. Box 830688, M/S AD 23, Richardson, TX 75083-0688**. Indication of ethnicity and sex are requested as part of the application, but not required.

UTD is an AA/EO university and strongly encourages applications from candidates who would enhance the diversity of the university's faculty and administration.

UTD

Erik Jonsson School of Engineering and Computer Science

Bioengineering

The Erik Jonsson School of Engineering and Computer Science is recruiting faculty to fill tenured and tenure-track positions in the area of Bioengineering. The new department of Bioengineering will be housed in a new $100 million building which will open in early 2007. We will accept applications at all levels but prefer funded investigators who will qualify for an appointment at the level of Full Professor with a Distinguished Chair. A startup package in seven figures has been budgeted to these positions, and successful senior candidates will be encouraged to recruit junior faculty to extend and complement their research areas. We are focusing this search on candidates working in the areas of: medical imaging, biological systems engineering, nanomedicine or neuroengineering. The successful candidates will benefit from the close working relationship between The University of Texas at Dallas and the U.T. Southwestern Medical Center, and where appropriate, the position will have a joint appointment with UTSW. Candidates must have a terminal degree in a relevant discipline, and must demonstrate evidence of the ability to conduct a nationally recognized research program.

Applicants should mail their curriculum vitae, a research and teaching plan, and the names and addresses of at least five academic or professional references as soon as possible to: **Academic Search #779, The University of Texas at Dallas, P. O. Box 830688, M/S AD 23, Richardson, TX 75083-0688**. Indication of ethnicity and sex are requested as part of the application, but not required.

UTD is an AA/EO university and strongly encourages applications from candidates who would enhance the diversity of the university's faculty and administration.

Faculty Scientists - Pediatrics

The Department of Pediatrics at The University of Texas Medical School at Houston seeks faculty scientists with research interests in any of the following research areas: **complex genetic disorders, lung, heart and brain development, cell and cartilage biology**. These research interests will complement those already established in the Department of Pediatrics and allow for collaborations. The University of Texas Medical School at Houston is situated in the Texas Medical Center, the largest medical center in the world composed of 35 medical and research facilities including The University of Texas M. D. Anderson Cancer Center, The University of Texas School of Public Health at Houston, and Harris County Hospital District. Facilities within the university include state-of-the-art genomics, proteomics, histopathology and mouse cores and vivarium. Positions are available at the instructor, assistant and associate professor levels commensurate with previous experience. These positions are highly competitive with regard to salary, start-up funds and laboratory space. Applicants should have one of the following degrees: PhD, MD or MD/PhD. Successful candidates will be expected to develop and sustain research programs with extramural funding and play an integral role in new program initiatives.

Applicants should send a statement of research interests, curriculum vitae and names and addresses of three references to:

Dr. Jacqueline T. Hecht, PhD, The University of Texas Medical School
Department of Pediatrics, Rm. 3.316, Houston, TX 77030
Email: Jacqueline.T.Hecht@uth.tmc.edu

Women and minority candidates are encouraged to apply. The University of Texas Health Science Center at Houston is an EO/AA employer. M/F/D/V. This is a security sensitive position and thereby subject to Texas Education Code §51.215. A background check will be required for the final candidate.

The University of Texas
Health Science Center at Houston

Science
AAAS

West Coast Ad Sales Representative
SCIENCE

The American Association for the Advancement of Science (AAAS) is seeking a West Coast Advertising Sales Representative for its prestigious weekly journal *Science*. The West Coast Sales Representative will solicit and sell print and online advertising via telephone and face-to-face presentations to life science companies as well as to non-life science companies (computer, chemical, and new technology). Successful candidate will be an effective communicator and a team player with outstanding customer service and sales skills and a strong desire to pursue a career in the rewarding industry of Science, Technical and Medical publishing. Must be able to excel in an independent sales environment.

Position requires a bachelor's degree (or an equivalent combination of education and sales experience) and 2-3 years previous sales experience, preferably in a media/publishing environment. Familiarity with product advertising and online advertising preferred; proficient computer skills including Microsoft Office and contact management system required. 50-70% travel is required. AAAS offers a competitive base pay and benefits package plus commissions.

For consideration, please send resume and cover letter with salary requirements to: **The American Association for the Advancement of Science, 1200 New York Avenue, NW, Suite 100, Washington, DC 20005; Fax (202) 682-1630** or email to **hrtemp@aaas.org**. Please reference job: **BM001**.

Do you do aging research?

Aging Research Careers

Advertising Supplement

Get the experts behind you.

Be sure to read this special ad supplement devoted to aging research opportunities in the upcoming **21 April issue of *Science*.**

You can also read it online at **www.sciencecareers.org.**

To advertise in this issue, please contact:

U.S. Daryl Anderson
phone: 202-326-6543
e-mail: danderso@aaas.org

Europe and International
Tracy Holmes
phone: +44 (0) 1223 326 500
e-mail: ads@science-int.co.uk

Japan Jason Hannaford
phone: +81 (0) 52 789-1860
e-mail: jhannaford@sciencemag.jp

ScienceCareers.org
We know science AAAS

Forschungszentrum Jülich
in der Helmholtz-Gemeinschaft

We are the largest interdisciplinary research institution in Europe working in the fields of "Matter", "Energy", "Information", "Life" and "Environment".

The encouragement of young scientists, both male and female, is an explicit concern of ours. We are therefore eager to attract highly qualified young postdocs to enhance the work in our main research areas. With our

Tenure Track Programme 2007

we are offering outstanding young postdocs the opportunity to establish and head their own working groups at Research Centre Jülich (FZJ) for five years including responsibility for their staff and budget. After a successful interim assessment in the third year of employment, a tenure-track option will provide reliable prospects for the candidate's future career.

For 1 January 2007 we are therefore advertising

four positions as leaders of teams of young scientists,

of which

two positions are reserved for women scientists.

You have outstanding qualifications, a PhD in a scientific or technical subject and would like to work on cutting edge research topics in one of FZJ's departments. A six-month continuous period of research in a laboratory abroad during your PhD work or as a postdoc would be desirable for your application.

We offer you an excellent infrastructure and state-of-the-art equipment, family-oriented working conditions and a human resources development programme. The performance-related salary will conform to the provisions of the Collective Agreement for the Civil Service (TVöD).

Applications from disabled persons are welcomed.

Detailed information on the programme and application procedure can be found at www.fz-juelich.de/tenure-track

Please submit your application by **31 May 2006** to

Forschungszentrum Jülich GmbH
Stabstelle Wissenschaftlich-Technische Planung
Dr. Christoph Arens
52425 Jülich
Germany
E-mail:
ch.arens@fz-juelich.de
Telephone:
+49 2461 61-3394 or -3026

THE FUTURE IS OUR MISSION

Further information about FZJ at: www.fz-juelich.de

John Innes Centre

INDEPENDENT RESEARCH FELLOWSHIPS

The John Innes Centre (JIC), Norwich, UK is a world leading centre of excellence in plant and microbial sciences based on the Norwich Research Park. We are inviting applications from outstanding young researchers who either hold, or wish to apply for Independent Research Fellowships, to attend a conference at the JIC on 5/6 June 2006. At the meeting you will be able to present a talk about your proposed area of research and to discuss your proposals, the development of your group and your future career plans in depth with senior JIC scientists.

After the conference we will select and mentor outstanding candidates in writing Fellowship applications and/or offer the opportunity to move existing Fellowships to the JIC.

Further details and particulars can be found at
http://www.jic.ac.uk/corporate/opportunities/vacancies/fellows.htm

Please e-mail a 2-page summary of your research plan, a copy of your CV, and arrange for three letters of recommendation to be emailed to dee.rawsthorne@bbsrc.ac.uk by Friday 21st April 2006.

The John Innes Centre is a registered charity (No223852) grant-aided by the Biotechnology and Biological Sciences Research Council and is an Equal Opportunities Employer.

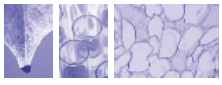

THE INSTITUTE OF MOLECULAR MEDICINE, LISBON, PORTUGAL

RESEARCH GROUP LEADERS

The INSTITUTE OF MOLECULAR MEDICINE, IMM, wishes to recruit young research group leaders in Neurosciences, Oncobiology and Systems Biology.

IMM is located at the Lisbon University campus. The Institute is currently funded by The Ministry of Science-*Fundação para a Ciência e Tecnologia,* and by the Faculty of Medicine-University of Lisbon.

IMM is committed to foster top quality, interdisciplinary bio-medical research.

The prime selection criterion for candidate group leaders is scientific excellence relevant to the research interests of the Institute, as described in the IMM Web site: **http://www.imm.ul.pt**

An initial contract of 5 years' duration will be offered to the successful candidates. This can be renewed, depending on circumstances at the time of the review.

Applicants should submit a curriculum vitae, with a concise description of research interests and future plans. Two letters of recommendation should be independently sent to: **Prof. M. Carmo-Fonseca, Institute of Molecular Medicine, Faculty of Medicine, Avenida Prof. Egas Moniz, 1649-028, Lisboa, Portugal.**
Fax: 351 21 7999412
Email: carmo.fonseca@fm.ul.pt

Deadline to submit applications: 12 May 2006

MICHIGAN STATE UNIVERSITY

ASSOCIATE PROFESSOR
Aquatic Resource Policy and Management/ Director for Michigan Sea Grant Extension Programs
Department of Fisheries and Wildlife
College of Agriculture and Natural Resources

Description: The primary responsibility is to serve as the Extension Program Coordinator for the Michigan Sea Grant College Program. Secondary responsibilities include developing and implementing an applied research program in support of Michigan Sea Grant College program centering on Great Lakes aquatic resource policy and management.

Responsibilities:
1. Coordinate Michigan Sea Grant Extension Program (75%)
Program Development and Management
- Serve as a member of the Michigan Sea Grant College Program Management Team.
- Assist Associate Director of Michigan Sea Grant College Program, as needed to enhance effectiveness of the program operations.
- Coordinate the development and implementation of strategic plans, Sea Grant Extension proposals and annual plans of work.
- Foster the development of each staff member's special talents and interests.
- Communicate program needs to upper-level university administrators.
- Maintain liaison between MSU Extension & Michigan Sea Grant College Program.
- Prepare the program for evaluation by the National Sea Grant College Program.
- Represent the Sea Grant Extension program within the university system and externally.
- Develop new funding opportunities to expand Sea Grant Extension programming in the State, region and Nation.
- Promote affirmative action.

Personnel Management
- Keep staff informed of Sea Grant institutional plans, activities and expectations.
- Encourage staff members to communicate ideas for improving the Sea Grant Extension program and Michigan Sea Grant as a whole.
- Monitor staff contributions.
- Supervise on campus and assigned off-campus Sea Grant extension staff members.
- Serve on interview committees for Sea Grant Extension personnel.
- Provide input to off-campus staff performance in cooperation with MSUE Regional Directors. - Make merit recommendations to Regional Directors for off-campus staff assigned to MSUE regions.

Financial Management
- Prepare and propose program budgets to the Director of MSU Extension and the Associate Director of Michigan Sea Grant Program
- Administer grant accounts through MSU departments and MSU Contract and Grants Administration.
- Encourage staff members to submit proposals for contracts and grants from outside sources and facilitate submission of proposed contracts and grants as necessary.
- Consult with Associate Director of Michigan Sea Grant in setting priorities for allocation of core funding.
- Prepare annual reports.
- Maintain budget records.

2. Research: (25%)
Establish an integrative applied research program that supports the programmatic activities of the Michigan Sea Grant College program. The research program may draw upon needs expressed in the current strategic plan or develop principles of successful interdisciplinary collaboration and adaptive management approaches to improve the scientific basis of Great Lakes policy decision making. Applicants are encouraged to propose a relevant research program that would be competitively funded externally to the Michigan Sea Grant College Program.

Qualifications: Ph.D. at the time of appointment, with an advanced degree in a field that relates to aquatic science or aquatic ecosystem policy and management and a record of scholarship that would qualify for appointment in the MSU tenure system.
The candidate is expected to have demonstrated leadership skills and experience in extension program development, administration and research.
The candidate should have:
- proficiency and demonstrated knowledge, through work experience, in the assessment of large aquatic ecosystem policy and resources issues;
- interest, skill, and experience in using science to improve public policy by synthesizing research which help policy makers and the public make better decisions regarding large aquatic ecosystem management.
- excellent written and oral communication skills;
- a demonstrated ability to write successful research proposals, mentor graduate students and publish research findings.
- A demonstrated ability to work in a collaborative environment, including with other faculty, staff, and external clientele groups.
- The ability to understand and integrate diverse cultural perspectives into decisions.
- Demonstrated experience in managing contracts, grants and financial management.
- Demonstrated ability to lead program planning and implementing and evaluating teams.
- Demonstrated experience in personnel management.

Appointment: Salary commensurate with experience and qualifications. Interested individuals should prepare (1) letter of interest, (2) resume, (3) description of relevant experience and expertise, and of professional goals, (4) names and contact information for three references. Application Deadline: April 30, 2006 or until filled. Please send application materials to William W. Taylor, Chairperson, Michigan State University, Dept. of Fisheries and Wildlife, 13 Natural Resources Building, East Lansing, MI 48824. E-mail: taylorw@msu.edu. Candidates should include "Job Sea Grant Coordinator" at the start of the subject line in all e-mail correspondence regarding this position.

MSU IS AN AFFIRMATIVE ACTION, EQUAL OPPORTUNITY INSTITUTION.

POSITIONS OPEN

TENURE-TRACK FACULTY POSITIONS
Departments of Pharmacology and Pathology
Columbia University
College of Physicians and Surgeons

The Departments of Pharmacology and Pathology at Columbia University invite applications for two tenure-track faculty positions at the **ASSISTANT** and **ASSOCIATE PROFESSOR** levels. Applicants must hold a Ph.D. and/or M.D. degree. Candidates whose fields of interest include mechanisms of cell signaling, membrane biophysics or biochemistry, or computational approaches to biological problems will be given the strongest consideration. Incoming faculty must be willing to teach pharmacology or related areas to graduate and professional students (M.D., Ph.D.), mentor thesis studies of Ph.D. students, and carry out a scholarly and contemporary research program. Incumbents will be expected to conduct an extramurally funded research program involving graduate students and postdoctoral fellows, and participate in administrative functions of the Departments and the University. Candidates will be expected to show evidence of their potential through letters of recommendation and a publication record appropriate for their experience.

Please send electronically curriculum vitae, three references, cover letter, and a brief statement of current and future research interests to: **Yudith Mahon-Campbell, e-mail: ym2197@columbia.edu.**

We are an Affirmative Action/Equal Opportunity Employer.

UNIVERSITY OF CALIFORNIA, IRVINE
Department of Medicine
Division of Infectious Diseases

The Division of Infectious Diseases and the Program in Public Health are seeking candidates for a position as **HOSPITAL EPIDEMIOLOGIST** at the University of California (UC) Irvine Medical Center. This is a tenure-track position at the Assistant Professor level. Candidates should have an M.D. degree, be Board-certified or Board-eligible in infectious diseases, and have previous training and experience in hospital epidemiology/infection control. A strong research background is required, and candidates should be in a position to successfully compete for NIH funding. Clinical responsibilities will be limited and flexible in accordance with the successful candidate's interests and the extent of extramural funding. Applicants should send a curriculum vitae and names and addresses of three references to: **Donald Forthal, M.D., Chief, Division of Infectious Diseases, Department of Medicine, University of California, Irvine Medical Center, 101 City Drive, Orange, CA 92868.** *The University of California, Irvine, has an active career partner program and an NSF ADVANCE Program for Gender Equity and is an Equal Opportunity Employer, committed to excellence through diversity.*

POSTDOCTORAL/RESEARCH ASSOCIATE POSITIONS are available to study signal transduction, mitochondrial biology, cell calcium, and ion channels in cardiovascular and respiratory systems. Research training in molecular/cell biology, electrophysiology, physiology, or pharmacology is desirable. Salary will be commensurate with experience. If interested, please e-mail application letter and curriculum vitae to **Dr. Yong-Xiao Wang** at **e-mail: wangy@mail.amc.edu, Center for Cardiovascular Sciences, Albany Medical College, Albany, NY 12208-3479.** *An Equal Opportunity/Affirmative Action Employer. Women and Minorities are encouraged to apply.*

The University of Colorado at Colorado Springs (UCCS) Biology Department seeks a **BIOLOGIST** for appointment to a tenure-track position at the Assistant Professor level to begin August 2006. Visit **website: http://web.uccs.edu/affirm/job%20announce/assistant_professor_biology480518.htm.**

The University of Colorado at Colorado Springs is committed to diversity and equality in education and employment.

POSITIONS OPEN

The Institute for Tropical Ecosystems Studies (ITES) at the University of Puerto Rico, Río Piedras, invites applications for one **TENURE-TRACK POSITION** in landscape ecology. The successful candidate should have experience with spatial analysis and geographic information system (GIS) and research interests in such areas as (but not limited to) applications of remote sensing, conservation ecology, or land-use change. Appointment will be at the Assistant or Associate Professor level depending on qualifications. Job duties will include research, managing the spatial analysis laboratory, securing external funds, a minimum load of three credits per semester, and directing students. ITES is an interdisciplinary unit with research projects in the Neotropics and Asia, and a Long-Term Ecological Research (LTER) site within 30 minutes of campus. The majority of our students are from Puerto Rico or other countries in Latin America. We encourage applications from women and minorities.

Applicants should submit curriculum vitae, statements of research and teaching interests, representative reprints, and contact information for three references to:

Dr. Alonso Ramírez
Search Committee Chair
Institute for Tropical Ecosystem Studies
University of Puerto Rico
P.O. Box 21910
San Juan, PR 00931-1910

The committee will receive and review applications from March 1, 2006, until the position is filled. The starting date is August 2006. For more information, see **website: http://ites.upr.edu** or **e-mail: aramirez@ites.upr.edu.**

The University of Puerto Rico is an Equal Opportunity/Affirmative Action Employer. Minorities/ Women/ Veterans/ Persons with Disabilities.

FACULTY POSITION, EPIDEMIOLOGY

The College of Veterinary Medicine at the University of Maryland, College Park invites applications for a nine-month, tenure-track **ASSISTANT/ ASSOCIATE PROFESSOR** position in Epidemiology. Minimum requirement: Ph.D. or equivalent degree in Epidemiology or related field for this 80 percent research, 20 percent teaching appointment. Demonstrated evidence of basic and applied research experience in epidemiology required for work in infectious diseases, zoonosis, disease transmission, and food safety. Epidemiologists using molecular tools are strongly encouraged to apply. Teaching responsibilities include lectures and clinical rotations, and mentoring graduate and veterinary students. Excellent benefits package and salary commensurate with qualifications. Submit a letter of application, curriculum vitae, statement of career goals, and names and contact information for three professional references to: **Chair, Epidemiologist Search Committee, Virginia - Maryland Regional College of Veterinary Medicine, University of Maryland, 8075 Greenmeade Drive, College Park, MD 20742-3711.** Applications will be accepted until June 1, 2006, or until a suitable candidate has been identified. The position is available immediately. *The University of Maryland is an Affirmative Action/Equal Opportunity Employer.*

POSTDOCTORAL RESEARCHER positions are open in the laboratory of **Dr. Ming You, M.D., Ph.D.,** Washington University School of Medicine, St. Louis, Missouri. Successful candidate will perform laboratory methods on the following projects: (1) identification of genes predisposed to cancer; (2) molecular basis of cancer; and (3) chemoprevention of cancer. Individuals with experience in molecular biology, transgenic animal models, or computational biology are welcome to apply. *Permanent residency is required.* Interested applicants should send curriculum vitae, statement of research interests, and the contact information of three references to: **Cindy Kaye, Washington University School of Medicine, 660 South Euclid Campus Box 8109, St. Louis, MO 63110. E-mail: kayec@wustl.edu.** Application deadline is May 1, 2006. *We are an Equal Opportunity Employer.*

Associate Provost and Vice President for Research

Boston University

Boston University seeks a dynamic individual with academic leadership experience, an international scholarly reputation, and proven success in acquiring external funding for research to serve as Associate Provost and Vice President for Research (AP/VPR). This position reports to the Provost and will coordinate and facilitate all research efforts at Boston University. The holder will chair the Research Advisory Council and will sit on the President's Administrative Council, Council of Deans, and University Leadership team.

The AP/VPR will assist and advise the President and Provost on all matters pertaining to the University's comprehensive research activities. Working with the Associate Provost of the Medical Campus, the successful candidate will work to evolve current strategic plans for research, including articulating and creating policies and procedures that enhance faculty research, technology transfer, and corporate outreach. This position will oversee, or share in the oversight of, the Office of Technology Development, Office of Sponsored Programs, Office of Research Compliance, the Undergraduate Research Opportunities Program, and all multi-school/college interdisciplinary laboratories and research centers. The AP/VPR will work collaboratively and proactively with the deans, directors, and faculty to achieve a greater integration of the University's research program with its graduate teaching program. The AP/VPR will also work with legislative bodies, government agencies, regulatory agencies, foundations, industry partners, and colleagues at other institutions to advance the research being undertaken at Boston University.

The successful candidate should have an earned Ph.D. and scholarly credentials to meet the standards for an academic appointment at the level of full professor in his or her field; experience with externally funded research; a successful track record of appropriate management and administrative experience; strong interpersonal skills; and the ability to foster collaborative efforts within the Boston University community and build links with industry nationally and internationally.

Boston University, with a total enrollment of more than 30,000 and a faculty of more than 3,500 in its 17 schools and colleges, is the fourth-largest independent university in the United States. The University supports a large and diverse research program, with sponsored research funding totaling over $300 million in 2005.

Persons interested in being considered for this position should submit a brief letter of interest and current curriculum vitae by April 30, 2006. Applications and nominations should be submitted to: Office of the Provost, One Sherborn Street, Boston, MA 02215, attn: Ms. Suzanne Kennedy.

BOSTON UNIVERSITY

An affirmative action, equal opportunity employer

MEDICAL OFFICERS AND INTERDISCIPLINARY SCIENTISTS
PANDEMIC INFLUENZA VACCINE

The Center for Biologics Evaluation and Research, Food and Drug Administration, Department of Health and Human Services is searching for outstanding physicians and scientists to assist in the Center's Pandemic Influenza Vaccine initiative. Center staff conducts biomedical research to provide a strong scientific base for the regulation of blood and blood-related products, vaccines, allergenic products, and gene therapies according to statutory authorities in order to protect and enhance the public health. In conjunction with regulatory and research responsibilities, the Center statistically evaluates clinical and pre-clinical studies of human biological products and vaccines and epidemiologically evaluates post-marketing studies and adverse biological reactions.

The Pandemic Influenza Vaccine initiative is to protect critical workers and the US population in the anticipation of an influenza pandemic as quickly as possible through the establishment of a pandemic influenza vaccine manufacturing capacity. FDA has dramatically expanded its pandemic influenza program in the clinical, statistical, epidemiological, manufacturing and facilities areas this past year. FDA will be required to perform additional data reviews and facility inspections both for assuring adequate annual flu vaccine and in response to the potential for a pandemic.

QUALIFICATIONS:

- **Physicians:** Applicants must have an M.D. or equivalent degree from an accredited institution and additional research experience. Graduates of foreign medical schools must submit a copy of their ECFMG certificates.
- **Scientists:** (Other than M.D.) An advanced degree in one or more of the following disciplines is highly desirable: Biology, Microbiology, Chemistry, Biochemistry; Toxicology/Pharmacology, or Mathematical Statistician.

CANDIDATES FOR CIVIL SERVICE OR COMMISSIONED CORPS APPOINTMENTS MUST BE U.S. CITIZENS. NON-U.S. CITIZENS MAY BE ELIGIBLE FOR SERVICE FELLOWSHIP APPOINTMENTS OR OTHER POST-DOCTORAL PROGRAMS.

SALARY:

- **Physicians:** salaries range from Selected Federal White-Collar Pay Schedules, $91,407 - $118,828. In addition, physicians may also be eligible for a Physician's Comparability Allowance (PCA) of $4,000 to $24,000 per annum, or be appointed under Title 42 Excepted Service. Salary and benefits are commensurate with education and experience. Positions may be filled by appointment in the US Public Health Service, Commissioned Corps.
- **Scientists:** salaries range from Selected Federal White-Collar Pay Schedules $54,272 - $118,828. Salary and level of responsibility are commensurate with education and experience.

LOCATION: CBER is actively recruiting applicants to fill positions located in Bethesda and Rockville, Maryland, involved in the regulation of biological and related products in support of the Pandemic Influenza Vaccine.

HOW TO APPLY: Applications are accepted and should indicate availability for employment. Interested candidates should submit a current Curriculum Vitae/Resume and cover letter to: **recruitment@cber.fda.gov** or **Food and Drug Administration, Center for Biologics Evaluation and Research; 1401 Rockville Pike, HFM-123, Rockville, MD 20852-1448; ATTENTION: Recruitment Coordinator**.

Additional information: **http://www.fda.gov/cber/inside/hirebkg.htm**.

FDA IS AN EQUAL OPPORTUNITY EMPLOYER WITH SMOKE FREE ENVIRONMENT
**FDA provides reasonable accommodations to applicants/employees with disabilities.*

POSITIONS OPEN

CHAIR
Department of Physiological Sciences
Eastern Virginia Medical School, Norfolk, Virginia

Eastern Virginia Medical School (EVMS) is seeking an extraordinary individual to Chair its Department of Physiological Sciences. This is an exciting time at EVMS and the Institution is committed to significant investment and growth in the basic sciences. The new Chair of Physiological Sciences will have exceptional support for recruiting new faculty and building nationally prominent research and education programs. Candidates for this position must have a Ph.D. and/or M.D. degree, a distinguished record of scholarly achievements including international recognition in research, an outstanding record of maintaining extramural funding, and demonstrated commitment to excellence in teaching. The area of research is open, but candidates should have superb leadership and interpersonal skills, and the ability to develop programmatic research areas that bridge the Department's three divisions (biochemistry, pharmacology, and physiology). Major current research focal areas are reproductive biology and cardiovascular science with funding from the National Institutes of Health and private foundations. Faculty provide instruction to students in the first and second year of medical school, in the allied health professions, and train M.S. and Ph.D. graduate students in the biomedical sciences. The successful candidate will be expected to articulate and implement a vision for improving faculty productivity and recruiting talented research scientists in ways that enhance current research and educational programs, and that may include strong programs in new areas of cutting edge research. For further information, please visit the Department **website: http://www.evms.edu.**

All inquiries, nominations, and applications will be held in strictest confidence. Applicants for this exceptional opportunity should forward (1) curriculum vitae, (2) research interests, and (3) the names of three references to:

Larry D. Sanford, Ph.D., Chair
Physiological Sciences Chair Search Committee
Department of Physiological Sciences
Eastern Virginia Medical School
P.O. Box 1980, Norfolk, VA 23501-1980
Telephone: 757-446-5619
E-mail: sanforld@evms.edu

EVMS is an Equal Opportunity/Affirmative Action and Drug Free Workplace Employer and encourages applications of women and minorities.

POSTDOCTORAL POSITION
Quantitative Toxicology/Pharmacology

The U.S. Environmental Protection Agency (EPA), National Center for Environmental Assessment in Cincinnati, Ohio, seeks Postdoctoral candidates in computational toxicology and biological modeling for human health risk assessments. Successful candidates will have experience in some of the following areas: toxicology, biochemistry, physiology, pharmacology, statistics, and computer modeling. Specialized education training and/or experience preferred include quantitative structure-activity (e.g., QSAR, SAR) modeling, pharmaco- or toxicokinetic modeling, or physiological or biologically-based dose response modeling. Salary ranges from $50,000 up to $70,000, commensurate with qualification plus benefits. Information on federal positions can be found at **website: http://cfpub.epa.gov/ncea/cfm/recordisplay.cfm?deid=134123 (CINCSAST-010406-01).** For additional information contact **Dorothy Carr** at **telephone: 919-541-4356.** Information on nonfederal positions can be found at **website: http://www.orau.gov/orise/edu/needs/EPA-NCEA-2006-01.pdf.** For additional information please contact **Karen Proffitt** at **telephone: 513-569-7099.**

US EPA is an Equal Opportunity Employer.

POSITIONS OPEN

FACULTY POSITION
in Cellular/Molecular Neuroscience

The Department of Neuroscience at Baylor College of Medicine is recruiting **ASSISTANT PROFESSORS** on the tenure-track who utilize contemporary tools of molecular and cellular neuroscience to investigate fundamental questions of nervous system function in health, disease, or injury. The successful candidate should have a Ph.D. and or M.D., postdoctoral experience, strong experimental skills, and a record of accomplishment in the application of molecular, imaging, biophysical, or electrophysiological approaches to nervous system function. The Department of Neuroscience is undergoing a major expansion, building on strengths in ion channel function, cellular/molecular imaging, synaptic plasticity, neuronal development, cell signaling, sensory processing, and cognitive/computational neuroscience. The position will provide highly competitive allowances for laboratory support and research program development. Send curriculum vitae and statement of research interests, and have at least three letters of reference sent to: **Michael J. Friedlander, Ph.D., Professor and Chair of Neuroscience, Director of Neuroscience Initiatives, Baylor College of Medicine, One Baylor Plaza, Suite S740A, Houston, TX 77030 (e-mail: friedlan@bcm.edu)** by April 30, 2006. Applications may be submitted electronically or by mail; reference letters must be submitted by mail.

Baylor College of Medicine is an Equal Opportunity Affirmative Action and Equal Access Employer.

POSTDOCTORAL FELLOWSHIP, Cancer Epidemiology and Prevention Research. The Robert H. Lurie Comprehensive Cancer Center and the Department of Preventive Medicine of Northwestern University Feinberg School of Medicine invite applications for the multidisciplinary Postdoctoral Training Program in Cancer Epidemiology and Prevention, an R25 Cancer Education and Career Development program directed by **Susan M. Gapstur, Ph.D., M.P.H.** The two-year program offers the option to complete a Master's of Public Health or M.S. in Clinical Investigation; it is organized around four thematic areas: (1) epidemiology and biomarkers; (2) screening and early detection; (3) chemoprevention; and (4) behavioral prevention. In collaboration with faculty, Fellows design an individualized didactic and research program emphasizing one of these four themes. Stipend is at least $50,000 annually plus benefits, with additional funds provided for tuition, travel, and supplies. Applicants must hold a doctoral level degree (Ph.D., M.D., Ed.D.) *and be a U.S. citizen or permanent resident at time of application.* Candidates interested in entering the Program in summer or fall 2006 should refer to our website for complete instructions at **website: http://www.preventivemedicine.northwestern.edu/r25.htm.** Send all materials to: **Paula Feldman, Program Coordinator, Department of Preventive Medicine, Feinberg School of Medicine, Northwestern University, 680 North Lake Shore Drive, Suite 1102, Chicago, IL 60611** by April 28, 2006. *Women and minorities are encouraged to apply. Northwestern University is an Equal Opportunity/Affirmative Action Employer.*

POSTDOCTORAL FELLOW. Aging of mitochondria in neuroscience using cell fluorescence and in situ PCR measures of mitochondrial function in the context of glutamate and beta-amyloid toxicity. Minimum qualifications are a Ph.D. in either cell biology or neuroscience with desired focus on neurotoxicity, in situ PCR or mitochondrial function. Apply to: **Dr. Gregory J. Brewer (website: http://www.siumed.edu/mmi/phdpages/gbpage2.HTM), Attn.: Ms. Barb Reichert (e-mail: breichert@siumed.edu), Southern Illinois University School of Medicine, P.O. Box 19626, Springfield, IL 62794-9626.**

POSITIONS OPEN

NEBRASKA CENTER FOR VIROLOGY

RESEARCH ASSISTANT PROFESSOR in molecular virology to participate in established research program of **Dr. Charles Wood** on HIV and AIDS-associated diseases including Kaposi's Sarcoma. Provide management of ongoing research projects and supervise research staff in his laboratory while developing independent research associated with the Nebraska Center for Virology **(website: http://www.unl.edu/virologycenter)** through the University of Nebraska, Lincoln School of Biological Sciences. Candidates should hold Ph.D. and/or M.D. and relevant postdoctoral research experience.

Review begins April 1, 2006. To be considered for this position, apply at **website: http://employment.unl.edu.**

Dr. Charles Wood, Director
Nebraska Center for Virology
E249 Beadle Center
Lincoln, NE 68588-0666
E-mail: cwood1@unl.edu

The University of Nebraska is committed to a pluralistic campus community through Affirmative Action and Equal Opportunity. We assure reasonable accommodation under the Americans with Disabilities Act; contact ***J. Walker*** *at* ***telephone: 402-472-4560*** *for assistance.*

SOUTHERN ILLINOIS UNIVERSITY
School of Dental Medicine
Department of Applied Dental Medicine
Section of Pharmacology

Southern Illinois University School of Dental Medicine (SIU-SDM) is seeking applicants for a full-time tenure-track position at the **ASSISTANT/ASSOCIATE PROFESSOR** level in the Section of Pharmacology. Responsibilities include pharmacology course development and didactic teaching of dental students with some teaching at advanced levels. Additionally, the candidate will be expected to be active in oral health care related research as well as service to the University. Candidates should possess a Ph.D. in pharmacology or a dental degree/Ph.D. Previous teaching experience and a record of research accomplishment are desirable. Academic rank and salary are commensurate with experience and qualifications. SIU-SDM is a suburban campus located in the St. Louis metropolitan area. Send a letter of application, including a statement of teaching philosophy and research interests, curriculum vitae and names and contact information for three references to: **Dr. Ann Boyle, Dean, School of Dental Medicine, Southern Illinois University, 2800 College Avenue, Alton, IL 62002-4900.** Review of applications will begin in April 2006, and continue until the position is filled.

SIUE is an Equal Employment Opportunity/Affirmative Action Employer committed to diversity in education and employment. SIUE is a State University; benefits under state sponsored plans may not be available to holders of F-1 or J-1 visas.

The Department of Biology at the University of Nevada, Reno, is seeking candidates for two non-tenure track, nine-month **LECTURER POSITIONS**. Full-time lecturer to teach human anatomy and physiology, evening sections of introductory organismal biology, and endocrinology or physiology course. Full-time lecturer to teach genetics, evening sections of introductory cell biology, and neurobiology or physiology course. Minimum qualifications include an earned Ph.D. degree in biology, physiology, or related discipline and previous teaching experience at the college level in a faculty position or as a graduate assistant. View complete position description, requirements and online application at **website: http://jobs.unr.edu.** Applications received by April 24, 2006, will receive full consideration. *Equal Employment Opportunity/Affirmative Action, women and under-represented groups are encouraged to apply.*

WORKSHOPS

Workshop on Computational Methods for Spatially Realistic Microphysiological Simulations

June 6-9, 2006

Hosted by The National Resource for Biomedical Supercomputing

This workshop will cover simulation of models focused on diffusion-reaction systems such as neurotransmission and biochemical networks. New versions of *MCell* and *DReAMM* software (www.mcell.psc.edu and www.mcell.cnl.salk.edu) will be introduced, highlighting models created from 3-D reconstructions or CAD tools, and new Monte Carlo methods for 3-D simulation of reactions in solution and on biological surfaces.

Application deadline is April 26, 2006.

www.nrbsc.org/education/workshops/cmms/

The NRBSC (an NIH Resource Center) pursues leading edge research and education in high performance computing and the life sciences, with focus areas in microphysiology, volumetric data visualization and analysis, and computational structural biology.

Direct inquiries to:
nrbsc@psc.edu
1-800-221-1641

Pittsburgh Supercomputing Center
300 S. Craig Street
Pittsburgh, PA 15213

PITTSBURGH SUPERCOMPUTING CENTER

NRBSC
www.nrbsc.org

SYMPOSIA

IOWA STATE UNIVERSITY
Plant Sciences Institute

8th annual Plant Sciences Institute Symposium

Plant Receptor Signaling

Photoreceptors
Emmanual Liscum
Keith Moffat
Peter Quail

Hormone Receptors
Joanne Chory
Mark Estelle
Dan Kliessig
G. Eric Schaller
Michael R. Sussman

Receptors in Biotic Interactions
Andrew Bent
Eric Davis
Greg Martin
Pam Ronald

Receptors in Growth and Development
Sacco de Vries
June Nasrallah
John Schiefelbein

Genomic/Proteomic Approaches for Plant Receptors
Scott Peck
Shinhan Shiu
Frans Tax
Roger Wise

Organizing Committee:
Philip W. Becraft
Roger P. Wise
G. Eric Schaller
Marit Nilsen-Hamilton

For more information or to register
visit: www.bb.iastate.edu/~gfst/phomepg.html
or e-mail: pbmb@iastate.edu

JUNE 22-25 2006
Iowa State University, Ames, Iowa

Immunology/ Infectious Disease Research Careers

Advertising Supplement

Get the experts behind you.

Be sure to read this special ad supplement devoted to immunology and infectious disease career opportunities in the upcoming **5 May issue of *Science*.**

Find immunology and infectious disease research jobs and other career resources online at **www.sciencecareers.org.**

For advertising information, contact:

U.S. Daryl Anderson
phone: 202-326-6543
e-mail: danderso@aaas.org

Europe and International
Tracy Holmes
phone: +44 (0) 1223 326 500
e-mail: ads@science-int.co.uk

Japan Jason Hannaford
phone: +81 (0) 52 789-1860
e-mail: jhannaford@sciencemag.jp

ScienceCareers.org
We know science AAAS

POSITIONS OPEN

BIOLOGY (Tenure Track)
Penn State Altoona

The Pennsylvania State University, the Altoona College invites applications for a Tenure-Track position in vertebrate physiology in the Division of Mathematics and Natural Sciences, beginning in fall 2006. The position requires a Ph.D. in biology or a closely related discipline. Teaching duties will include introductory biology, mammalian anatomy for allied health students, upper-level vertebrate physiology (lecture/laboratory), and a course in his/her area of expertise. The successful candidate should contribute to our new Baccalaureate Program in Biology. Only 40 miles from the University Park campus, Altoona College offers the advantages of small college teaching with the readily available resources of a major research university. Applicants should present a record of evidence and potential effectiveness in teaching, research, and service. Penn State Altoona offers a competitive salary and an attractive benefits package. Applicants should send a letter of application establishing their qualifications; current curriculum vitae; a description of teaching philosophy and evidence of teaching effectiveness; a statement of research interests; transcripts (official transcripts required at the time of an interview); and a minimum of three letters of reference. Applicants are strongly encouraged to submit their applications and accompanying materials electronically to **e-mail: mnsdiv@psu.edu** in Word or PDF formats. Review of applications will begin the week of April 15, 2006, and continue until the position is filled. Nonelectronic inquiries, applications, and additional materials should be sent to: **Chair, Search Committee for Biology, Penn State Altoona, Box A-22006, 3000 Ivyside Park, Altoona, PA 16601-3760.** For additional information about Penn State Altoona, please visit our web page at **website: http://www.aa.psu.edu.**

Penn State is committed to Affirmative Action, Equal Opportunity and the diversity of its workforce.

POSITIONS OPEN

FACULTY POSITION
Bilkent University
Ankara, Turkey

Bilkent University Department of Molecular Biology and Genetics, seeks applicants at the **ASSISTANT** or **ASSOCIATE PROFESSOR** levels. We are particularly interested in outstanding candidates who have special expertise on cancer biology, signalling, or functional genomics. The candidate is expected to take on academic responsibilities in addition to conducting research. Bilkent University is a private university and the Department is widely acknowledged as one of the leading research institutes in Turkey. The medium of instruction in the University is English. Applicants should send a letter of intent and curriculum vitae to:

Professor Dr. Mehmet Ozturk
Bilkent University
Department of Molecular Biology and Genetics
Ankara 06800 Turkey
E-mail: jobappl@fen.bilkent.edu.tr
Website: http://www.mbg.bilkent.edu.tr

ANGIOGENESIS/CARCINOGENESIS/ STEM CELL RESEARCHERS

Temple University School of Medicine is currently seeking researchers (Ph.D. or M.D.) at the **ASSISTANT/ASSOCIATE** or **FULL PROFESSOR** level who are trained in cell, molecular or immunobiology (preferably with a history of grant funding) and whose research interests lie in the areas of angiogenesis, stem cell biology, or carcinogenesis.

Please send curriculum vitae and bibliography to: **Henry Simpkins, M.D., Ph.D., Professor and Chairperson, Department of Pathology and Laboratory Medicine, Temple University School of Medicine, 3401 North Broad Street, Philadelphia, PA 19140.** *Temple University is an Equal Opportunity/ Affirmative Action Employer and strongly encourages applications from women and minorities.*

POSITIONS OPEN

The University of Texas Southwestern Medical Center at Dallas, Division of Nephrology seeks faculty at the **ASSISTANT/ASSOCIATE/ FULL PROFESSOR** level who will develop independent research programs in kidney biology and disease. Individuals with interests in genetics or glomerular biology are particularly encouraged to apply. Brand new, state-of-the-art laboratory facilities and competitive startup packages will be provided. M.D. candidates should be Board-certified/ Board-eligible in nephrology. Visit our **website: http://www.utsouthwestern/nephrology.** Send curriculum vitae, description of research, and names of three references to: **Peter Igarashi, M.D., Chief of Nephrology, University of Texas Southwestern, 5323 Harry Hines Boulevard, Dallas, TX 75390-8856. E-mail: peter.igarashi@utsouthwestern.edu.** *University of Texas Southwestern is an Equal Opportunity/ Affirmative Action Employer.*

SYMPOSIUMS

Fourth International Symposium on Cell/Tissue Injury and Cytoprotection/Organoprotection Focus on Gastrointestinal Tract
Co-Chairs: Drs. S. Szabo and A. Tarnawski
May 17 - 19, 2006, Long Beach, California

Goals: To provide updates on cell and tissue injury, protection, repair and healing, including the role of stem cells. The focus will be on gastrointestinal tract injury, protection, and healing of esophageal, gastric, duodenal mucosal injury and ulcers, liver injury, inflammatory bowel disease. Injury and healing of other tissues will also be discussed.

Format: Minisymposia, e.g., two to three invited speakers, followed by short presentations selected from submitted abstracts and poster session. Registration fee: $200 (includes program and abstract booklet, opening reception, lunch, and symposium dinner). To obtain registration and abstract forms please contact: **Frances Walker, Veterans Affairs Medical Center (05/113), e-mail: frances.walker@med.va.gov; telephone: 562-826-5513.** Abstract submission deadline: April 15, 2006.

MARKETPLACE

MARKETPLACE

MARKETPLACE

Simplify Gene Silencing Experiments with *Silencer*® Pre-designed siRNA

Fast. Easy. Guaranteed.

- Ready to use siRNAs provided in as little as 4 days
- Searchable database makes it simple to find siRNAs to your genes of interest
- Efficient gene knockdown guaranteed
- Now save 18% when you purchase 3 siRNAs per gene

Tired of wasting time with poorly designed siRNAs? *Silencer*® Pre-designed siRNAs—highly effective, ready-to-use siRNAs available for all human, mouse and rat genes—provide guaranteed gene silencing. Each one has been designed using a carefully optimized algorithm and then manufactured to exacting quality standards to provide potent and specific gene silencing.

Verify Gene Silencing Results and Save 18%

Journal article reviewers generally require that you verify gene silencing results with a second siRNA. *Silencer* Pre-designed siRNAs make it easy to comply. Ambion guarantees that at least two *Silencer* Pre-designed siRNAs will knockdown target mRNA levels by ≥70% when three are purchased for the same gene.

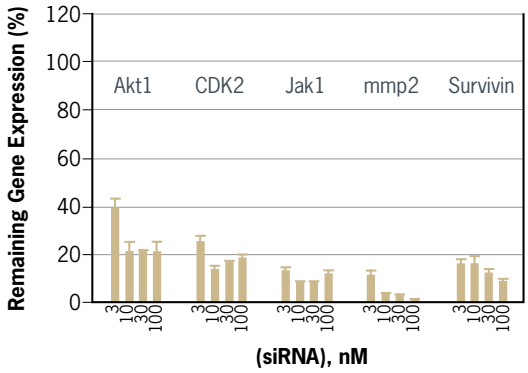

Potency of *Silencer*® siRNAs at Low Concentrations. The algorithm Ambion uses to design *Silencer* Pre-designed siRNAs results in efficient gene silencing. Most *Silencer* siRNAs are effective at 3-10 nM.

Ambion RNAi Resources

On the Web: RNA Interference Resource
Protocols, data, references, and more
www.ambion.com/RNAi

Via Mail: RNA Interference Research Guide
New tools and techniques for performing RNAi
Request a free copy at **www.ambion.com/contact/litreq**

Via e-mail: Silencer E-Newsletter
Experimental tips, new tools for RNAi, and exclusive special offers
Sign up at **www.ambion.com/contact/litreq**

Via phone: RNAi Specialists
Assistance with experimental setup, design, and troubleshooting
See **www.ambion.com/contact**
for our full list of toll free phone numbers

Learn how you can get fast, easy and guaranteed siRNAs at
www.ambion.com/info/siRNA

Ambion®
THE RNA COMPANY®

Ambion, Inc.
U.S. 800-888-8804 • Canada 800-445-1161
fax +1-512-651-0201

Ambion (Europe) Ltd
tel +44 (0)1480-373-020
fax +44 (0)1480-373-010

Ambion K.K. (Japan)
tel +81 (0)3-5638-2181
fax +81 (0)3-5638-2182

For a list of Ambion direct free phone numbers and distributors in your country, go to www.ambion.com/contact